Investigating Metabolic Dysfunction and Microbiome Imbalance as a Driver in the neurodegenerative Disease Amyotrophic Lateral Sclerosis

Fiona Dresel

2026

A thesis presented for the degree of

Doctor of Philosophy in Cell Biology



School of Biosciences

University of Kent

I Declaration

No part of this thesis has been submitted in support of an application for any degree or other qualification of the University of Kent or any other University or Institution of learning.

Fiona Dresel

March, 2026

II Acknowledgments

I would like to thank my supervisors, Prof Campbell Gourlay, Prof Martin Michaelis and Dr Becky Hall for their scientific advice and support. I would also like to thank my funding body, SoCoBio and the BBSRC, for supporting this work.

Finally, I wish to express my gratitude to my family and friends for their encouragement throughout this journey.

III Abbreviations

α-syn	A-synuclein
AC	Adenylate cyclase
ALS	Amyotrophic lateral sclerosis
AMP	Adenosine monophosphate
AMPA	A-amino-3-hydroxy-5-methyl-4-isoxazoleproprionic acid
ATP	Adenosine triphosphate
AUC	Area under the curve
BCL	B-Cell leukaemia
BMI	body mass index
C. albicans	*Candida albicans*
C. elegans	*Caenorhabditis elegans*
C9orf72	Chromosome 9 open reading frame 72
CaBPs	Calcium buffering proteins
cAMP	Cyclic adenosine monophosphate
CAT	Catalases
CCS1	Copper chaperone for Sod1
cDCs	Conventional dendritic cells
CDRE	Calcineurin-dependant response element
CFU	Colony forming units
Cn	Calcineurin
CNS	Central nervous system

Coel	Coelenterazine
CREBP	cAMP-response element binding protein
CRISPR	Clustered regularly interspaced short palindromic repeats
Cu	Copper
CV	Crystal violet
dH_2O	Distilled water
DNA	Deoxyribonucleic acid
DPRs	Dipeptide repeat proteins
ECL	Enhanced Chemiluminescence
EDTA	Ethylenediaminetetraacetic acid
ER	Endoplasmic reticulum
ETC	Electron transport chain
fALS	Familial ALS
FBS	Foetal bovine serum
FDA	Food and Drug administration
FFARs	Free fatty acid receptors
FK506	Tacrolimus
FKBP	FK-binding protein
FLIM/FRET	Fluorescence lifetime microscopy/ Förster's resonance energy transfer
FTLD	Frontotemporal dementia
FUS1	Fused in sarcoma
GAPDH	Glyceraldehyde phosphate dehydrogenase

GFP	Green fluorescent protein
GPCRs	G-protein-coupled receptors
GPX	Glutathione peroxidases
H_2O_2	Hydrogen peroxide
HATs	Histone acetyl transferases
HDAC	Histone deacetylase
His	Histidine
hnRNP	Heterogeneous nuclear ribonucleoprotein
IMM	Inner mitochondrial membrane
IMS	Mitochondrial intermembrane space
MAPK	Mitogen-activated protein-kinase
MBR	Metal-binding region
MFI	Mean fluorescence intensity
mRNA	Messenger RiboNucleic Acid
mTOR	Mammalian Target of Rapamycin
mTORC1	Mammalian target of rapamycin complex 1
NaB	Sodium Butyrate
NADH	Nicotinamide adenine dinucleotide hydrogen
NADPH	Nicotinamide adenine dinucleotide phosphate
NGM	Nematode growth medium
NMJ	Neuromuscular junction
NO•	Nitric oxide
$O_2•^-$	Superoxide

OH•	Hydroxyl radicals
OMM	Outer mitochondrial membrane
$ONOO^-$	Peroxynitrite
OXPHOS	Oxidative phosphorylation
PAS	Phagosome assembly site
PBS	Phosphate-buffered-saline
PBS/T	Phosphate Buffered Saline and Tween
PKA	Protein kinase A
PRX	Peroxiredoxins
PT	Permeability transition pore
RNA	Ribonucleic acid
RNAi	RNA interference
ROS	Reactive oxygen species
S. cerevisiae	*Saccharomyces cerevisiae*
sALS	Sporadic ALS
SCFAs	Short-chain fatty acids
Sod1	Superoxide dismutase 1
TARDBP	TAR DNA binding protein
TCA	Tricarboxylic Acid cycle/Krebs cycle
TDP-43	TAR DNA-binding protein 43
TF	Transcription factor
TSA	Trichostatin A
V-ATPase	Vacuolar-ATPase

VDAC	Voltage dependent ion channel
VPA	Valproic acid
WT	Wild type
WTL	Wild type like
YFP	Yellow fluorescence protein
Zn	Zinc

IIII Contents

Table of Contents

I Declaration ..... *II*

II Acknowledgments ..... *III*

III Abbreviations ..... *IV*

IIII Contents ..... *IX*

V Abstract ..... *XVI*

1. Introduction *1*

1.1 Amyotrophic Lateral Sclerosis (ALS) **1**

1.1.1 Clinical Phenotypes and Diagnosis **1**

1.2 *SOD1*-associated ALS **4**

1.2.1 Sod1p and Ccs1p Interaction in *S. cerevisiae* **8**

1.2.2 Mutations in *SOD-1* associated with fALS and its aggregation **9**

1.3 Current Model of ALS-linked pathology **11**

1.3.1 Mitochondrial dysfunction **11**

1.3.2 Lysosome and autophagy dysfunction in ALS **15**

1.3.3 Calcium regulation in ALS **17**

1.4 Calcineurin and ALS **22**

Calcium regulation and Calcineurin function in *S. cerevisiae* **25**

Labile Zinc accumulation due to disturbed Calcineurin-Sod1 interaction **30**

1.10 The Gut Microbiome **31**

1.12 Gut Microbiome and neurodegenerative diseases **32**

1.12.1 Amyotrophic Lateral Sclerosis and the gut microbiome **34**

1.13 The short chain fatty acid Sodium Butyrate 37

The antimicrobial properties of Butyrate 42

1.5 Models of ALS 43

1.5.1 *Saccharomyces cerevisiae* as a model organism for motor neuron diseases 43

1.5.2 SH-SY5Y human neuroblastoma cells as a model for neurodegenerative diseases 44

1.5.3 *C. elegans* and their lifecycle 45

***C. elegans* as a model organism in neurodegenerative diseases 46**

Aims 47

Chapter 2 - Butyrate can ameliorate Sod1 aggregation and restore motility in a C. elegans ALS model system 50

2.1 Introduction 50

2.2 Materials and Methods 54

2.2.1 *C. elegans* Strains and maintenance 54

2.2.1.1 Synaptic transmission assay using aldicarb 55

2.2.1.2 Thrashing assay 56

2.2.1.3 Confocal Microscopy of *C. elegans* 56

2.2.2 Tissue culture: SH-SY5Y neuroblastoma cell line 57

2.2.2.1 Maintenance of SH-SY5Y 57

2.2.2.2 Cell viability assay 58

2.2.2.3 Preparation of total cell lysates and immunoblotting 58

2.2.2.4 Transfection 60

2.2.2.7 Widefield microscopy 61

2.3 Results 62

2.3.1 The impact of Butyrate supplementation on SOD1-mediated motor defects in an ALS *C. elegans* model 62

3.3.2 Investigating the impact of the SCFA Butyrate and Histone deacetylase inhibitor (HDAC inhibitors) supplementation on SOD1-mediated neuromuscular junction (NMJ) dysfunction 65

2.3.3 The Effect of NaB and TSA exposure on h:Sod1 and h:Sod1G85R aggregation in C. *elegans*..... 69

2.3.4 The Effect of NaB and histone deacetylase inhibitor VPA on mutated Sod1 aggregation in the neuroblastoma cell line SH-SY5Y 72

2.4 Discussion 78

2.4.1 Supplementation of butyrate and the HDAC inhibitor TSA can improve Sod1-mediated motor defects and Sod1-mediated neuromuscular junction dysfunction in *C. elegans*..... 78

2.4.2 Addition of Butyrate and HDAC inhibitors TSA and VPA can clear Sod1^{mut} aggregations in *C. elegans* and the neuroblastoma cell line SH-SY5Y 83

Chapter 3 – An analysis of the antifungal effects of Butyrate on C. albicans reveals pH dependent modes of action – implications for ALS linked dysbiosis 85

3.1 Introduction 85

3.1.1 Gut dysbiosis in ALS patients 86

3.1.2 Importance of HDAC and TF regulation for hyphae formation in *C. albicans* 89

3.2 Materials and Methods 92

3.2.1 Media preparation and growth conditions for *Candida albicans*..... 92

3.2.2 Preparation of total cell lysates and immunoblotting..... 94

3.2.3 *C. albicans* chemical transformation 95

3.2.4 Restriction enzyme digest of DNA 98

3.2.5 Purification of plasmids from *E. coli*..... 99

3.2.6 Agarose gel electrophoresis..... 99

3.2.7 Absorbance assays for growth rate analysis of *C. albicans* 100

3.2.8 Biofilm Growth assay 101

3.2.9 XTT assay..... 102

3.2.10 Crystal Violet assay 102

3.2.11 Hyphae Extension Measurement 103

3.2.12 Agar Invasion Assay 103

3.2.13 Metastasis Assay 104

3.2.14 Colony Forming Unit assay/Viability assay 105

3.2.15 Reactive Oxygen Species (ROS) and Necrosis Assay 105

3.2.16 Cytosolic Calcium concentration measurement using ApoAequorin luminescence 106

3.2.17 mitochondrial fragmentation using mitotracker green FM 107

3.2.18 relative GFP intensity as indicator for intracellular pH 107

3.2.19 High Resolution Respirometry 107

3.3 Results 108

3.3.1 Effect of NaB addition on *C. albicans* planktonic cells SC5314 108

3.3.2 Effect of NaB addition on *C. albicans* SC5314 biofilms 111

3.3.3 Effect of NaB addition on *C. albicans* SC5314 agar invasion 115

3.3.4 Effect of NaB addition on hyphae formation of *C. albicans* SC5314 117

3.3.5 Effect of NaB addition on histone acetylation status in planktonic *C. albicans* SC5314 cells 119

3.3.6 Effect of HDAC deletions and of NaB on SC5314 planktonic and biofilm growth .. 122

3.3.7 Effect of HDAC deletions in addition to NaB treatment on biofilm growth 126

3.3.8 Effect of HDAC deletions and of NaB on invasion 128

3.3.9 Effect of HDAC deletions and of NaB on filamentation 133

3.3.10 Effect of combining Set3C HDAC component deletion with NaB exposure on H4 acetylation dynamics 136

3.3.11 Effect of TF deletions and of NaB on SC5314 planktonic and biofilm growth 139

3.3.12 Effect of TF deletions in addition to NaB treatment on biofilm growth 142

3.3.13 Effect of pH on NaB action in SC5314 *C. albicans* 144

3.3.14 Calcium chelation or catalase overexpression prevents NaB induced cell death at pH 4 155

3.4 Discussion 158

Chapter 4 New Roles and Interactions for Sod1 and Sod1^{A4V} under conditions of stress 166

4.1 Introduction 166

4.1.1 Expression of single copy *SOD1* and mutant *sod1^{A4V}* alleles in *S. cerevisiae* 166

4.1.2 Overexpression of ALS-linked mutant isoforms of Sod1 into *S. cerevisiae* causes cytotoxicity, metabolic dysfunction, and a vacuole acidification defect 168

4.1.3 Vacuolar functions 170

4.1.4 Aims of this chapter 174

4.2 Materials and Methods 174

4.2.1 Media preparation and growth conditions for *Saccharomyces cerevisiae*, and *Escherichia coli* 174

4.2.1.1 Yeast growth media 174

4.2.1.2 Yeast extract, peptone, dextrose (YPD) growth media 174

4.2.1.3 Synthetic complete (SC) drop-out medium 175

4.2.1.4 *E. coli* growth and selection 175

4.2.2 Yeast and bacterial strains used in this project 176

4.2.2.1 *E. coli* strains 176

4.2.2.2 *S. cerevisiae* 176

4.2.3 Molecular Biology methods 176

4.2.3.1 Plasmids used in this project 176

4.2.3.2 High efficiency yeast transformation using the LiAc/SS carrier DNA/PEG method for *S. cerevisiae* 178

4.2.3.3 Quick genomic DNA extraction and PCR in *S. cerevisiae* 178

4.2.3.4 Restriction enzyme digest of DNA 179

4.2.3.5 Purification of plasmids from *E. coli* 180

4.2.3.6 Agarose gel electrophoresis 180

4.2.3.7 Transformation of *E. coli* with plasmid DNA 181

4.2.3.8 *E. coli* competent cell preparation 182

4.2.3.9 Invitrogen Gateway cloning reaction 182

4.2.3.9.1 BP cloning reaction 183

4.2.3.9.2 LR cloning reaction 184

4.2.4 Cell biology whole cell experimental procedures 184

4.2.4.1 Vacuole knockout library screen: Absorbance assays for growth rate analysis of *S. cerevisiae* cells 184

4.2.4.2 Quantification of calcineurin activity by flow cytometry 186

4.2.4.3 Cytosolic Calcium concentration measurement using ApoAequorin luminescence 187

4.2.5 Fluorescence microscopy of yeast cells 188

4.2.5.1 Sample preparation 188

4.2.5.2 Fluorescence microscopy 189

4.2.5.3 FLIM/FRET microscopy 189

4.3 Results 191

4.3.1 Interaction between Sod1 and parts of the vATPase (VMA2) using FLIM/FRET 191

4.3.2 Generation of new strains to complete the knockout library 195

4.3.3 Assessment of effects of Sod1^{A4V} expression in vacuole KO library in YPD 197

4.3.4 Assessment of effects of Sod1^{A4V} expression in vacuole KO library under 50 mM Calcium stress 200

4.3.5 Assessment of effects of Sod1^{A4V} expression in vacuole KO library under Calcineurin inhibition (FK506) 203

4.3.6 Assessment of effects of Sod1^{A4V} expression in vacuole KO library under 4 mM Zinc stress 207

4.3.7 Summary of reproducible potential synthetic interactions between Sod1^{A4V} and vacuole KO strains in YPD media and under 50 mM Calcium, calcineurin inhibition, and 4 mM Zinc stress 210

4.3.8 Sod1 and Sod1^{A4V} regulation of calcium response 212

4.3.9 Sod1^{A4V}-induced calcium toxicity is not linked to cell death in *Δras2* and *Δyvc1* .. 219

4.3.10 Sod1^{A4V} expression induces calcium flux imbalance 223

4.3.11 The loss of Sod1 interacting proteins leads to the perturbation of Cn signalling 232

4.3.12 Sod1^{A4V}-induced Crz1 mislocalisation under calcium stress 237

4.4 Discussion 247

4.4.1 Introduction 247

4.4.2 Vacuolar Function and Trafficking 249

4.4.3 Autophagy 251

4.4.4 Metabolic Signalling and Stress Response 252

4.4.5 Ionic homeostasis and Calcineurin Signalling 255

4.4.6 Summary 261

5. Final discussion 263

5.1 Consistent themes across our model systems 263

5.2 Link between metabolism, ion signalling and microbial metabolites 264

6. Implications 265

7. Limitations 268

8. Concluding remarks 269

References: 272

V Abstract

The neurodegenerative disorder Amyotrophic lateral Sclerosis (ALS) leads to a progressive loss of motor neurons controlling voluntary muscles ultimately leading to paralysis and death usually through respiratory paralysis. Recent findings suggest that metabolic defects in combination with lower abundance and diversity of the microbial profile in ALS patients play an important role in the onset and progression of ALS. Dietary compounds are metabolised by the gut microbiota yielding metabolites altering the metabolic status of the host influencing host health. In addition, research also suggests that a cell's response to metabolic changes can contribute to the toxicity associated with ALS when placed in the context of mutations in the protein Superoxide dismutase 1 (Sod1) and the regulation of calcium homeostasis, mediated by Calcineurin. Understanding these interactions may help in our understanding of familial and sporadic forms of ALS.

In this thesis we used a multi-model approach to investigate how *SOD1* mutations interrupt calcium and energy homeostasis, particularly in the absence of specific metabolites and vacuolar membrane transporters using *S. cerevisiae* as a simple ALS model. We further examined the therapeutic potential of butyrate, a short-chain fatty acid reduced in ALS patients, which has been linked to gut health, microbial diversity, and histone deacetylase (HDAC) inhibition. Using *C. elegans* and human neuroblastoma cell models, we assessed the effects of butyrate on $Sod1^{mut}$ aggregation, motor function, and neuromuscular junction integrity. In addition, we investigated the antifungal properties of butyrate against *C. albicans*, considering fungal dysbiosis as an emerging factor in ALS pathology.

Our findings show that butyrate supplementation could reduce $Sod1^{mut}$ aggregation, rescue

motor and neuromuscular defects in *C. elegans*, and decrease aggregation in human cell, thereby validating these systems as platforms for testing HDAC inhibitors. We could show that the mode of action of butyrate is pH-dependent: under acid conditions it interrupts calcium homeostasis, impairs mitochondrial function, and induces ROS accumulation, whilst simultaneously exerting anti-fungal activity against *C. albicans*. Finally, we could show that the $Sod1^{A4V}$ mutation alters calcium sensitivity and impairs calcineurin-Crz1 signalling, exacerbating neurodegenerative processes.

In summary, my work demonstrates how a single mutated protein ($Sod1^{A4V}$) can interrupt multiple, highly conserved cellular systems including vacuolar (lysosomal) function, autophagy, metabolic signalling, and calcium homeostasis, each of which are implicated in ALS. Our findings reinforce the concept of ALS as both proteopathy and an endosomal-lysosomal disorder. Importantly, by linking reduced butyrate levels and gut mycobiome dysbiosis in ALS patients to cellular dysfunction, this thesis underscores the potential role of gut-derived factors in ALS pathology.

1. Introduction

1.1 Amyotrophic Lateral Sclerosis (ALS)

1.1.1 Clinical Phenotypes and Diagnosis

The neurodegenerative disorder Amyotrophic lateral Sclerosis (ALS) leads to a progressive loss of motor neurons controlling voluntary muscles responsible for eating, speaking, walking, and breathing, ultimately leading to paralysis and death usually through respiratory paralysis within a couple of years post diagnosis (Brown and Al-Chalabi, 2017). ALS is also known as Lou Gehrig Disease and is 100% fatal leading to 30,000 deaths per year in the USA (http://www.als.org) (Olanow, 1993). There are two types of ALS which are pathologically indistinguishable from one another: familial ALS (fALS) is caused by mutations in around 40 genes, with mutations in four – C9orf72, SOD1, FUS1 and TARDBP- accounting for the majority of cases (Nijs and Van Damme, 2024). *SOD1* encodes the enzyme superoxide dismutase 1, which plays a key role in managing oxidative stress and will be explored in detail later. *C9orf72* codes for a protein believed to possess guanine nucleotide exchange factor activity and is implicated in neuronal autophagy and endosomal trafficking (Manal A Farg *et al.*, 2014). *TARDBP* produces TDP-43 (TAR DNA-binding protein 43), a protein involved in RNA metabolism (King *et al.*, 2014; Ma *et al.*, 2021), while *FUS* encodes an RNA-binding protein originally identified in sarcoma (Crozat *et al.*, 1993; Rabbitts *et al.*, 1993). Loss-of-function mutations in each of these genes contributes to ALS pathogenesis through distinct but sometimes overlapping molecular pathways (Manal A. Farg *et al.*, 2014; Nijs and Van Damme, 2024). A polymorphic hexanucleotide repeat “GGGGCC” is contained in *C9orf72* that can be expanded up to many hundreds of repeats (Manal A. Farg *et al.*, 2014).

Although the precise physiological role of *C9ORF72* has yet to be fully defined, the gene is evolutionarily conserved and expressed across multiple tissues, e.g. in the spinal cord, cerebral cortex, and cerebellum. The mechanisms by which hexanucleotide repeat expansions in *C9ORF72* contribute to ALS are also still unknown, however, several hypotheses have been proposed. These include partial loss of function due to reduced mRNA processing or splicing, resulting in lower levels of the *C9ORF72* protein (by as much as 50 %) (Fratta *et al.*, 2012) as well as toxic gain-of-function effects stemming from abnormal RNA structures or the generation of aggregation-prone dipeptide repeat proteins through non-canonical translation mechanisms (Ash *et al.*, 2013; Mori *et al.*, 2013; Manal A. Farg *et al.*, 2014). An additional proposed mechanism in mutant *C9orf72*-linked ALS involves disrupted endosomal and autophagic pathways. The expansion of hexanucleotide repeats is thought to interfere with the normal role of C9ORF72 in intracellular trafficking, particularly in relation to lysosomal function. Under nutrient-deprived conditions, C9ORF72 normally interacts with SMCR8 and relocates to lysosomal membranes, where it plays a key role in activating the mTORC1 complex. Studies have demonstrated that in the absence of C9ORF72, cells exhibit abnormalities in lysosomal morphology, suggesting that the protein is essential for maintaining lysosomal homeostasis and proper autophagy signalling (Manal A. Farg *et al.*, 2014; Amick, Roczniak-Ferguson and Ferguson, 2016).

The *FUS* gene encodes a multifunctional RNA-binding protein involved in gene regulation and the cellular response to DNA damage, in part through its interaction with histone deacetylase 1 (HDAC1). The exact disease mechanism associated with *FUS* mutations remains unknown, however, current evidence supports a dual mechanism involving both loss-of-function and toxic gain-of-function effects. For instance, ALS-associated *FUS* mutations can lead to enhanced vulnerability to DNA damage, coupled with impaired

recruitment of HDAC1, pointing to disrupted DNA repair processes as a potential pathogenic factor (W.-Y. Wang *et al.*, 2013). Furthermore, mutant FUS often mislocalises from the nucleus to the cytoplasm, forming aggregates that interfere with its normal nuclear functions (An *et al.*, 2019). Interestingly, some FUS variants implicated in fALS do not form cytoplasmic inclusions, indicating that nuclear dysfunctions may also contribute to toxicity through gain-of-function mechanisms (An *et al.*, 2019).

TARDBP encodes TDP-43, a nuclear RNA/DNA-binding protein involved in RNA metabolism and neuronal gene regulation (Tollervey *et al.*, 2011). In ALS, TDP-43 is frequently mislocalised to the cytoplasm where it forms insoluble, ubiquitinated aggregates—present in ~ 97 % of ALS and ~ 45 % of frontotemporal dementia (FTLD) cases—highlighting its central role in disease pathology. While the causative role of these aggregates remains debated, most ALS-linked mutations occur in the glycine-rich C-terminal region, increasing aggregation tendency (Johnson *et al.*, 2009). Cytoplasmic accumulation of mutant TDP-43 leads to nuclear depletion, disrupting RNA processing, and also impairs translation through aberrant interactions with ribosomal complexes (Freibaum *et al.*, 2010; Russo *et al.*, 2017).

The second type of ALS is called sporadic ALS (sALS) which does not possess any obvious genetically inherited components. However, 90 % of ALS cases are sporadic (Pansarasa *et al.*, 2018; Kim *et al.*, 2019). Symptoms most often start to develop between the ages 50 and 65 (Logroscino *et al.*, 2008), initially presenting as either weakness in the limbs (spinal onset) or a difficulty with swallowing or speaking (bulbar onset). Spinal onset is present in ~ 70 % of ALS cases and combines upper motor neuron and lower motor neuron degeneration signs in the limbs. In comparison, bulbar onset presents in ~ 25 - 30 % of ALS cases and is associated with difficulties in swallowing and speech before degeneration signs in the limbs

become visible (Corcia *et al.*, 2008). At present, treatment and therapy options for ALS remain limited, with only two drugs, Riluzole and Edaravone, having been approved by the Food and Drug Administration (FDA). These drugs have limited efficacy, prolonging life of ALS patients by only a few months (Lacomblez *et al.*, 1996).

1.2 *SOD1*-associated ALS

The highly evolutionary conserved cytosolic enzyme Sod1 is an abundant antioxidant that converts superoxide into the less reactive oxygen species hydrogen peroxide (Figure 1).

In eukaryotes, toxic reactive oxygen species (ROS) can cause damage to vital cellular components ultimately causing cell death. ROS are released into the mitochondrial matrix and mitochondrial intermembrane space (IMS) by NADH dehydrogenase enzyme and ubisemiquinone anion as a by-product of the electron transport chain (Sturtz *et al.*, 2001). Human Sod1 detoxifies superoxide ROS within the intermembrane space of the mitochondria, as well as the cytosol and peroxisome whilst Sod2 detoxifies ROS in the mitochondrial matrix (Sturtz *et al.*, 2001; Islinger *et al.*, 2009).

In addition to its well-established role in antioxidative defence, SOD1 is also an important regulator of redox signalling. The product of SOD1 activity, hydrogen peroxide (H_2O_2), can act as a secondary messenger that can modulate signalling pathways through reversible oxidation of protein cysteine residues (Winterbourn and Metodiewa, 1999; Kwon, 2003; Bienert, Schjoerring and Jahn, 2006; Banerjee *et al.*, 2007; Giorgio *et al.*, 2007; Block *et al.*, 2008; Niethammer *et al.*, 2009; Paulsen and Carroll, 2010). This redox-dependent regulation affects various cellular targets, including kinases and phosphatases, thereby influencing cell growth, metabolism, and stress responses. Recent findings highlight that SOD1 contributes

to intracellular signalling by maintaining localized H_2O_2 gradients and modulating thiol-based redox switches, further positioning it as a dynamic player in signal transduction beyond its canonical detoxification activity (Y. Wang *et al.*, 2018; Eleutherio *et al.*, 2021).

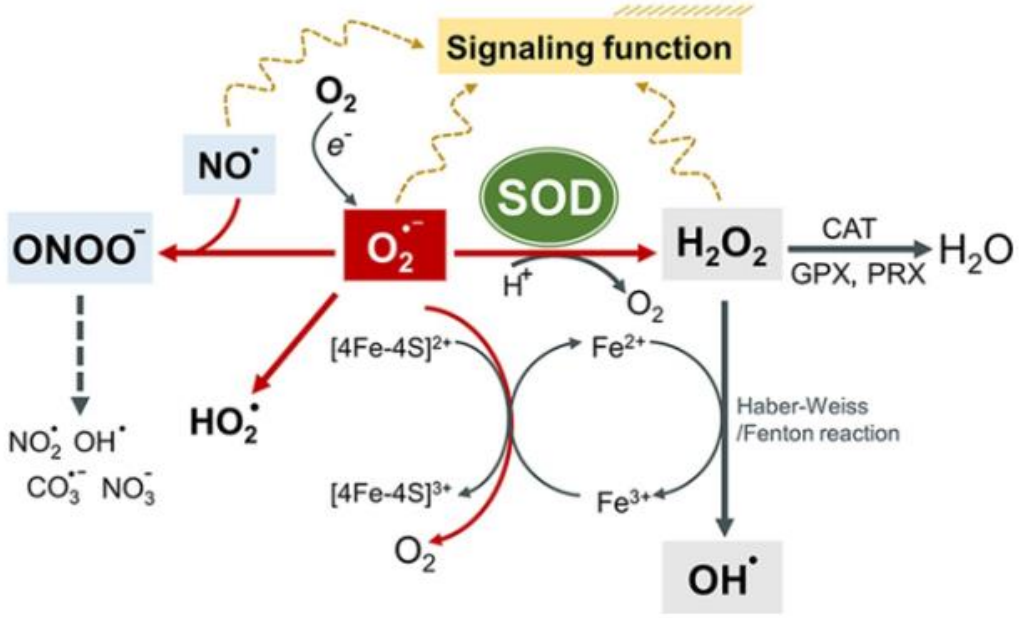


Figure 1 Reactive Oxygen species generation and detoxification pathways.
Generation of reactive oxygen species are prevented through the action of SODs which coverts superoxide ($O_2•^-$) to hydrogen peroxide (H_2O_2) which is then further broken down by catalases (CAT), glutathione peroxidases (GPXs), and peroxiredoxins (PRXs) to water. Through redox reactions with iron hydroxyl radicals (OH•) can be generated. Oxidative stress is also promoted when nitric oxide (NO•) availability is decreased through reactions of $O_2•^-$ with NO• generating peroxynitrite ($ONOO^-$) resulting in the formation of reactive intermediates like $NO_2•$, OH•, and $CO_3•^-$.
Superoxide can also reduce Fe^{3+} to Fe^{2+} in iron-sulphur clusters thus disrupting those and forming more radicals. $O_2•^-$ can also transform to the more reactive radical hydroperoxyl ($HO_2•$).
(Wang et al., 2018). Image from (Wang et al., 2018)

Each Sod1 subunit is made up of a ß-barrel core and seven loops held together by a disulphide bond, a binuclear metal binding site and a network of hydrogen bonds. Pivotal for the catalysing activity of Sod1 is the copper and zinc ions held together by the metal binding site (Banci *et al.*, 2002; Arnesano *et al.*, 2004; Estácio *et al.*, 2015; Sea *et al.*, 2015). Eukaryotic wild type Sod1 usually forms a homodimer which presents a remarkably stable quaternary structure providing Sod1 with the ability to function under denaturing

conditions and in the reducing environment of the cytosol (Arnesano *et al.*, 2004). Studies of the human Sod1 showed that this stability may be subject to both the metal occupancy and the disulphide bonds contained in Sod1, and that pathogenic misfolding may be induced when Cu/Zn cofactors and the disulphide bonds are disrupted (Hough *et al.*, 2004; Tiwari, Xu and Hayward, 2005; Nordlund *et al.*, 2009). Multiple misfolded conformations and different structural variants have been associated with fALS (Prudencio and Borchelt, 2011).

Human and yeast Sod1 proteins are not only similar in structure, but also in their maturation process. While the human Sod1p comprises 154 amino acids and requires two cysteine residues for protein stability, yeast Sod1p consists of 153 amino acids and requires two proline residues in order to bind to Ccs1p – a copper chaperone. There is another SOD enzyme expressed in both yeast and humans, called Sod2p which resides in the mitochondria and has a manganese ion in its active site. However, mammals also express a third SOD1 enzyme, Sod3p which is not expressed in yeast. The extracellular Sod1p has four subunits and contains copper and zinc ions (Askwith and Kaplan, 1998) (Figure 2 A, B).

A

```
Human_SOD1      MATKAVCVLKGDGPVQGIINFEQKESNGPVKVWGSIKG-LTEGLHGFHVHEFGDNTAGCT    59
Yeast_SOD1      -MVQAVAVLKGDAGVSGVVKFEQASESEPTTVSYEIAGNSPNAERGFHIHEFGDATNGCV    59
                  .:**.*****. *.*:::*** ... *..*  .* *   :. :***:***** * **.

Human_SOD1      SAGPHFNPLSRKHGGPKDEERHVGDLGNVTADKDGVADVSIEDSVISLSGDHCIIGRTLV    119
Yeast_SOD1      SAGPHFNPFKKTHGAPTDEVRHVGDMGNVKTDENGVAKGSFKDSLIKLIGPTSVVGRSVV    119
                ********:.:.**.*.** *****:***.:*::***. *::**:*.* *  .::**::*

Human_SOD1      VHEKADDLGKGGNEESTKTGNAGSRLACGVIGIAQ     154
Yeast_SOD1      IHAGQDDLGKGDTEESLKTGNAGPRPACGVIGLTN     154
                :*   ******..*** ****** * ******:::
```

B

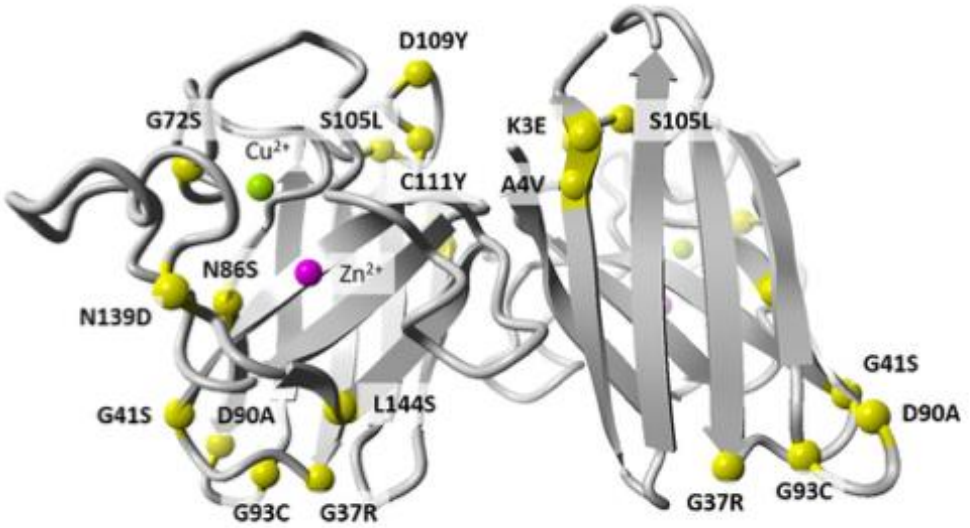


Figure 2 ***Sequence alignment and structure of human and yeast Cu/Zn superoxide dismutase (SOD1).*** *(A) Sequence alignment of human and Saccharomyces cerevisiae SOD1. Protein sequences were obtained from UniProt (human SOD1, P00441; S. cerevisiae SOD1, P00445) and aligned using Clustal Omega. Blue highlights Cu-binding residues, green highlights Zn-binding residues, and yellow highlights Cys58 and Cys147, which form the conserved intramolecular disulfide bond. (B) Structure of the SOD1 homodimer, with familial amyotrophic lateral sclerosis (fALS)-associated mutations highlighted in yellow. The positions of the copper (Cu) and zinc (Zn) ions are indicated. Panel B adapted from (Berdyński et al., 2022)*

1.2.1 Sod1p and Ccs1p Interaction in *S. cerevisiae*

Maturation of Sod1p, its proper folding, and thus Sod1p's correct function is mediated by the copper chaperone Ccs1p (Sturtz *et al.*, 2001). Ccs1p is made up of three domains: a copper-binding motif required for copper binding in copper-scarce cellular conditions (Puig and Thiele, 2002), the main Sod1p interaction domain which has a strong homology to the overall structure of Sod1p (Bleackley and MacGillivray, 2011), and the third domain which contains a CxC motif allowing the transfer of the copper ion to Sod1p.

In *S. cerevisiae*, Ccs1p-Cu specifically binds to immature Sod1p to donate its copper ion into Sod1p's active site (Furukawa, Torres and O'Halloran, 2004). During this interaction, Sod1p also gets oxidised to generate an intra-molecular disulphide bond within Sod1p. The incorporation of copper is eventually further stabilised by binding of zinc to Sod1p (Bleackley and MacGillivray, 2011). Disruption or misfunction of Sod1p and Ccs1p interaction leads to incorrect formation of disulphide bonds resulting in misfolded proteins being susceptible to aggregation. It can also prevent completing the maturation process of Sod1p as Ccs1p may no longer activate Sod1p, thus allowing aggregation of immature Sod1p which are more prone to oxidative damage (Sturtz *et al.*, 2001).

In general, yeast Sod1p requires the aid of Ccs1p in order to be properly activated, whereas human Sod1p may be activated through other mechanisms (Bastow, Gourlay and Tuite, 2011). Regulation of SOD1 activation might be performed by glutathionylation in yeast and humans alike (Mannarino *et al.*, 2011; Brasil *et al.*, 2013).

1.2.2 Mutations in *SOD-1* associated with fALS and its aggregation

SOD1 was the first gene to be linked to ALS (Rosen *et al.*, 1993). Since its first discovery, more than 217 mutations causing ALS have been identified. These mutations can be found in all five axons of the genes and comprise point mutations, truncations, deletions and substitutions. The ALS online database (ALSod: https://alsod.ac.uk/) provide a list of all ALS-linked *SOD1* variants discovered so far. The most common fALS-linked mutations in *SOD1* are D90A, A4V and G93A whereby the A4V mutation is the most frequently found in the US and the D90A around the world (Gurney *et al.*, 1994).

fALS-linked mutations are classified into two main forms: metal-binding region mutants (MBR) and WT-like (WTL) mutants. MBR mutants e.g. H48R, H48Q, G85R, D124V, S134N and C146R show impaired metal binding and a diminished superoxide activity of the enzyme and impair the full formation of the mature holo-Sod1 increasing the propensity of Sod1 aggregation (Wang *et al.*, 2003; Rodriguez *et al.*, 2005). On the other hand, WTL mutants have similar metal binding affinities and structures to that of the WT Sod1 and include mutations like A4V, G37R, D90A, G93A and N139K.

The mutation of Sod1 appears to lead to changes in stability that lead to its aggregation (Kato *et al.*, 2000; DiDonato *et al.*, 2003; Stathopulos *et al.*, 2003). In its misfolded state, SOD1 exposes hydrophobic regions that are normally buried within its stable structure, leading to self-association into soluble oligomers and, eventually, larger insoluble aggregates. These aggregates may be disordered or take on the more ordered structure of amyloid fibrils, depending on the conformation of the misfolded monomers. In some cases, aggregation follows a seeding mechanism, where small fibrils accelerate the accumulation of additional SOD1 species (Tsekrekou *et al.*, 2024). This aggregation process is cytotoxic and contributes to multiple pathogenic mechanisms in ALS, including the loss of antioxidant

protection, increased oxidative stress, excitotoxicity, disrupted axonal transport, mitochondrial dysfunction, and neuroinflammation (Ferraiuolo *et al.*, 2011; Saccon *et al.*, 2013).

Sod1 aggregation was seen in spinal cord and brain samples from ALS-patients spreading from cell to cell in a prion-like manner (Münch, O'Brien and Bertolotti, 2011). In studies using *SOD1*-ALS mouse models which overexpress WT Sod1 it was found that overexpression of WT Sod1 inhibited protein aggregation formation of mutant Sod1 isoforms. Interestingly, inhibition of protein aggregation accelerated progression of the disease. This suggests that soluble misfolded Sod1 mutants are the toxic agent (J. Wang *et al.*, 2009).

Moreover, it was also observed that WT Sod1 can become oxidised, giving it a conformational epitope similar to those found in Sod1 mutants and not the unoxidized WT Sod1 protein (Bosco *et al.*, 2010). Generally, WTL mutations decrease the ability of apo-Sod1 monomers to form dimers and increase the rate of unfolding at physiological temperature (Broom *et al.*, 2015).

A4V is among the most frequently observed mutation in North America. Patients carrying this variant typically face a very rapid disease trajectory, often with survival averaging just over a year post-symptom onset. This severe phenotype is thought to result from extreme instability and aggregation-prone behaviour of the mutant SOD1 protein (Matamala and Kiernan, 2017; Huang *et al.*, 2024).

The G37R mutation is linked to a more moderate disease course compared to A4V (Berdyński *et al.*, 2022). While it still leads to ALS, the progression is comparatively slower than that observed with the A4V mutation. The G37R variant exhibits a higher stability,

resulting in a reduced tendency to form toxic aggregates, which may account for the less aggressive disease phenotype (Prudencio *et al.*, 2009).

D90A is the most prevalent SOD1 mutation in Europe and can be inherited dominantly or recessively (Parton *et al.*, 2002; Andersen, 2006). Homozygote D90A-associated ALS tends to have a slower progression, with patients often surviving for extended periods post-diagnosis (Broom *et al.*, 2006; Luigetti *et al.*, 2009).

The G93A mutation is the most studied SOD1 mutation in rodents. The amino acid change leads to misfolded and aggregated proteins resulting in toxicity to motor neurons (Synofzik *et al.*, 2010; Kreilaus *et al.*, 2020).

N139K is rare and less characterized but has been associated with a milder disease presentation. Individuals with this mutation often show slower progression, suggesting that this variant might impair SOD1 function without inducing rapid cellular damage (Prudencio *et al.*, 2009; Berdyński *et al.*, 2022).

1.3 Current Model of ALS-linked pathology

With the help of multiple animal models studying mutations linked to ALS multiple interconnected mechanisms of toxicity linked to mutant isoforms of Sod1, *C9ORF72 and TARDP* have been proposed and include mitochondrial dysfunction, protein aggregation and misfolding, and metabolic dysfunction.

1.3.1 Mitochondrial dysfunction

Mitochondria are essential organelles found in nearly all eukaryotic cells, responsible for managing crucial cellular processes such as energy generation, calcium buffering, and the

regulation of cell death. Structurally complex, they respond dynamically to changing energy demands, for example by increasing their size or number in response to stimuli like physical activity or hormonal signals. Through processes known as fusion and fission, mitochondria continuously remodel themselves to maintain efficiency and adapt to cellular needs (Valero, 2014; Magner *et al.*, 2015; Bravo-Sagua *et al.*, 2017). Their key role lies in oxidative phosphorylation (OXPHOS), a process that produces the cell's main energy source, ATP, primarily for energy-intensive organs like the brain and heart (Kausar, Wang and Cui, 2018). However, as a byproduct of this process, mitochondria also generate reactive oxygen species (ROS). While ROS play signalling roles at low levels, excessive production can lead to oxidative stress, a known contributor to neurodegenerative diseases including ALS. Within the inner mitochondrial membrane, a series of enzyme complexes facilitates electron transport and proton pumping to generate the electrochemical gradient required for ATP synthesis. Disruptions in these complexes impair mitochondrial function and energy metabolism, with long-term consequences including neuronal damage (Kausar, Wang and Cui, 2018). Furthermore, mitochondria regulate intracellular calcium levels in close interplay with other organelles, such as the endoplasmic reticulum. This tight regulation is critical for both mitochondrial performance and cellular homeostasis, highlighting mitochondria's central role in health and disease (Rizzuto, Duchen and Pozzan, 2004; Zhao *et al.*, 2022). In addition, mitochondria are also associated with apoptosis through the control of membrane permeability via actions of outer-membrane Bcl2 family proteins such as Bcl2, Bax/Bak and the voltage dependent ion channel, VDAC (Shimizu *et al.*, 1999). Studies have shown that misfolded ALS-linked Sod1 mutants may associate with the outer mitochondrial membrane at the cytoplasmic face (Vande Velde *et al.*, 2008), and can interact with Bcl2 in spinal cord mitochondria inducing a conformational change that exposes the toxic BH3 (Bcl2 homology)

domain (Pedrini *et al.*, 2010). As mentioned, above, the key roles of mitochondria include energy metabolism and calcium regulation. Disruption of these may contribute to neuronal damage (Kausar, Wang and Cui, 2018; Zhao *et al.*, 2022). An overview of the key mitochondrial functions and the potential consequence of their disruption is shown in Figure 3.

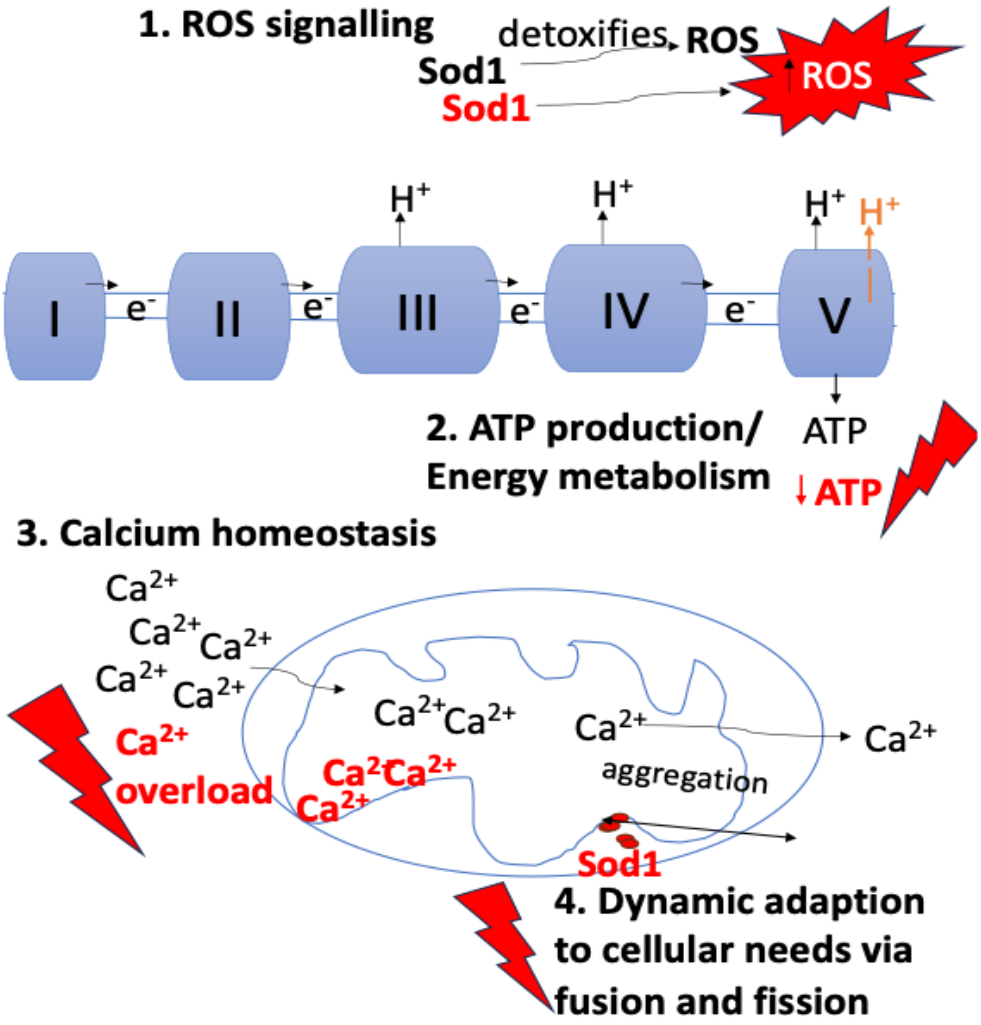


Figure 3 Mitochondrial functions and their potential contribution to disease. *Mitochondria are multifunctional organelles that contribute to cellular homeostasis through several interconnected processes. These include (1) reactive oxygen species (ROS) signalling and detoxification, (2) ATP production through oxidative phosphorylation and the electron transport chain, (3) regulation of calcium (Ca^{2+}) homeostasis, and dynamic adaptation to cellular demands through mitochondrial fusion and fission (4). Disruption of these mitochondrial functions can result in altered ROS signalling and accumulation, impaired ATP production, disturbed mitochondrial dynamics and Ca^{2+} overload. Red indicates dysfunction, red SOD1 indicates dysfunctional SOD1, and ↓ indicates decrease.*

As touched on above and in Figure 3, mutations in *SOD1* result in toxic gain- or loss-of-function effects that can disturb cellular homeostasis including mitochondrial function (Brown and Al-Chalabi, 2017). Sod1 aggregates may localise to the outer mitochondrial membrane in motor neurons (Rakhit *et al.*, 2002; Higgins, Jung and Xu, 2003) and interfere with mitochondrial respiration, increase ROS production, reduce membrane permeability, and promote cytochrome c release, leading to mitochondrial damage (Pickles *et al.*, 2013). Mutant SOD1 can also bind to the voltage-dependent anion channel (VDAC) on the outer mitochondrial membrane (OMM), impairing adenine nucleotide exchange and further disrupting energy supply and redox balance (Israelson *et al.*, 2010).

The *C9ORF72* gene encodes a protein which is primarily expressed in neurons (Renton *et al.*, 2011). Mitochondrial dysfunction associated with *C9ORF72* mutations includes increased oxygen consumption, mitochondrial hyperpolarization, elevated ROS production, and increased ATP levels in mutant fibroblasts (Onesto *et al.*, 2016). Arginine-rich dipeptide repeat proteins (DPRs), especially poly(GR), could be imported into mitochondria, causing aggregation and interference with mitochondrial function (Lopez-Gonzalez *et al.*, 2016; Li *et al.*, 2020). Poly(GR) may alter mitochondrial membrane potential, dysregulate mitochondrial dynamics via changed DRP1 and OPA1 levels, and impair oxidative phosphorylation by degrading ATP synthase subunit ATP5A1 (Choi *et al.*, 2019). Moreover, defects in complexes I and IV of the respiratory chain and elevated ROS were observed in *C9ORF72* mutant models (Dafinca *et al.*, 2016).

The mislocalisation and aggregation of the RNA-binding protein TDP-43 were associated with mitochondrial abnormalities and oxidative stress in ALS. Animal studies showed that overexpression of TDP-43 led to neurodegeneration with abnormal mitochondrial

distribution in motor neurons, including mitochondrial accumulation in cytoplasmic inclusions and loss from axon terminals (Shan *et al.*, 2010; Xu *et al.*, 2010; Magrané *et al.*, 2014). It was also shown that TDP-43 ALS mutants could localize to mitochondria affecting mitochondrial morphology and reducing mitochondrial density and length through interactions with mitophagy and fusion-related proteins such as prohibitin 2 and MFN2 (W. Wang *et al.*, 2013; Davis *et al.*, 2018).

1.3.2 Lysosome and autophagy dysfunction in ALS

Lysosomes are also pivotal in protein sorting and degradation, ion storage, autophagy, and stress responses in the cell. Lysosomal defects are associated with neurodegenerative diseases involving protein misfolding, like Alzheimer's disease (Lee *et al.*, 2010; Coffey *et al.*, 2014; X. Guo *et al.*, 2017), Parkinson's disease (Perrett, Alexopoulou and Tofaris, 2015; Moors *et al.*, 2017; Rahman and Rhim, 2017), Huntington's disease (Pircs *et al.*, 2018; Chen *et al.*, 2023), and ALS (Chen *et al.*, 2012; Han *et al.*, 2015; Xia *et al.*, 2016; Koh *et al.*, 2019). Proteostasis is crucial for neuronal health and preventing neurodegenerative diseases. One of the key cellular mechanisms maintaining proteostasis is autophagy. Autophagy is a conserved process responsible for the degradation and recycling of cellular components under stress or during development (Klionsky, 2008). There are several forms of autophagy: macroautophagy, microautophagy, and chaperone-mediated autophagy. Additionally, there are also organelle-specific pathways such as mitophagy (mitochondria), granulophagy (RNP granules), and others ensuring selective degradation of damaged or excess cell components (Chua *et al.*, 2022).

The most studied type is macroautophagy, which involves the formation of double-membraned vesicles called autophagosomes that enclose cytoplasmic contents (Parzych and Klionsky, 2014). This process begins at the phagophore assembly site, regulated by key protein complexes including ULK kinases, ATG13, and FIP200 (Ganley *et al.*, 2009; Jung *et al.*, 2009; Yang and Klionsky, 2009; Itakura and Mizushima, 2010; Chen and Klionsky, 2011). Upon nutrient depletion or pharmacological inhibition of mTOR, autophagy is initiated, and membrane nucleation begins with a PI3K complex including BECN1 and PIK3C3 (Itakura *et al.*, 2008; Hosokawa *et al.*, 2009; Jung *et al.*, 2009). The membrane then expands with the help of the ATG12–ATG5–ATG16L1 complex (Geng and Klionsky, 2008; Weidberg, Shvets and Elazar, 2011). Once formed, autophagosomes fuse with lysosomes to create autolysosomes, where the internalized material is degraded by lysosomal enzymes (Yorimitsu and Klionsky, 2005; Mizushima and Komatsu, 2011; Lamb, Yoshimori and Tooze, 2013). In microautophagy, cargo is taken up directly into lysosomes via its membrane, forming intraluminal vesicles that are later degraded (Li, Li and Bao, 2012).

Studies have shown that survival of motor-neurons could strongly be decreased when autophagy is impaired, however, deletion of *ATG7*, which is crucial in inducing autophagy did not cause ALS-related TDP-43 toxicity in mice (Fulceri *et al.*, 2011; Tashiro *et al.*, 2012a). The effects of compounds promoting autophagy on survival in various *SOD1*-ALS models have been investigated in multiple studies receiving mixed results: the autophagic inducer trehalose acts independently of mTORC1 signalling improved motor-neuron diseases in ALS mouse models (X. Zhang *et al.*, 2014). Lithium, which also stimulates autophagy independently of mTORC1 signalling, also slowed the progression of ALS in humans and provided protection against motor-neuron diseases in ALS-mouse models (Fornai *et al.*,

2008). Studies using the mTORC1-dependent activator of autophagy, rapamycin, found that motor-neuron loss was increased and reduced survival of $Sod1^{G93A}$ mouse models was shown. On the other hand, survival in immunodeficient ALS mouse models was increased (Zhang *et al.*, 2011; Staats *et al.*, 2013). In mammals, autophagy could also be regulated through lysosomal calcium signalling activating calcineurin which could then dephosphorylate TFEB which in turn upregulates autophagy (Medina *et al.*, 2015; Tong and Song, 2015).

In *S. cerevisiae*, the vacuole shares many functional similarities to the mammalian lysosome. Interestingly, a link has been found between overexpression of ALS-linked Sod1 and vacuole dysfunction in *S. cerevisiae*, such as defects in vacuole acidification and a decrease in autophagy (Bastow *et al.*, 2016). Constitutive functions of the yeast vacuole include degradation, storage, buffering, and detoxification. Together with proteasomes, vacuoles represent one of the two main degradation systems within the yeast cell where hydrolytic enzymes break down a wide range of proteins (Zubenko, Park and Jones, 1983; Knop *et al.*, 1993; van den Hazel, Kielland-Brandt and Winther, 1996). A more detailed introduction to the functions of the vacuole in yeast will be given later in chapter 5.

1.3.3 Calcium regulation in ALS

Another causative factor of ALS to be considered is calcium dysregulation. A prominent feature of motor neurons compared to other cells is their vulnerability to calcium overload. This vulnerability is due to the high expression of calcium permeable AMPA receptors (Williams *et al.*, 1997; Shaw and Eggett, 2000; Van Den Bosch *et al.*, 2000; Guatteo *et al.*, 2007). In contrast, the endogenous expression of calcium buffering proteins (CaBPs), e.g.

parvalbumin and calbindin, is low (Alexianu *et al.*, 1994; Palecek, Lips and Keller, 1999; Jaiswal, 2013). However, EF-hand calcium binding proteins are still present in motor neurons (Migheli *et al.*, 1999; M.-D. Zhang *et al.*, 2014).

Several studies could detect intracellular calcium overload and a further decrease in calretinin and parvalbumin in motor neuron axons in ALS patients (Siklós *et al.*, 1996, 1998; Kruman *et al.*, 1999; Grosskreutz, Van Den Bosch and Keller, 2010; Kawamata and Manfredi, 2010; Hayashi, Amari and Okamoto, 2013).

Another pathological pathway in ALS causing calcium overload is that mutated SOD1 was found to accumulate in the mitochondrial intermembrane space which impairs normal mitochondrial function. This is interesting as mitochondria are supposedly crucial in buffering calcium in motor neurons (Jaarsma *et al.*, 2001; Liu *et al.*, 2004; Jaiswal and Keller, 2009; Lautenschläger *et al.*, 2013). Thus, SOD1 mutations can lead to disturbances in calcium homeostasis.

In this context, it was also shown that calcium can bind to immature SOD1 increasing its accumulation (Leal *et al.*, 2013; Estácio *et al.*, 2015). In agreement, overexpression of CaBPs and AMPA channel antagonists could decrease calcium overload, neurodegeneration, and abnormal SOD1 accumulation in ALS1 models (Van Damme *et al.*, 2003; Tateno *et al.*, 2004; Tortarolo *et al.*, 2006; Yin, Tang and Weiss, 2007; Beers *et al.*, 2008; Parone *et al.*, 2013).

Figure 4 depicts calcium signalling in motor neurons and highlights key consequences of calcium overload.

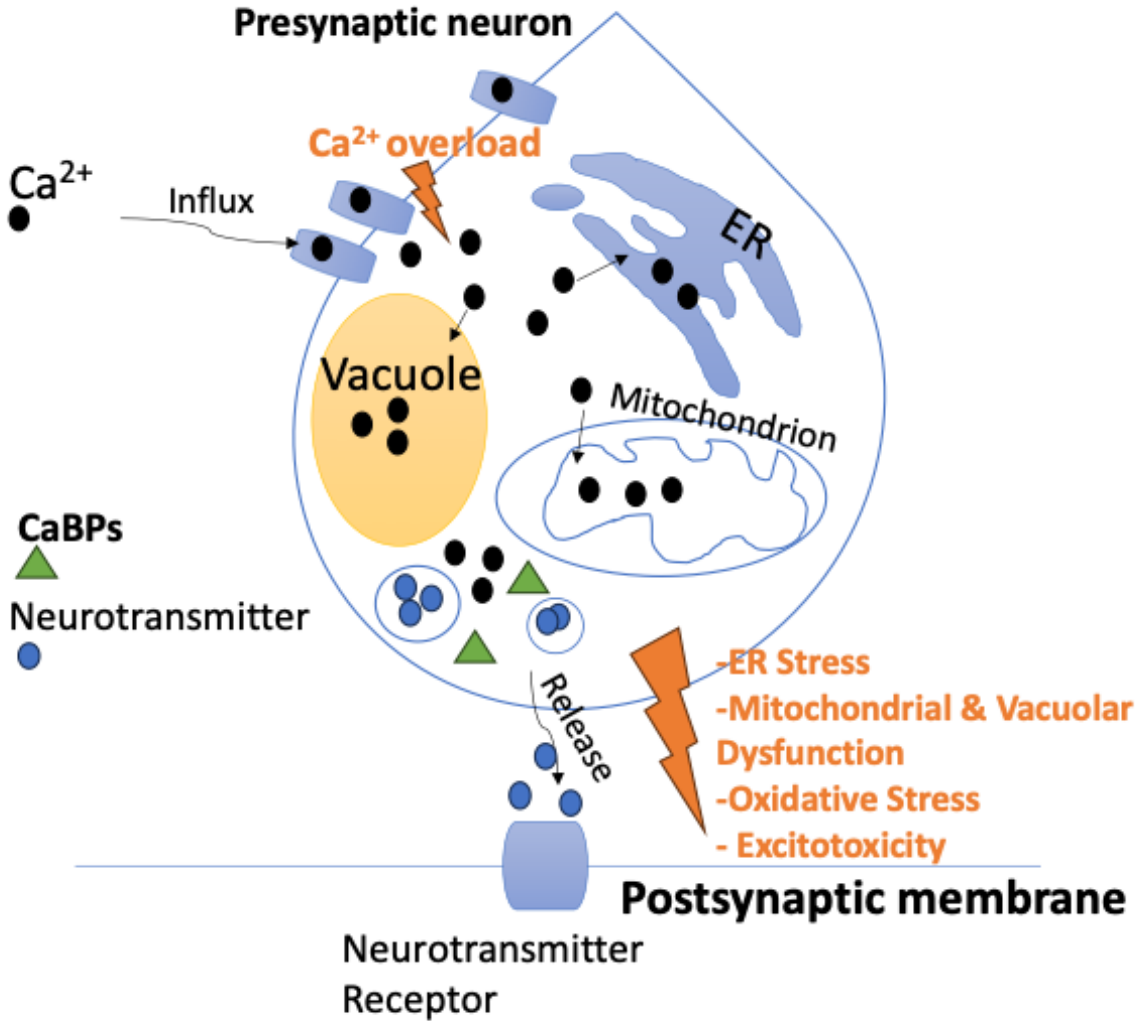


Figure 4 Calcium signalling in motor neurons. Influx of calcium into the motor neuron causes release of neurotransmitters e.g. Acetylcholine into the synaptic cleft where it binds to receptors leading to muscle contraction. Calcium buffering proteins (CaBPs) regulate free intracellular calcium levels through binding to calcium ions controlling timing and intensity of calcium signals. Low CaBPs expression and prolonged increased intracellular calcium impairs mitochondrial, vacuolar and ER function resulting in excitotoxicity, and muscle atrophy. Oxidative stress is also triggered by excessive intracellular calcium levels.

Calcineurin (Cn), or protein phosphatase 2B, is a heterodimeric Ser/Thr protein phosphatase involved in a wide range of cellular signalling pathways and is a major component in calcium signalling. The highly evolutionary conserved complex consists of a catalytic A and a

regulatory B subunit, 58-64 kDa and 19 kDa, respectively. The protein phosphatase activity of Cn is dependent on both the binding of one calcium ion to the regulatory B subunit and the binding of one calmodulin molecule causing a confirmatory change thus activating the complex. The Cn complex remains in an autoinhibitory confirmation where the A and B subunits are bound to each other in the absence of calcium or calmodulin (Kissinger *et al.*, 1995). Being highly expressed in the central nervous system (CNS) and playing a major part in many pathways involving modulation of immune responses and signal transduction in the nervous system through regulating neuronal excitability, the release of neurotransmitters and hormones, gene transcription and calcium-dependent apoptosis, Cn activity is thought to be pivotal in motor neuron diseases (Morioka *et al.*, 1999; Wang *et al.*, 1999; Rusnak and Mertz, 2000).

Loss of calcium homeostasis may also play a role in mitochondrial dysfunction as it is a key regulator of mitochondrial function such as ATP synthesis (McCormack and Denton, 1993; Hansford and Zorov, 1998; Balaban, 2002), and *vice versa* maintaining calcium homeostasis is a central role of mitochondria (Gunter et al., 2000, 2004). In higher eukaryotes, calcium entry across the double membrane and into the mitochondrial matrix is highly regulated through outer membrane voltage-gated anion channels (VDAC) (Gincel, Zaid and Shoshan-Barmatz, 2001) and mitochondrial Ca^{2+} uniporters (MCU) (Mishra et al., 2017). The membrane potential is also crucial in calcium influx and efflux by using the large negative membrane potential and the Na^{+} gradients to drive calcium efflux via NCLX. This can also be reversed if the membrane potential dissipated (Carafoli, 1974). The mitochondrial membrane potential is therefore consumed by both calcium influx and efflux and both rely on the maintenance of the H^{+} gradient through the respiratory chain (Carafoli, 1974; Brookes et al., 2004). Under elevated calcium conditions the entire respiratory chain is

upregulated resulting in enhanced respiration and ATP output (McCormack, Halestrap and Denton, 1990; Kavanagh, Ainscow and Brand, 2000; Territo et al., 2000). The permeability transition pore (PT) comprises another mechanism through which calcium exits the mitochondria (Bernardi and Petronilli, 1996): high calcium levels in the mitochondrial matrix can activate the PT and acidic pH can inhibit it (Gogvadze et al., 2001; Halestrap and Brenner, 2003). PT, however, also has a role in cell death as the apoptosis inducing molecule cytochrome c is released upon its opening albeit the precise mechanism how cytochrome c is released is not known and it is not always calcium-dependent (Loeffler and Kroemer, 2000; Gogvadze et al., 2001). Furthermore, components of the PT may interact with cell-death-regulating Bcl proteins (Narita et al., 1998; Shimizu et al., 1999; Tsujimoto and Shimizu, 2000). Cell death is also marked by loss of membrane potential thus recruiting Bcl proteins to the mitochondrion (De Giorgi et al., 2002). Another player in calcium homeostasis is the endoplasmic reticulum (ER). Being a major intracellular calcium store, its calcium release is highly regulated to ensure cellular signalling (Panda et al., 2021) and studies have shown that mitochondria locate specifically to calcium releasing sites of the ER (Mannella et al., 1998). During calcium imbalance the stress response via the ER releases more calcium which may promote mitochondria fragmentation and apoptosis (Hom et al., 2010). Studies have also shown that cytochrome c interacts with the ER's primary calcium release channel IP_3R magnifying ER calcium release (Boehning et al., 2003; Boehning, Patterson and Snyder, 2004).

1.4 Calcineurin and ALS

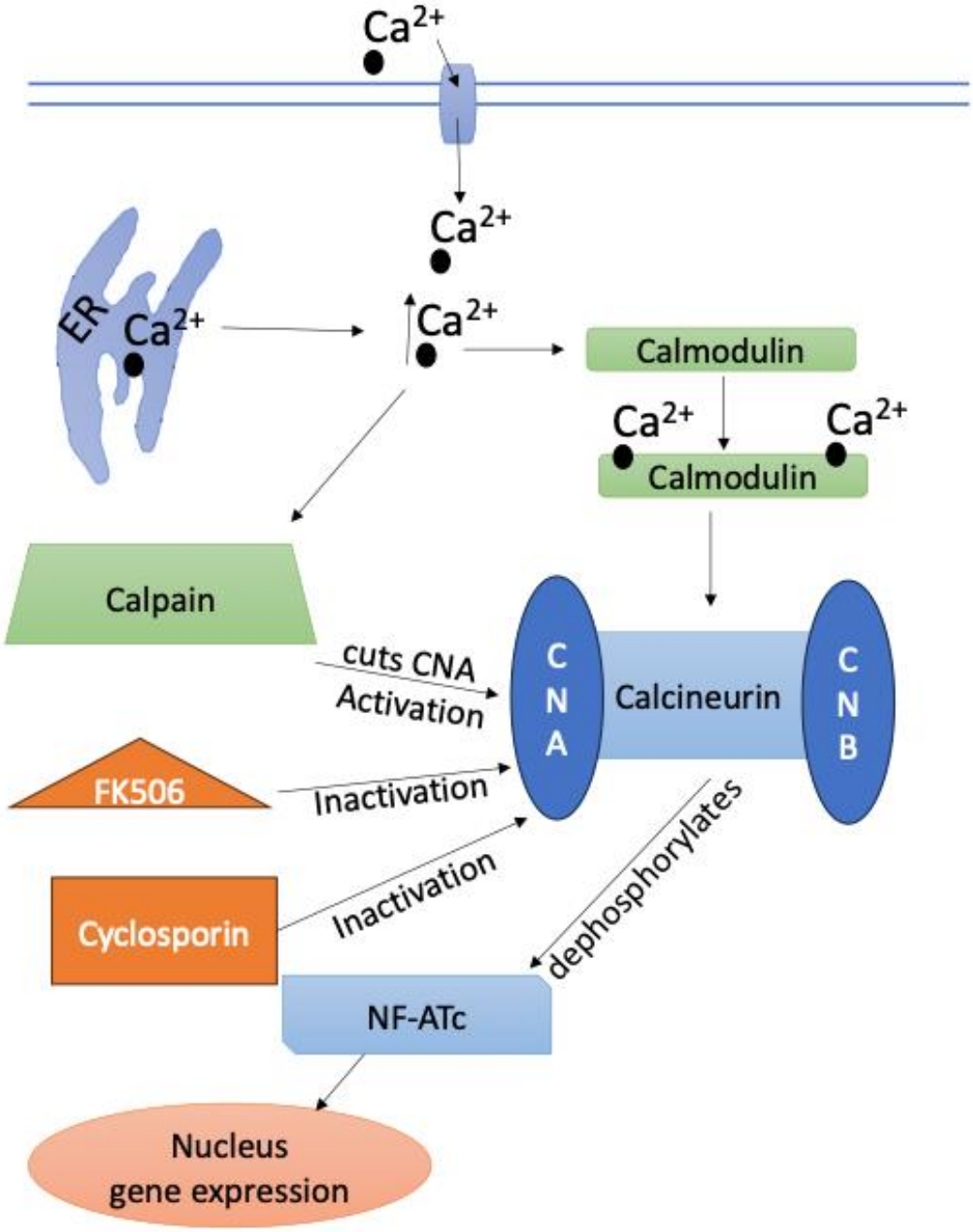


Figure 5 Schematic of the activation of the calcineurin complex and its functions.
ER stress caused by protein misfolding leads to Ca^{2+} release from the ER, activating Cn. Reversible activation is Ca^{2+}/calmodulin (CaM)-dependent and transient, while irreversible activation results from calpain-mediated proteolytic cleavage of the C-terminal regulatory region of CNA, including CaM-binding and autoinhibitory domains, generating a constitutively active catalytic fragment. Hyperactive Cn dephosphorylates cytoplasmic NFAT (NF-ATc), promoting its nuclear translocation and sustained pro-apoptotic gene expression. Cn inhibitors (tacrolimus/FK506, cyclosporin A) inhibit this pathway indirectly through their respective immunophilin complexes: FK506 binds FKBP12, while CsA binds cyclophilin A. These drug–immunophilin complexes bind to and inhibit the CNA catalytic subunit, thereby preventing Cn-mediated NFAT dephosphorylation and reducing downstream apoptotic signalling (Shah et al., 2017).

The Cn complex is a heterodimer composed of a catalytic subunit, CNA (~ 60 kDa), and a smaller regulatory subunit, CNB (~ 19 kDa). CNA contains the phosphatase catalytic domain as well as the CaM-binding and autoinhibitory domains. CNB is a Ca^{2+}-binding regulatory subunit containing four EF-hand motifs and contributes to the structural stability and Ca^{2+}-dependent regulation of the complex. Binding of Ca^{2+} to CNB and Ca^{2+}/CaM to CNA promotes activation of the phosphatase by relieving autoinhibition of CNA (Connolly *et al.*, 2018). Pharmacological inhibition of Cn can be achieved using FK506 and cyclosporine A which will together with immunophilin, such as cyclophilin and FK-binding proteins (FKBPs) form a drug-immunophilin complex which depresses Cn activity (Salowe and Hermes, 1998) (Figure 5).

Cn is highly expressed in the CNS and plays a role in many pathways involving modulation of immune responses and signal transduction by regulating neuronal excitability, the release of neurotransmitters and hormones, gene transcription and calcium-dependent apoptosis. As the only Ca^{2+}-dependent phosphatase in neurons, Cn is key to neuronal homeostasis: Its very high affinity (0.1 - 1 nM) to Ca^{2+} ensures its rapid activation when Ca^{2+} levels rise in the neuronal cytosol (Klee, Crouch and Krinks, 1979; Hubbard and Klee, 1987). To prevent further cytosolic Ca^{2+} influx, activated Cn may weaken voltage-gated Ca^{2+} channels and ER-induced Ca^{2+} release through dephosphorylation of IP3 and RyR (Armstrong, 1989; Zhu and Yakel, 1997; Burley and Sihra, 2000; Day *et al.*, 2002; Mukherjee and Soto, 2011). Cn also regulates the transcription factor cAMP-response element binding protein (CREB) in neurons by dephosphorylation thus switching CREB off and therefore stopping CREB-dependent gene expression (Bito, Deisseroth and Tsien, 1996; Rusnak and Mertz, 2000; Shibasaki, Hallin and Uchino, 2002). Cn also regulates the nuclear factor of activated T-cell (NFAT4) through its dephosphorylation which leads to nuclear translocation of NFAT4

inducing the expression of neutrophilin and netrin dependent gene expression needed for axonal outgrowth (Graef *et al.*, 2003; Groth and Mermelstein, 2003). Hyperactivation of Cn, however, may lead to neuronal apoptosis: Here, high cytosolic Ca^{2+} levels results in overactivation of Cn which dephosphorylates the pro-apoptotic protein BAD which thus disassociates from the scaffolding protein 14-3-3 to interact with Bcl-x in the mitochondrial membrane facilitating apoptosis (Wang *et al.*, 1999; Strasser, O'Connor and Dixit, 2000; SHOU *et al.*, 2004; Yang *et al.*, 2004). Mouse prion disease models have shown that normalisation of Cn activity through administration of the Cn inhibitor FK506 could reverse this apoptotic effect and therefore prevent neuronal loss (Mukherjee *et al.*, 2010). Moreover, mouse models of several neurodegenerative disorders showed low levels of BAD in its phosphorylated/scaffolding form (Agostinho *et al.*, 2008; Reese *et al.*, 2008). Interestingly, inhibition of overactivated Cn in Huntington disease mouse models showed restoration of neuronal death (Pineda *et al.*, 2009).

Cn activity has been shown to play an important role in motor neuron diseases (Morioka *et al.*, 1999; Wang *et al.*, 1999; Rusnak and Mertz, 2000). Previous studies using human neuroblastoma cells expressing fALS-SOD1 and mice models expressing fALS SOD1 showed that the phosphatase activity of Cn is depressed when mutant SOD1 is present (Ferri *et al.*, 2002) suggesting that Cn is redox regulated. This is further supported by experiments that show that wild type SOD1 functions as a protective element for Cn (Wang, Culotta and Klee, 1996), and fALS-SOD1 can directly deactivate Cn (Ferri *et al.*, 2008). The target of such oxidation of Cn is suggested to be the iron atom at its active site (Namgaladze, Hofer and Ullrich, 2002). Decreased Cn activity has been reported in ALS patients: a study reported significantly decreased Cn activity in lymphocytes in 37 sporadic and eight fALS patients with an increase in protein oxidation which was not found in the control subjects (Ferri *et al.*,

2004). Interestingly, a yeast Parkinson's disease model showed that Cnb1p overexpression could decrease protein aggregation and α-synuclein toxicity (Chawla *et al.*, 2023).

Calcium regulation and Calcineurin function in *S. cerevisiae*

In yeast, calcium homeostasis is tightly controlled to regulate cellular processes like cell growth (K. W. Cunningham and Fink, 1994; Cui, Kaandorp, Ositelu, *et al.*, 2009). Calcium-mediated signalling in yeast involves responses to alkaline environments (Serrano *et al.*, 2002) as well as to hypotonic shock via MAP kinase activation (Batiza, Schulz and Masson, 1996). In yeast, the level of free calcium in the cytoplasm is carefully controlled and kept low (50 – 200 nM) by storing calcium in compartments like the vacuole, ER, Golgi, and mitochondria (K. W. Cunningham and Fink, 1994; Cui, Kaandorp, Ositelu, *et al.*, 2009; Cyert and Philpott, 2013). Extracellular calcium mainly enters through the Cch1/Mid1 channel in the plasma membrane, which is activated by signals like depolarization, hypotonic shock, pheromones, and the unfolded protein response (Iida *et al.*, 1994; Fischer *et al.*, 1997; Bonilla, 2002).

A key protein in the calcium signalling cascade is Cn. The yeast *S. cerevisiae* has two isoforms of the Cn A subunit, namely Cna1 encoded by *CNA1* and Cmp2 encoded by *CMP2*. Cn activity is not lost if either one of them is deleted from the cell, making their functions redundant (Cyert *et al.*, 1991). However, Cn activity is dysfunctional if both isoforms are deleted at the same time. The B subunit in yeast is called Cnb1 and is crucial for the phosphatase activity (Cyert *et al.*, 1991; Liu *et al.*, 1991).

Normal Cn activity is essential for viability and growth in *S. cerevisiae* when exposed to high levels of ions, such as Na+, Li+, Mn2+, and OH-, or the α-factor yeast mating pheromone

suggesting a role in adaptive signalling (Cyert and Thorner, 1992; Mendoza *et al.*, 1994; Farcasanu *et al.*, 1995; Moser, Geiser and Davis, 1996; Withee, Sen and Cyert, 1998). The best-known substrate of Cn in yeast is the transcription factor Crz1. Cn dephosphorylates and activates this transcription factor and thus elicits a cell survival response under stress in a similar way to Cn-dependent regulation of the mammalian NFATc transcription factors (Stathopoulos-Gerontides, Guo and Cyert, 1999; Yoshimoto *et al.*, 2002).

Cytosolic calcium levels are low under standard laboratory conditions thus presenting inactive Cn. However, calcium levels increase under stress conditions, like hyperosmotic shock, activate Cn in order to elicit an adaptive response. A study showed that the hyperosmolarity-induced calcium release from the yeast main intracellular calcium store, the vacuole, is mediated via the vacuolar membrane channel Yvc1p. Low cytosolic calcium levels are restored through the calcium/H+ exchanger Vcx1p (Denis and Cyert, 2002).

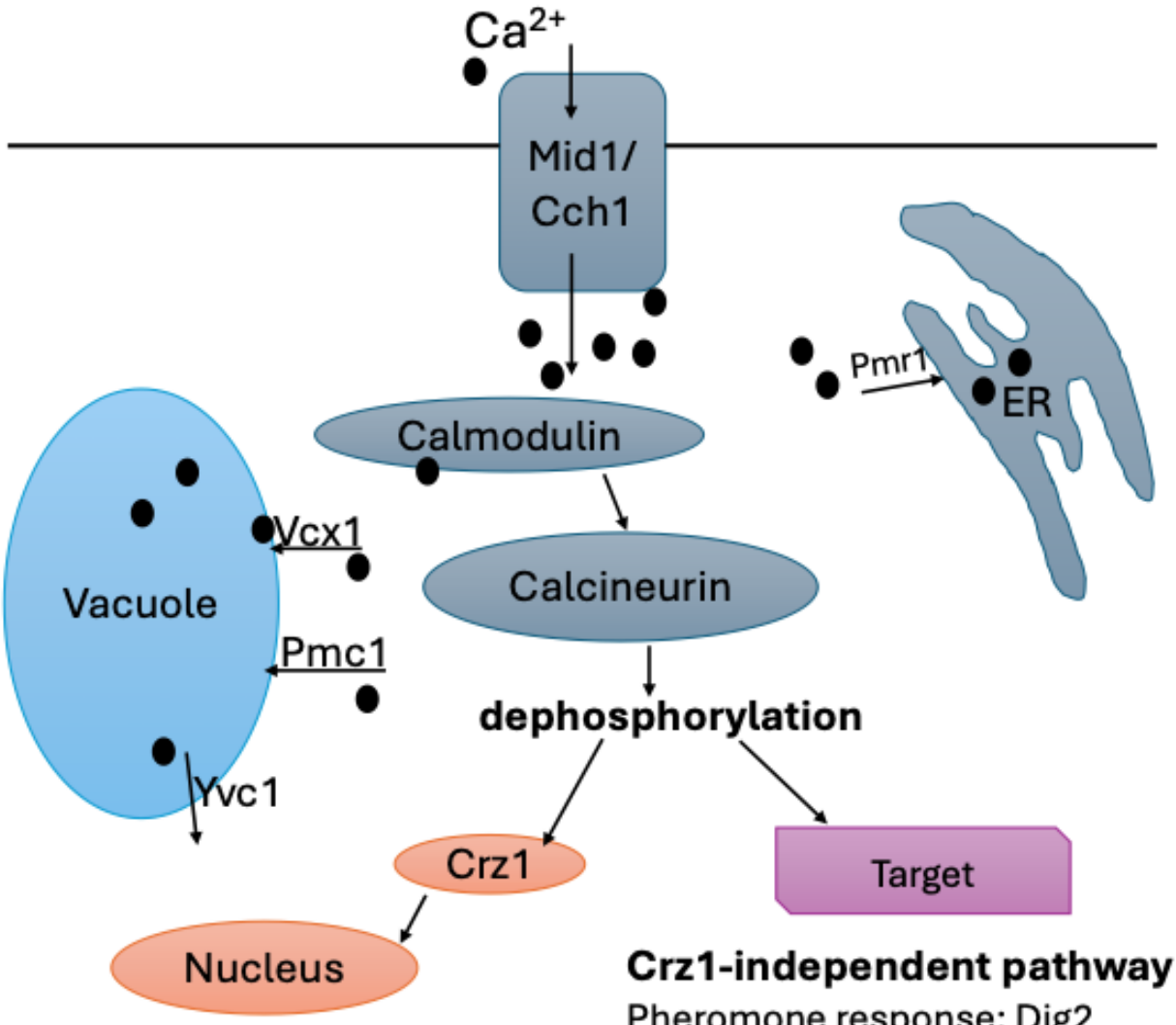
When calcium enters the cell, cytosolic calcium levels increase which is sensed by calmodulin as calcium binds to it (Stull, 2001). The calcium-calmodulin-complex binds to the phosphatase Cn via its calmodulin-binding-site and its Cnb1 domain causing a conformational change in Cnb1, exposing the Cna1 catalytic site of Cn which can now interact with calmodulin releasing the autoinhibitory domain of Cn from its substrate-binding site activating Cn. This triggers dephosphorylation of Cn targets such as Crz1. The dephosphorylated Crz1 transcription factor (TF) enters the nucleus via the importin Nmd5 (Polizotto and Cyert, 2001) and can now bind to its target promotors through calcineurin-dependent response element (CDREs) inducing the transcription of genes needed for cell growth and response to pheromones (K. Cunningham and Fink, 1994; Withee *et al.*, 1997; Park *et al.*, 2019). Crz1 is phosphorylated and exported out of the nucleus through the exportin Msn5 (Boustany and Cyert, 2002; Koike *et al.*, 2012; Thewes, 2014).

Studies have shown that to activate downstream Crz1 targets, the frequency of localising Crz1 to the nucleus is more important than the TFs abundance (Cai, Dalal and Elowitz, 2008). This frequency was controlled by calcium concentration. However, the nuclear residence time of Crz1 (about 2 min) was not regulated by calcium concentration (Cai, Dalal and Elowitz, 2008).

In *S. cerevisiae* Cn can dephosphorylate Cn targets by recognizing short, degenerate docking motifs called PxIxIT and LxVP which are different from the dephosphorylation sites. Thus, Cn can regulate autophagy, cell cycle progression, zinc homeostasis and calcium regulation independently from Crz1 signalling (Roy and Cyert, 2009; Goldman *et al.*, 2014). Dig2, which controls pheromone responses and is negatively regulated by Cn, and Elm1, which controls cell cycle progression, were found to be Cn targets (Goldman *et al.*, 2014; Park *et al.*, 2019) (Figure 4). Under alkaline stress, Cn can negatively regulate the kinase Elm1 thus affecting the activation of the energy-sensing kinase Snf1, ultimately influencing the expression of stress-responsive genes such as *HXT2* and *ENA1*. So, whilst gene expression via Crz1 is elicited through Cn, Cn also suppresses Elm1/Snf1 signalling. Thus, cell cycle progression may be regulated by limiting Elm1 activity during G1 phase allowing slower growth under stress through Cn (Goldman *et al.*, 2014).

The calcium signal ends when Ca^{2+} is stored in the main calcium reservoir, vacuole, via the Ca^{2+} pump Pmc1 and the Ca^{2+}/H^{+} exchanger Vcx1, which may also help regulate pH. The ER and Golgi may also act as additional calcium storage sites (K. W. Cunningham and Fink, 1994; Miseta *et al.*, 1999; D'hooge *et al.*, 2015). Recently, a new channel protein Ycx1 - localised to the ER and Golgi- has been identified to play a crucial role in calcium and Cn signalling: It was shown that Cn activation was reduced when the gene *YDL206W* which

encodes Ycx1 was disrupted leading to reduced calcium accumulation in the cytosol in *S. cerevisiae* (G. M. Lee *et al.*, 2023) (Figure 6).



Crz1-dependent pathway
Cell wall synthesis: Fks2, Rho1
Ion transport: Pmc1, Pmr1
Glucose metabolism: Gpx2
Signalling: Rcn1, Rcn2
Lipid synthesis: Sur1, Csg2, Hes1
Degradative enzymes: Apg5, Cps1

Crz1-independent pathway
Pheromone response: Dig2
Ubiquitin signalling: Ubx7
Cell cycle: Rts1, Hsl1, Elm1
Ca^{2+}signalling: Rcn1, Cch1
Glucose sensing: Tda1
Autophagy: Atg13

Figure 6 Schematic of calcium signalling and calcineurin functions in S. cerevisiae. Increased cytosolic Ca^{2+}, resulting from vacuolar release or extracellular influx through the Cch1/Mid1 channel complex, activates calmodulin. Ca^{2+}-bound calmodulin binds the calmodulin-binding domain of the Cn catalytic subunit (Cna), while Ca^{2+} binding to the regulatory subunit Cnb contributes to Cn activation. Activated Cn dephosphorylates Crz1, promoting its nuclear translocation and binding to Cn-dependent response elements (CDREs) in target gene promoters, thereby inducing stress-response genes. Cn also mediates Crz1-independent responses through the dephosphorylation of other targets, including Dig2.

As in mammals, calcium homeostasis has been shown to play a role in cell death. However, unlike in mammals where a mitochondrial Ca^{2+} uniporter mediates rapid equilibration of Ca^{2+} across the inner mitochondrial membrane, yeast cells do not possess the uniporter, which complicates the understanding how calcium homeostasis is linked in yeast apoptosis compared to mammals (Carafoli and Lehninger, 1971; Carraro and Bernardi, 2016). In yeast, programmed cell death involves steps like an increase in intracellular calcium levels and the build-up of ROS (Madeo *et al.*, 1999). These changes play a direct role in cell death induced by stresses such as oxidative damage (Madeo *et al.*, 1999), acetic acid (Chaves *et al.*, 2021), pheromones (Severin and Hyman, 2002), ethanol (Kitagaki *et al.*, 2007), and ER (Kajiwara *et al.*, 2012) or osmotic stress (Huh *et al.*, 2002).

Labile Zinc accumulation due to disturbed Calcineurin-Sod1 interaction

The metalloproteins calcineurin and SOD1 both contain zinc (King and Huang, 1984; Mera-Adasme *et al.*, 2016; Sirangelo and Iannuzzi, 2017). Metal cations and oxidative injury have been implicated in ALS (Cuajungco and Lees, 1997; Li *et al.*, 2013).

Studies have shown that Cn-SOD1 interactions are necessary for Cn activity, as SOD1 functions as a protection element from oxidative stress (Agbas *et al.*, 2007). Failure of this interaction may cause increased labile zinc accumulation which may cause motor neuron death (Tiwari and Hayward, 2005; Kim *et al.*, 2009). Failure of controlling ROS through Sod1 may also lead to Cn regulation dysfunction as superoxide for example can oxidise the catalytically active Cn Fe^{2+}-Zn^{2+} centre (Namgaladze, Hofer and Ullrich, 2002).

1.10 The Gut Microbiome

The combination of the entire population of microorganisms, including bacteria, viruses, protozoa, and fungi together with their genetic material found in the gastrointestinal tract define the gut microbiome. The gut microbiota also comprises commensals, opportunistic and dedicated pathogens (Brody, 2020). Some of the main functions of the gut microbiota is to absorb nutrients and minerals, synthesise amino acids, enzymes and vitamins, and to create short-chain fatty acids (SCFAs). SCFAs are crucial for the protection and maintenance of gut health but also serve as an energy supply for epithelial cells. SCFAs such as acetate or butyrate may modulate the guts immune system and prevent pathogens from breaking through the epithelial barrier by making it less permeable (den Besten *et al.*, 2013). There are four phyla which make up the majority of the gut microbiota: *Firmicutes*, *Bacteroidetes*, *Actinobacteria*, and *Proteobacteria*. Around 500 to 1000 bacterial species with each having genomes made up of thousands of genes colonise the human body. This means human bodies are not only influenced by human genes but also by microbial genes and microbial metabolic by-products (Thursby and Juge, 2017). A stable gut microbiome is established as early as birth. It has been shown that the method of delivery has an impact of the development of the gut microbiota, for example caesarean-born children have microbiomes mainly consisting of skin microbes such as *Staphylococcus ssp*. Other factors including breast feeding and antibiotic use affect microbiome development as well. For example breast feeding promotes *Bifidobacterium* colonisation while through food consumption especially indigestible carbohydrates other phyla like *Bacteroidetes* and *Firmicutes* colonise the gut in infants (Palmer *et al.*, 2007; Fallani *et al.*, 2011; Vallès *et al.*, 2014; Tanaka and Nakayama, 2017). Events interfering with the establishment of the gut microbiome e.g. antibiotic use may result in impaired immune function causing allergies and asthma (Tanaka and

Nakayama, 2017). Adulthood is marked by a relatively stable microbiome, however, as ageing occurs diversity of the microorganisms colonising the gut decreases affecting gut and immune function. This allows for increased gut permeability causing microbes to pass through the epithelial layer ultimately resulting in inflammation including neuroinflammation, chronic inflammation and impaired mitochondrial function (Nagpal *et al.*, 2018; Conway and A Duggal, 2021). Ageing may be associated with a decrease in SCFAs produced in the gut, possibly due to change of diet and appetite (Salazar *et al.*, 2019). SCFAs are a major energy source for the gut epithelial cells and contribute 5 - 10 % of the total energy required by the human body. Maintaining a low luminal pH, and promoting the increase of microbial biomass SCFAs play a critical role in mucus production and the colonising of beneficial bacteria (LeBlanc *et al.*, 2017).

Butyrate is a SCFA that is generated by the gut microbiota. Multiple studies have shown that butyrate acts as an histone deacetylase inhibitor (HDAC inhibitor) that has multiple health benefits, for example it has been linked to the prevention of proliferation of colorectal cancer cells (Donohoe *et al.*, 2014; Pascale *et al.*, 2018; Chen, Zhao and Vitetta, 2019).

1.12 Gut Microbiome and neurodegenerative diseases

The “Gut-Microbiota-Brain” axis describes the crosstalk between the central, the enteric, the autonomic nervous system and the hypothalamic pituitary adrenal axis. The bidirectional network sends afferent signals from the autonomic system through enteric pathways to the central nervous system which in turn then sends efferent signals to the intestinal wall (Tsigos and Chrousos, 2002; Carabotti *et al.*, 2015). Normal functioning of the central nervous system could be linked to healthy gut function (Carabotti *et al.*, 2015;

Daulatzai, 2015), and in turn mental health conditions such as depression and anxiety were linked to dysbiosis and inflammation of the gut (Daulatzai, 2015; Foster and Zhou, 2015). Existence of the "Gut-Brain-axis" is supported by studies using germ-free mice which showed impaired stress response (Sudo *et al.*, 2004; Ait-Belgnaoui *et al.*, 2012) and reduced anxiety-like behaviour (Heijtz *et al.*, 2011; Neufeld *et al.*, 2011). In addition, it is well known that the gut releases hormones, neurotransmitters and immunological factors that either signal to the central nervous system directly or through autonomic neurons (Ma *et al.*, 2019).

Neurodegenerative diseases such as ALS, Alzheimer's, Huntington's, and Parkinson's disease are all characterised by aggregation of misfolded and thus malfunctioning proteins which causes impairment or loss of tissue function and worsens with disease progression (Soto, 2003). No effective treatment or cure could be established so far mostly due to the fact that the exact aetiology of the diseases still remain unidentified (Durães, Pinto and Sousa, 2018). However, links between age, diet, stress, trauma, infections and antibiotics use and the risk of developing a neurodegenerative protein conformational disease could be established (Esch *et al.*, 2002; Honjo, Reekum and Verhoeff, 2009; Dominy *et al.*, 2019; Sun *et al.*, 2019; Mertsalmi, Pekkonen and Scheperjans, 2020; Bianchi, Herrera and Laura, 2021). Factors like stress, antibiotic use and trauma could also be linked to microbiome changes (Dethlefsen *et al.*, 2008; Hemmings *et al.*, 2017; Jin *et al.*, 2017), which might highlight the importance of bacteria and other microorganisms colonising the human body in disease onset. Evidence exists showing that gut dysbiosis or enteric infection may play a crucial role in neurodegenerative protein conformational disease (Scheperjans *et al.*, 2015; Gerhardt and Mohajeri, 2018; Mazzini *et al.*, 2018). Furthermore, butyrate-producing bacteria have been

shown to be effective in suppressing protein aggregation in *C. elegans.* This highlights the importance of microbial metabolites on host health (Walker *et al.*, 2021). In addition, studies in ALS mouse models have shown that gut integrity and microbial homeostasis is improved when butyrate is supplemented thus prolonging life span (Zhang *et al.*, 2017).

1.12.1 Amyotrophic Lateral Sclerosis and the gut microbiome

The fatal incurable disease ALS is characterised by a progressive degeneration of motor neurons. Its aetiology and pathophysiology are mostly unknown. Whilst only 10 - 15 % of ALS cases are familial cases i.e. ALS is caused through mutations in various genes, the majority of ALS cases are, however, sporadic (Turner *et al.*, 2017). The current view on ALS disease development suggests a complex interplay among host factors, microbiome, and environmental factors with risk factors being smoking, lower body mass index (BMI), extreme physical exercising, and trauma e.g. through military service that contribute to the disease development (Wang *et al.*, 2017). The composition of the gut microbiome is dependent on various factors, such as genetics, gender, age, geographic location, lifestyle, and diet (Ballan *et al.*, 2020; de Vos *et al.*, 2022). In addition, compounds from the diet are metabolised by the gut microbiota yielding various metabolites that will interact with cell receptors and signalling pathways of the host influencing the host's health. Thus, various compositions of the gut microbiota will provide different metabolite profiles leading to different impacts on different signalling pathways, and therefore may contribute to or impede host health (Ballan *et al.*, 2020; de Vos *et al.*, 2022).

Studies using transgenic ALS mice carrying either SOD1G86R or SOD1G93A showed an altered metabolic status whereby energy homeostasis was drastically impaired leading to

hypermetabolism largely of muscular origin. This metabolic phenotype of SOD1G86R mice as well as later disease onset could be improved when an energy-rich diet was given (Dupuis *et al.*, 2004). Recently, diet has been shown to be a crucial contributing factor to ALS risk, onset, and progression: high-calorie fat or sugar-rich diets showed to positively affect ALS patients to help combat fast weight loss and hypermetabolism seen in ALS patients (Desport *et al.*, 2001; Bouteloup *et al.*, 2009; Vaisman *et al.*, 2009; Dupuis *et al.*, 2011; Ferri and Coccurello, 2017; Steyn *et al.*, 2018). In addition, alterations in mitochondrial function, including fragmentation, and aggregation are a hallmark in ALS patients (Vielhaber, 2000; Krasnianski *et al.*, 2005; Echaniz-Laguna *et al.*, 2006; Crugnola *et al.*, 2010; Cozzolino and Carrì, 2012).

The antioxidant resveratrol which is found in grapes exerts neuroprotective properties, and may decrease neurotoxicity of cerebrospinal fluid from ALS patients *in vitro* contributing to neuronal health and Ca^{2+} homeostasis (Yáñez *et al.*, 2011).

Probiotics supplementation to ALS patients increased the presence of bacterial groups related to butyrate and propionate generation which may be beneficial to energy provision and metabolising neurotoxic compounds (Di Gioia *et al.*, 2020). Previous work conducted by Zhang *et al.*, 2017 showed delayed disease progression and extended survival time of SOD1G93A mice upon butyrate supplementation. Furthermore, the gut microbiome was improved and Paneth cells – the gut's main immune cells – together with signalling of lysozyme 1 anti-microbial peptide defensin 5 alpha was restored in these mice mutants (Zhang *et al.*, 2017). Butyrate treatment also decreased intestinal SOD1G93A aggregation in mice (Zhang *et al.*, 2017). Most recently, butyrate treatment was found to improve healthy metabolites in ALS (Ogbu *et al.*, 2022). Longitudinal studies provided evidence that early microbial changes are linked to autoimmunity (e.g. *Clostridium sp.ASF502*), inflammation

(*Enterohabdus Muris*), and metabolism (*Desulfovibrio fairfieldensis*) in SOD1G93A mice (Zhang *et al.*, 2021). Another study showed that nicotinamide delayed disease progression in the ALS SOD1G93A mice. It was also found that the gut microbiome in these mice mutants varied to the control mice, and that antibiotic use exacerbated motor abnormalities (Blacher *et al.*, 2019). Differences in the gut microbiome were also found in other ALS mouse models carrying the SOD1G93A mutation (Figueroa-Romero *et al.*, 2019). Human ALS studies could identify that the microbiome of ALS patients is significantly different to healthy controls: *Bacteroidetes Bacteriodales Dorea* were substantially higher than in healthy controls and phyla *Firmicutes* were significantly higher in healthy controls compared to ALS patients. Furthermore, species *Oscillibacter, Anaerostipes,* and *Lachnospiraceae* were substantially decreased in ALS patients (Fang *et al.*, 2016). It was reported (Rowin *et al.*, 2017) that dysbiosis and decreased diversity of the microbiome compared to healthy controls was present in all ALS patients examined. Furthermore, other studies investigating the microbiome of ALS patients found that there was a significantly lower abundance and diversity of the bacterial profile in ALS patients compared to healthy controls; here higher abundance of *E. coli* and *Enterobacteria* combined with lower abundance of *Clostridium* and yeast was identified in ALS patients (Mazzini *et al.*, 2018; Di Gioia *et al.*, 2020).

A recent comparison of the gut microbiota of ALS patients with the patients' spouses as healthy controls found that ALS patients were lacking butanoate metabolic pathway enzymes (Hertzberg *et al.*, 2022). Furthermore, they found that enzymes involved in metabolic pathways including response regulators and carbon metabolism pathways were low in ALS patients. Decreased amounts of enzymes involved in butyrate metabolism was also established.

1.13 The short chain fatty acid Sodium Butyrate

SCFA are organic acids which are generated through fermentation of dietary carbohydrates and fibres, starch and some endogenous proteins by bacteria residing in the proximal colon. Butyrate production via bacterial fermentation of dietary fibres is coordinated through two metabolic pathways. The first pathway involves phosphorylation of butyryl-CoA generating butyryl-phosphate which is a substrate for butyrate kinase ultimately producing butyrate. The second pathway involves the transfer of the CoA moiety of butyryl-CoA onto acetate through an enzyme called butyryl-CoA: acetate CoA transferase which ultimately results in the generation of butyrate and acetyl-CoA (Trachsel *et al.*, 2016; Esquivel-Elizondo *et al.*, 2017) (Figure 7).

In addition to these pathways, fructolysine can contribute to butyrate production through the lysine pathway: Whilst breaking down dietary protein usually produces toxic waste products, this pathway allows specialised bacteria e.g. *Intestinimonas butyriciproducens* to use unique enzymes to ferment the amino acid lysine directly into butyrate. Interestingly, *Intestinimonas butyriciproducens* can switch between the carbohydrate pathway and the protein-based lysine pathway depending on the diet. Fructolysine is produced when sugars and proteins fuse together at high heat when cooked, and it is commonly found in modern Western diets such as in grilled meats, roasted snacks and packaged ready-to-eat meals. Normally, fructolysine is degraded into toxic Advanced Glycation End-products (AGEs). *Intestinimonas butyriciproducens*, however, may feed on both carbohydrate and fructolysine converting one molecule of this byproduct into three molecules of butyrate. Essentially fructolysine is taken up by ABC transporters which is phosphorylated into

fructolysine-6-phosphate by fructolysine kinase which is then cleaved into lysine and glucose6-phosphate by fructoseamine deglycase. Lysine is subsequently degraded via the lysine pathway eventually to crotonyl-CoA which is converted to butyryl-CoA and then to butyrate (Smith and Macfarlane, 1997; Vital, Howe and Tiedje, 2014; Bui *et al.*, 2015) (Figure 7).

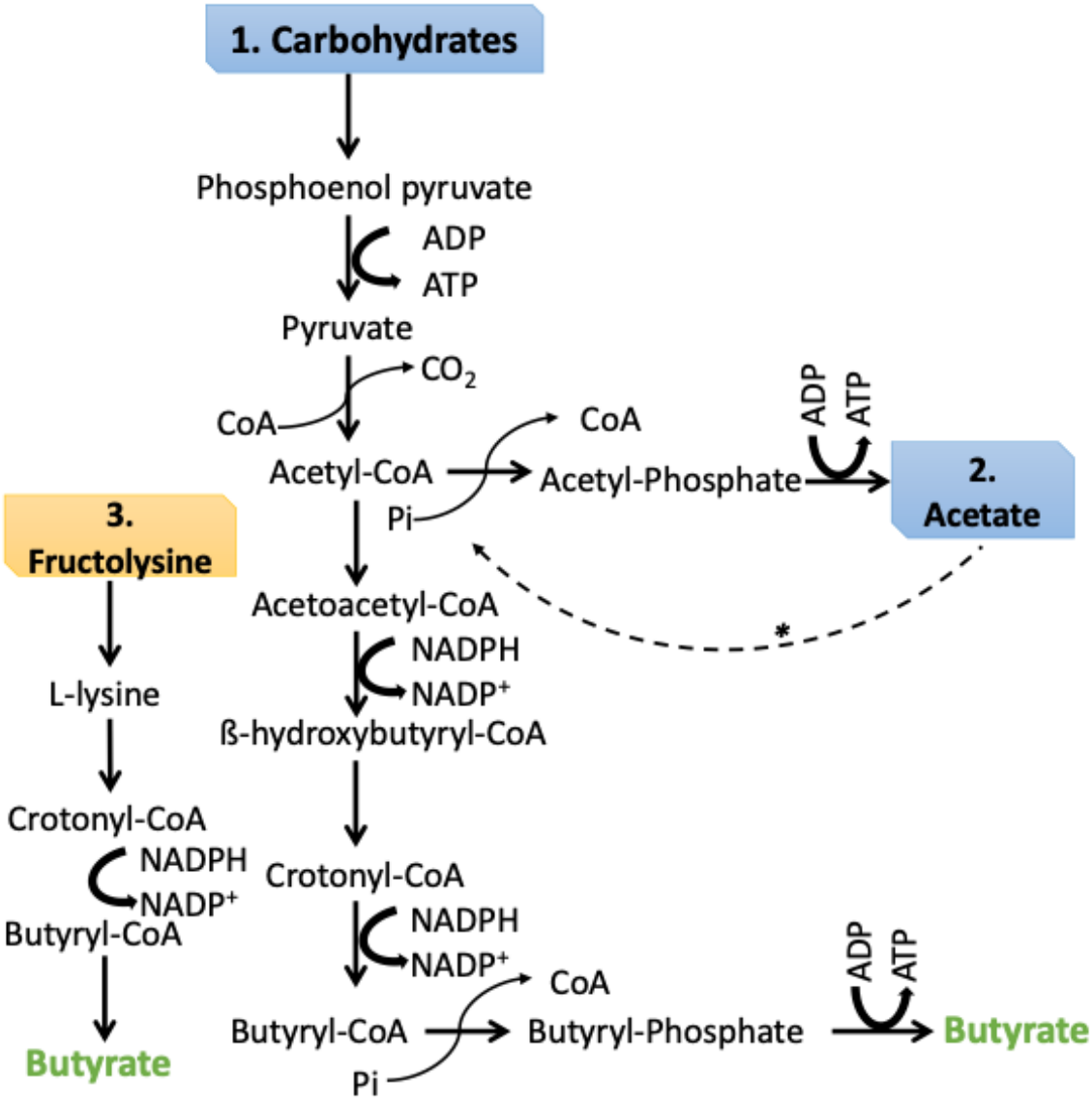


Figure 7 Metabolic routes for butyrate production. (1) The butyrate kinase pathway, in which carbohydrates are directly converted to butyrate via butyryl-CoA and butyryl-phosphate; (2) the butyryl-CoA:acetate CoA transferase (*) pathway, in which a CoA moiety is transferred from butyryl-CoA to acetate, generating butyrate and acetyl-CoA; and (3) the lysine pathway, in which fructolysine is converted to L-lysine, which subsequently feeds into the butyrate biosynthetic pathway at crotonyl-CoA. The lysine pathway is simplified in the figure for clarity, with its subsequent metabolic steps described in the text.

Around 60 - 70 % of the energy requirements of epithelial cells of the colon are provided by SCFA (Canani, 2011; Brahe, Astrup and Larsen, 2013; P. Fan *et al.*, 2015; Ma *et al.*, 2017).

SCFAs are crucial for the protection and maintenance of the gut health but also for the energy supply of epithelial cells. SCFAs such as acetate or butyrate may modulate the gut's immune system and prevent pathogens from breaking through the epithelial barrier by making it less permeable (den Besten *et al.*, 2013).

The most important bacterial groups producing butyrate are *Faecalibacterium prausnitzii* and *Eubacterium rectale/Roseburia* spp. (Quesada-Vázquez *et al.*, 2020).

The SCFA butyrate is the least produced SCFA with only 15 % of total SCFAs in humans (Liu *et al.*, 2018). Acetate and propionate, however, have an abundance of 60 % and 25 %, respectively (Slavin, 2013; Conlon and Bird, 2014; Liu *et al.*, 2018). Despite being the least abundant SCFA, butyrate has crucial roles in colon function of ruminants and other mammalians: it prevents inflammation in the small intestine (Wächtershäuser and Stein, 2000), provides energy of colonocytes (Donohoe *et al.*, 2011), stimulates mucin synthesis by upregulating the MUC2 expression thus increasing the mucosal defence layer (Willemsen, 2003; HAMER *et al.*, 2007), regulates growth of enterocytes (Hodin *et al.*, 1996; Wächtershäuser *et al.*, 2000; Wächtershäuser, Loitsch and Stein, 2000) and cell proliferation and apoptosis of colon and cancer cells (S. Archer *et al.*, 1998; S. Y. Archer *et al.*, 1998; Donohoe *et al.*, 2014). A study using germfree mice showed that butyrate could rescue mitochondria respiration, and prevent autophagy: Here, germ-free mice colonocytes induce an energy-deprived state and low enzyme expression thereby failing to maintain metabolism and the TCA cycle and inducing autophagy. Butyrate enters the mitochondria where ß-oxidation takes places producing acetyl-CoA, which then enters the TCA cycle where NAD^+ is reduced to NADH. NADH can enter the electron transfer chain (ETC) ultimately leading to ATP and CO_2 generation. Thus, butyrate may regulate energy metabolism and autophagy in the mammalian colon (Donohoe *et al.*, 2011).

Butyrate may mediate some of its metabolic effects through binding to glucose receptors in the portal vein thus increasing insulin sensitivity and hence reducing hepatic gluconeogenesis. Butyrate thus mediates its signalling via gluconeogenesis from the gut epithelium using the cAMP signalling pathway (Stilling, Dinan and Cryan, 2014; Keenan *et al.*, 2015).

Butyrate can bind to several G-protein-coupled receptors (GPCRs), such as GPR41 and GPR43. GPR41 is expressed in adipose tissue, the pancreas, spleen, lymph nodes, bone marrow, and blood mononuclear cells (Byrne *et al.*, 2015). Through binding of butyrate to GPR41 body energy expenditure and the maintenance of metabolic homeostasis is directly controlled by sympathetic nervous system activity (Kimura *et al.*, 2011). Upon butyrate binding to GPR41 the production of intracellular cAMP is reduced mediating intracellular stress response in mammary epithelial cells (Le Poul *et al.*, 2003; Yonezawa, Kobayashi and Obara, 2007). It was also observed that butyrate can activate the entire cAMP-PKA-CREB pathway in the human cell line Caco-2 independently of GPR41 or GPR43 (Hilgers, Conradi and Burton, 1990; Wang *et al.*, 2012). In the cAMP-PKA-CREB pathway, intracellular cAMP activates PKA which then translocates into the nucleus to phosphorylate CREB at serine 133. Phosphorylated CREB may then recruit its coactivator CREB-binding protein (CREBP). Transcriptional activation may then be initiated through association with RNA polymerase II via CREBP (Altarejos and Montminy, 2011). Butyrate may phosphorylate CREB at serine 133, activate PKA and elevate cAMP concentrations in Caco-2 cells (Wang *et al.*, 2012). However, these effects of butyrate may not be mediated through GPCR but may be mediated by direct or indirect activation of soluble adenylate cyclase (AC) to increase cAMP (Wang *et al.*, 2012).

GPR109A is another GPCR that is directly activated by butyrate and mediates signalling in the inflammasome pathway in colonic macrophages and dendritic cells. Thus, controlling differentiation of regulatory T-cells and IL-10-producing T-cells (Singh *et al.*, 2014). Another study has shown that butyrate may increase intracellular free cytosolic Ca^{2+} via binding to GPR41 suggesting butyrate a metabolic intermedate (Miletta *et al.*, 2014).

HDAC is the enzyme responsible for catalysing the removal of acetate from modified lysine residues at the N-terminal region of histones H2A, H2B, H3 and H4 which form a histone octamer core where 146bp of DNA is wrapped around (Luger *et al.*, 1997). Preventing the removal of acetyl groups from lysine residues on histone and non-histone proteins leaves the DNA more tightly bound (compaction of chromatin) as the lysine residues retain their positive charge thus preventing gene transcription (Davie, 2003). However, this affects only the expression of about 2 % of mammalian genes (Davie, 2003) and the precise mechanism remains unclear.

The antimicrobial properties of Butyrate

Butyrate has also been reported to show an antimicrobial activity against fungi, yeast, and bacteria at high concentrations. It has been supposed that toxicity is caused by the production of secondary metabolites through inhibiting histone deacetylases (Beau *et al.*, 2012; Zutz *et al.*, 2013, 2014) or by destabilisation of the intracellular pH level due to its chemical nature as weak organic acid (Browning *et al.*, 2006). Recent studies (Zutz *et al.*, 2017) showed that butyrate at concentrations ranging from high 3 - 30 mM significantly reduced fungal biomass in *Penicillium restrictum*. However, treatment of *Penicillium restrictum* with 0.03 mM of butyrate had the highest antimicrobial activity. It was

furthermore shown that intracellular levels of adenine and its derivatives were significantly increased upon butyrate treatment (Zutz *et al.*, 2017). Other studies have also shown that butyrate supresses fungal growth of *C. albicans, Trichosporon* and *C. neoformans* and their virulence (Nguyen *et al.*, 2011; Cordeiro *et al.*, 2019). It was also shown that butyrate prevents biofilm formation of *C. albicans, C. parapsilosis,* and *C. neoformans* in a dose-dependent manner and make those species more susceptible to treatment with the antifungal fluconazole (Nguyen *et al.*, 2011).

1.5 Models of ALS

Since SOD1-associated ALS was discovered in 1993 (Rosen *et al.*, 1993), numerous models have been used to elicit more understanding of the complexity of the disease and the factors that influence ALS especially how mutations linked to ALS affect cell and whole animal function. Various animal models also provide a platform to perform pre-clinical tests and small molecule screens (Bonifacino *et al.*, 2021). Below we focus on ALS models in *Saccharomyces cerevisiae*, SH-SY5Y human neuroblastoma cells, and *C. elegans*.

1.5.1 *Saccharomyces cerevisiae* as a model organism for motor neuron diseases

Saccharomyces cerevisiae is a single-celled budding yeast that has been used as the primary model organism in the discovery of molecular signalling pathways (Botstein and Fink, 2011). Due to its easy genetic manipulation, rapid growth and a vast amount of resources and molecular tools (Mohammadi *et al.*, 2015), *S. cerevisiae* has not only elucidated our understanding in human disorders, such as cancer (Pereira, Coutinho, *et al.*, 2012;

Guaragnella *et al.*, 2014) and neurodegenerative disorders (Pereira, Bessa, *et al.*, 2012; Tenreiro *et al.*, 2013), but also in ageing research (Bonawitz *et al.*, 2007). In 1996, its genome was the first eukaryotic genome to be sequenced (Goffeau *et al.*, 1996) revealing strong conservation between humans and yeast in key functional pathways regulating cell cycle (Liu *et al.*, 2015) and metabolism (Petranovic *et al.*, 2010) e.g. mitogen-activated protein-kinase (MAPK) (Madrid *et al.*, 2016). Dysfunction or mis-regulation in any of these pathways are associated with many diseases in humans (Foury, 1997).

As mentioned above, many signalling pathways and molecular mechanisms, such as protein trafficking defects, mitochondrial dysfunction and transcriptional dysregulation, are highly conserved between yeast and humans. This is why yeast can be utilised to study fundamental molecular events underlying neurodegenerative disorders (Gitler, 2008). Moreover, genes, such as the *SOD1* gene involved in ALS can be successfully studied using yeast (Bastow *et al.*, 2016).

1.5.2 SH-SY5Y human neuroblastoma cells as a model for neurodegenerative diseases

The *in vitro* model cell line SH-SY5Y is a common neuronal model used in neuroscience research to investigate nervous system disorders on molecular and cellular basis (Hoffmann *et al.*, 2023). SH-SY5Y is a subline of the neuroblastoma cell line SK-N-SH that was derived from a 4-year-old female patient. SH-SY5Y is commonly used to help model neurological disorders such as Alzheimer's disease, Parkinson's disease, and ALS (Xicoy, Wieringa and Martens, 2017; Hoffmann *et al.*, 2023). Unlike primary rodent cell cultures, the SH-SY5Y cell line expresses human-specific proteins (Kovalevich and Langford, 2013). However, being a

cancer cell line SH-SY5Y has also limitations in modelling actual neurons (Xicoy, Wieringa and Martens, 2017; Hoffmann *et al.*, 2023).

1.5.3 *C. elegans* and its lifecycle

Caenorhabditis elegans or *C. elegans* is a eukaryotic multicellular organism possessing homologs of about two-thirds of all human disease genes. Its genome is completely sequenced making it an invaluable tool for experimental research at both metabolic and genomic levels covering research areas ranging from ageing and age-related diseases to drug screening. The ease of genetic manipulation and short lifespan of *C. elegans* also make this organism attractive when modelling human disorders (Brenner, 1974; Moreno-Arriola *et al.*, 2014).

The harmless nematode feeds on microorganisms such as *E. coli* and is easy to maintain in laboratory settings. When cultured at 20 °C the around 1 mm long adults which are self-fertilising hermaphrodites exhibit a 2.5 to 4 day reproductive cycle and possess a mean lifespan of about 18 to 20 days (Hertweck, 2003; Schaffitzel and Hertweck, 2006; Golden, 2007; Chew *et al.*, 2017). Although being self-fertilising hermaphrodites male *C. elegans* can be found albeit less commonly in nature (Devaney, 2006).

Under normal conditions *C. elegans* can develop into four larval stages (L1-L4). After 12 hours L1 larva hatch from the eggs and develop into L2 larva which lasts around 7 hours. During this L2 stage germ cell divisions proceeds, and the elongation of the gonad starts. Within the next 16 hours, gonadogenesis and vulval and uterine development are completed, allowing L4 stage larva to develop into adults (Brenner, 1974; Hall, D., Herndon, L. and Altun, 2017). However, under extreme conditions, development can be arrested after

the L2 larval stage, and the organism proceeds with the so called dauer larval stage. Once conditions become more favourable again, the dauer stage *C. elegans* may recover by moulting into the L4 larval stage thus proceeding normal development (Chen, Scarcelli and Legouis, 2017) (Figure 6).

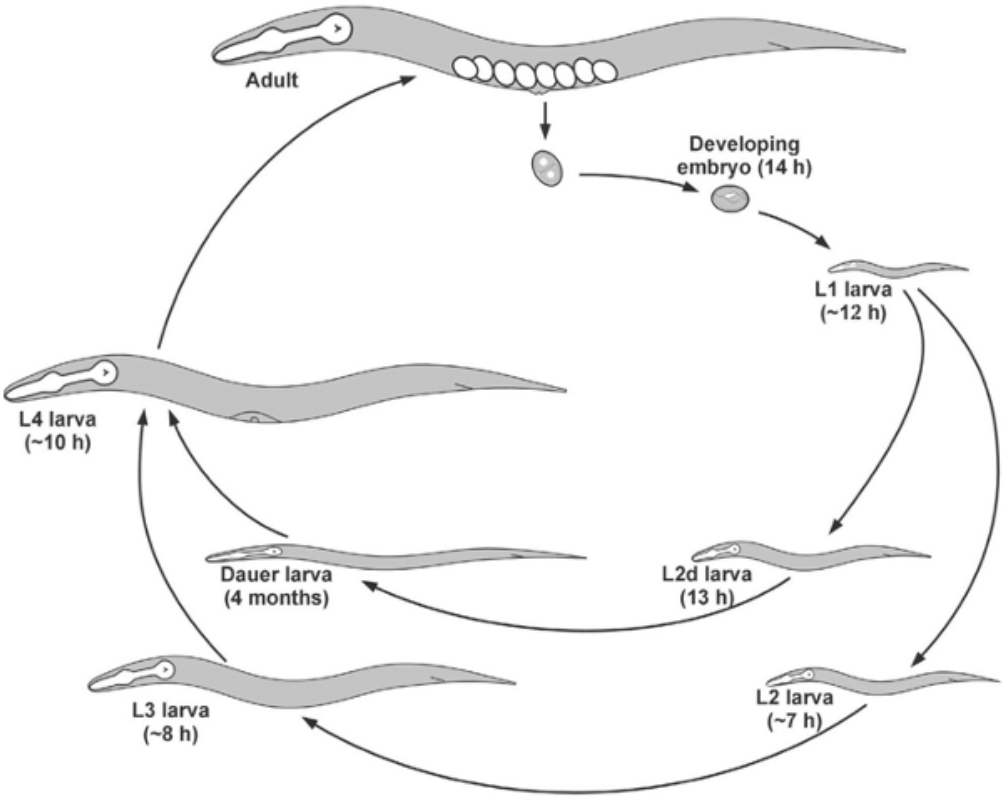


Figure 6 The life-cycle of the nematode C. elegans.
Under normal conditions, C. elegans develop through four larval stages (L1-L4). After hatching, L1 larvae develop into L2 larvae, where germ cell divisions and gonad elongation occur. Over the next 16 hours, gonadogenesis and vulval development complete, allowing progression to the L4 stage and adulthood. Under adverse conditions, development can arrest at the L2 stage, initiating the dauer larval stage. Upon favorable conditions, dauer larvae can recover and resume normal development by moulting into the L4 stage.
Image from (Strange, 2003).

C. elegans as a model organism in neurodegenerative diseases

The *C. elegans* nervous system is composed of 302 neurons whose signalling is controlled by nearly all neurotransmitters used in the mammalian neuron system (Kuwahara *et al.*, 2008; Therrien and Parker, 2014). Their easy genetic manipulation through for example RNA

interference (RNAi) makes them an attractive model organism. Here, double stranded RNA expressed in bacteria is exploited by regulating and silencing gene expression in worms via feeding the worms with said transformed bacteria. Another advantage is their transparent body enabling *in vivo* visualisation of neurons (Li, Huang and Le, 2013).

Motor neuron diseases such as ALS can also be nicely simulated using *C. elegans*. Multiple groups have been able to express mutant human Sod1p in *C. elegans* thus simulating the degeneration of neurons and paralysis two of the hallmarks of ALS (Gidalevitz *et al.*, 2009; Jiou Wang *et al.*, 2009; Li *et al.*, 2014). Recent findings (Li, Huang and Le, 2013) support that expression of mutant SOD1 leads to protein aggregation indicating a major role in the progression of ALS. When mutant SOD1 was expressed in *C. elegans* motor neurons it was also found that more than 80 % of the transgenic worms were paralysed by day 12 of their study (Li, Huang and Le, 2013). Other studies showed that mutant *SOD1* expression caused a dysfunctional response mechanism during oxidative stress (Oeda, 2001). In addition, expressing mutant SOD1 in the entire nervous system leads to impaired neuronal transmission and motor defects (Jiou Wang *et al.*, 2009). However, it has been reported (Gidalevitz *et al.*, 2009) that mutant SOD1 aggregates could form in other parts of the body in *C. elegans* as well when SOD1 mutants were expressed in body wall muscles in *C. elegans*. However, the majority of times protein aggregation takes place in motor neurons.

Aims

The aims of this thesis is to investigate how metabolic dysfunction contributes to impaired cellular health, homeostasis, and viability in the context of amyotrophic lateral sclerosis (ALS) pathology. Using *Saccharomyces cerevisiae*, *Caenorhabditis elegans*, and human

neuroblastoma cells as complementary model systems, this thesis aims to: (1) determine whether the microbial metabolite butyrate can influence mutant Sod1 aggregation and associated cellular phenotypes; (2) investigate the contribution of mycobiome dysbiosis to ALS pathology and determine whether butyrate can modulate the effects of fungal dysbiosis; and (3) elucidate how the ALS-associated $Sod1^{A4V}$mutation alters cellular metabolic processes, with particular emphasis on vacuolar function and calcium homeostasis. Together, these aims seek to provide insight into the relationship between metabolic dysfunction and cellular pathology in ALS and to identify metabolic pathways that may contribute to disease progression.

Chapter 2 - Butyrate can ameliorate Sod1 aggregation and restore motility in a *C. elegans* ALS model system

Abstract

Amyotrophic lateral sclerosis (ALS) is a progressive neurodegenerative disease characterized by motor neuron loss and protein aggregation, commonly driven by mutations in superoxide dismutase 1, Sod1. Recent evidence implicates gut microbiota-derived metabolites, such as butyrate, in modulating neurodegeneration, but the underlying mechanisms remain unclear. Here, we demonstrate that sodium butyrate (NaB), a histone deacetylase inhibitor and microbial metabolite, ameliorates ALS-related phenotypes in *C. elegans* and mammalian cell models expressing mutant isoforms of Sod1 linked to ALS. NaB treatment prevented Sod1 aggregation and restored motor function and axonal integrity in transgenic worms overexpressing $Sod1^{G85R}$. Mechanistically, NaB recapitulated the effects of the pan-HDAC inhibitor Trichostatin A, suggesting HDAC inhibition as key to a reduction in Sod1 aggregation and its downstream effects. Application of NaB or the HDAC inhibitor Valproic Acid, also prevented aggregation of $Sod1^{A4V}$, $Sod1^{G85R}$ or $Sod1^{G37R}$ in transfected human neuroblastoma cells. These findings support a conserved neuroprotective role for NaB and HDAC inhibitors via their anti-aggregation activity. Our findings also verify *C. elegans* and neuroblastoma cell lines as excellent research tools to explore the mechanism of NaB and HDAC inhibitors anti-aggregation action and their potential for future therapy development.

2.1 Introduction

The neurodegenerative disorder Amyotrophic lateral Sclerosis (ALS) leads to a progressive loss of motor neurons controlling voluntary muscles responsible for eating, speaking, walking, and breathing, ultimately leading to paralysis and death usually through respiratory paralysis within a couple of years post diagnosis (Brown and Al-Chalabi, 2017). ALS is also known as Lou Gehrig Disease and is 100 % fatal leading to 30,000 deaths per year in the USA (http://www.als.org) (Olanow, 1993; Mehta *et al.*, 2023). There are two types of ALS which are pathologically indistinguishable from one another: familial ALS (fALS) is caused by mutations in various proteins, and sporadic ALS (sALS) which does not possess any obvious genetically inherited components. However, 90 % of ALS cases are sporadic (Pansarasa *et al.*, 2018; Kim *et al.*, 2019). Whilst the aetiology and pathophysiology of ALS are well documented, it has recently been demonstrated that the gut microbiota may play a substantial role in the progression of the disease (Wang *et al.*, 2017).

The gut microbiota functions to absorb nutrients and minerals, synthesise amino acids, enzymes and vitamins, and to create short-chain fatty acids (SCFAs). As such it has a profound influence on human health and has been linked to a wide range of disease pathologies (Thursby and Juge, 2017). Variation in gut microbiota composition and activity may result in different metabolite profiles with a direct impact upon cell signalling pathways, and downstream effects that may contribute to or impede host health (Ballan *et al.*, 2020; de Vos *et al.*, 2022). Differences in gut microbiome were found in ALS mice trials carrying the $SOD1^{G93A}$ mutation (Figueroa-Romero *et al.*, 2019). Human ALS studies also identified that the microbiome of ALS patients is significantly different to healthy controls: *Bacteroidetes Bacteriodales Dorea* were substantially higher than in healthy controls and

phyla *Firmicutes* were significantly higher in healthy controls compared to ALS patients. Furthermore, *Oscillibacter, Anaerostipes,* and *Lachnospiraceae* were substantially decreased in ALS patients (Fang *et al.*, 2016). It has been reported that dysbiosis and decreased diversity of the microbiome was present in ALS patients when compared to healthy controls (Rowin *et al.*, 2017).

Such findings have led to attempts to treat ALS with dietary interventions that might redress the dysbiosis, such as via probiotic supplementation containing lactic acid bacteria e.g. *Streptococcus thermophilus*, *Lactobacillus fermentum*, *Lactobacillus delbrueckii*, *Lactobacillus plantarum*, and *Lactobacillus salivarius.* Whilst a 6-month probiotic treatment did alter the gut microbiota composition, it did not restore biodiversity to levels seen in healthy controls or affect disease progression, as measured by the ALS functional rating scale (Di Gioia *et al.*, 2020).

SCFAs are a major energy source for gut epithelial cells and contribute 5 - 10 % of the total energy required by the human body (Donohoe *et al.*, 2011; Rivière *et al.*, 2016; Parada Venegas *et al.*, 2019). SCFAs help to maintain a low luminal pH, and promote an increase of microbial biomass as well as playing a critical role in mucus production and the colonising of beneficial bacteria (LeBlanc *et al.*, 2017). Gut bacteria degrade non-digestible polysaccharides e.g. dietary fibres to produce SCFAs (Fusco *et al.*, 2023). The SCFA butyrate is generated by the gut microbiota and has shown to have clinical benefit, for example it is known to be beneficial in targeted cancer treatment (Donohoe *et al.*, 2014), for example butyrate can inhibit histone deacetylase – an enzyme whose activity that has been linked to the proliferation of colorectal cancer cells (Donohoe *et al.*, 2014; Pascale *et al.*, 2018; Chen,

Zhao and Vitetta, 2019). Fifteen bacterial species, including the butyrate-producing bacteria *Roseburia intestinalis* and *Eubacterium rectale* have been reported to be significantly lower in ALS patients when compared to healthy controls (Niccolai *et al.*, 2021; Hertzberg *et al.*, 2022). Furthermore, ALS patients display a reduction in the activity of enzymes involved in butyrate metabolism (Hertzberg *et al.*, 2022). These data suggest that decreased butyrate production may play a key role in ALS pathology. Evidence to suggest this has been generated in a mouse model, with butyrate treatment leading to an improvement in motor function in the $Sod1^{G93A}$ ALS model system (Zhang *et al.*, 2021). It is believed that one mode of action of butyrate is through HDAC inhibition (Candido, 1978; Vidali *et al.*, 1978; Donohoe *et al.*, 2014; Pascale *et al.*, 2018; Chen, Zhao and Vitetta, 2019). Other HDAC inhibitors such as Valproic acid (VPA) and Trichostatin A (TSA) have been considered as potential ALS treatments (Yoo and Ko, 2011) whereby VPA has been tested in clinical trials (Piepers *et al.*, 2009; Boll *et al.*, 2022) and TSA in more lab-based studies (Yoo and Ko, 2011; Bennett *et al.*, 2021; Klingl, Pakravan and Van Den Bosch, 2021).

In this study we aimed to investigate the effect of butyrate supplementation on $Sod1^{mut}$ aggregation clearance and motor defects in transgenic $Sod1^{mut}$ *C. elegans* models and in $Sod1^{mut}$ transfected neuroblastoma cells. Here, we found that butyrate supplementation could ameliorate motor and neuromuscular junction defects observed in transgenic $Sod1^{mut}$ *C. elegans* and could also decrease Sod1 aggregation in both models. These findings demonstrate that *C. elegans* and cell-based models may be employed to determine how butyrate and other clinically used HDAC inhibitors function to limit Sod1 aggregation, providing a platform for pre-clinical evaluation.

2.2 Materials and Methods

2.2.1 *C. elegans* Strains and maintenance

For *C. elegans* culture and maintenance, the uracil auxotroph *E. coli* strain OP50 was used. The N2 strain of *C. elegans was used as a* wild type strain control. The transgenic *C. elegans* strains express the human wild type SOD1 protein and the $SOD1^{G85R}$ mutant protein in an integrated manner and both transgenes are C-terminally fused to YFP. A pan-neuronal promotor was used to express the proteins in the 302 neurons of a *C. elegans* hermaphrodite. Both strains were created by Prof. Jiou Wang (John Hopkins Bloomberg School of Public Health). The strains are Psnb-1::hSOD1-YFP and Psnb-1::hSOD1G85R-YFP and were a kind gift from the lab of Professor Alan Morgan (University of Liverpool) (Jiou Wang *et al.*, 2009).

The worms were maintained on standard NGM (0.3 % w/v NaCl, 0.25 % w/v bactopeptone, 1.7 % w/v granulated agar, 2.5 % v/v KH_2PO_4 (pH6), 0.1 % v/v $MgSO_4$ (1M), 0.1 % v/v $CaCl_2$ (1 M), 0.1 % v/v cholesterol (5 mg/ml dissolved in ethanol)) containing 200 µl *E.coli* OP50 at 20 °C. Standard NGM agar plates were supplemented with the following additives after autoclaving, 0.5 mM Aldicarb (Sigma-Aldrich), 100 mM Sodium Butyrate NaB (Sigma-Aldrich), 150 µg/ml Trichostatin A (TSA) (Cayman Chemical).

For synchronisation procedures, plates containing plenty of eggs and gravid adult worms were washed with M9 buffer (3 g KH_2PO_4, 6 g Na_2HPO_4, 5 g $NaCl_2$, 1 ml 1 M $MgSO_4$, dH_2O to 1 L) to obtain all worms in a centrifuge tube. Worm pellets were exposed to a 1:1 bleach 4 M NaOH for 5-6 min until the mothers have almost completely disintegrated. The bleach was immediately quenched by making the solution up to 15 ml with M9 buffer. To complete

this wash step the tube was centrifuged at 3000 rpm for 1 min. The wash step was repeated twice and around 200 µl of the re-suspended M9/egg solution was pipetted onto fresh NGM OP50 plates or supplemented NGM OP50 plates.

2.2.1.1 Synaptic transmission assay using aldicarb

NGM plates containing 0.5 mM aldicarb were prepared one day before use and stored at 4 °C. 30-40 L4 stage larvae of strains of interest were picked using a sterile platinum wire and transferred onto fresh NGM plates seeded with OP50 *E. coli* with or without supplements (100 mM NaB or 150 µg/ml Trichostatin A) but not aldicarb. The worms were then incubated at 20 °C for 24 h. Copper rings were then dipped into 70 % ethanol and flamed for a few seconds before placing them onto the 0.5 mM aldicarb containing NGM plate. This will corral worms inside the rings allowing for several genotypes to be assayed on the same plate. 10 µl of OP50 *E. coli* were pipetted into the centre of the ring to keep the worms in this area. 20 day 1 adults of each genotype were transferred to the centre of each ring. The worm transfer was staggered every 3 min so that all 3 phenotypes could be examined within an interval of 10 min. Worms were counted as paralysed and removed from the plate when they failed to move their head even if touch was applied. A Two-Way repeated measures ANOVA applying the Geisser-Greenhouse correction and using a Tukey's post hoc multiple comparison test was used to measure statistical significance.

2.2.1.2 Thrashing assay

Using bleach, worms were age synchronised and time points day 1, 2, 6, and 7 were used to perform this experiment. At each time point 15 worms were tested individually. 200 µl of M9 buffer were pipetted into each well of a 96 well plate. One worm at a time was picked and transferred onto an unseeded plate to remove any OP50 attached to the worm. The worm was then placed into one of the wells and left to settle for 1 min before counting its body bends for 30 seconds. A thrash was characterised when the worm moved its head and tail towards each other. A One-Way repeated measures ANOVA (RM-ANOVA) applying the Geisser-Greenhouse correction and using a Tukey's post hoc multiple comparison test was used to measure statistical significance.

2.2.1.3 Confocal Microscopy of *C. elegans*

C. elegans were grown on either standard NGM OP50 plates or NGM OP50 supplemented with 100 mM of NaB or 150 µg/ml Trichostatin A (TSA). Worms were picked and immobilised using 0.2 % tricaine combined with 0.02 % levamisole in M9 buffer. The anaesthetized worms were then transferred onto an agarose pad on a glass slide. A coverslip was then placed on top of the worms leaving two small gaps along the sides to allow for gas exchange. The slides were viewed under a Zeiss LSM880/Elyra/Axio Observer.Z1 Confocal Microscope (Carl Zeiss Inc.) using the 488 nm argon and the 561 nm DP55 lasers and 60x objective. The image acquisition software used was ZENBlack (Carl Zeiss Inc.) and the image processing software was ZENBlue (Carl Zeiss Inc.). Z-stacks were taken allowing for collection of multiple images across the entire thickness of the worm. Those images can then either be viewed separately or stitched together into a 3D image.

To analyse the measurement of mean fluorescence intensity (MFI) in a region of interest Fiji (Fiji is just ImageJ) was used. Here, focus was laid on the head section of the worms. The control and treated samples were acquired using the same acquisition parameters.

For each worm, a fixed-size square region of interest (ROI) was positioned over the head region and the mean fluorescence intensity was recorded. A second ROI of the same dimensions was used to measure background fluorescence in a nearby region without detectable YFP signal. The background MFI was subtracted from the MFI measured in the head ROI to obtain the background-corrected MFI. The same ROI dimensions were used throughout the analysis to ensure consistency between measurements.

2.2.2 Tissue culture: SH-SY5Y neuroblastoma cell line

2.2.2.1 Maintenance of SH-SY5Y

The human neuroblastoma cell line SH-SY5Y was derived from ATCC (Manassas, US) and maintained in Iscove's Modified Dulbecco's (IMDM; Fisher Scientific, UK) supplemented with 10 % (v/v) foetal bovine serum (FBS; Sigma-Aldrich, Germany), 100 IU/ml penicillin, and 100 µg/ml of streptomycin (Life Technologies, UK; cell culture medium), at 37 °C in a humidified 5 % CO_2 incubator. 70 - 80 % confluent cultures were washed with phosphate-buffered-saline (PBS), detached with 0.05 % w/v aqueous trypsin-EDTA solution (Sigma-Aldrich, Germany), and reseeded at an appropriate ratio into a new flask. To prevent genetic deviation, cell populations were passaged continuously for no longer than five months. Fresh stocks were made from a subpopulation of each cell line from the earliest passage possible.

2.2.2.2 Cell viability assay

Cell viability was measured by (3-(4,5-dimethylthiazol-2-yl)-2,5-diphenyltetrazolium bromide) MTT assay modified after Mosmann (Mosmann, 1983) as previously described (Onafuye *et al.*, 2019). Here, the yellow tetrazole 3-(4,5-dimethylthiazol-2-yl)-2,5-diphenyltetrazolium bromide (MTT; Universal Biologicals UK) is metabolically reduced to purple formazan only in living cells (Mosmann, 1983). 5000 cells /well suspended in 200 µl of cell culture medium were plated in 96-well plates and incubated in the presence of the indicated drug concentrations. The 96-well plates were then incubated at 37 °C for five days or until the max wells had a confluency of 80 %. Then, 25 µl of MTT reagent (2 mg/ml MTT (w/v) in PBS) was added and cells were incubated for 4 hours. Subsequently, the cells were lysed using 200 µl of sodium dodecylsulfate (SDS, Fisher Scientific) buffer (20 % (w/v) SDS in 50 % (v/v) N, N-dimethylformamide, pH adjusted to 4.7 at 37 °C) and incubated overnight. Absorbance was read at 600 nm wavelength in a Victor X4 Multilabel Plate reader (PerkinElmerLife Sciences, USA).

2.2.2.3 Preparation of total cell lysates and immunoblotting

Cells were grown to a confluency of 70 % in TF25 flasks. The cells were washed with ice cold PBS twice after the culture medium was removed and exposed to 100 µl of lysis buffer (50 mM HEPES pH7.4, 250 mM $NaCl_2$, 0.1 % NP40, 1 mM DTT, 1 mM EDTA, 1 mM NAF, 10 mM β Glycerophosphate, 0.1 mM sodium orthovanadate and Complete™ protease inhibitor cocktail (Roche, Switzerland)). The cells were scraped into cold microcentrifuge tubes and

incubated on ice for 30 min before centrifugation at 13,000 rpm for 10 min at 4 °C to remove insoluble material. The lysate was then transferred to a sterile microcentrifugation tube and kept on ice or frozen on dry ice and stored at - 80 °C. Protein concentrations were determined by sodium salt Bicinchoninic acid (BCA) method. 30 µg/well of proteins were separated on 4 - 12 % SDS-polyacrylamide gels and transferred to PVDF membranes (Thermo Fisher). The PVDF membranes were placed in blocking solution (5 % w/v dried skimmed milk (Oxoid) and PBS (Phosphate Buffered Saline)) for 45 mins with rotation at room temperature followed by incubating in blocking solution containing the rabbit polyclonal Histone H4 (Acetylated) primary antibody (Bio-Rad, Cat# AHP418) in a 1/800 dilution overnight at 4 °C. The following day, membranes were washed with PBS/T (Phosphate Buffered Saline and 0.2 % Tween 20 (Sigma)) before being exposed to the horse-radish peroxidase conjugates anti-rabbit secondary antibody (1/10000) for 45 mins at room temperature and further washed 6x with PBS/T. The immunoreactivity was visualised using Enhanced Chemiluminescence (ECL) using a SynGene gel doc. To analyse the blots the GeneSys Software (Version 1.6.5.0) was used and a Synoptics 6MP camera was used to capture the images. The programme Fiji (ImageJ) version (2.1.0/1.53c) was used to normalise to the control by calculating the integrated intensity of the protein band which was then divided by the integrated intensity of the loading control band of anti-alpha-tubulin anti mouse (Sigma-Aldrich).

2.2.2.4 Transfection

We generated transfected SH-SY5Y cells containing $Sod1^{mut}$ using the Ionza nucleofector tool kit. The transfected cells were selected using G418 in cell culture medium. All transgenes are C-terminally fused to GFP and a pAcGFP1-N1 vector backbone was used.

The Lonza Amaxa® Cell Line Nucleofector® Kit V and the amaxa nucleofector® II transfection device was used to transfect the cell line SHSY5Y. Pre-nucleofection procedures were followed per manufacturer's instructions for SH-SY5Y cells: the media was changed twice a week, and cells were passaged as normal at 75 - 80 % confluency. Cells were seeded out at 2 x 10^5 cells/cm^2. Cells were again grown to 75 - 80 % confluency. Medium was then removed from the cultured cells and washed once with PBS. The cells were then trypsinised as usual for about 5 min at 37 °C. The trypsin was inactivated with cell culture medium once the cells had detached. For one nucleofection sample, 1-2 x 10^6 cells, 2 µg plasmid DNA, and 100 µl Cell Line Nucleofector® Solution V were needed. T75 cell flasks containing 400 µg/ml G418 in cell culture medium were prepared and pre-incubated in a humidified 37 °C/5 % CO_2 incubator. 1-2 x 10^6 cells were centrifuged at 90 xg for 10 min at room temperature. After removal of the supernatant, the pellet was resuspended in 100 µl Nucleofector® Solution. Combining 100 µl of this cell suspension with 2 µg plasmid DNA, the cell/DNA mix was transferred into certified cuvettes. The Nucleofector® Program A-023 was used for high viability. 500 µl of pre-warmed medium was added immediately after transfection and the whole sample was transferred either into the pre-equilibrated cell flasks or chambered cover slips in the 37 °C/5 % CO_2 incubator. Cells were analysed after 4 and 24 h post transfection. Transfected cell lines were maintained in Neomycin (select with G418). The plasmids used for transfection are provided in Table 1.

TABLE 1 LIST OF PLASMIDS USED FOR TRANSFECTION

Product Ref	Product	Supplier	Vector type	Selectable Marker
26407	pF146 pSOD1WTAcGFP1	Addgene Inc	Mammalian Expression	Neomycin (select with G418)
26408	pF147 pSOD1A4VAcGFP1	Addgene Inc	Mammalian Expression	Neomycin (select with G418)
26410	pF149 pSOD1G85RAcGFP1	Addgene Inc	Mammalian Expression	Neomycin (select with G418)
26411	pF150 pSOD1G93AAcGFP1	Addgene Inc	Mammalian Expression	Neomycin (select with G418)
26409	pF148 pSOD1G37RAcGFP1	Addgene Inc	Mammalian Expression	Neomycin (select with G418)

2.2.2.7 Widefield microscopy

After transfection, cells transferred into a chambered cover slip with 8 individual wells and high walls for cell culture (ibidi) were left untreated or 5 mM NaB or 1 mM VPA treatment was added. Cells were incubated for 24 h before being analysed using widefield microscopy. Images were captured using an Olympus IX81 fluorescence microscope using either GFP filter set (395/509 excitation/emission) or using DIC at 100x magnification using an Andor Xyla 4.2 CMOS digital camera.

2.3 Results

2.3.1 The impact of Butyrate supplementation on SOD1-mediated motor defects in an ALS *C. elegans* model

Short-chain fatty acids (SCFAs, including acetate, propionate and butyrate) are generated in the colon through bacterial fermentation of dietary fibres and starch. It has been reported that ALS patients lack butyrate-producing bacteria (Niccolai *et al.*, 2021) and that butyrate supplementation could improve motor function in a mouse model of ALS (Zhang *et al.*, 2017).

We sought to determine the effects of sodium butyrate (NaB) supplementation in a *C. elegans* model of ALS. We conducted a thrashing assay in untreated and NaB treated transgenic animals to provide the first insights into its effect on Sod1 or Sod1^{G85R} induced motor defects in a *C. elegans* model of ALS.

As reported in previous studies (Jiou Wang *et al.*, 2009; Baskoylu *et al.*, 2018), it was noted that both h:Sod1 or h:Sod1G85R overexpression led to decreased thrashing frequencies over a 7 day time-course, when compared to the wildtype N2 worm (Figure 1A). The h:Sod1G85R overexpression animals had the most severe thrashing impairment compared to both strains and would curl up or only move their head when gently prodded instead of moving freely in a sinusoidal pattern seen in the wild type N2 and h:Sod1 overexpression worms (Jiou Wang *et al.*, 2009; Baskoylu *et al.*, 2018).

To determine the effects of NaB activity three separate thrashing assays experiments were devised (Figures 1B-D).

In the first instance worms were grown and eggs transferred onto either NGM or NGM NaB supplemented plates. This meant that the synchronised embryos transferred onto butyrate plates were exposed to NaB from hatching and throughout development (Figure 1B). NaB supplementation had no significant effect on the thrashing activity of the N2 wild type strain (Figure 1B). The thrashing defect phenotype observed in both h:Sod1 and h:Sod1G85R overexpression animals could be rescued by around 30 % and 50 %, respectively, when grown on 100 mM NaB supplemented plates. A significant difference in thrashing behaviour was still observed when h:Sod1 and the mutant h:Sod1G85R NaB treated cells were compared to the wild type strain, suggesting a partial rescue of motor activity (Figure 1 B). In addition, the mobility issues shown by h:Sod1 and h:Sod1G85R worms was also markedly improved when supplemented with NaB (link to MP4's held in Kent Academic Repository: http://doi.org/10.22024/UniKent/01.01.604).

Following this we cultivated the animals on standard NGM OP50 plates from hatching until they reached their L4 larvae stage. The animals were then transferred onto NaB supplemented plates prior to assessing thrashing activity (Figure 1C). In this experiment the transgenic animals were only exposed to NaB from early adulthood. We could identify a slight variation in thrashing behaviour between the NaB-treated N2 (Figure 1C) and the untreated N2 control (Figure 1A) on the 3rd (p value: 0.0143) and the 6th (p value: 0.0024) day of the experiment. Here, the NaB-treated N2 strain showed a slightly higher thrashing frequency than the untreated N2 animals on days 3 and 6 (Figure 1 A, C). NaB-treated h:Sod1 overexpression animals showed a partial thrashing phenotype rescue (Figure 1C) and on days 6 and 7 these animals behaved almost coequal to the untreated N2 control (Figure

1 A, C). We could identify a about a 50 % phenotype rescue in h:Sod1G85R overexpression animals, albeit with a slight delay compared to the first experiment (Figure 1 A-C) where animals were exposed to NaB since hatching. However, on days 6 and 7 the transgenic mutant NaB-treated h:Sod1G85R worms behaved almost coequally to the untreated N2 control (Figure 1 A, C).

In the third thrashing experiment (Figure 1 D), transgenic L4 larvae were cultivated on NaB supplemented plates for one generation and then transferred back onto untreated NGM plates. We found that sudden NaB withdrawal reversed the rescue effects in both h:Sod1 and h:Sod1G85R overexpression animals. However, interestingly the h:Sod1G85R animals showed a slight increase in thrashing frequency much alike the h:Sod1 overexpression animals (Figure 1 D).

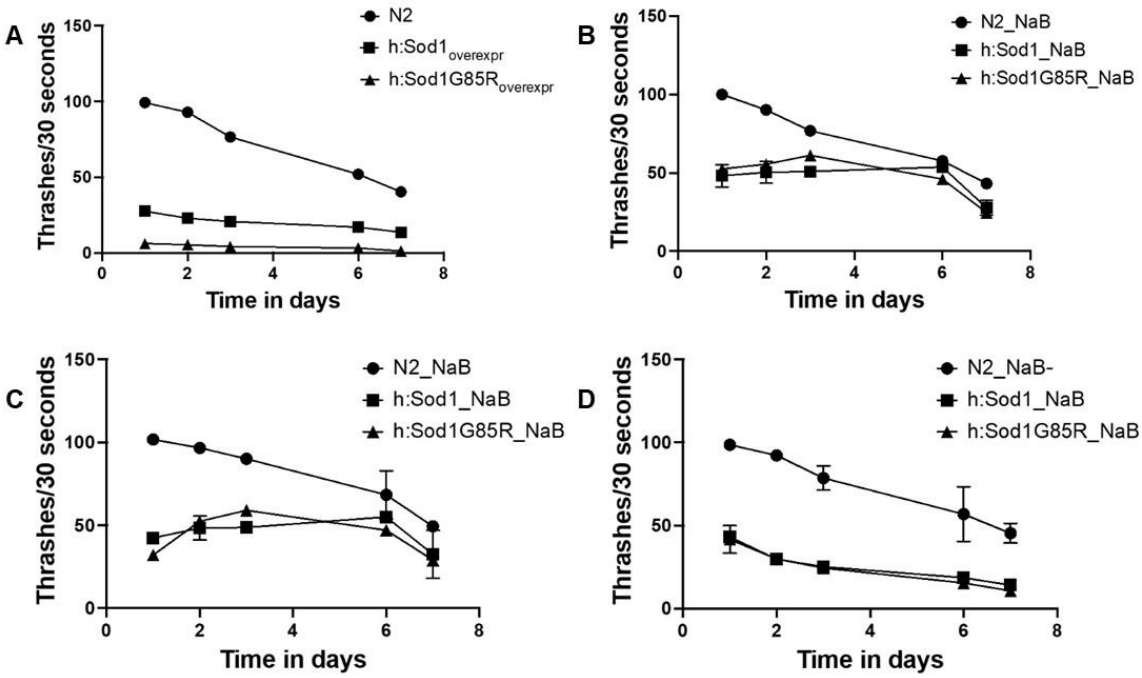


Figure 1 Thrashing assay showing the effect of NaB and NaB withdrawal on transgenic ALS C.elegans strains.
The body bends of 15 worms in liquid medium (M9 media) was recorded at 30 seconds intervals for each strain on days 1, 2, 3, 6 and 7. Age synchronisation was performed prior to the experiment by picking 100 L4 larvae per strain and per plate. Transgenic strains were compared to the standard N2 strain. The experiment was carried out in triplicates and the data represented displays an average of the three biological repeats. The error bars indicate the standard deviation. A One-Way repeated measures ANOVA (RM-ANOVA) applying the Geisser-Greenhouse correction and using a Tukey's post hoc multiple comparison test was used to measure statistical significance.
A) Thrashing curve of untreated animals.
B) Thrashing curve of 100 mM NaB exposure since hatching.
C) Thrashing curve of 100 mM NaB exposure since early adulthood.
D) Thrashing curve of 100 mM NaB withdrawal after 1 generation.

2.3.2 Investigating the impact of the SCFA Butyrate and Histone deacetylase inhibitor (HDAC inhibitors) supplementation on SOD1-mediated neuromuscular junction (NMJ) dysfunction

NMJ dysfunction is a common symptom in the early stages of ALS (Fischer *et al.*, 2004). We therefore sought to examine NMJ function in a *C. elegans* model of ALS and the effects of NaB upon this. In addition, as NaB is a known HDAC inhibitor, we examined whether the

well-characterised HDAC inhibitor Trichostatin A (TSA) had similar effects. Locomotion in *C. elegans* is exerted through excitatory motor neurons releasing acetylcholine and inhibitory motor neurons which release GABA y-aminobutyric acid (Richmond and Jorgensen, 1999; Zhen and Samuel, 2015). Thus, cholinergic motor neurons will release acetylcholine activating acetylcholine receptors located on muscles exciting them. Conversely, the break-down of acetylcholine is performed by acetylcholinesterase in the synaptic cleft terminating neurotransmission and thus muscle contraction. NMJ function can be studied in *C. elegans* using aldicarb which inhibits acetylcholinesterase, causing acetylcholine accumulation in the synaptic cleft of the NMJ. Inhibiting acetylcholinesterase by aldicarb application causes continuous muscle contraction and dysfunction of the NMJ can be determined by either aldicarb resistance or sensitivity. Typically, low synaptic transmission is correlating to increased aldicarb resistance whilst increased synaptic transmission may be characterised by increased aldicarb sensitivity or faster paralysis (Rand, 2007).

Multiple studies have shown that butyrate can act as an HDAC inhibitor (Candido, 1978; Vidali *et al.*, 1978; Donohoe *et al.*, 2014; Pascale *et al.*, 2018; Chen, Zhao and Vitetta, 2019). HDAC is the enzyme responsible for catalysing the removal of acetate from modified lysine residues at the N-terminal region of histones H2A, H2B, H3 and H4 which form a histone octamer core (Luger *et al.*, 1997). Preventing the removal of acetyl groups from lysine residues on histone and non-histone proteins leaves the DNA more tightly bound (compaction of chromatin) as the lysine residues retain their positive charge thus preventing gene transcription (Davie, 2003). However, this affects only the expression of about 2 % of mammalian genes (Davie, 2003) and the precise mechanism remains unclear.

The antifungal antibiotic Trichostatin A (TSA) is derived from *Streptomyces* and is a selective class I and II histone deacetylase (HDAC) inhibitor. Furthermore, TSA inhibits the cell cycle in eukaryotes and induces morphological reversion in transformed cells (Hsu *et al.*, 2019).

We observed that 100 % of wild type worms achieved paralysis within 3 h when exposed to aldicarb (Figures 2A-D). The pattern of paralysis adopted a sigmoidal curve, suggesting that worms within a population may react differently to aldicarb exposure. Interestingly, although all animals were paralysed with 3 h, the treatment of wild type with NaB led to a reduction in aldicarb sensitivity within part of the population (Figure 2A-2D). We could confirm that both transgenic ALS strains overexpressing either h:Sod1 or h:Sod1G85R showed NMJ dysfunction when compared to the wild type (Figure 2A and 2B). We found that the h:Sod1 and h:Sod1G85R transgenic strains were more aldicarb sensitive, achieving paralysis in 100 % of the population within 120 and 100 mins respectively (Figures 2A and 2B).

Treatment of h:SOD1 or h:SOD1G85R with NaB led to a wild type aldicarb resistance profile (Figure 2A and B) suggesting a rescue of the observe NMJ defect. Treatment of wild type *C. elegans* with 150 µg/ml TSA led to no difference in aldicarb sensitivity (Figure 2C and D). However TSA supplementation led to a rescue in NMJ function in transgenic animals overexpressing either human h:Sod1 or h:Sod1G85R that mirrored the wild type aldicarb response (Figure 2C and D).

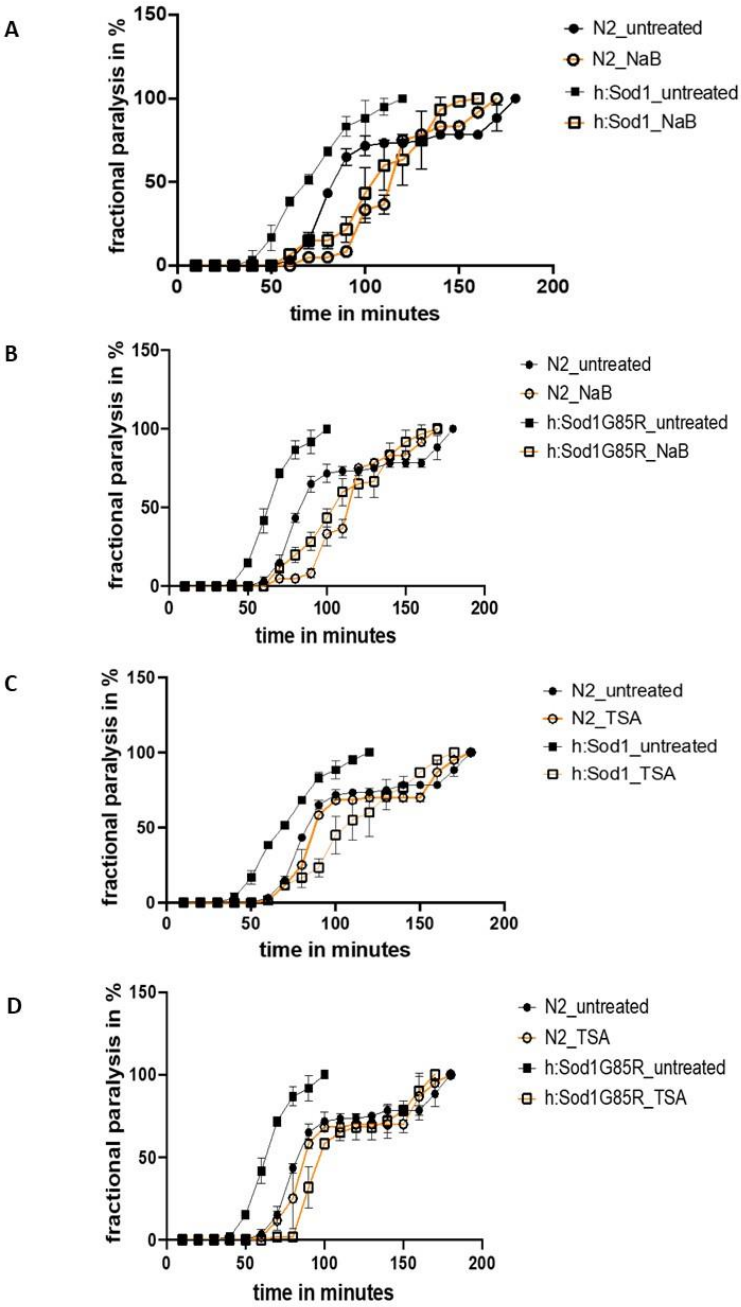


Figure 2 Aldicarb-response curves of wild type N2 and transgenic animals overexpressing human Sod1 or Sod1G85R after 100 mM NaB or 150 µg/ml Trichostatin A (TSA) treatment.
The control worms were grown on standard NGM OP50 plates and synchronised with the NaB or TSA plates. Age synchronisation was also performed prior to the experiment by picking 100 L4 larvae per strain and per plate. The experiment was carried out in triplicates and the data represented displays an average of the three biological repeats. The error bars indicate the standard deviation. A Two-Way repeated measures ANOVA applying the Geisser-Greenhouse correction and using a Tukey's post hoc multiple comparison test was used to measure statistical significance.
A-B) Aldicarb response curves after NaB exposure for transgenic h:Sod1 and h:Sod1G85R animals.
C-D) Aldicarb-response curves after TSA treatment for transgenic h:Sod1 and h:Sod1G85R animals.

2.3.3 The Effect of NaB and TSA exposure on h:Sod1 and h:Sod1G85R aggregation in C. *elegans*

The effects of Sod1 stability and aggregation on cellular dysfunction and in the promotion of ALS pathology is well documented. As we had observed a significant improvement in motility and NMJ function we sought to investigate whether NaB and TSA exposure had an effect on h:Sod1 and h:Sod1G85R aggregation. We therefore carried out confocal microscopy to measure fluorescence intensity of YFP-labelled h:Sod1 or h:Sod1G85R animals in transgenic animals.

The overexpression of h:Sod1 and h:Sod1G85R *C. elegans* led to visible aggregation as has been previously reported (Jiou Wang *et al.*, 2009; Baskoylu *et al.*, 2018). Clear aggregation of h:Sod1 and h:Sod1G85R were visible in the head ganglia and ventral cord (Figure 3 A-C). Upon 24 h of exposure with NaB we observed a significant and reproducible reduction in aggregate formation animals expressing either h:Sod1 or h:Sod1G85R (Figure 3 A-C). A significant reduction in Sod1 and Sod1G85R aggregate formation was also observed following exposure to TSA. However, the effect of TSA was not more pronounced than that of NaB. (Figure 3A-C).

The observed differences in fluorescence intensity are consistent with changes in SOD1 aggregation; however, it is important to consider that differences in total SOD1 protein abundance could also contribute to the observed fluorescence signal. Therefore, confirmation that SOD1 protein levels are comparable between conditions will be important to determine whether the differences observed reflect changes in aggregation rather than differences in overall SOD1 abundance.

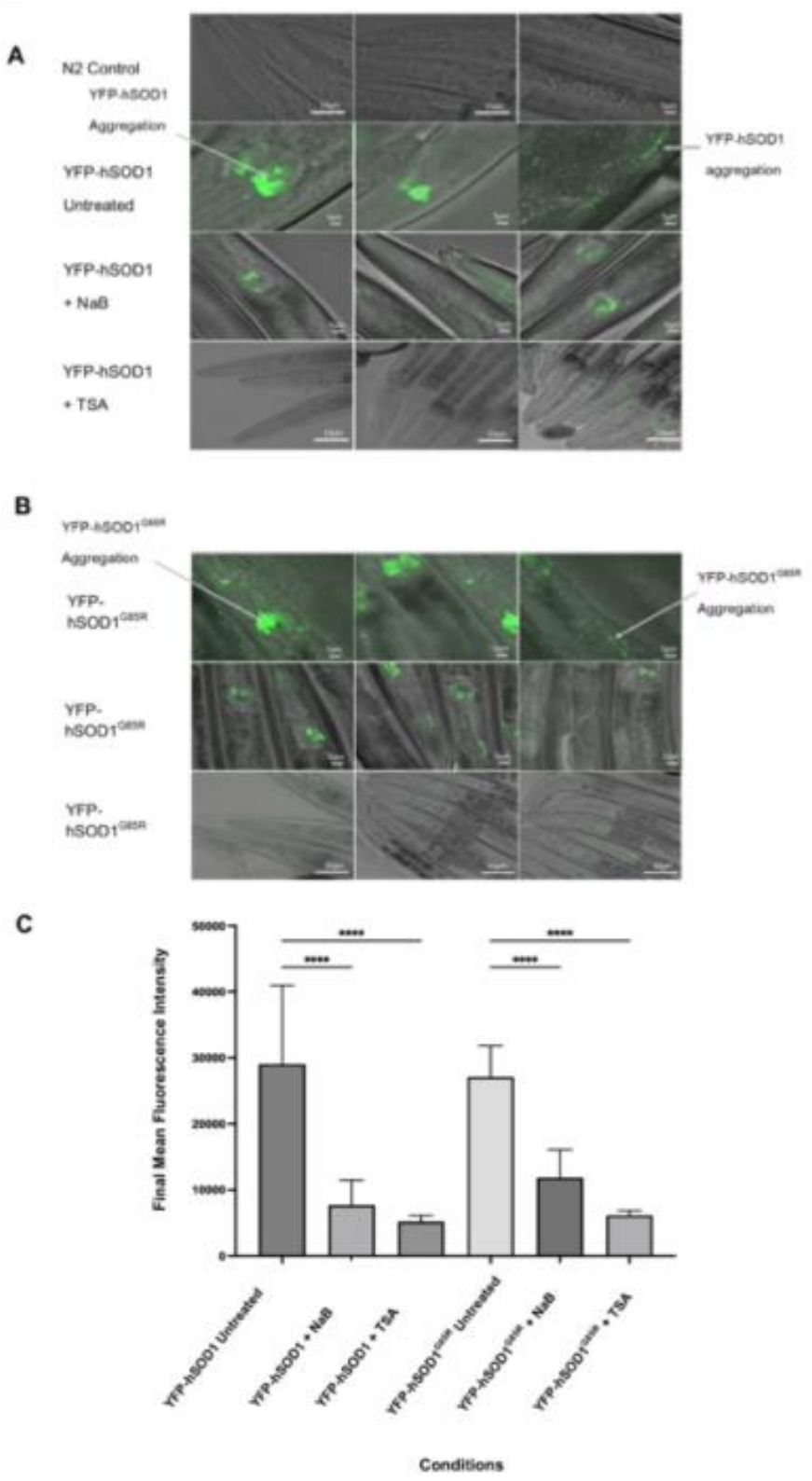


Figure 3 Effects of NaB and TSA on SOD1 aggregation in C. elegans. Confocal images and MFI of transgenic hSOD1 and hSOD11^{G85R}. C. elegans grown with and without supplementation of 100mM NaB or 150µg/mL trichostatin A (TSA). (A–B) Confocal images of untreated and NaB or TSA-treated animals. (C) Mean fluorescence intensity (MFI) of YFP-hSOD1 and YFP-hSOD1^{G85R} expression. Each graph represents an average of three biological repeats (n = 10). The error bars display the standard deviation. A one-way ANOVA using a Tukey multiple comparison test was used to determine statistical significance. (*) flags levels of significance compared with the untreated strains.

2.3.4 The Effect of NaB and histone deacetylase inhibitor VPA on mutated Sod1 aggregation in the neuroblastoma cell line SH-SY5Y

Our results demonstrate that NaB and TSA treatment can prevent Sod1 and Sod1G85R aggregation and the resultant motor defects in *C. elegans*. To further investigate this finding, we tested the effects of NaB and the HDAC inhibitor Valproic acid on SH-SY5Y cells expressing a range of Sod1 mutants that have been linked to ALS. We first performed MTT assays to identify non-toxic working concentrations for both NaB and VPA in SH-SY5Y cells, using NaB and VPA concentrations ranging from 0.07 - 5 mM. 1 mM was selected for VPA and 5 mM for NaB as non-toxic working concentrations showing minimal effect on viability.

We hypothesised that Sod1 aggregation inhibition may occur as a result of HDAC inhibition. We therefore examined whether the selected concentrations of 1 mM and 5 mM for VPA NaB respectively demonstrated HDAC inhibition in a western blot analysis to detect H4 acetylation (Figure 4). The western blot was performed using a rabbit polyclonal anti-acetylated histone H4 antibody (AHP418, Bio-Rad). The antibody was raised against the tetra-acetylated form of histone H4 and recognizes acetylated isoforms of histone H4 (Bio-Rad). Both 24 h 5 mM NaB and 1 mM VPA treatment significantly increased the intensity of the acetylated H4 signal in SH-SY5Y cells compared with the untreated control (Figure 4B, C). The immunoblot showed a predominant band corresponding to the expected molecular weight of histone H4, alongside additional higher- or lower-molecular-weight immunoreactive bands that may represent different H4 isoforms or other antibody-reactive species. These results suggest an increase in H4 acetylation following NaB and VPA treatment; however, changes in total H4 protein abundance could also contribute to the

increased signal. Therefore, in the absence of normalisation to total histone H4, the results are interpreted as an increase in acetylated H4 signal rather than definitive evidence of increased H4 acetylation.

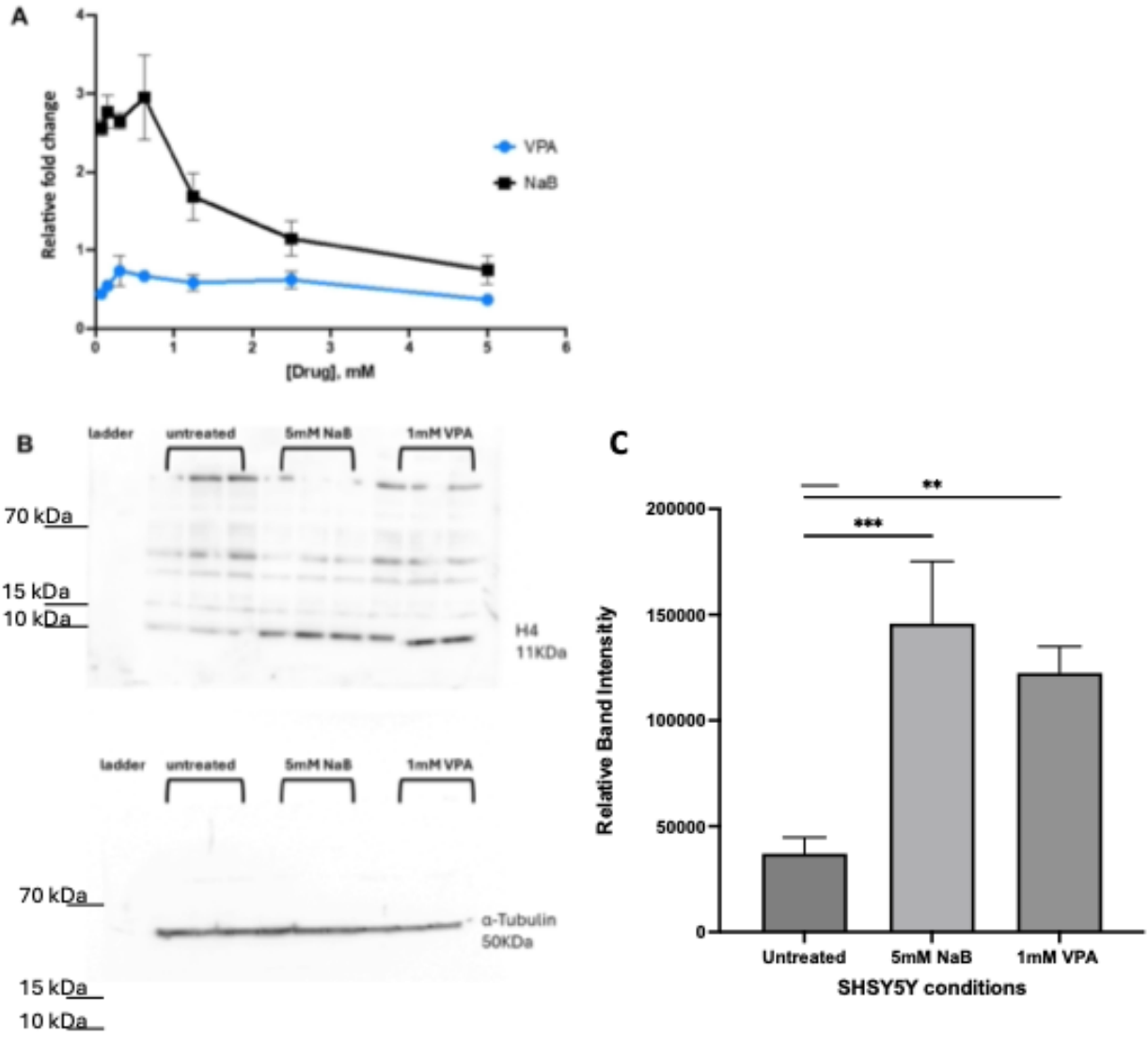


Figure 4 Effects of NaB and VPA on GFP tagged SOD1 and SOD1A4V aggregation in SH-SY5Y cells.
A) Dose-response curve of NaB and VPA in SH-SY5Y testing concentrations ranging from 0.07-5 mM in a MTT assay.
B) A western blot showing the detection of H4 in SH-SY5Y cells after 5 mM NaB or 1 mM VPA treatment after 24 h.
C) A bar chart representing the change in H4 acetylation relative to α-tubulin loading control in SH-SY5Y following exposure to either 1mM VPA or 5mM NaB for 24h. Uniform protein loading was ensured by probing levels of α-tubulin after probing for H4. The bar chart and dose-response curve represent an average of three biological repeats. The error bars display the standard deviation. A One-Way ANOVA using a Tukey multiple comparison test was used to determine statistical significance. (*) flags levels of significance compared to the untreated cells.

We then investigated the effect of 5 mM NaB and 1 mM VPA on Sod1 aggregation. We conducted widefield microscopy after incubating Sod1 or Sod1^{mut} transfected SH-SY5Y cells for 24 h with either 5 mM NaB or 1 mM VPA (Figure 5, 6). As expected, untreated and 5 mM NaB-treated WT-SOD1 expression in SH-SY5Y cells led to a diffused and cytoplasmic localisation of SOD1 (Figure 5). 1 mM VPA treatment showed minimal SOD1 aggregations after 24 h (Figure 5). Untreated SOD1A4V expressing SH-SY5Y cells showed many SOD1A4V aggregations which could be significantly reduced and a more WT-like SOD1 distribution could be achieved after 5 mM NaB or 1 mM VPA treatment (Figure 5).

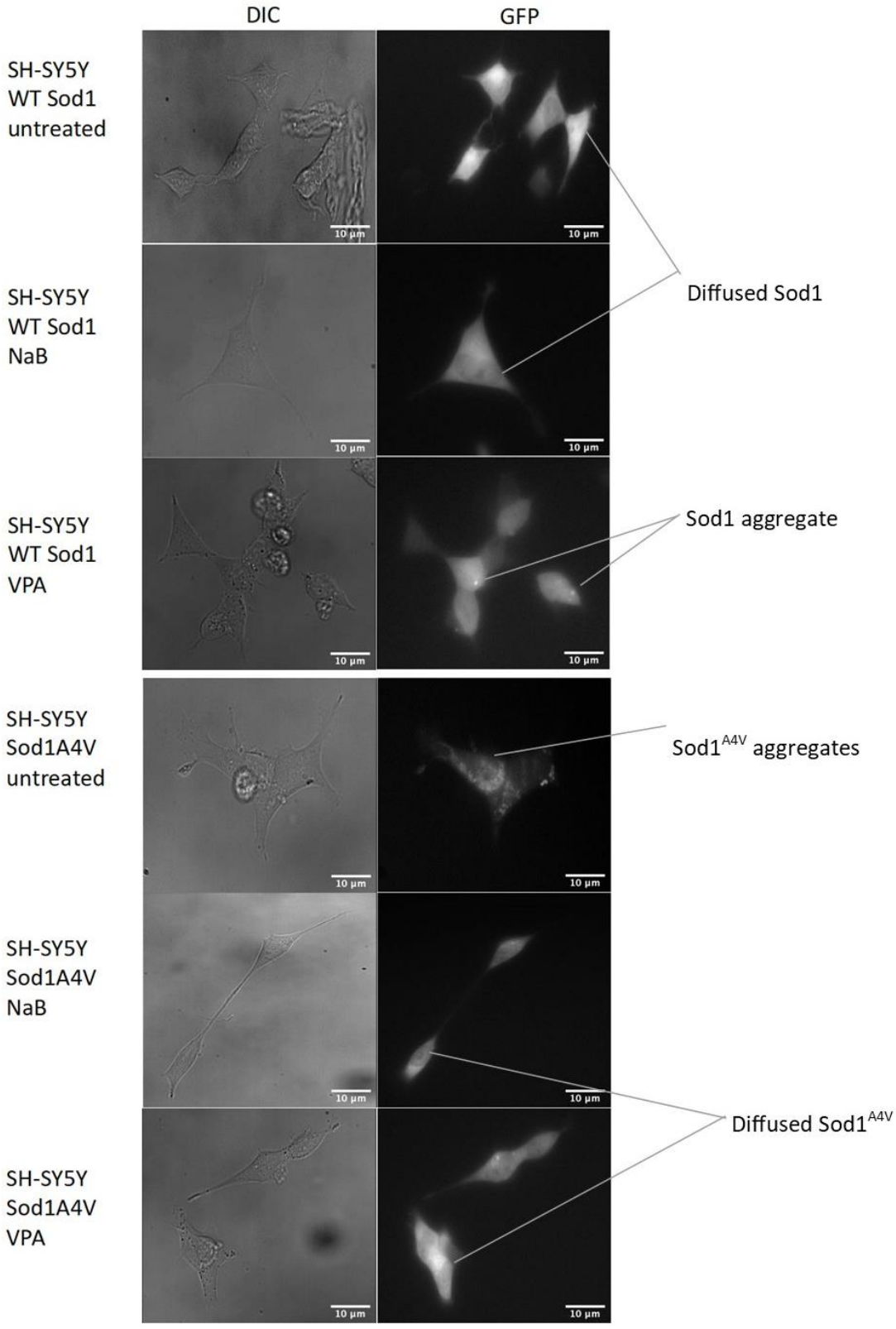


Figure 5 Widefield DIC and GFP images of Sod1 and Sod1^{A4V} transfected SH-SY5Y before and after 5 mM NaB or 1 mM VPA incubation.
Cells were incubated in standard IMDM media supplemented with G418 to select for successfully transfected cells. The cells were then incubated with either 5 mM NaB or 1 mM VPA for 24 h. The slides were viewed under an Olympus 1X81 inverted microscope and 60x objective.

Untreated SOD1G85R expressing SH-SY5Y cells showed mutant SOD1 aggregates. This could be completely reversed after NaB and VPA treatment (Figure 6). High levels of mutant SOD1 aggregation could be detected in untreated SOD1G37R expressing SH-SY5Y cells (Figure 6). However, after NaB or VPA treatment cytoplasmic diffused mutant SOD1 localisation was seen (Figure 6).

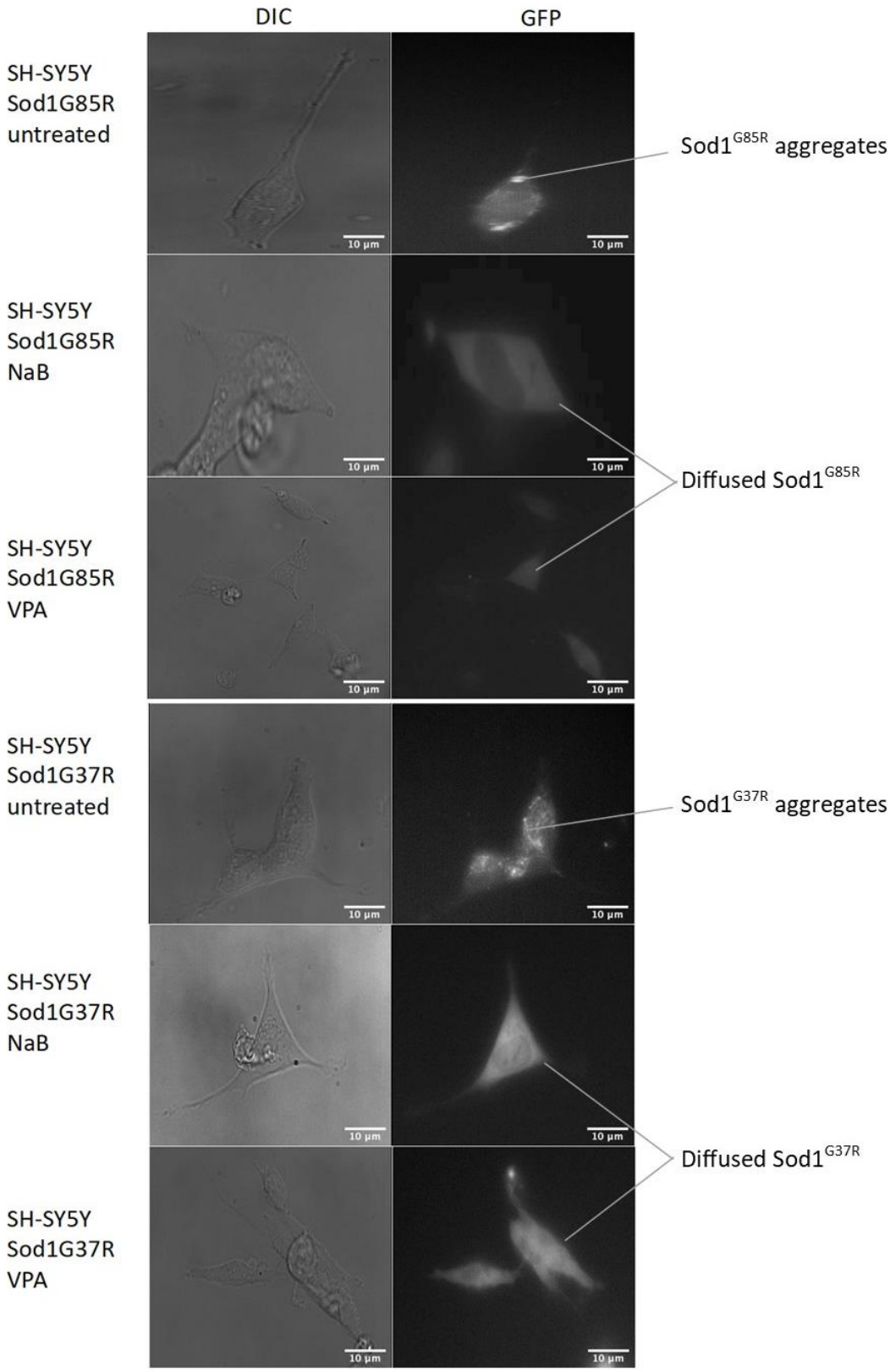


Figure 6 Widefield DIC and GFP images of Sod1^{G85R} and Sod1^{G37R} transfected SH-SY5Y before and after 5 mM NaB or 1 mM VPA incubation.
Cells were incubated in standard IMDM media supplemented with G418 to select for successfully transfected cells. The cells were then incubated with either 5 mM NaB or 1 mM VPA for 24 h. The slides were viewed under an Olympus 1X81 inverted microscope and 60x objective.

2.4 Discussion

In the present study we sought to further investigate the impact of butyrate and HDAC inhibitors such as TSA and VPA on Sod1-mediated toxicity in ALS. We made use of two systems: *C. elegans* to investigate the linkage of the gut microbiome to ALS, and the neuroblastoma cell line SH-SY5Y allowing us to further our findings in a human-derived model.

2.4.1 Supplementation of butyrate and the HDAC inhibitor TSA can improve Sod1-mediated motor defects and Sod1-mediated neuromuscular junction dysfunction in *C. elegans*

Hallmarks of the neurodegenerative disease ALS are progressive loss of motor neurons responsible for e.g. walking, eating, and breathing resulting in paralysis and death (Brown and Al-Chalabi, 2017), and NMJ dysfunction in early stages of ALS (Fischer *et al.*, 2004). In our study we could confirm the findings of (Jiou Wang *et al.*, 2009) where locomotor defects and paralysis in both human SOD1 and human mutant SOD1 G85R could be reported albeit to a lesser extent in the human SOD1 overexpressing strain in *C. elegans*. The distinct motor defective phenotype of the G85R strain (Figure 1B) suggests a mutant protein specific paralysing effect. We could also confirm that both transgenic ALS strains overexpressing either human SOD1 or human mutant SOD1 G85R show NMJ dysfunction (Baskoylu *et al.*, 2018). However, in our study the transgenic strains were more aldicarb sensitive than non-transgenic wild type *C. elegans*, achieving paralysis in 100 % of the population within 120 and 100 mins respectively (Figures 2A and 2B).

This is different to the findings by (Baskoylu *et al.*, 2018), who reported stronger resistance to aldicarb compared to the non-transgenic wild type N2. We also noticed an overall sensitivity to 1 mM aldicarb, so we had to adjust the concentration to 0.5 mM. Strain dependent differences could be a potential reason for the different findings and a direct comparison would be needed to be made with the strains from the Baskoylu study and the ones we used to investigate further.

Furthermore, in our study we could show that supplementation of butyrate or the HDAC inhibitor TSA was able to rescue both Sod1 protein aggregation and the locomotor and NMJ defects in *C. elegans*. This may suggest that butyrate acts as an HDAC inhibitor to exert protective functions in neurons.

The reversible actions of histone acetylation and deacetylation catalysed by histone acetyl transferases (HATs) and histone deacetylases (HDACs), respectively, are pivotal in gene regulation, crucial for cell proliferation and differentiation (Icardi, De Bosscher and Tavernier, 2012; Rousseaux and Khochbin, 2015). Gene activation is accelerated through hyperacetylation of N-terminal of histones H3 and H4 whereby transcriptional repression is regulated through deacetylation (Strahl and Allis, 2000). Homeostasis of these opposing enzymatic actions is often imbalanced in diseases such as cancer and neurodegenerative diseases (Rouaux, 2003; Fraga *et al.*, 2005). In neurodegenerative illnesses homeostasis in histone acetylation tends towards hypoacetylation (Saha and Pahan, 2006). To date eighteen mammalian HDACs have been characterised and grouped into four classes. Classical HDACs are Class I, II, and IV and are zinc-dependent whilst Class III HDACs are NAD-dependent. Class III HDACs share similarities to yeast SIR2 and are also called sirtuins, SIRT 1-7 are mainly involved in metabolism, stress response and ageing regulative mechanisms

(Michan and Sinclair, 2007; Wiech *et al.*, 2009). HDAC inhibitors lead to the prevention of the removal of acetyl groups from lysine residues on histone and non-histone proteins. This generally means that DNA exists in a more tightly bound state (compaction of chromatin) as the lysine residues retain their positive charge thus preventing gene transcription (Davie, 2003). Structurally, HDAC inhibitors can be grouped into four groups: hydroxamates, cyclic peptides, aliphatic acids, and benzamides (Kim and Bae, 2011). The antifungal Trichostatin A (TSA) is a selective HDAC inhibitor of Class I and II HDACs (Vanhaecke *et al.*, 2004). TSA can cease the cell cycle and controls gene expression (Zhang *et al.*, 2012). Valproic acid or VPA is an established drug used in epilepsy treatment and is well tolerated, however, may cause birth defect if given during early pregnancy (Nau, Hauck and Ehlers, 1991; Gottlicher, 2001; Phiel *et al.*, 2001). However, VPA is also considered a novel class of HDAC inhibitor inducing differentiation of carcinoma cells (Gottlicher, 2001; Phiel *et al.*, 2001).

The impact of the microbiome on ALS disease onset and progression has been subject of discussion for several years: Several studies have shown that gut health is linked to brain pathology providing evidence of a two-way communication system called the gut-brain axis important in many neurodegenerative diseases (Carabotti *et al.*, 2015; Ryman *et al.*, 2023). Gut dysbiosis and a general alteration and imbalance of the gut microbiome could be observed in both human ALS patients and animal models (Toepfer, C Folwaczny, A Klauser, RL, 2000; Blacher *et al.*, 2019; Burberry *et al.*, 2020; Boddy *et al.*, 2021; Parra-Cantu *et al.*, 2021; Samara *et al.*, 2021). A study conducted in mice showed that microbiota composition may limit neurodegenerative microglia which are the primary immune cells in the central nervous system and thus influence ALS disease progression. This study also reported that antibiotics usage decreases butyrate-producing bacteria (Cox *et al.*, 2022). Another pre-clinical mice study showed that changes in the gut microbiome occur at early stages in

SOD1^{G93A} animals which subsequently displayed muscle atrophy, motor dysfunction and activation of immune cells in the nervous system (Figueroa-Romero *et al.*, 2019). Compared to healthy individuals, human ALS studies report that the gut microbiome of ALS patients differs immensely in terms of increased abundance of various pathobionts rather than bacterial phyla e.g. *Firmicutes* which are beneficial to healthy metabolic function (Zhai *et al.*, 2019; Goutman *et al.*, 2022; Guo *et al.*, 2024). Furthermore, human ALS gut microbiota studies reported deficiency in butyrate-producing microbes (Fang *et al.*, 2016; Nicholson *et al.*, 2021). Another study showed that ALS patients lacked microbial enzymes thus decreasing the activity of metabolic pathways such as carbon and butyrate metabolism (Hertzberg *et al.*, 2022).

Butyrate is one of the main SCFA generated through fermentation of dietary carbohydrates and fibres, starch and some endogenous proteins by bacteria residing in the proximal colon. Around 60 - 70 % of the energy requirements of epithelial cells of the colon are provided by SCFA (Canani, 2011; Brahe, Astrup and Larsen, 2013; P. Fan *et al.*, 2015; Ma *et al.*, 2017).

SCFAs are crucial for the protection and maintenance of the gut health but also for energy supply for epithelial cells. SCFAs such as acetate or butyrate may modulate the guts immune system and prevent pathogens from breaking through the epithelial barrier by making it less permeable (den Besten *et al.*, 2013).

Although not thoroughly comprehended yet, it is known that SCFAs bind to G-protein-coupled receptors (GPCRs) such as the free fatty acid receptors FFAR2 and FFAR3, the hydrocarboxylic acid receptor GPR109a/HCAR2, and GPR164. These receptors are widely expressed in cells from both the gastrointestinal mucosa and the immune and nervous systems (Bolognini *et al.*, 2016; Mohajeri *et al.*, 2018).

Inhibition of histone deacetylase (HDAC) activity is another mechanism SCFA may act on systemic functions and could be found in gut and immune tissue (Kien *et al.*, 2008) as well as in the peripheral and central nervous system (Stilling *et al.*, 2016). Neuroinflammation and activation of microglia play an important role in many neurodegenerative diseases (Silva, Bernardi and Frozza, 2020; Caetano-Silva *et al.*, 2023): Several studies showed that butyrate acts on inflammatory microglia and decreases pro-inflammatory cytokines secretion through HDAC inhibition (Patnala *et al.*, 2017; P. Wang *et al.*, 2018; Reddy *et al.*, 2018; Yamawaki *et al.*, 2018; Silva, Bernardi and Frozza, 2020; Caetano-Silva *et al.*, 2023). Studies in Parkinson's disease revealed that structural changes in gut microbiota and sodium butyrate administration may ameliorate motor malfunctioning and deficiency in dopamine levels (St. Laurent, O'Brien and Ahmad, 2013; Sharma, Taliyan and Singh, 2015; Liu *et al.*, 2017; Paiva *et al.*, 2017; W. Li *et al.*, 2017; Sun *et al.*, 2018).

The many and sometimes contradictory effects of butyrate are all dependent on its physiological concentrations that appear to form as a gradient along the lumen-to-crypt axis and the proximal-distal axis in the lumen (Csordas, 1996; Sengupta, Muir and Gibson, 2006). Mice studies showed that administration of high levels of butyrate (40 mM or 200 mM) were safe to use (Andrusaite *et al.*, 2024; Ma *et al.*, 2024). They also showed that whilst low butyrate concentrations (1 mM) may promote lung cancer cell proliferation, higher butyrate concentrations (5 mM) may supress lung cancer cell proliferation (Ma *et al.*, 2024). In immune responses e.g. via conventional dendritic cells (cDC) butyrate at a low concentration (0.5 mM) acts as a HDAC inhibitor preventing cDC development and thus their ability to prime T-cells (Andrusaite *et al.*, 2024). In humans butyrate administered orally or using enemas at concentrations of 100 mM or more has been used as a treatment in colonic inflammation patients (Scheppach *et al.*, 1992; Lührs *et al.*, 2002; Vernia *et al.*,

2003; HAMER *et al.*, 2007; Hamer *et al.*, 2010) suggesting butyrate potential as a therapeutic approach.

2.4.2 Addition of Butyrate and HDAC inhibitors TSA and VPA can clear Sod1^{mut} aggregations in *C. elegans* and the neuroblastoma cell line SH-SY5Y

Another hallmark of the ALS disease are mutant SOD1 aggregations in neurons and skeletal muscle cells (Redler and Dokholyan, 2012).

We found that butyrate administration and usage of the widely used HDAC inhibitors TSA and VPA to the culture media of the *C. elegans* and SH-SY5Y models decreased mutant SOD1 aggregations. In our SH-SY5Y model we could decrease mutant SOD1 aggregation in a variety of the most prevalent SOD1 mutations found in ALS and in our *C. elegans* model we could show a more pronounced reduction in Sod1 and Sod1G85R aggregation formation upon exposure to NaB, VPA and TSA (Figure 3A-C). TSA also led to an aldicarb profile identical to the wild type whilst NaB did not (Figures 2, 3) suggesting a correlation between aggregate prevention and NMJ function. A study showed that mutant SOD1^{G93A} aggregations could also be found in intestinal cells of ALS mice and human intestinal epithelial cells. In this study the administration of butyrate could decrease abnormal Paneth cells as well as restore abnormal intestinal function and increase life span in these ALS mice (Zhang *et al.*, 2017). Another G93A ALS mouse study focusing on NF-kappaB and bcl-2 demonstrated that sodium phenylbutyrate increased life span and shapes anti-apoptotic gene expression through HDAC inhibition (Ryu *et al.*, 2005). Interestingly, a study using *Drosophila melanogaster* showed that TSA and butyrate both influence autophagy and

chaperones assisting in correctly folding newly synthesised proteins (Chen *et al.*, 2002). Interestingly, a study using motorneuron-like NSC34 and HEK293 cell lines showed that HDAC6 knockdown could increase mutant SOD1 aggregation instead of decreasing (Gal *et al.*, 2013).

Other studies using *C. elegans* have shown that gut colonisation of butyrate producing bacteria supress aggregation of proteins thus preventing proteotoxicity and thus emphasising the impact of microbial metabolites on host health (Walker *et al.*, 2021). In conclusion, we demonstrated that NaB may act as an HDAC inhibitor preventing or decreasing a range of mutant SOD1 accumulations which also might correlate with NMJ function. Further studies investigating the exact mechanism of Sod1 aggregation inhibition in our models may provide a useful platform for the design of new therapeutic approaches to utilise HDAC inhibition to treat ALS.

Chapter 3 – An analysis of the antifungal effects of Butyrate on *C. albicans* reveals pH dependent modes of action – implications for ALS linked dysbiosis

Abstract

Candida species contribute to both normal gut microbiome dynamics and a range of medical conditions where maintaining microbial balance is crucial for health. In this context, butyrate, a short-chain fatty acid produced by various gut bacteria and known to play a critical role in intestinal homeostasis, has been shown to influence *Candida* levels. Here, we investigate the antifungal effects of sodium butyrate (NaB) on *Candida albicans* under pH conditions that are found within the gut. We find that NaB has a rapid histone deacetylase inhibitor activity against *C. albicans* and inhibits growth, hyphal transition, respiration and biofilm formation at neutral pH. In contrast, at pH 4.0 NaB has fungicidal effects that are accompanied by mitochondrial depolarisation, accumulation of reactive oxygen species (ROS), and dysregulation of intracellular calcium homeostasis. Our data confirm that oxidative stress and loss of calcium regulation are responsible for NaB-induced death under acidic conditions. These findings highlight the pH-dependent effects of butyrate and have relevance for both our understanding of the microbiome and its potential as a therapeutic to control *Candida albicans* overgrowth.

3.1 Introduction

3.1.1 Gut dysbiosis in ALS patients

The composition of the gut microbiome is dependent on various factors, such as genetics, gender, age, geographic location, lifestyle, and diet (Ballan *et al.*, 2020; de Vos *et al.*, 2022). In addition, compounds from the diet are metabolised by the gut microbiota yielding various metabolites that will interact with cell receptors and signalling pathways of the host influencing the host's health. Thus, various compositions of the gut microbiota will provide different metabolite profiles leading to different impacts on different signalling pathways, and therefore may contribute or impede host health (Ballan *et al.*, 2020; de Vos *et al.*, 2022).

The current view on ALS disease development and progression suggests a complex multi-factor interplay of both genetic and non-genetic elements (Fang *et al.*, 2009; Al-Chalabi *et al.*, 2014; Renton, Chiò and Traynor, 2014; Marangi and Traynor, 2015; Wang *et al.*, 2017).

External risk factors such as smoking, diet, heavy metals, and pesticide exposure were identified in epidemiological studies (Fang *et al.*, 2015). Recently, diet had been shown to be a crucial contributing factor to ALS risk, onset, and progression: high-calorie fat or sugar-rich diets showed to positively affect ALS patients (Desport *et al.*, 2001; Bouteloup *et al.*, 2009; Vaisman *et al.*, 2009; Dupuis *et al.*, 2011; Ferri and Coccurello, 2017; Steyn *et al.*, 2018).

Human ALS studies could identify that the microbiome of ALS patients is significantly different to healthy controls: *Bacteroidetes Bacteriodales Dorea* and phyla *Firmicutes* levels were significantly higher in healthy controls compared to ALS patients. Furthermore, *Oscillibacter, Anaerostipes,* and *Lachnospiraceae* were substantially decreased in ALS patients (Fang *et al.*, 2016). It was reported (Rowin *et al.*, 2017) that dysbiosis and

decreased diversity of the microbiome compared to healthy controls was present in all ALS patients examined. Furthermore, other studies investigating the microbiome of ALS patients found that there was a significant lower abundance and diversity of the bacterial profile in ALS patients compared to healthy controls; here higher abundance of *E. coli* and *Enterobacteria* combined with lower abundance of *Clostridium* and yeast was identified in ALS patients (Mazzini *et al.*, 2018; Di Gioia *et al.*, 2020). A recent study identified that 15 bacterial species including butyrate-producing bacteria *Roseburia intestinalis* and *Eubacterium rectale* levels were significantly lower in ALS patients when compared to healthy controls (Niccolai *et al.*, 2021). Comparison (Hertzberg *et al.*, 2022) of the gut microbiota of ALS patients with the patients' spouses as healthy controls found that ALS patients were lacking butanoate metabolic pathway enzymes. Furthermore, they found that enzymes involved in metabolic pathways including response regulators, carbon and butyrate metabolism pathways were expressed at low levels.

An interesting external factor which may promote ALS disease are fungal infections. These can be acquired through spores from plants or soil that are inhaled. Many fungi produce neurotoxins that can promote motor neuron degeneration (Castanedo-Vazquez *et al.*, 2019; French, Ludowyke and Guillemin, 2019). Mycotoxins or neurotoxins are secondary metabolites generated by fungi such as *Aspergillus*, *Fusarium,* and *Penicillium* (Sweeney, 1998). Mycotoxins may be ingested through spoiled food contaminated with fungi and may have carcinogenic, nephrotoxic, mutagenic and neurotoxic effects (Alshannaq and Yu, 2017). Many filamentous species such as *Aspergillus* and *Penicillium* generate Ochratoxin A which has been noted in Parkinson's disease (Sava *et al.*, 2006; El Khoury and Atoui, 2010). Another hallmark of ALS is excessive secretion of the excitatory neurotransmitter glutamate in the synaptic cleft (Van Den Bosch *et al.*, 2006; Arnold *et al.*, 2024). *In vivo* studies in sheep

and rats showed that the mycotoxins virulome and penitrem A may cause increased glutamate secretion (Norris *et al.*, 1980; Peterson *et al.*, 1982; Bradford, Norris and Smith, 1990). Increased glutamate levels were also shown to increase the toxicity of mutant SOD1 (Roy *et al.*, 1998) and induce post-translational modifications in TDP-43 leading to ALS development or progression (Scofield *et al.*, 2012). Riluzole is the first approved drug for ALS treatment inhibiting glutamate secretion as well as showing moderate antifungal activity (Doble, 1996; LaFleur *et al.*, 2011; Lasiene and Yamanaka, 2011; Bhandari, Kuhad and Kuhad, 2018). Fungal SOD1 is not only important for virulence in pathogenic fungi but also helps evade the human immune defence system by increasing oxidative stress resistance (Cox *et al.*, 2003; Cox, Banack and Murch, 2003). Although fungal SOD1 is genetically and structurally different to human SOD1, fungal SOD1 may prolong fungal infection by mycotoxigenic molds, such as *Aspergillus*, *Fusarium*, and *Penicillium* species, and therefore extend host exposure to their secondary metabolites (Huang, Kuo and Jinn, 2012; French, Ludowyke and Guillemin, 2019). Notably, this toxic exposure profile excludes common yeast pathogens like *C. albicans*, which do not produce classic secondary-metabolite mycotoxins made by filamentous molds.

C. albicans infection leading to gut inflammation could be observed in ALS studies (Rowin *et al.*, 2017; Fournier *et al.*, 2020). Other studies showed that bacterial and fungal infections in the CNS coexist in ALS patients (Alonso *et al.*, 2017; Alonso, Pisa and Carrasco, 2019). Gut dysbiosis and reduced diversity within the gut microbiome in ALS patients has been reported in multiple studies (Fang *et al.*, 2016; Rowin *et al.*, 2017; Zhang *et al.*, 2017) and it has been suggested that gut dysbiosis can directly affect the central nervous system through

the gut-brain-axis (Forsyth *et al.*, 2011; Hsiao *et al.*, 2013; Sampson *et al.*, 2016).

Butyrate is a known inhibitor of the histone deacetylase (HDAC) (Candido, 1978; Vidali *et al.*, 1978; Donohoe *et al.*, 2014; Pascale *et al.*, 2018; Chen, Zhao and Vitetta, 2019). HDAC inhibitors were found to show neuroprotective properties in ALS studies whereby the genetic silencing of HDAC6 reversed axonal transport defects in ALS-patient-derived motor neurons (W. Guo *et al.*, 2017). Furthermore, the HDAC6 inhibitor Trichostatin A (TSA) could protect axons from excitotoxin-induced degeneration in mice (Hanson *et al.*, 2018; Phipps *et al.*, 2024). The studies suggest that the regulation of HDAC activity may provide an approach to develop new therapeutic treatments for ALS. It is also of interest to consider how the levels of HDAC inhibitors, such as butyrate, may affect the prevalence and activity of microbes linked to ALS pathology, such as *C. albicans*.

3.1.2 Importance of HDAC and TF regulation for hyphae formation in *C. albicans*

The opportunistic pathogen *Candida albicans* is a commensal yeast found on the mucosal surfaces of the oral cavity, gastrointestinal tract, and the urinary tract of healthy people (Douglas, 2003; Ganguly and Mitchell, 2011; Cottier and Hall, 2020). However, *C. albicans* can cause severe infections in immunocompromised individuals (Ghrenassia *et al.*, 2019). *C. albicans* is a dimorphic fungus able to switch between a yeast and a pseudohyphal or hyphal form. This yeast-to-hyphae switch is strongly correlated to virulence and critical for biofilm formation due to expression of cell surface adhesins critical for cell-cell and cell-surface attachment (Berman and Sudbery, 2002; Nobile *et al.*, 2008). In addition, hyphal cells

secrete candidalysin, a 31-amino-acid cytolytic peptide toxin derived from the Ece1 protein, which contributes to *C. albicans* virulence by disrupting host cell membranes and promoting tissue damage (Lin and Filler, 2025).

Biofilms are communities of single or multi species microorganisms which attach to a surface or cells generating extracellular polymers forming a structural matrix. Antimicrobial drug resistance is significantly higher than in planktonic free-living systems (Talpaert *et al.*, 2015; Cavalheiro and Teixeira, 2018).

Epithelial and endothelial cells can be invaded by *C. albicans* when they are in their hyphae form through active invasion not requiring host cell uptake mechanisms. Another mechanism by which this occurs is called induced endocytosis. Here, epithelial cells generate pseudopodia-like structures upon fungi interaction via the fungal adhesin Als3 and human E-cadherin or Her2 – the epidermal growth factor receptor 2 located on epithelial cells (Phan *et al.*, 2007; Zhu *et al.*, 2012; Maza *et al.*, 2017). This interaction causes a rearrangement in the actin filaments in the host cells leading to the uptake of the fungus (Phan *et al.*, 2007; Zhu *et al.*, 2012; Yang *et al.*, 2014; Maza *et al.*, 2017). Invasion can also occur through clathrin-dependent endocytosis involving dynamin and cortactin (Moreno-Ruiz *et al.*, 2009).

Transcriptional hyphal regulation is influenced by environmental and nutritional signals such as pH, *N*-acetylglucosamine, serum, CO_2, temperature, O_2 (Villa *et al.*, 2020). Signalling pathways such as the Efg1-cAMP and the Cph1-mediated MAPK pathways control the yeast-to-hyphae switch in *C. albicans* (Biswas, Van Dijck and Datta, 2007).

To date, there are 11 HDACs identified in *C. albicans* and *C. glabrata* which are grouped into three main classes: Class I contains Rpd31, Rpd32, Hos1, and Hos2. Class II entails Hda1 and

Hos3, and Class III contains Sir2 and Hst proteins. Set3 is an NAD+-dependent HDAC (Garnaud *et al.*, 2016). Virulence factors in *C. albicans* such as hyphae formation are regulated through transcriptional mechanisms (Garbe *et al.*, 2023; Luther *et al.*, 2023; Y. Lee *et al.*, 2023), but also through chromatin modification (Lopes da Rosa and Kaufman, 2012; Garnaud *et al.*, 2016). The class I HDAC Rpd31 for example is necessary to initiate filamentous growth (Xie *et al.*, 2016; X. Li *et al.*, 2017), hyphal development and elongation. These processes are also regulated by the class II HDAC Hda1 (Zacchi, Schulz and Davis, 2010; Kim, Lee and Lee, 2015; X. Li *et al.*, 2017). During hyphal initiation Nrg1 is repressed enabling the recruitment of Hda1 through Brg1. Hda1 binds to hyphae promotors restructuring nucleosomes blocking Nrg1 binding sites thus upholding hyphae development (Lu, Su and Liu, 2012). In line with their roles, hyphae development and azole resistance respectively (Lu, Su and Liu, 2012; X. Li *et al.*, 2017) deletion of Hda1 or Rpd31 led to a decrease in virulence in a mouse study investigating *C. albicans* pathogenicity (Simonetti *et al.*, 2007). Another important HDAC class crucial for morphological transition is the sirtuin family including Sir2, Hst1, Hst2, Hst3 (Zhao and Rusche, 2021). Hst3 is crucial for normal hyphae growth as it deacetylates H3K56 thus reducing virulence in *C. albicans* (Wurtele *et al.*, 2010). The precise functions of Sir2, Hst1, and Hst2 in *C. albicans* have not been characterised well yet, however, studies showed that expression levels of hyphae-specific genes decreased in the absence of *SIR2* (Zhao and Rusche, 2021). It was further found that Hst1 and Sir2 localised to the nucleus suggesting they function in gene expression (Zhao and Rusche, 2021). In *C. albicans* the Set3C complex behaves as cofactor in transcribing genes needed in metabolism and morphogenesis. Set3C also restricts the regulatory circuit cluster of Nrg1, Efg1, Brg1, and Tec1 controlling hyphal differentiation by changing their

transcription kinetics (Hnisz *et al.*, 2012). Furthermore, the Set3/Hst1 complex is reducing signalling via the cAMP/PKA promoting the white-to-opaque switch (Su *et al.*, 2020).

In the current study, we aimed to characterise the effects of butyrate on *C. albicans*. Here, we found that high levels of NaB could decrease hyphae formation and biofilm growth in *C. albicans*, potentially through SET3C H4 acetylation dynamics. We could also show that NaB mode of action is pH dependent and that under acidic conditions can cause a loss of calcium homeostasis leading to cell death characterised by a loss of mitochondrial function and ROS accumulation. Our findings demonstrate that butyrate can supress a range of *C. albicans* virulence traits and under acidic conditions, as are found in the gut, can act as fungicidal agent.

3.2 Materials and Methods

3.2.1 Media preparation and growth conditions for *Candida albicans*

All components of the media were mixed in to deionised distilled water prior to autoclaving. All media was sterilised using a Prestige Medical bench-top autoclave at 121 °C, 15 Ib/sQ.in for 11 min. All liquid cultures of *C. albicans* were incubated at 30 °C with constant rotation at 180 rpm. 2 % w/v granulated agar (Oxoid technical agar No. 3) was added prior to autoclaving for solid medium and glucose, if required, was added after autoclaving. The YPD growth medium contained 2 % w/v glucose (Fisher), 1 % w/v yeast extract (BD) and 2 % w/v Bactopeptone (BD). The RPMI-1640 medium was provided by Sigma-Aldrich, R8755. The

HDAC deletions (Table 2) used in this study were a kind gift from the lab of Prof Alessia Buscaino (University of Kent).

TABLE 2 LIST OF HDAC DELETION STRAINS

Strain Name	**Isogenic background**	**Genotype**
Δrpd31	*Candida albicans* SC5314	*rpd31*Δ::*C.d.HIS1*/*rpd31*Δ::*C.m.LEU2* *arg4*Δ/*arg4*Δ *his1*Δ/*his1*Δ *leu2*Δ/*leu2*Δ *URA3*/*ura3*Δ::λimm434 *IRO1*/*iro1*Δ::λimm434 a/a mating type Transformant 1
Δ*sir2*	*Candida albicans* BWP17	*ura3*Δ::λimm434/*ura3*Δimm434 *his1*::*hisG*/*his1*::*hisG* *arg4*::*hisG*/*arg4*::*hisG* *sir2*::*HIS1*/*sir2*::*ARG4*
Δ*hos2*	*Candida albicans* SC5314	*hos2*Δ::*C.d.HIS1*/*hos2*Δ::*C.m.LEU2* *arg4*Δ/*arg4*Δ *his1*Δ/*his1*Δ *leu2*Δ/*leu2*Δ *URA3*/*ura3*Δ::λimm434 *IRO1*/*iro1*Δ::λimm434 a/a mating type Transformant 1
Δ*hst1*	*Candida albicans* SC5314	*hst1*Δ::*C.d.HIS1*/*hst1*Δ::*C.m.LEU2* *arg4*Δ/*arg4*Δ *his1*Δ/*his1*Δ *leu2*Δ/*leu2*Δ *URA3*/*ura3*Δ::λimm434 *IRO1*/*iro1*Δ::λimm434 a/a mating type Transformant 2
Δ*hst2*	*Candida albicans* SC5314	*hst2*Δ::*C.d.HIS1*/*hst2*Δ::*C.m.LEU2* *arg4*Δ/*arg4*Δ *his1*Δ/*his1*Δ *leu2*Δ/*leu2*Δ *URA3*/*ura3*Δ::λimm434 *IRO1*/*iro1*Δ::λimm434 a/a mating type Transformant 2
Δ*set3*	*Candida albicans* SC5314	*arg4*Δ/*arg4*Δ *his1*Δ/*his1*Δ *leu2*Δ/*leu2*Δ *URA3*/*ura3*Δ::λimm434 *IRO1*/*iro1*Δ::λimm434 *set3*Δ::*C.d.HIS1*/*set3*Δ::*C.m.LEU2* a/a mating type Transformant 2
Δ*hda1*	*Candida albicans* Ca159 (*ura3*Δ::λimm434/*ura3*Δ::λimm434 *his1*::*hisG*/*his1*::*hisG*	*ura3*Δ::λimm434/*ura3*Δ::λimm434 *his1*::*hisG*/*his1*::*hisG* *arg4*::*hisG*/*arg4*::*hisG* *hda1*Δ::*arg4*/*hda1*Δ::*his1*

arg4::*hisG*/*arg4*::*hisG* *hda1*Δ::*arg4*/*HDA1*)	

3.2.2 Preparation of total cell lysates and immunoblotting

Overnight precultures of *C. albicans* in appropriate media were grown to log phase (OD600 nm of 0.6) before adding desired stresses such as 200 mM NaB. $1x10^8$ cells were sampled after 0 min, 15 min, 30 min, and 60 min after NaB exposure and exposed to 200 µl of the lysis buffer (1 ml of 1 M NaOH; 1 ml of 0.5 M EDTA pH8; 2 ml of 10 % SDS; 200 µl ß-mercaptoethanol). The lysates were heated for 10 min at 90 °C before 5 µl of 4 M Acetic acid was added to each sample. Lysates were vortexed for 30 seconds before incubating them for 10 min at 90 °C. 50 µl of loading buffer (50 % glycerol, 0.25 M Tris-HCl pH 6.8, 0.05 % bromophenol blue) was added to each sample. The samples were then centrifuged at 10,000 rpm for 1 min in a bench microcentrifuge to clear the lysate before loading onto 4 - 12 % SDS-polyacrylamide gels for protein separation. Separated proteins were transferred onto PVDF membranes (Thermo Fisher), which were placed in blocking solution (5 % w/v dried skimmed milk (Oxoid) and PBS (Phosphate Buffered Saline)) for 45 mins with rotation at room temperature followed by incubating in blocking solution containing the anti-rabbit H4 primary antibody (Biorad AHP418) in a 1/800 dilution overnight at 4 °C. The following day, membranes were washed with PBS/T (Phosphate Buffered Saline and 0.2 % Tween 20 (Sigma)) before being exposed to the horse-radish peroxidase conjugates anti-rabbit Pgk1 secondary antibody (1/10000) for 45 mins at room temperature and further washed 6 x with PBS/T. The immunoreactivity was visualised using Enhanced Chemiluminescence (ECL) using a SynGene gel doc. To analyse the blots, the GeneSys Software (Version 1.6.5.0) was

used and a Synoptics 6MP camera was used to capture the images. The programme Fiji (ImageJ) version (2.1.0/1.53c) was used to normalise to the control by calculating the integrated intensity of the protein band, which was then divided by the integrated intensity of the loading control band of anti-Pgk1 anti- rabbit (Sigma-Aldrich).

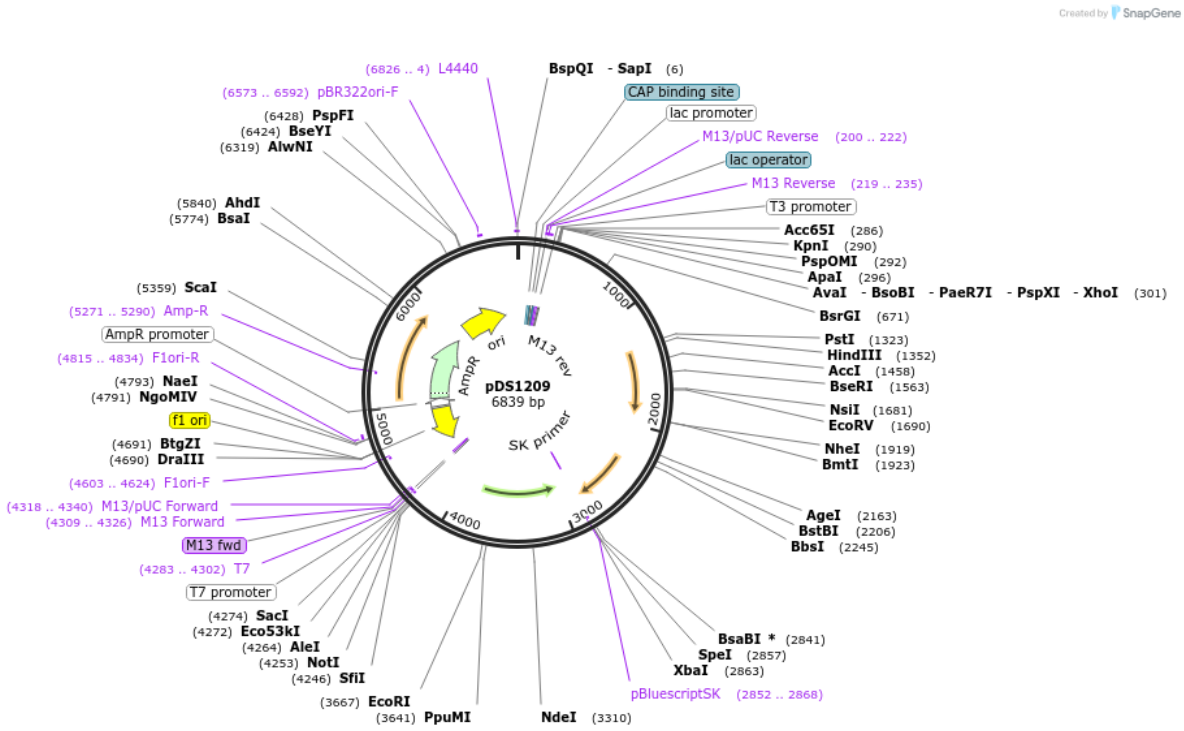
3.2.3 *C. albicans* chemical transformation

Overnight precultures of *C. albicans* strains in YPD medium were diluted to an OD600 nm of 0.1 in 5 ml of fresh YPD and incubated at 30 °C with shaking at 180 rpm until an OD600 nm of 0.6 - 0.8 was reached. Cells were then pelleted in a cooled centrifuge for 5 min at 4000 rpm and resuspended in 1 ml sterile water three times before resuspending the pellet in 1/100th of its original volume. Competent cells were mixed with 10 µl of 10 mg/ml single stranded DNA (boiled herring sperm DNA), 20 µl of digested plasmids of interest – a kind gift from Prof Dominique Sanglard (Sanglard, 2021) (Table 3), 50 µl of washed cell suspension, 875 µl of 50 % PEG 3350, 100 µl 10 X TE (100 mM Tris pH 7.4, 10 mM EDTA pH 8), and 25 µl 1 M LiOAc pH 7. The cell mixture was incubated overnight at 30 °C without shaking before placed into a 44 °C water bath for 15 min. Transformed cells were centrifuged at 5000 rpm for 2 min and resuspended into 15 ml YPD at 30 °C with shaking for recovery. The suspension was pelleted for 2 min at 5000 rpm and cells were plates onto selective media. Plates were incubated at 30 °C for at least two days to allow colony growth.

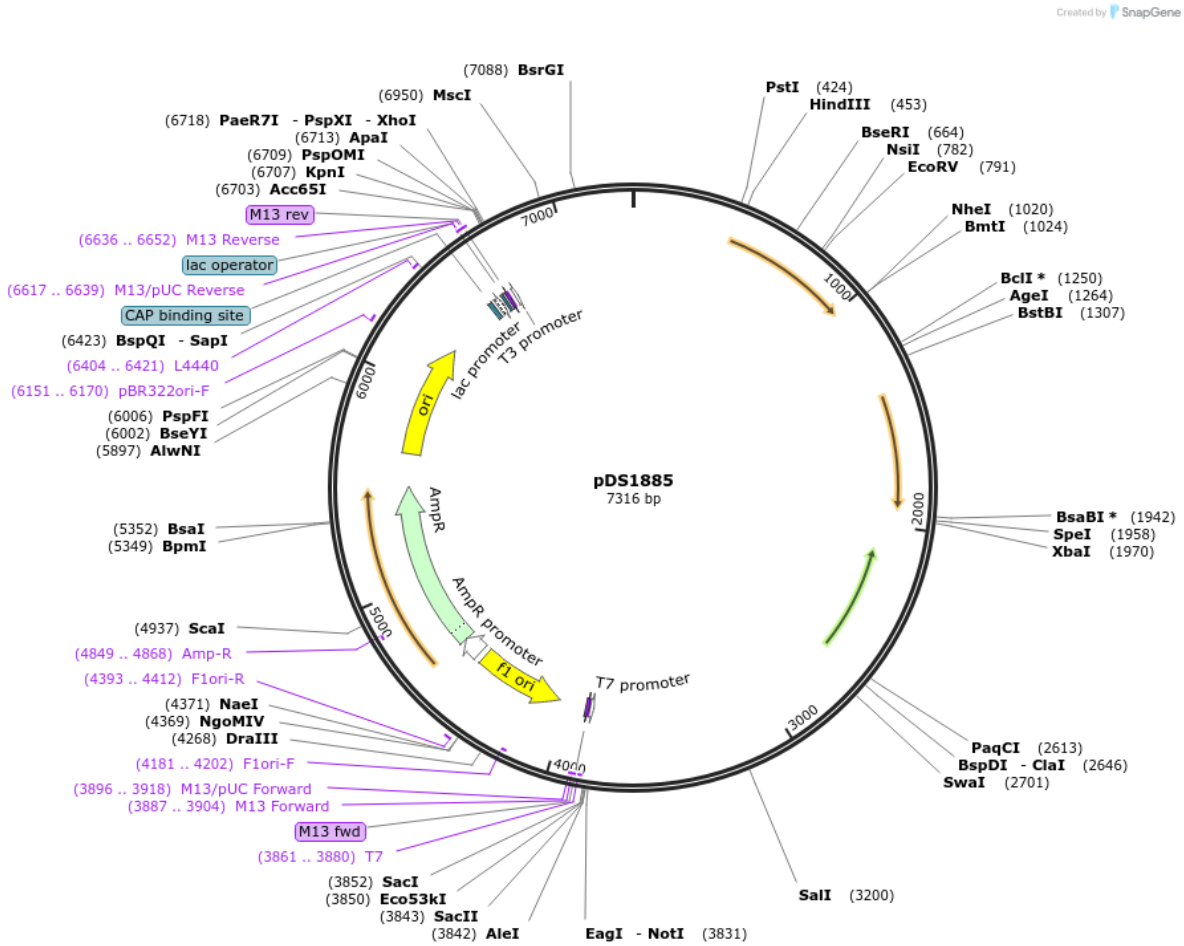
TABLE 3 PLASMIDS USED

Plasmid	**Restriction enzyme**	**Selective Marker**
pds1207 Aequorin	StuI	NAT
pds1865 Aequorin	StuI	NAT

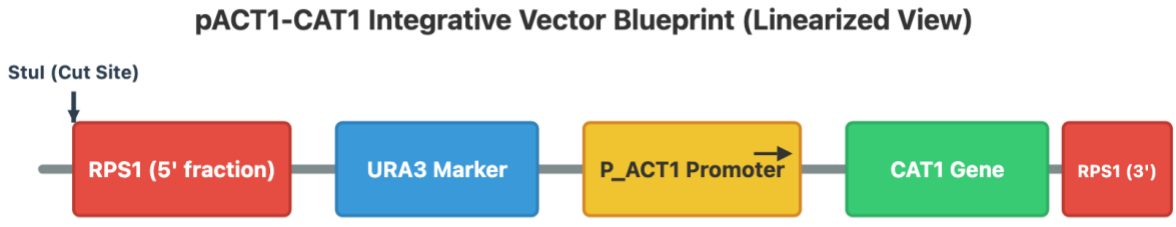
pACT CAT1	StuI	URA3



Plasmid map 1 of the URA3-selectable aequorin reporter vector. *The map illustrates the architectural layout of the reference vector pDS1209 (available via Addgene, plasmid #177340), which is structurally identical to the pDS1207 construct utilized in this study.*



Plasmid map 2 of the SAT1-selectable aequorin reporter vector. *The map illustrates the architectural layout of the reference vector pDS1885 (available via Addgene, plasmid #177341), which is structurally identical to the pDS11885 construct utilized in this study.*



Vector layout following StuI digestion within the RPS1 sequence to direct homologous recombination into the C. albicans genome.

Plasmid map 3 Structural layout of the linearized integrative pACT1-CAT1 overexpression vector. Diagram reconstructed based on the known molecular components of the custom construct provided by the Quinn Lab. The vector contains the Candida albicans CAT1 open reading frame under the regulatory control of the strong, constitutive ACT1 promoter (P_ACT1).

3.2.4 Restriction enzyme digest of DNA

Using restriction endonucleases from New England Biolabs (StuI), enzymatic scission of DNA at specific sequence points was carried out. The manufacturer's protocol was used, and the buffer was supplied by the manufacturer. The reagents listed below (Table 4) were added together to create a 20 µl reaction mix. The incubation time for the digests was at least 1 hour (sometimes 4 h) at 37 °C. 10 µl of the samples was loaded onto an agarose gel to analyse the digested products.

TABLE 4 BASIC REACTION MIXTURE USED FOR THE RESTRICTION ENZYME DIGEST USED IN THIS STUDY

Reagent	**Volume**	**Concentrations**
Sterile water	14.8 µl	
Plasmid DNA of interest	2 µl	2 µg/µl
BSA	0.2 µl	10 µg/µl
Multicore 10x buffer	2 µl	10X
StuI (restriction enzyme)	1 µl	5 u/µl

3.2.5 Purification of plasmids from *E. coli*

Overnight *E. coli* cultures grown in LB medium supplemented with the appropriate antibiotic (Ampicillin stock concentration: 100 mg/ml in sterile deionised water, Sigma-Aldrich) at 37 °C with constant rotation at 180 rpm were harvested at 8000 rpm for 3 mins at room temperature. The supernatant was removed, and the plasmid DNA of interest was extracted from the cell pellet using a Qiagen QIAprep Spin Miniprep Kit according to the manufacturer's instructions.

3.2.6 Agarose gel electrophoresis

To analyse DNA fragments and plasmids, agarose gel electrophoresis was carried out. The agarose gels were composed of 0.8 % (w/v) agarose (Melford, MB12000) in 1x TAE buffer containing 0.5 µg/ml final concentration of ethidium bromide (Table 5). The Invitrogen Fisher 1 kb + gene ruler DNA ladder and the 10 X blue juice loading dye was used.

TABLE 5 RECIPE FOR 1X TAE BUFFER

Ingredient	**amount**
Tris base	4.84 g
Glacial acetic acid	1.14 ml
0.5 M EDTA, pH 8.0	2 ml
Milli-Q water	To 1 L final volume

3.2.7 Absorbance assays for growth rate analysis of *C. albicans*

Precultures of *C. albicans* strains grown overnight in YPD medium at 30 °C with shaking at 180 rpm were inoculated to an OD600 nm of 0.1 in 100 µl of appropriate medium with or without supplements or pH adjustments (pH 8: adjusted with 0.1 M NaOH to raise pH or pH 4: adjusted with 1.0 M HCl to lower pH) (Table 6) into a sterile 96-well plate (Greiner). Media at the initial values of pH 4.0 and pH 8.0 were unbuffered. Consequently, it should be noted that the extracellular pH likely drifted during the course of the growth curve due to cellular metabolic activity, ion transport, and the accumulation of metabolic waste products. The 96-well plate was placed into a BMG LABTECH FLUOstar OPTIMA or a BMG LABTECH SPECTROstar Nano plate reader for 24 h where the growth was measured (Table 7). The protocol setting used can be found in the table below (Table 7). To analyse the data, the software BMG LABTECH MARS was used. The data was then exported to Microsoft Excel for further analysis. The area under the curve (AUC) was calculated using GraphPad Prism. Here, the trapezoidal method was applied where each connecting segment under the growth curve describes a trapezoid. The sum of each segmental trapezoid forms the total AUC.

TABLE 6 A LIST OF SUPPLEMENTS ADDED TO YPD MEDIA

Supplement	**Concentration**
NaB (Sigma Aldrich)	Various concentrations
H_2O_2	5 mM
$CaCl_2$ (Sigma Aldrich)	50 mM

TABLE 7 THE PROTOCOL SETTING USED TO MEASURE GROWTH RATE

Cycle Time	**1800 seconds**
Flashes per Well	3
Excitation	600 nm
Shaking Frequency	400 nm
Shaking Mode	Double Orbital
Additional Shaking Time	30 seconds before each cycle
Temperature	30 °C
Positioning Delay	0.5 seconds

3.2.8 Biofilm Growth assay

The surface of a 96 well plate upon which the biofilm was to grow was coated by adding 100 µl of 50 % Donor Bovine Serum (DBS) and left for at 30 mins at 30 ^{o}C without shaking. The 50 % DBS was removed by inverting the plate and washing with 1 X PBS solution. Cells washed and resuspended in 1 X PBS at a density of 1 x 10^{6} CFU/ml (OD600 nm of 1.0 for 24 well plate, OD600 nm 0.1 for 96 well plate) were added and left for 90 mins to adhere to the surface at 37 °C without shaking. Non-adhered cells were then removed by washing the plate once with 100 µl of 1 X PBS as before. 100 µl of fresh media and supplements of choice were added to the wells and the plate returned to incubator without shaking for up to 24 h (mid stage) or 48 h (mature Biofilm). Once biofilms had grown the plate was washed twice with 1 X PBS, inverting on tissue and tapping it gently to remove detached cells before proceeding to XTT assay or crystal violet assay (CV).

3.2.9 XTT assay

To assess biofilm growth, an XTT (2,3-bis-(2-methoxy-4-nitro-5-sulfophenyl)-2H-tetrazolium-5-carboxanilide) (XTT Assay Kit ab232856, Abcam) reduction assay was used. This is a readout of the metabolic activity of viable cells in the biofilm and is used as a readout of cell number. The XTT assay was performed by adding 200 µl of 1 X PBS to each well and then adding 10 µl of the XTT labelling reagent to each well. To make the XTT labelling mixture, 1.5 ml of XTT labelling reagent (XTT Developer Reagent) was mixed with 30 µl of the electron coupling reagent (Electron Mediator Solution). The plate was incubated in a non-shaking incubator at 37 °C for 4 - 5 h before being centrifuged for 5 mins at 4000 g. The red product was then removed from each well and the XTT formazan in the supernatant was determined spectrophotometrically at 492 nm using a plate reader. The conversion of the XTT substrate to a soluble coloured formazan product correlates with metabolic activity.

3.2.10 Crystal Violet assay

Biofilm formation was quantified by crystal violet staining. 100 µl of 0.1 % (w/v) crystal violet was added to each well and incubated at room temperature for 15 mins. The liquid was poured out and the wells washed with sterile water four times before leaving the plates to dry for 24 h. After 24 h 100 µl of 30 % acetic acid was added to each well and incubated for 15 mins. The plate was then spun down at 4000 rpm for 5 mins. The acetic acid/ crystal violet solution was then read using a plate reader at 550 nm to quantify the biofilms. Biofilms were also visualised using an Olympus IX81 fluorescence microscope using either

RFP filter set (488/583 excitation/emission) or using DIC at 20x magnification using an Andor Xyla 4.2 CMOS digital camera.

3.2.11 Hyphae Extension Measurement

C. albicans strains were grown in YPD overnight at 30 °C with shaking at 180 rpm. The cultures were diluted to an OD600 nm of 0.5 in RPMI medium with and without 200 mM NaB supplementation and incubated at 30 °C at 180 rpm. Measurements were taken at timepoints 2 h, 4 h, and 6 h by pipetting 2 µl of the culture mixed with 2 µl of the ready to use Calcofluor white stain (1 g/L, Sigma Aldrich) onto a microscope slide. The slide was covered with a 20 mm by 20 mm cover slip. A single drop of Olympus Immoil-F30CC immersion oil was applied to the surface of the 100x (1.4 NA) objective lens prior to the examination under the microscope. Images were captured using an Olympus IX81 fluorescence microscope using either DAPI filter set (350/465 excitation/emission) or using DIC at 100x magnification using an Andor Xyla 4.2 CMOS digital camera.

3.2.12 Agar Invasion Assay

C. albicans strains were grown in YPD overnight at 30 °C with shaking at 180 rpm. The cultures were harvested at 1,000 xg for 5 min in a 1 ml centrifuge tube, washed 3x with PBS and centrifuged at 1,000 xg for 5 min. The cell number was adjusted to 1 x10^7 cells/ml (about OD600 nm 0.1) in PBS. The adjusted cells were then exposed to 200 mM NaB for either 1 h, 6 h or 24 h. The cells were then washed with PBS once, before pipetting a spot of each sample onto the surface of a 10 cm YPD agar plate. Once dry, the plates were inverted

and incubated at 37 °C for 2 - 5 days or as soon as hyphae formation (initiation of invasive growth) could be observed at the edge of the colony. An image of the colony from above was then taken before the surface of the colony was washed off my gently rubbing the surface with a gloved finger under running water. The same colony was then imaged after washing. The invading cells will not have washed off leaving invasive growth visible.

3.2.13 Metastasis Assay

10 x 14 mm sterile silicone leaflets were attached to a modified 24 well plate lid.
1 ml of 50 % Donor Bovine Serum (DBS) was added to a 24 well plate and left for at 30 mins at 30 ^{o}C. This helps with the adherence of cells. Excess 50 % DBS was removed by dipping the plate lid with the attached leaflets in a new 24 well plate containing 1 ml PBS. The washed plastics are then transferred to a new 24 well plate containing washed and resuspended in PBS cells at a density of 3 x 10^7 CFU/mL (roughly OD600 nm 1.0) and incubated 90 mins at 37 °C and 5 % CO_2 without shaking. Non-adhered cells were removed by washing twice with PBS as described above. Fresh media with and without 200 mM NaB was then added to the wells and incubated without shaking at 37 °C for 48 h until a mature biofilm has formed. Following Biofilm growth on leaflet as above for 48 h the lid plus leaflets were transferred to a fresh plate containing fresh non-supplemented media. The pate was then incubated for another 48 h to allow dispersion and formation of a secondary biofilm at the bottom of the plate. The leaflets were then removed, and media was aspirated from the well. The secondary biofilm at the bottom of the well can then be quantified by XTT, Crystal violet stain and microscopy.

3.2.14 Colony Forming Unit assay/Viability assay

C. albicans strains were grown in YPD overnight at 30 °C with shaking at 180 rpm. The overnight cultures were washed once with PBS and subsequently used to inoculate RPMI medium, with or without supplements and pH adjustment, to an OD600 nm of 0.5. The cultures were then incubated for 1 h at 30 °C at constant shaking at 180 rpm. The number of cells in a culture was counted under a microscope using a haemocytometer. For 100 % viability, 300 colony forming units (CFUs) should grow. The plates were incubated at 30 °C for 48 h prior counting. The percentage viability was determined by the dividing the number of observed CFUs by the number of expected CFUs and multiplied by 100.

3.2.15 Reactive Oxygen Species (ROS) and Necrosis Assay

C. albicans strains were grown overnight at 30 °C with 180 rpm shaking in YPD medium. Overnight cultures were inoculated in RPMI at desired pH with or without 200 mM NaB to an $OD_{600\ nm}$ of 0.5. H2DCF-DA at a concentration of 5 µg/ml (stock of 5 mg/ml in DMSO) were added to all samples before incubating them at 30 °C with constant shaking at 180 rpm for 1 h. Cultures were then washed thrice in sterile 1x PBS and resuspended in 1x PBS containing 2 µg/ml propidium iodide (PI) stain. H2DCF-DA intensity of cells was analysed using the BD AccuriTM C6 Plus Personal Flow Cytometer (BD Biosciences). Measurement events were gated based on forward scatter (FSC) and side scatter (SSC) to identify the yeast cell population and exclude cellular debris. Singlet yeast cells were subsequently identified by gating the FSC-A versus FSC-H population to exclude cell aggregates and doublets. This ensures that only singlet yeast cells were being recorded. The flow cytometer was equipped

with a blue laser (488 nm) and a red laser (640 nm). The FL1 (533/30 nm) filter was used to detect the DCF fluorescence (H2DCF-DA) and the FL2 (585/40 nm) filter for propidium iodide from cells. Approximately 25,000 events were collected per sample and the data was acquired and analysed using the BD Accuri C6 Plus software. The CGY638 strain (lacking *COX4*) was used as positive ROS control (Leadsham *et al.*, 2013), and a heat-killed necrotic (80 °C for 2 min) *C. albicans* culture sample was used as a positive PI control.

3.2.16 Cytosolic Calcium concentration measurement using ApoAequorin luminescence

C. albicans strains expressing aequorin from an integrated plasmid (a kind gift from Prof Dominique Sanglard) were grown in appropriate medium at 30 °C under constant shaking after successful transformation (refer to 3.2.3 *C. albicans* chemical transformation and 3.2.4 Restriction enzyme digest of DNA). Cells were then sub-cultured to mid log-phase around OD600 nm 0.5 - 0.7. Log- phase cells were then re-suspended at a density of ~108 cells/ml in fresh SD selective medium. The substrate Coelenterazine (Invitrogen, Thermo Fisher) was added to a final concentration of 5 µM. As a negative control, cells were treated with the equivalent volume of solvent (methanol). The samples were incubated in the dark for 5 h at 30 °C before collected by centrifuging at 5000 rpm for 5 min. The samples were washed three times with PBS, resuspended in 200 µl of medium, and incubated for 30 min in the dark at 30 °C to reconstitute functional aequorin within the cells. After the incubation, cells were transferred into a 96 well microplate. Luminescence readings were taken every 1 min with 40 secs shaking in between each read using a BMG LABTECH FLUOstar OPTIMA or a BMG LABTECH SPECTROstar Nano plate reader. The gain has been adjusted to 3600. After

10 cycles to record the baseline luminescence, the plate was ejected to add 50 mM $CaCl_2$. The plate was returned to the plate reader and readings were taken for a further 1 h.

3.2.17 Mitochondrial fragmentation using MitoTracker Green FM

Cells were resuspended at 10^6 cells/ml in pH (pH 4, pH 8) adjusted media and incubated with 200 mM NaB for 1 h. Cells were then washed with PBS three times before incubating the cultures at room temperature for 30 min with 100 nM of Mitotracker Green FM (1 mM stock). Cells were washed with 1x PBS before capturing the image using an Olympus IX81 fluorescence microscope using GFP filter set (395/509 excitation/emission) at 100x magnification using an Andor Xyla 4.2 CMOS digital camera.

3.2.18 Relative GFP intensity as indicator for intracellular pH

The SN250 mtGFP *C. albicans* strain (Duvenage *et al.*, 2019) was grown overnight in YPD at 30 °C under constant rotation. Cells were sub-cultured to an OD600 nm of 0.2 in a white 96-well plate for fluorescence work containing appropriate medium with or without stresses (200 mM NaB and/or 2 µM Antimycin A). Readings were taken every 5 min with shaking in between at 37 °C. 20 readings (20 cycles) were taken in total.

3.2.19 High Resolution Respirometry

To examine the consumption of oxygen from mitochondria in cell suspensions, the Orobus O2K Oxygraph High Resolution Respirometer was used. For the acquisition and analysis of data generated, the Datlab 4 software was used. The respirometer was air calibrated using

1x PBS. *C. albicans* precultures grown overnight in YPD medium were sub-cultured in pH 4 or pH 8 adjusted RPMI medium to an OD600 nm of 0.1. 2.5 ml of each diluted culture was then pipetted into one of the two chambers. The chamber stoppers were placed into closed position and any residual liquid culture was removed. To obtain an accurate oxygen flux/cell reading, the precise cell concentration was entered into the Datlab4 software. After obtaining the routine respiration, 200 mM NaB was added either gradually or at once. A 5 min interval between the addition of each drug was left to facilitate the detection of a full drug response. 2 µM Antimycin A (Anti A; 2 mM stock solution in ethanol) (Sigma-Aldrich) was added after each trial.

3.3 Results

3.3.1 Effect of NaB addition on *C. albicans* planktonic cells SC5314

First, we wished to assess the effect of NaB addition on planktonic *C. albicans* cells grown in rich (YPD) and defined media that promotes hyphal growth (RPMI). The growth of *C. albicans* was assessed in YPD and RPMI media supplemented with a range of NaB concentrations (1 mM, 10 mM, 50 mM, 100 mM, 200 mM, 300 mM, 400 mM) that represent normal levels found in the gut (Louis and Flint, 2017; Tahara *et al.*, 2018; Yang *et al.*, 2020; Pant *et al.*, 2023; Andrusaite *et al.*, 2024) as well as levels that have been used in mammalian studies as potential therapeutic strategies (Jiminez *et al.*, 2017). To compare the growth curves and assess statistical significance, the areas under the curves (AUCs) were calculated using GraphPad Prism. Here, the trapezoidal method was applied where each connecting segment under the growth curve describes a trapezoid. The sum of each segmental trapezoid forms the total AUC.

In YPD medium no significant difference in growth was observed between the untreated WT and 1 mM, 10 mM, 50 mM, and 100 mM NaB *C. albicans* cultures (Figure 1 A, B). A significant decrease in growth could be seen at 200 mM and above with treatment at 400 mM resulting in negligible growth (Figure 1 A, B). In RPMI medium, no significant difference in growth was observed between the untreated WT and 10 mM, and 50 mM NaB treated cells (Figure 1 C, D). A significant decrease in growth was observed between 100 mM - 400 mM NaB treated cells. However, in contrast to YPD medium no additional reduction in growth was observed above 200 mM (Figure 1 C, D). Interestingly, a significant difference in

growth reduction could also be observed when 1 mM NaB was added (Figure 1 C, D).

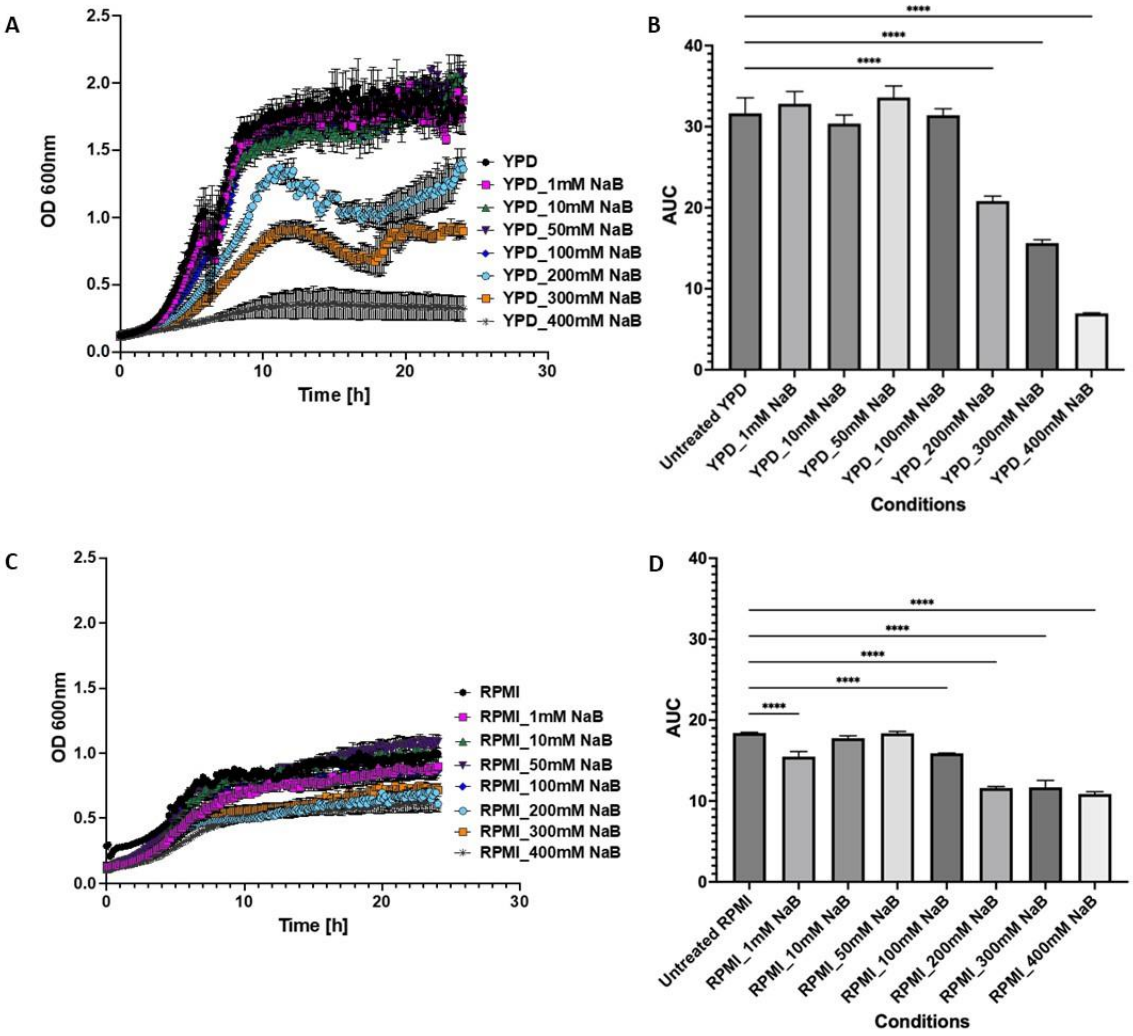


Figure 1 Growth analysis of SC5314 C. albicans in YPD and RPMI media supplemented with various NaB concentrations.
The growth analysis was undertaken through 24 h growth curves and AUC data. Each graph represents an average of three biological repeats. The error bars display the standard deviation. A One-Way ANOVA using a Tukey multiple comparison test was used to determine statistical significance. (*) flags levels of significance compared to the untreated WT.
A) SC5314 Growth curves in YPD media supplemented with various NaB concentrations.
B) SC5314 AUC YPD.
C) SC5314 Growth curves in RPMI media supplemented with various NaB concentrations.
D) SC5314 AUC RPMI.

3.3.2 Effect of NaB addition on *C. albicans* SC5314 biofilms

C. albicans can exist within a mixed-species biofilm within the gut and several resident bacteria can produce the SCFA butyrate (Wong *et al.*, 2006; Peleg, Hogan and Mylonakis, 2010; Biddle *et al.*, 2013). In addition, butyrate can be found within the diet and administered as a therapeutic (Liu *et al.*, 2018). We therefore assessed the effect of a range of butyrate concentrations on the ability of *C. albicans* to establish a biofilm.

To do this XTT assays and crystal violet assays (CV) were performed after 24 h of growth in RPMI medium in the presence of a range of concentrations of butyrate. NaB was added at concentrations between 100 mM – 400 mM after a 90 min attachment phase. The XTT analysis showed a clear reduction in metabolic activity within the biofilm after supplementation of 50 mM – 400 mM (Figure 2 A). The CV analysis showed a reduction in biofilm mass when 200 mM – 400 mM NaB was added. Lower NaB concentrations did not show any biofilm mass reduction (Figure 2 B). When 50 mM or 100 mM of NaB was supplemented the XTT value was reduced (Figure 2 A) but CV levels, which represent biofilm biomass, remained at the same level as untreated cells (Figure 2 B).

To identify any changes in morphology in 24 h *C. albicans* SC5314 RPMI biofilms formed in the presence of NaB, widefield fluorescence microscopy was utilised. In line with CV staining, which labels proteins and glucan within the matrix and cell surface, we did not observe a difference between control and 100 mM NaB treated biofilms. However, a clear reduction in biofilm formation was visible at NaB concentrations above 100 mM (Figure 2 C).

Candida biofilms are more resistant to antifungal drugs in comparison to planktonic cells. This is due to multifactorial reasons, some of which are the independent upregulation of drug-efflux pumps and the presence of the extracellular matrix which acts as a physical

barrier but also stabilises the biofilm structure. There are only three classes of antifungal drugs available for both systemic and superficial fungal infections, one of them being azoles. In *Candida*, the stress gene *MKC1* is upregulated upon azole exposure and is involved in drug resistance. The azole resistance through Mkc1 – the terminal mitogen-activated protein kinase of the protein kinase C pathway - is mediated by Hsp90 and calcineurin (Kumamoto, 2005; Uppuluri *et al.*, 2008; LaFayette *et al.*, 2010; Robbins *et al.*, 2011; Robbins, Caplan and Cowen, 2017; Kaur and Nobile, 2023). Fluconazole is a commonly used antifungal drug to treat candidiasis and interrupts the conversion of lanosterol to ergosterol ultimately leading to disruption of fungal membranes.

After observing a loss of matrix (Figure 2 C), we sought to investigate whether NaB addition could have an effect on *C. albicans* SC5314 biofilms sensitivity to fluconazole.

A significant decrease in biofilm growth could be observed when fluconazole was added at concentrations of 60 µg/ml, 120 µg/ml or 240 µg/ml (Figure 2 D, E). However, no additional decrease in biofilm growth could be observed in combination with 200 mM NaB (Figure 2 D,

E).

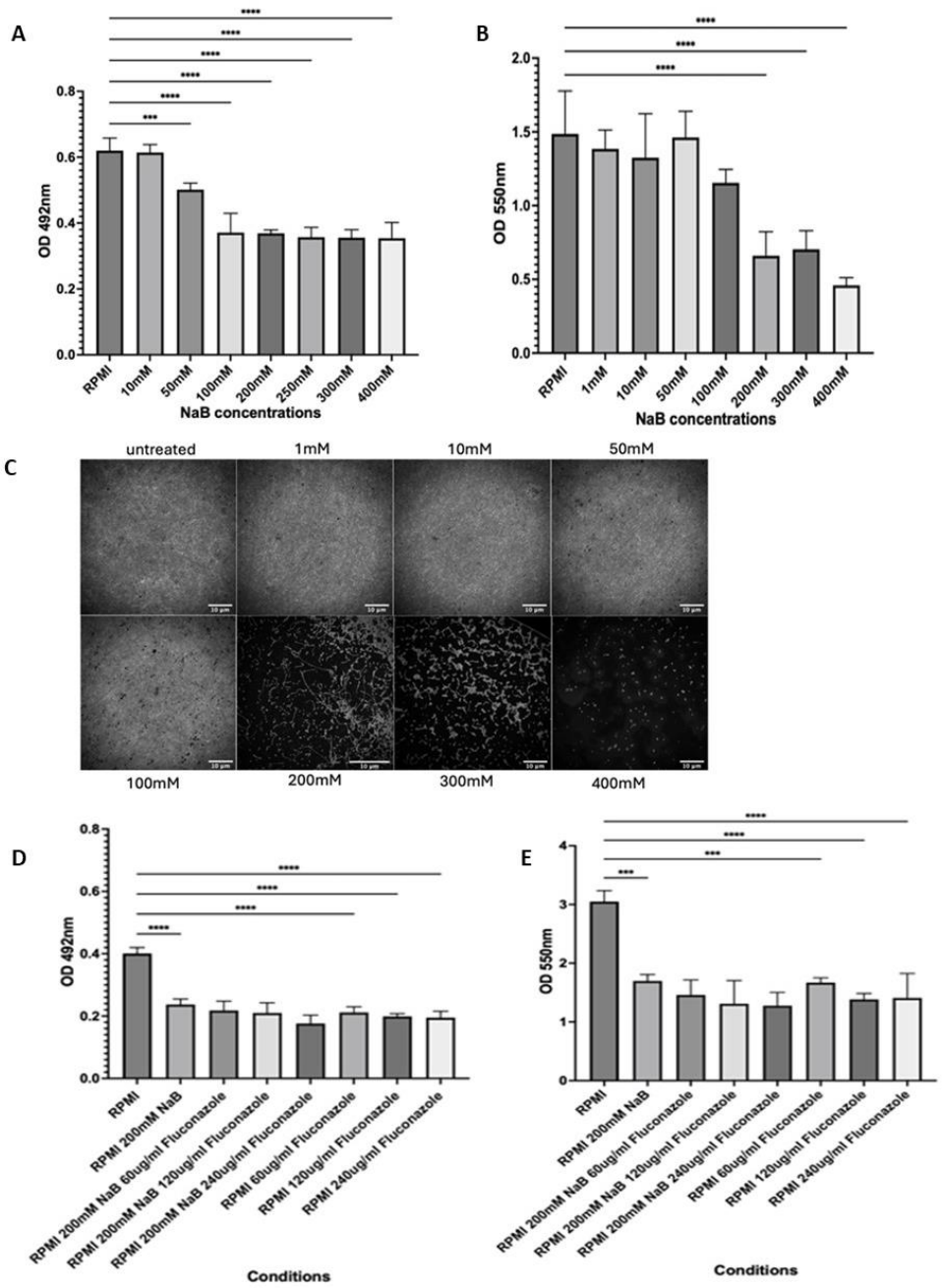


Figure 2 The effect of NaB on SC5314 24 h biofilm formation in RPMI media.
A, B) XTT and crystal violet (CV) quantifications of 24 h SC5314 biofilms with NaB supplementation after the attachment phase.
C) CV images (RFP 488/583 excitation/emission) of 24 h SC5314 biofilms with NaB supplementation after the attachment phase. Images represent three biological repeats. The scale bar is 10 µm and the magnification is x20.
*D, E) XTT and CV quantifications of 24 h SC5314 biofilms. 200 mM NaB was added after the attachment phase. Fluconazole concentrations were added after 24 h biofilm growth and incubated for another 24 h. XTT and CV quantifications represent an average of three biological repeats. The error bars display the standard deviation. A One-way ANOVA using a Tukey multiple comparison test was used to determine statistical significance. Non-significant = NS, * = adjusted p-value ≤ 0.05 and *** = adjusted p value ≤ 0.001.*

Once a biofilm is established, yeast cells from the top hyphae layer may detach from the biofilm and infect other areas. These dispersal cells are elongated yeast cells with enhanced virulent properties such as increased adhesion and filamentation as well as drug resistance (Uppuluri, Chaturvedi, *et al.*, 2010; Uppuluri *et al.*, 2018).We therefore sought to investigate whether NaB had an effect on *C. albicans* SC5314 dispersion from biofilms. A *C. albicans* SC5314 biofilm was grown on plastic leaflets for 48 h in the presence or absence of 200 mM NaB and 5 % CO_2 exposure. Secondary biofilm formation because of shedding was then analysed after another 48 h in the absence of NaB. The XTT analysis revealed a significant decrease in metabolic activity in the NaB pre-treated secondary biofilm formed after shedding (Figure 3 A). CV quantification showed a significant loss of biofilm mass in the NaB pre-treated secondary biofilm formed after shedding (Figure 3 B). CV images confirmed the loss of biofilm mass in NaB pre-treated secondary biofilm formed after shedding (Figure 3 C).

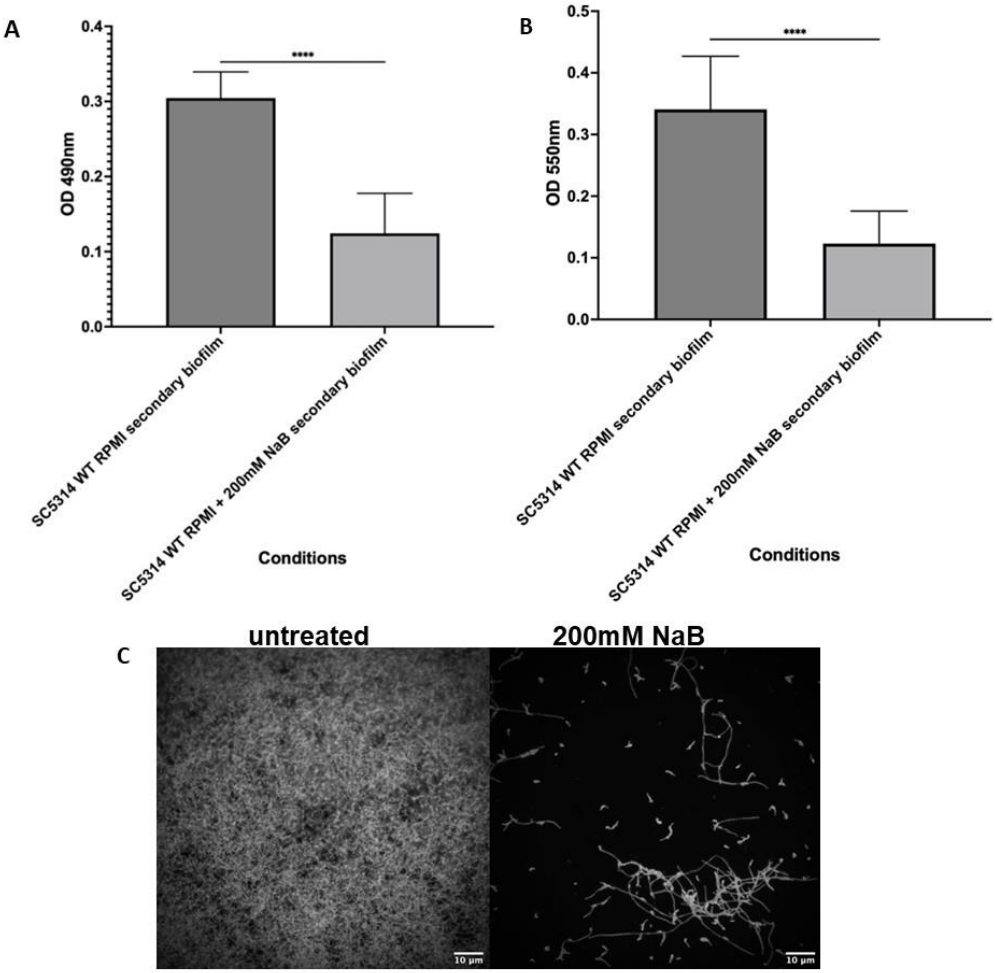


Figure 3 C. albicans SC5314 Metastasis assay in RPMI in presence or absence of 200 mM NaB.
*C. albicans SC5314 biofilms were grown on plastic leaflets for 48 h in the presence or absence of 200 mM NaB and 5 % CO_2 exposure. Secondary biofilm formation as a result of shedding was then analysed after another 48 h in untreated RPMI media. The data shown represent an average of three biological repeats. The error bars display the standard deviation. A One-way ANOVA using a Tukey multiple comparison test was used to determine statistical significance. Non-significant = NS, * = adjusted p-value ≤ 0.05 and *** = adjusted p value ≤ 0.001.*
A) XTT analysis.
B) CV analysis.
C) CV images (RFP 488/583 excitation/emission) of secondary untreated biofilms or secondary biofilms after 200 mM NaB treatment, x20 magnification, the scale bar is 10 µm.

3.3.3 Effect of NaB addition on *C. albicans* SC5314 agar invasion

C. albicans is able to invade epithelial cell layers effectively when it transitions to hyphal growth (Desai, 2018). To investigate whether NaB addition has an effect on *C. albicans*

invasion, an agar invasion assay was performed. The assay was performed on three different types of media commonly used for biofilm studies: YPD, RPMI, and spider media. *C. albicans* SC5314 were incubated with 200 mM NaB for 1 h, 6 h, 24 h before plating on plates lacking NaB, or constantly exposed where NaB was contained within the agar plates. Colonies were imaged before washing plates to remove all cells above the agar surface to reveal those that had invaded into the plate.

On YPD agar, invasion could be observed in both the untreated *C. albicans* SC5314 control strain and in NaB-pre-treated colonies. It was noted that the centres of pre-treated colonies appeared different to the untreated control. However, it is unclear from the images whether these areas were comprised uninvaded or morphologically different areas (Figure 4).

On RPMI agar, a thick layer of hyphae could be observed at the edges of the untreated control colony before and after washing (Figure 4). However, strong hyphae filamentation and invasion could be also observed in NaB-treated colonies, with again some differences in the centre as observed on YPD (Figure 4).

On spider media, a thick layer of hyphae could be observed at the edges of the untreated control colony before and after washing (Figure 4). Interestingly, the strongest reproducible effect of limited hyphae growth could be observed after 1 h of 200 mM NaB exposure before and after washing (Figure 4). After 6 h NaB exposure, an increase in filamentation and invasion could be observed which then decreased again after 24 h NaB exposure. Constant NaB exposure appeared to have similar invasion effects to those observed following 24 h NaB exposure (Figure 4). This may suggest that NaB pre-treatment can

reduce filamentation and invasion in media promoting hyphal transition such as spider media, however, not in rich media that promotes cell division such as YPD.

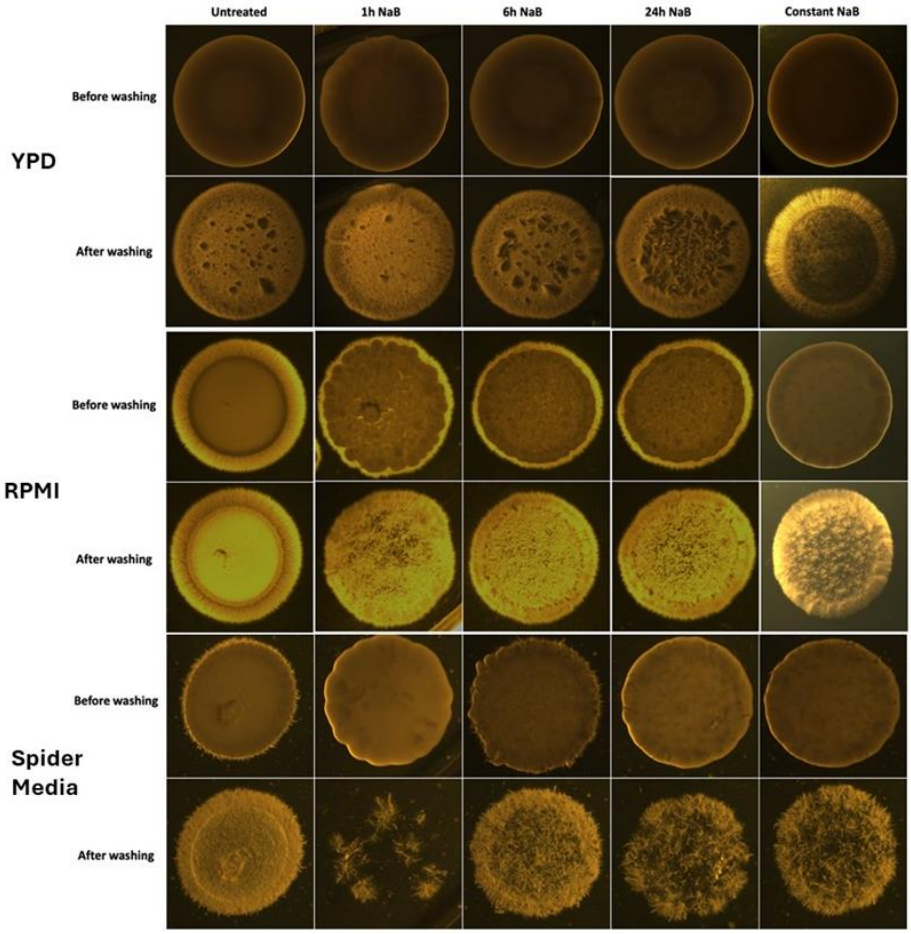


Figure 4 C. albicans SC5314 Agar Invasion on YPD, RPMI, and Spider Media agar.
C. albicans SC5314 were incubated with 200 mM NaB for 1 h, 6 h, 24 h, or constantly exposed to 200 mM NaB agar plates. Cells were adjusted to 1 x 107 cells/ml in PBS and 3 µl of 1 x 107 cells/ml were spotted onto YPD, RPMI, and Spider media agar plates. Images before and after washing were taken after 3 days when first signs of invasion became visible. The images above are representative of an average of three biological repeats.

3.3.4 Effect of NaB addition on hyphae formation of *C. albicans* SC5314

Since our results shown above indicate that NaB treatment could reduce invasion of agar under filamenting conditions and reduce biofilm formation we sought to investigate the

effect of NaB on hyphal initiation and growth. Cells were incubated in RPMI medium at 37 °C to induce hyphal transition, and the effects of supplementation with 200 mM NaB were observed over a 6 h period. Calcofluor white was used to visualise the fungal cell wall and assess morphological changes associated with hyphal initiation and growth. Calcofluor white binds to β-linked polysaccharides, including chitin and glucans, present in the fungal cell wall, producing fluorescence that outlines the cells and enables visualisation of their morphology (Rasconi *et al.*, 2009). Calcofluor white staining therefore allowed differentiation of yeast-form cells from germ tubes and hyphal structures, with the appearance and elongation of hyphal extensions used to assess hyphal initiation and growth. In the untreated *C. albicans* SC5314 samples, early signs of hyphal formation were observed after 2 and 4 h, while long hyphal extensions were seen after 6 h (Figure 5). In contrast, when cells were incubated with 200 mM NaB, hyphal initiation was not observed over the 6 h experimental period, with cells remaining in the yeast form (Figure 5).

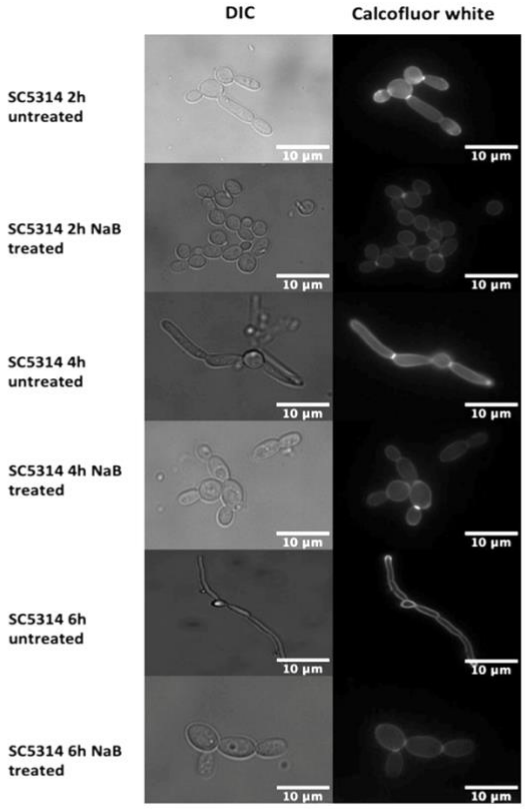


Figure 5 C. albicans SC5314 Filamentation assay in RPMI in presence or absence of 200 mM NaB over 2 h, 4 h, 6 h.
C. albicans SC5314 were incubated with or without 200 mM NaB for 2 h, 4 h, 6 h in RPMI. Cells were visualised at x100 magnification under Bright field (BF) or Dapi channel (Calcofluor white stain). Images represent three biological repeats. The scale bar is 10 µm.

3.3.5 Effect of NaB addition on histone acetylation status in planktonic *C. albicans* SC5314 cells

NaB has been shown to act as an HDAC inhibitor in several systems. To assess whether NaB addition induces changes in histone H4 acetylation consistent with HDAC inhibition and to obtain information of the temporal nature of this action we carried out a western blot to detect Histone H4 acetylation levels in planktonic *C. albicans* SC5314 cells. Proteins were extracted after 0 min, 15 min, 30 min, 60 min, 6 h, and 24 h following 200 mM NaB

exposure in YPD medium at 30 °C and probed with the anti-rabbit H4 primary antibody and the anti-rabbit Pgk1 loading control.

A rapid increase in the histone H4 acetylation signal could be observed upon NaB exposure after 30 min until 6 h, before decreasing slightly at 24 h (Figure 6 A, B). However, as total H4 protein levels were not assessed, it cannot be determined whether the observed changes in H4 acetylation signal reflect altered H4 acetylation, changes in H4 protein abundance, or a combination of both. The 0 min sample represents the initial baseline following NaB addition, rather than a time-matched untreated control. As untreated samples were not included at the corresponding time points, time-dependent changes in H4 acetylation in the absence of NaB cannot be excluded.

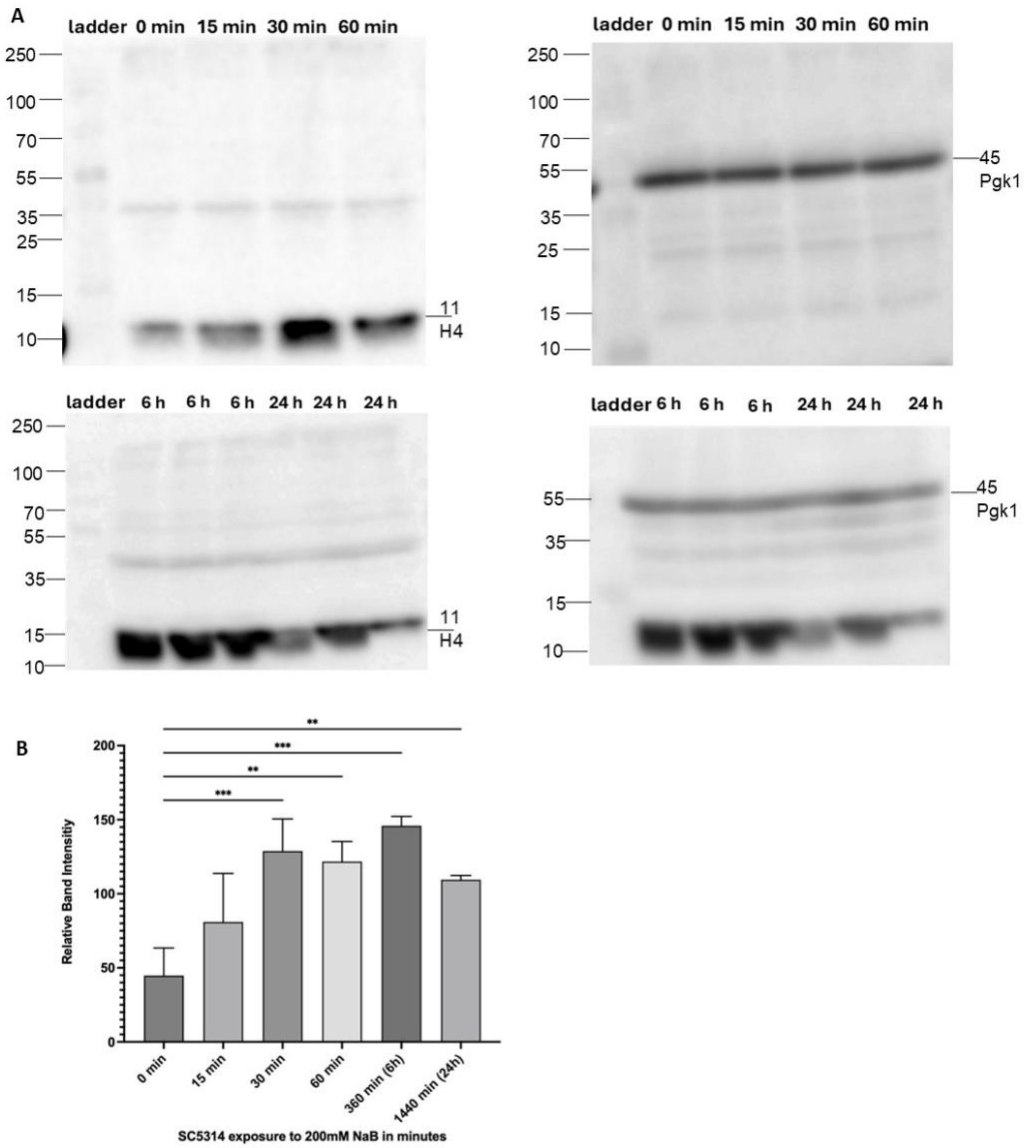


Figure 6 Western blot analysis displaying the detection of H4 (A) in a SC5314 background and a bar chart (B) representing the change in H4 acetylation relative to Pgk1 loading control. The cells were cultured in YPD media and sampled during log phase of growth at 0 min, 15 min, 30 min, 60 min, 6 h, 24 h after incubation with 200 mM NaB. Uniform protein loading was ensured by probing levels of Pgk1 after probing for H4. This experiment is a representative data set of three repeats.

3.3.6 Effect of HDAC deletions and of NaB on SC5314 planktonic and biofilm growth

As we could see an increase in H4 acetylation in NaB treated *C. albicans* SC5314 cells, we wanted to determine whether loss of any particular HDAC gene produced the same phenotype. To test this, we obtained the following HDAC deletion strains: Δ*sir2* (Class III; part of sirtuin family, NAD^+ dependent HDAC), Δ*rpd31* (Class I; necessary to initiate filamentous growth), Δ*hos2* (Class I; part of the Set3 complex' core; essential for Set3C assembly), Δ*hst1* (Class III; members of sirtuin family, part of the peripheral part of the Set3 HDAC complex), Δ*hst2* (Class III; crucial in morphological transition), Δ*set3* (Class III; Set3 is an NAD^+ dependent HDAC, important for morphogenesis), Δ*hda1* (Class II; important in hyphal development).

Firstly, we sought to identify the effect of HDAC deletions on growth of planktonic cells. We therefore conducted a growth curve assay in YPD and RPMI media supplemented with 200 mM NaB.

In YPD media a small but significant decrease in growth, based on AUC values could be seen in all strains apart from Δ*hst1*, Δ*sir2* and Δ*hda1* compared to the SC5314 wild type (WT) strain. The more pronounced effect on growth was observed in cells lacking *SIR2* (26.6 units) or *HDA1* (26.4 units) (Figure 7 A, B).

In YPD medium supplemented with 200 mM NaB, significant differences in growth based on AUC values were observed for all strains compared to the untreated YPD WT (Figure 7 B, C, D). Compared to the NaB treated WT differences in growth were seen in *Δsir2*, and *Δhda1* (Figure 7 C, D). Fold change of NaB-treated strains and their corresponding untreated strains compared to the fold change of treated/untreated WT strain showed only a significant difference in growth in *Δsir2*, and *Δhda1* (Figure 7 E).

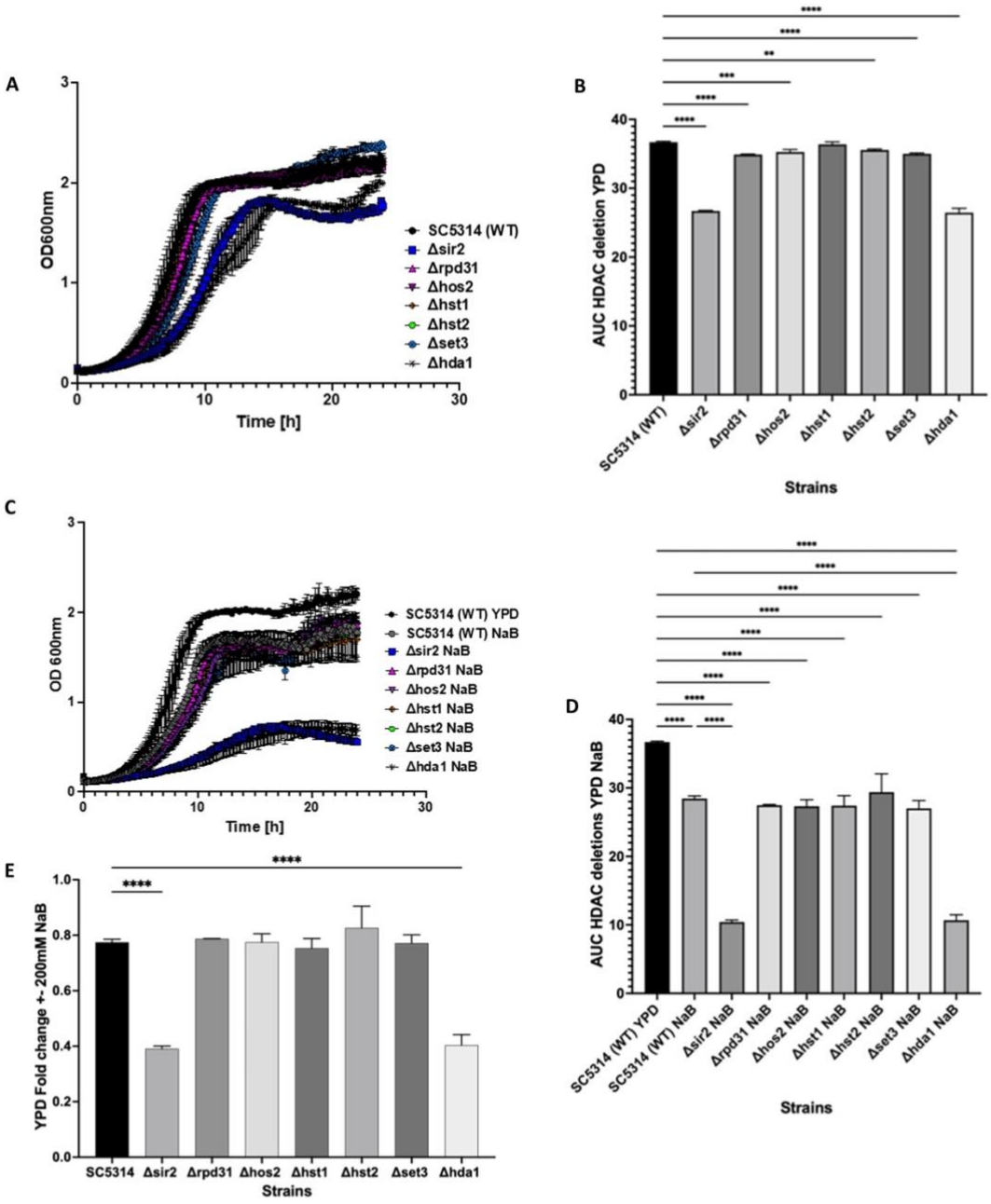


Figure 7 24 h Growth curve analysis of SC5314 and HDAC deletion strains in YPD media with or without NaB supplementation.

A) 24 h Growth curves of SC5314 and HDAC deletions strains in YPD media.

B) AUC analysis of 24 h growth curves in YPD.

C) 24 h Growth curves of SC5314 and HDAC deletions strains in YPD media supplemented with 200 mM NaB.

D) AUC analysis of 24 h growth curves in YPD supplemented with 200 mM NaB.

E) Bar chart representing the fold change of untreated/NaB treated strains.

The data represents an average of three biological repeats. The error bars represent the standard deviation. A One-Way ANOVA using a Tukey multiple comparison test was used to determine statistical significance.

In RPMI medium, *Δsir2*, *Δhda1* showed severe growth defects compared to the WT control (Figure 8 A, B). *Δset3* also showed some reduction in growth compared to the WT control (Figure 8 A, B). 200 mM NaB supplementation led to a significant reduction in growth in the treated WT control strain compared to its untreated control (Figure 8 C, D). NaB-treatment showed no effect on growth in *Δsir2* and *Δhda1* strains (Figure 8). Fold change analysis showed that all strains with the exceptions of *SET3* deletion showed a fold change reduction in growth equivalent to the wild type. These findings suggest that the deletion of *SET3* leads to an insensitivity of *C. albicans* to exposure of NaB with respect to planktonic growth (Figure 8 E).

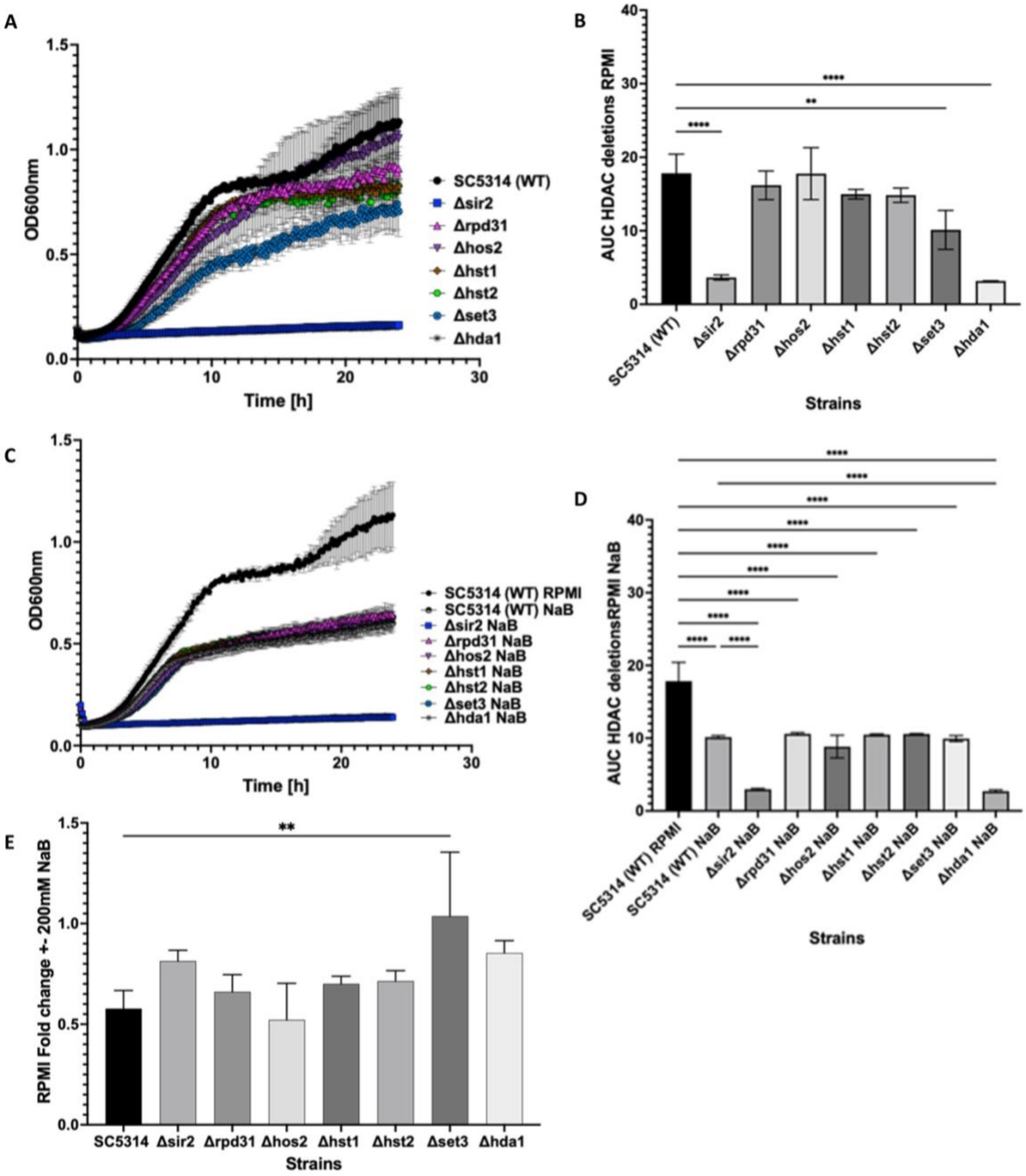


Figure 8 24 h Growth curve analysis of SC5314 and HDAC deletion strains in RPMI media with or without NaB supplementation.
A) 24 h Growth curves of SC5314 and HDAC deletions strains in RPMI media.
B) AUC analysis of 24 h growth curves in RPMI.
C) 24 h Growth curves of SC5314 and HDAC deletions strains in RPMI media supplemented with 200 mM NaB.
D) AUC analysis of 24 h growth curves in RPMI supplemented with 200 mM NaB.
E) Bar chart representing the fold change of untreated/NaB treated strains.
The data represents an average of three biological repeats. The error bars represent the standard deviation. A One-Way ANOVA using a Tukey multiple comparison test was used to determine statistical significance.

3.3.7 Effect of HDAC deletions in addition to NaB treatment on biofilm growth

As we had observed significant effects for NaB addition on biofilm growth, we wished to determine the effect of combining NaB supplementation with the deletion of HDAC genes. To do this, XTT and crystal violet assays were performed on biofilms grown in the presence and absence of 200 mM NaB in RPMI medium. A clear reduction in metabolic activity compared to the WT could be observed when *SIR2, HOS2, HST1, SET3*, or *HDA1* were deleted, but not in *RPD31* or *HST2* deletion strains (Figure 9 A). Significant reduction in biofilm mass compared to the WT was detected when *SIR2*, *RPD31*, *HOS2*, *HST1*, *HST2*, *SET3*, or *HDA1* were deleted (Figure 9 B). In NaB-treated biofilms reduced metabolic activity compared to the treated WT could be detected in *Δrpd31*, *Δhos2*, *Δhst1*, *Δhst2*, and *Δhda1*, but not in *Δsir2* and *Δset3* strains (Figure 9 C). Reduced biofilm mass compared to the NaB-treated WT could be observed in *Δsir2*, *Δhst1*, and *Δset3*, but not in *Δrpd31, Δhos2, Δhst2*, and *Δhda1* strains (Figure 9 D). Fold change analysis showed that all strains except for the *SET3* deletion had fold change reduction in metabolic activity (XTT) equivalent to the wild type (Figure 9 E). However, fold change reduction in biomass as seen in the WT were observed in all strains except for *Δsir2, Δhos2*, and *Δhda1*. The fold change of the biofilm mass remained unchanged in the *SET3* deletion (Figure 9 F).

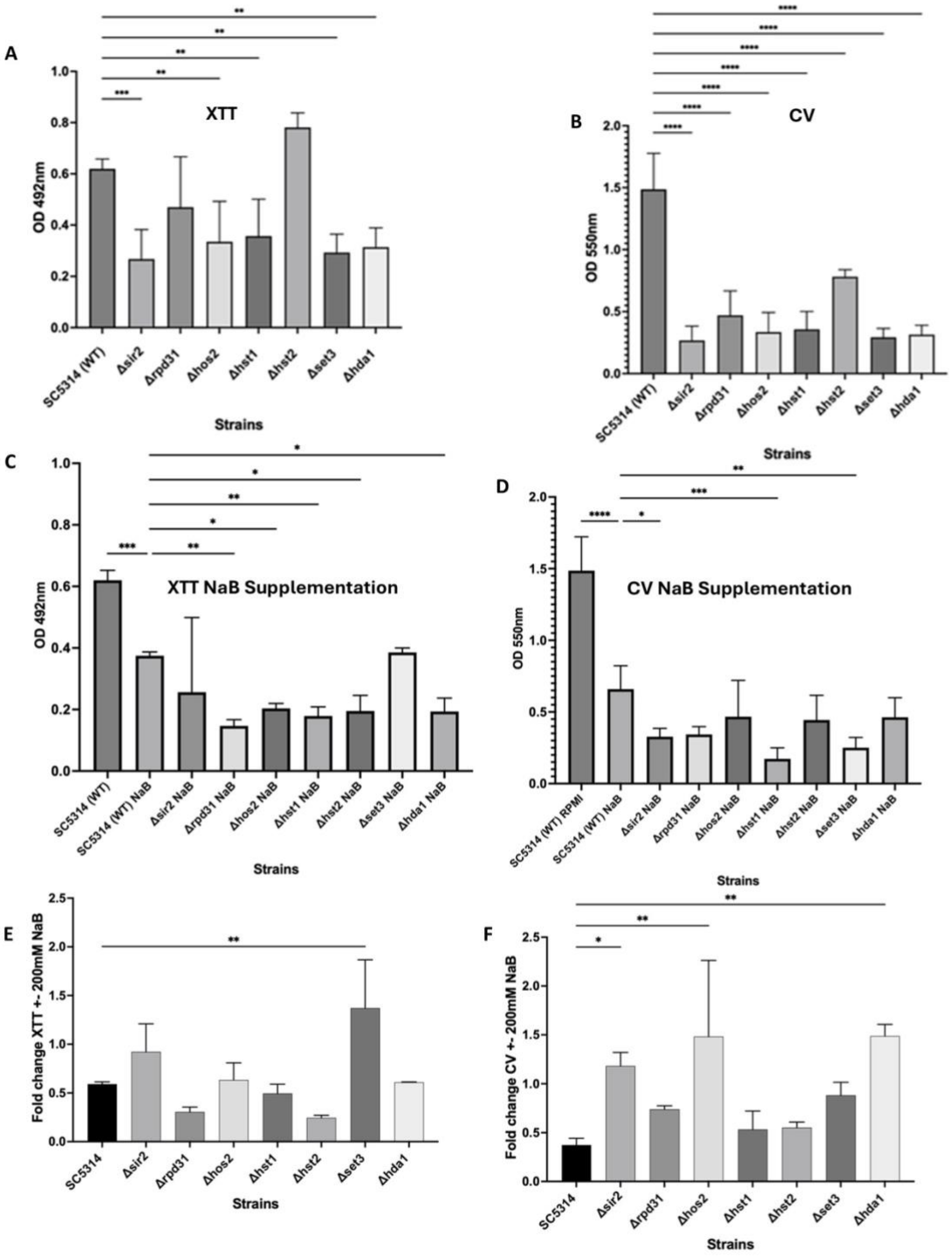
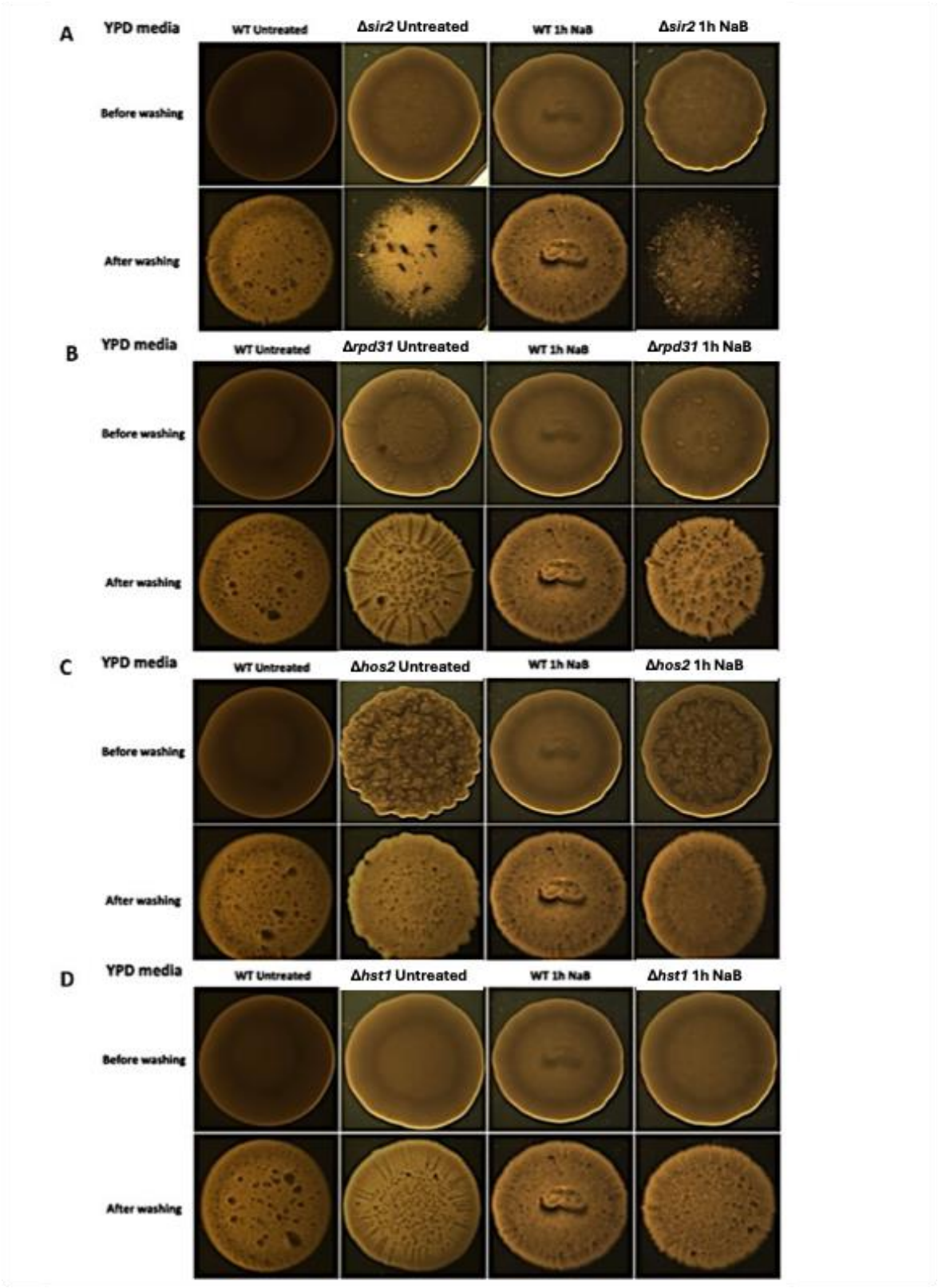


Figure 9 C. albicans SC5314 and HDAC deletions 24 h biofilm quantification with and without NaB using XTT and CV.

*Biofilms were grown in 96 well plates in RPMI media. 200 mM NaB was added to the media after the attachment phase. XTT (A,C) and CV (B, D) quantifications represent an average of three biological repeats. Fold changes (E, F) of NaB-treated/untreated biofilms were calculated for both XTT and CV data comparing to the fold change of the WT. The error bars display the standard deviation. A One-way ANOVA using a Tukey multiple comparison test was used to determine statistical significance. Non-significant = NS, * = adjusted p-value ≤ 0.05 and *** = adjusted p value ≤ 0.001.*

3.3.8 Effect of HDAC deletions and of NaB on invasion

Next, we investigated how HDAC deletions impact the effect of NaB on agar invasion. On YPD agar, less invasion could be observed with the untreated and NaB-treated *Δsir2* and *Δhda1* strains when compared to the untreated and NaB-treated WT control (Figure 10 A, G). No obvious difference in invasion could be observed in the other untreated or treated deletion strains (*RPD31, HOS2, HST1, HST2, SET3*) compared to the untreated or treated WT controls (Figure 10). Colony morphology changes in both untreated and treated colonies compared to the untreated and NaB-treated WT control could be observed in *HOS2* and *SET3* deletions (Figure 10 C, F). It should be noted that the one-hour NaB treatment may not have been sufficient to elicit a detectable effect. Furthermore, as NaB was not present in the YPD agar plates, cells were subsequently grown under standard conditions, which may have limited the ability to observe any sustained effects of NaB treatment.


A
YPD media
WT Untreated
Δsir2 Untreated
WT 1h NaB
Δsir2 1h NaB
Before washing
After washing
B
YPD media
WT Untreated
Δrpd31 Untreated
WT 1h NaB
Δrpd31 1h NaB
Before washing
After washing
C
YPD media
WT Untreated
Δhos2 Untreated
WT 1h NaB
Δhos2 1h NaB
Before washing
After washing
D
YPD media
WT Untreated
Δhst1 Untreated
WT 1h NaB
Δhst1 1h NaB
Before washing
After washing

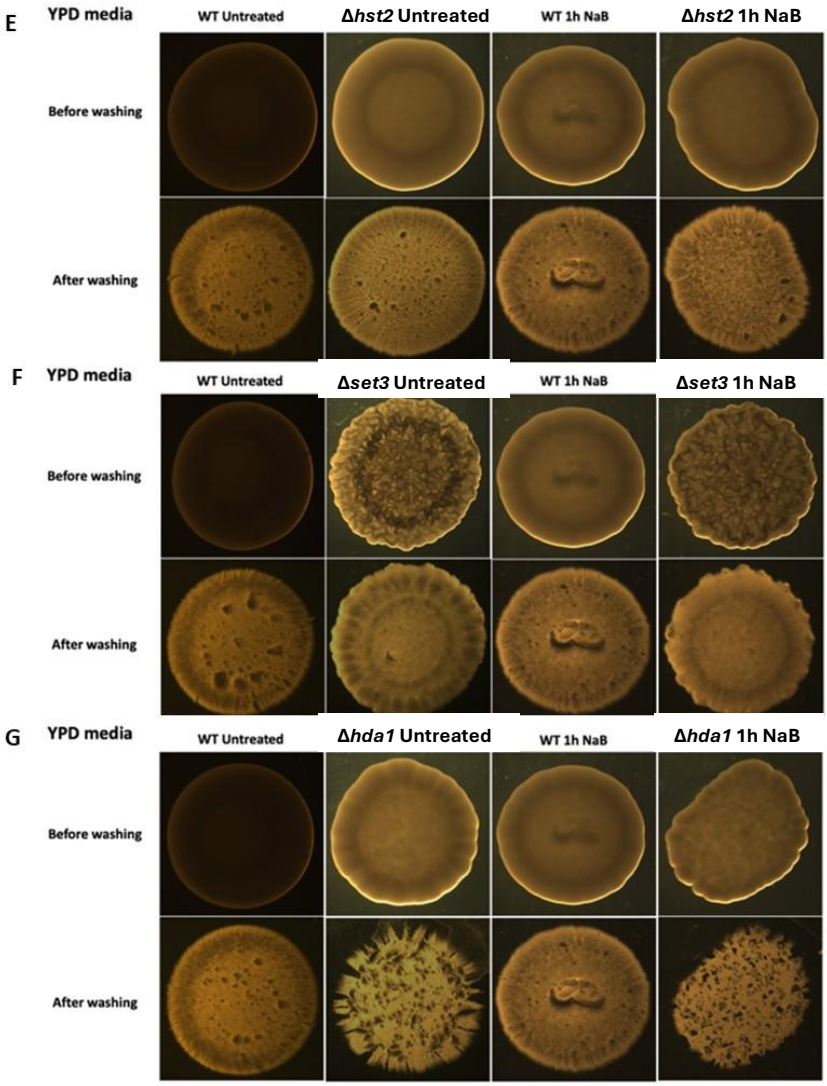
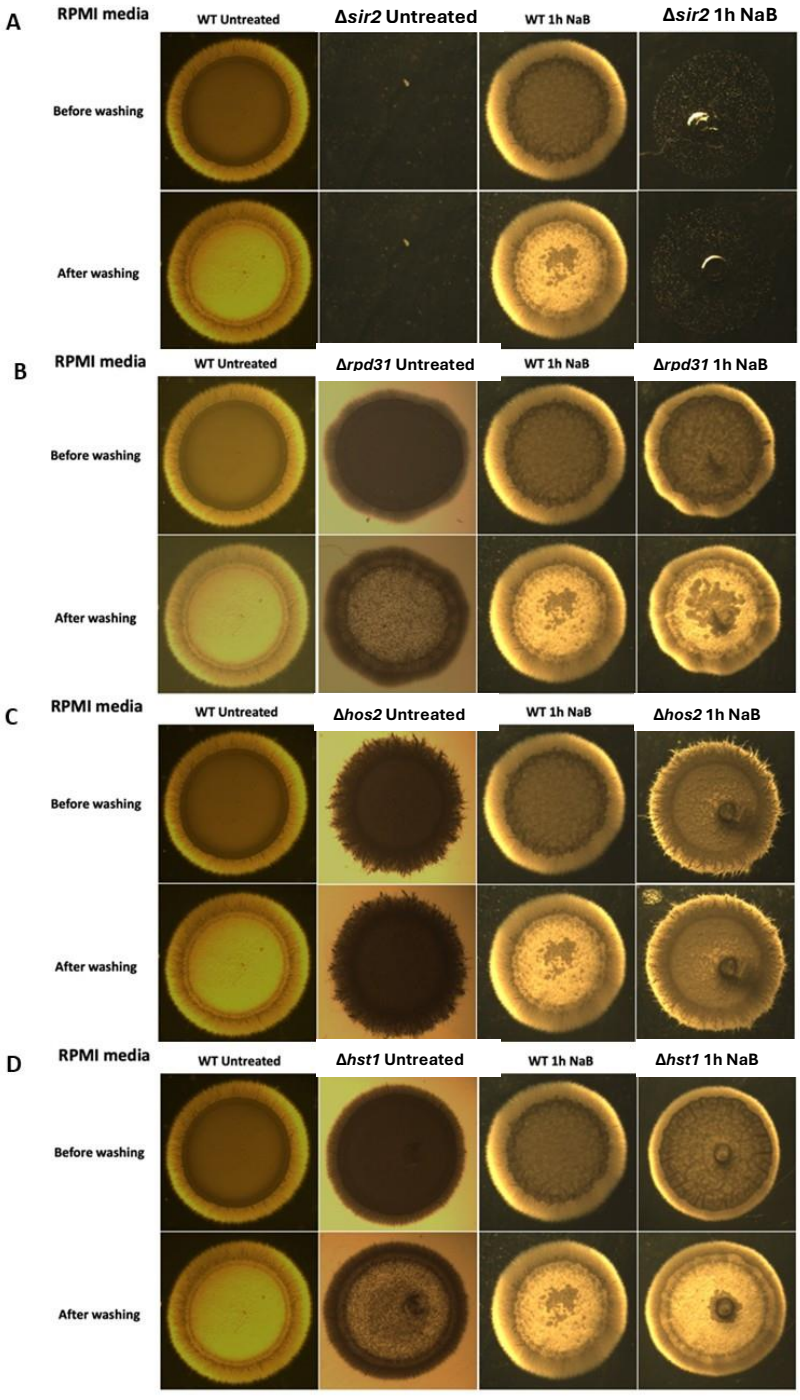


Figure 10 C. albicans SC5314 and HDAC deletions Agar Invasion on YPD agar.
C. albicans SC5314 and HDAC deletion strains were incubated with 200 mM NaB for 1 h. Cells were adjusted to 1 x 107 cells/ml in PBS and 3 µl of 1 x 107 cells/ml were spotted onto YPD agar plates. Images before and after washing were taken after 3 days when first signs of invasion became visible. The images above are representative of an average of three biological repeats.
A) WT and Δ sir2 agar invasion comparison.
B) WT and Δrpd31 agar invasion comparison.
C) WT and Δhos2 agar invasion comparison.
D) WT and Δhst1 agar invasion comparison.
E) WT and Δhst2 agar invasion comparison.
F) WT and Δset3 agar invasion comparison.

On RPMI agar, no colony growth could be observed for untreated *Δsir2* and *Δhda1* strains before and after washing. Some agar invasion could be detected before and after washing when *Δsir2* or *Δhda1* strains were treated with NaB for 1 h (Figure 11 A, G).

No obvious difference in invasion could be observed in the other untreated or treated deletion strains (*RPD31, HOS2, HST1, HST2, SET3*) compared to the untreated or treated WT control (Figure 11). Loss of *HOS2* and *SET3* seem to affect colony morphology but NaB addition did not add to this effect (Figure 11 C, F).



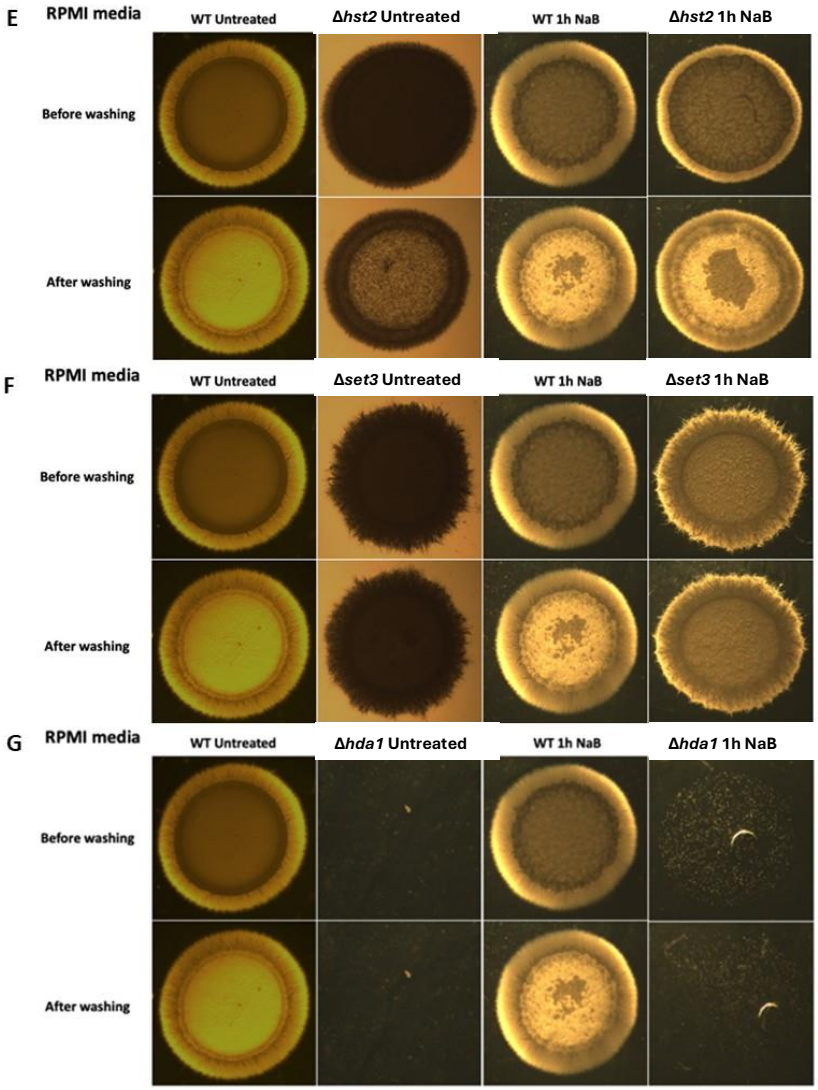
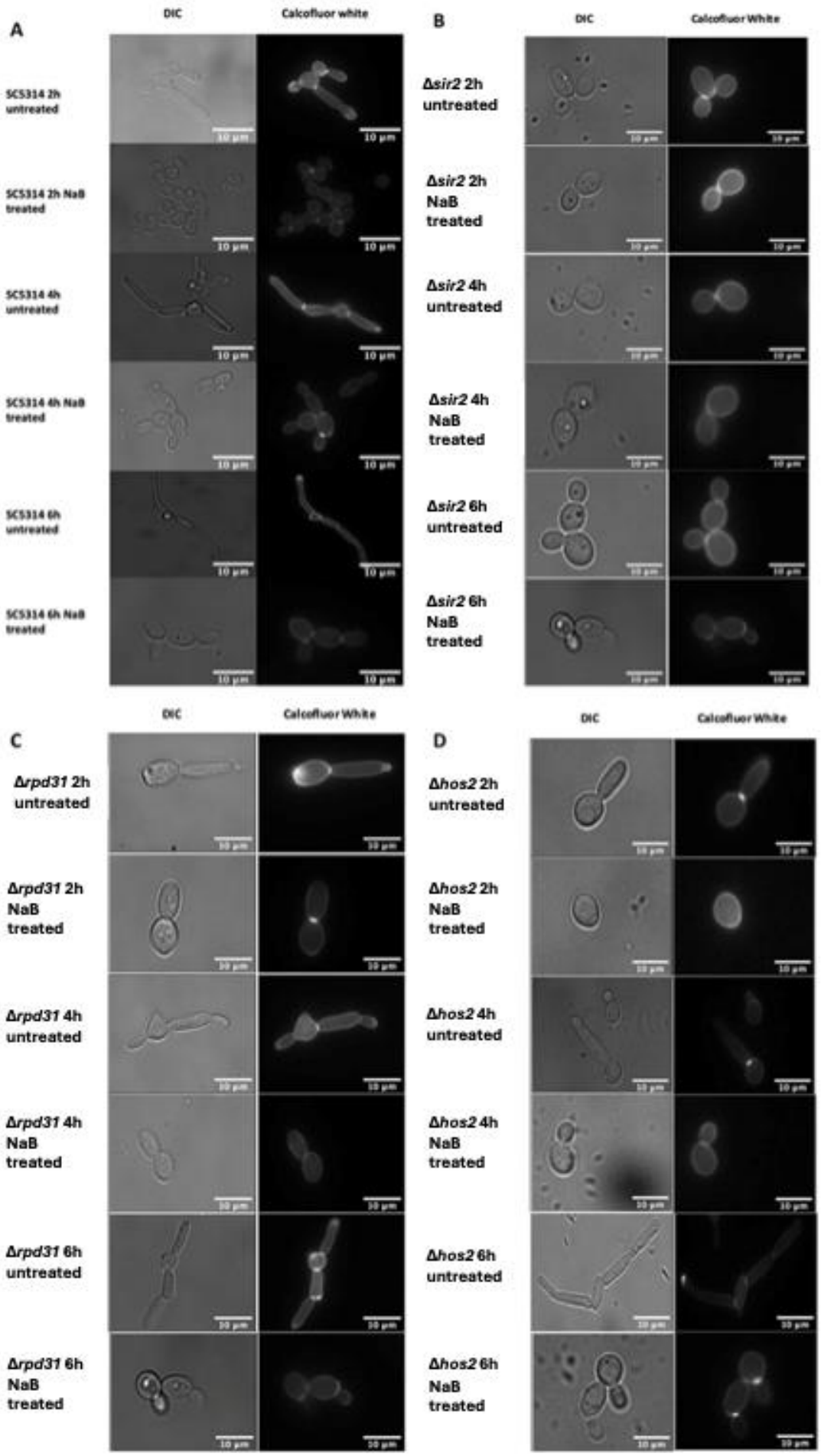


Figure 11 C. albicans SC5314 and HDAC deletions Agar Invasion on RPMI agar.
C. albicans SC5314 and HDAC deletion strains were incubated with 200 mM NaB for 1 h. Cells were adjusted to 1 x 107 cells/ml in PBS and 3 µl of 1 x 107 cells/ml were spotted onto RPMI agar plates. Images before and after washing were taken after 3 days when first signs of invasion became visible. The images above are representative of an average of three biological repeats.
A) WT and Δ sir2 agar invasion comparison.
B) WT and Δrpd31 agar invasion comparison.
C) WT and Δhos2 agar invasion comparison.
D) WT and Δhst1 agar invasion comparison.
E) WT and Δhst2 agar invasion comparison.
F) WT and Δset3 agar invasion comparison.
G) WT and Δhda1 agar invasion comparison.

3.3.9 Effect of HDAC deletions and of NaB on filamentation

To obtain a better understanding of which class of HDACs NaB inhibits in *C. albicans* we carried out widefield microscopy on NaB-treated and non-treated HDAC deletions strains over a time course of 2-6 h in RPMI medium at 37 °C. Our images showed that hyphae induction was prevented in all NaB-treated HDAC deletion strains as in the SC5314 control, so we could not identify a clear HDAC target of NaB (Figure 12). Interestingly, neither untreated nor NaB-treated *Δsir2* (Figure 12 B), and *Δhda1* (Figure 12 H) cells were able to form hyphae over a time frame of 6 h. This is in accordance with our observations in agar invasion assays (Figure 11 A, G). Induction of hyphae formation could be seen after 2 h of growth in RPMI, and upon 6 h growth in RPMI long hyphae extensions were visible in untreated *Δrpd31, Δhos2, Δhst1, Δhst2,* and *Δset3* (Figure 12 C-G).


A
DIC
Calcofluor white
SC5314 2h untreated
SC5314 2h NaB treated
SC5314 4h untreated
SC5314 4h NaB treated
SC5314 6h untreated
SC5314 6h NaB treated
B
DIC
Calcofluor White
Δsir2 2h untreated
Δsir2 2h NaB treated
Δsir2 4h untreated
Δsir2 4h NaB treated
Δsir2 6h untreated
Δsir2 6h NaB treated
C
DIC
Calcofluor White
Δrpd31 2h untreated
Δrpd31 2h NaB treated
Δrpd31 4h untreated
Δrpd31 4h NaB treated
Δrpd31 6h untreated
Δrpd31 6h NaB treated
D
DIC
Calcofluor White
Δhos2 2h untreated
Δhos2 2h NaB treated
Δhos2 4h untreated
Δhos2 4h NaB treated
Δhos2 6h untreated
Δhos2 6h NaB treated

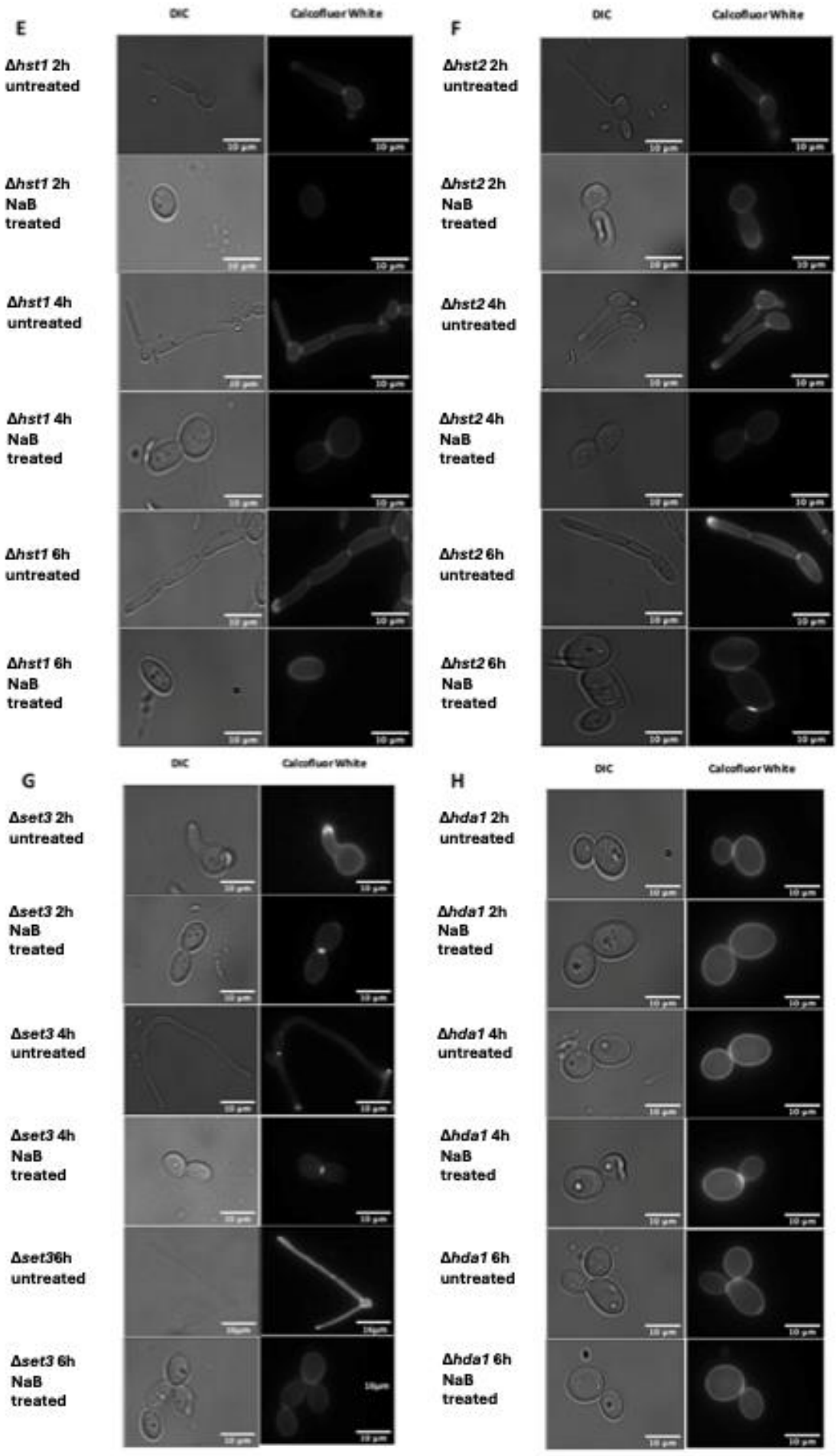

E
DIC
Calcofluor White
Δhst1 2h untreated
Δhst1 2h NaB treated
Δhst1 4h untreated
Δhst1 4h NaB treated
Δhst1 6h untreated
Δhst1 6h NaB treated
F
DIC
Calcofluor White
Δhst2 2h untreated
Δhst2 2h NaB treated
Δhst2 4h untreated
Δhst2 4h NaB treated
Δhst2 6h untreated
Δhst2 6h NaB treated
G
DIC
Calcofluor White
Δset3 2h untreated
Δset3 2h NaB treated
Δset3 4h untreated
Δset3 4h NaB treated
Δset36h untreated
Δset3 6h NaB treated
H
DIC
Calcofluor White
Δhda1 2h untreated
Δhda1 2h NaB treated
Δhda1 4h untreated
Δhda1 4h NaB treated
Δhda1 6h untreated
Δhda1 6h NaB treated

Figure 12 C. albicans SC5314 and HDAC deletion strains filamentation assay in RPMI in presence or absence of 200 mM NaB over 2 h, 4 h, 6 h.
C. albicans SC5314 and HDAC deletion strains were incubated with or without 200 mM NaB for 2 h, 4 h, 6 h in RPMI. Cells were visualised at x100 magnification under Bright field (BF) or Dapi channel (Calcofluor white stain). The scale bar is 10 µm. The image represent three biological repeats.
A) Filamentation images of WT
B) Filamentation images of Δsir2
C) Filamentation images of Δrpd31
D) Filamentation images of Δhos2
E) Filamentation images of Δhst1
F) Filamentation images of Δhst2
G) Filamentation images of Δset3
H) Filamentation images of Δhda1

3.3.10 Effect of combining Set3C HDAC component deletion with NaB exposure on H4 acetylation dynamics

Set3, Hst1 and Hos2 are the HDACs that are found within the Set3C complex, a seven-member complex with Set3, Hos2, Snt1 and Sif2 forming part of the core and are crucial for the assembly of the complex, whilst Hos4, Hst1 and Cpr1 a peripheral member of the complex. The Set3C complex has been directly linked to the regulation of the biofilm regulatory network as it can control the activity of five of the six core biofilm regulatory transcription factors *NRG1, BRG1, TEC1, NDT80*, and *ROB1* (Garnaud *et al.*, 2016).In addition, Set3C can control the expression of Nrg1, which is involved in the regulation of cellular dispersion (Uppuluri, Pierce, *et al.*, 2010). We decided to investigate whether the pattern of HDAC activity observed upon deletion of *SET3*, *HST1* or *HOS2* was affected by NaB treatment and may suggest a target for its action. To investigate histone H4 acetylation status in planktonic *C. albicans* HDAC deletion cells, Western blotting was carried out. Proteins were extracted immediately following NaB addition (0 min), and after 15 min, and 30 min following 200 mM NaB exposure in YPD medium at 30 °C and probed with the anti-

rabbit H4 acetylated primary antibody and the anti-rabbit Pgk1 loading control. An increase in the histone H4 acetylation signal could be observed upon NaB exposure after 15 min and increased further after 30 min NaB exposure in *Δhst1* (Figure 13 A, B). No clear increase in the H4 acetylation signal could be seen in *Δset3* within 30 min of NaB exposure (Figure 13 A, B). A relatively high H4 acetylation signal was observed in Δ*hos2* compared to the SC5314 control (Figure 6), but no increase could be detected upon NaB exposure (Figure 13 A, B). The 0 min sample represents the initial baseline following NaB addition, rather than a time-matched untreated control. As untreated samples were not included at the corresponding time points, time-dependent changes in H4 acetylation in the absence of NaB cannot be excluded. Furthermore, as total H4 protein levels were not assessed, changes in the H4 acetylation signal cannot be distinguished from changes in total H4 abundance. The corresponding SC5314 experiment is shown in Figure 6.

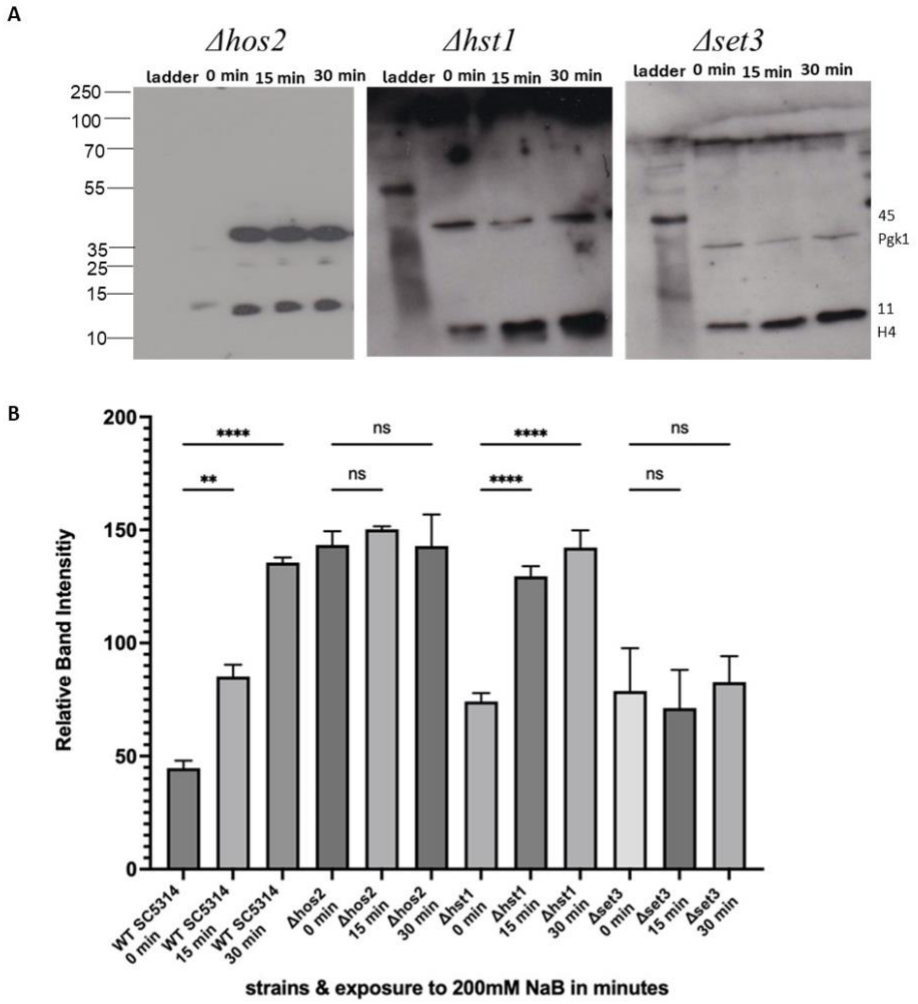


Figure 13 Western blot analysis displaying the detection of H4 (A) in a HDAC deletion strains (HOS2, HST1, SET3 deletions) and a bar chart (B) representing the change in H4 acetylation relative to Pgk1 loading control.
The cells were cultured in YPD media and sampled during log phase of growth at 0 min, 15 min and 30 min of 200 mM NaB incubation. Uniform protein loading was ensured by probing levels of Pgk1 after probing for H4. This experiment is a representative data set of three repeats.

Taken together, the observed differences in H4 acetylation following NaB exposure suggest that the Set3C components may have distinct roles in the regulation of H4 acetylation. The increase in H4 acetylation observed in Δ*hst1* following NaB exposure was not observed in Δ*set3* or Δ*hos2*, while Δ*hos2* exhibited a higher H4 acetylation signal under basal conditions compared with the SC5314 control. This may indicate that Hst1 contributes to the regulation of H4 acetylation in response to NaB, whereas deletion of *SET3* or *HOS2* does not

result in a comparable response within the time frame examined. However, the absence of time-matched untreated controls and measurements of total H4 means that changes in H4 acetylation cannot be attributed exclusively to NaB exposure. The results therefore provide an indication of differential effects of Set3C component deletion on H4 acetylation dynamics, but do not establish a direct role for individual components in the response to NaB.

3.3.11 Effect of TF deletions and of NaB on SC5314 planktonic and biofilm growth

The deletion of HDAC genes leads to a range of effects on *C. albicans* growth, suggesting that they provide a key point of regulation. We have observed that loss of core Set3C complex components leads to a loss of the expected increased H4 acetylation upon NaB exposure, suggesting that NaB action upon HDAC regulation of key transcription factors may underpin the morphological effects that we have observed.

We therefore investigated the effects of deleting transcription factors that are important in hyphae and biofilm formation in *C. albicans* using deletion strains: *Δefg1*, *Δnrg1, Δtec1, Δndt80,* and *Δrob1*. The wild type SN152 was used for comparison. We first investigated the effect of NaB on growth in transcription factor deletion strains in a planktonic system grown in RPMI for 24 h. Growth curve analysis showed that there was no significant difference in growth compared to the WT SN152 in *Δefg1*, *Δnrg1, Δtec1,* and *Δrob1*. Significant difference in growth compared to the WT SN152 was detected in *Δndt80* (Figure 14 A, B). When treated with 200 mM NaB significant growth differences compared to the WT SN152 could be seen in *Δndt80,* and *Δrob1* (Figure 14 C, D). No difference in growth compared to the

NaB-treated WT SN152 was detected in NaB-treated *Δefg1*, *Δnrg1,* or *Δtec1* (Figure 14 C, D). Fold change analysis demonstrated that all strains showed the same fold change reduction in growth as the WT except for *Δrob1* which showed further decrease in growth compared to the WT (Figure 14 E).

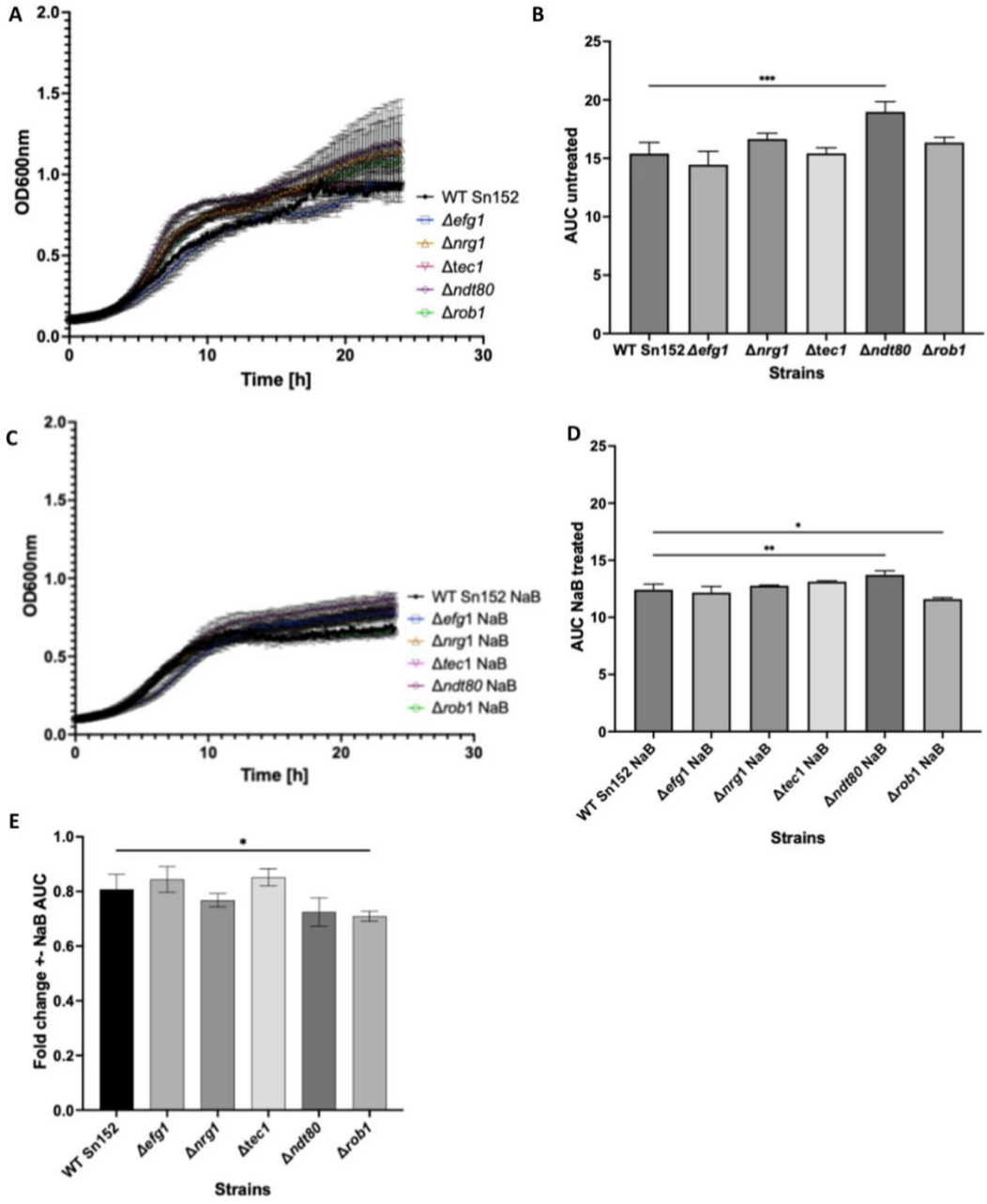


Figure 14 24 h Growth curve analysis of Sn152 and TF deletion strains in RPMI media with or without NaB supplementation.
A) 24 h Growth curves of Sn152 and TF deletion strains in RPMI media.
B) AUC analysis of 24 h growth curves in RPMI of Sn152 and TF deletion strains.
C) 24 h Growth curves of Sn152 and TF deletion strains in RPMI media supplemented with 200 mM NaB.
D) AUC analysis of 24 h growth curves in RPMI supplemented with 200 mM NaB of Sn152 and TF deletion strains.
E) Bar chart representing the fold change of untreated/NaB treated strains.
*The data represents an average of three biological repeats. The error bars represent the standard deviation. A One-way ANOVA using a Tukey multiple comparison test was used to determine statistical significance. Non-significant = NS, * = adjusted p-value ≤ 0.05 and *** = adjusted p value ≤ 0.001.*

3.3.12 Effect of TF deletions in addition to NaB treatment on biofilm growth

As we had observed significant effects for NaB addition on biofilm growth in SC5314, we wished to determine the effect of NaB supplementation on TF deletions. To do this XTT and crystal violet assays were performed on biofilms grown in the presence and absence of 200 mM NaB in RPMI medium. No reduction in metabolic activity compared to the WT SN152 could be observed in Δ*efg1,* Δ*nrg1*, Δ*tec1*, Δ*ndt80*, or Δ*rob1* (Figure 15 A). Significant reduction in biofilm mass compared to the WT was detected when *ROB1* was deleted (Figure 15 B).

In NaB-treated biofilms, no reduction in metabolic activity compared to the WT SN152 was observed in Δ*efg1,* Δ*nrg1*, Δ*tec1*, Δ*ndt80*, or Δ*rob1* (Figure 15 C). However, reduced biofilm mass compared to the NaB-treated WT was observed in Δ*tec1* and Δ*rob1* (Figure 15 D). Fold change analysis revealed that there were no significant differences in metabolic activity in all strains (Figure 15 E). However, fold change reduction in biomass as seen with the WT were observed in all strains except for Δ*tec1*, which showed a significant fold change reduction in biomass compared to the WT (Figure 15 F).

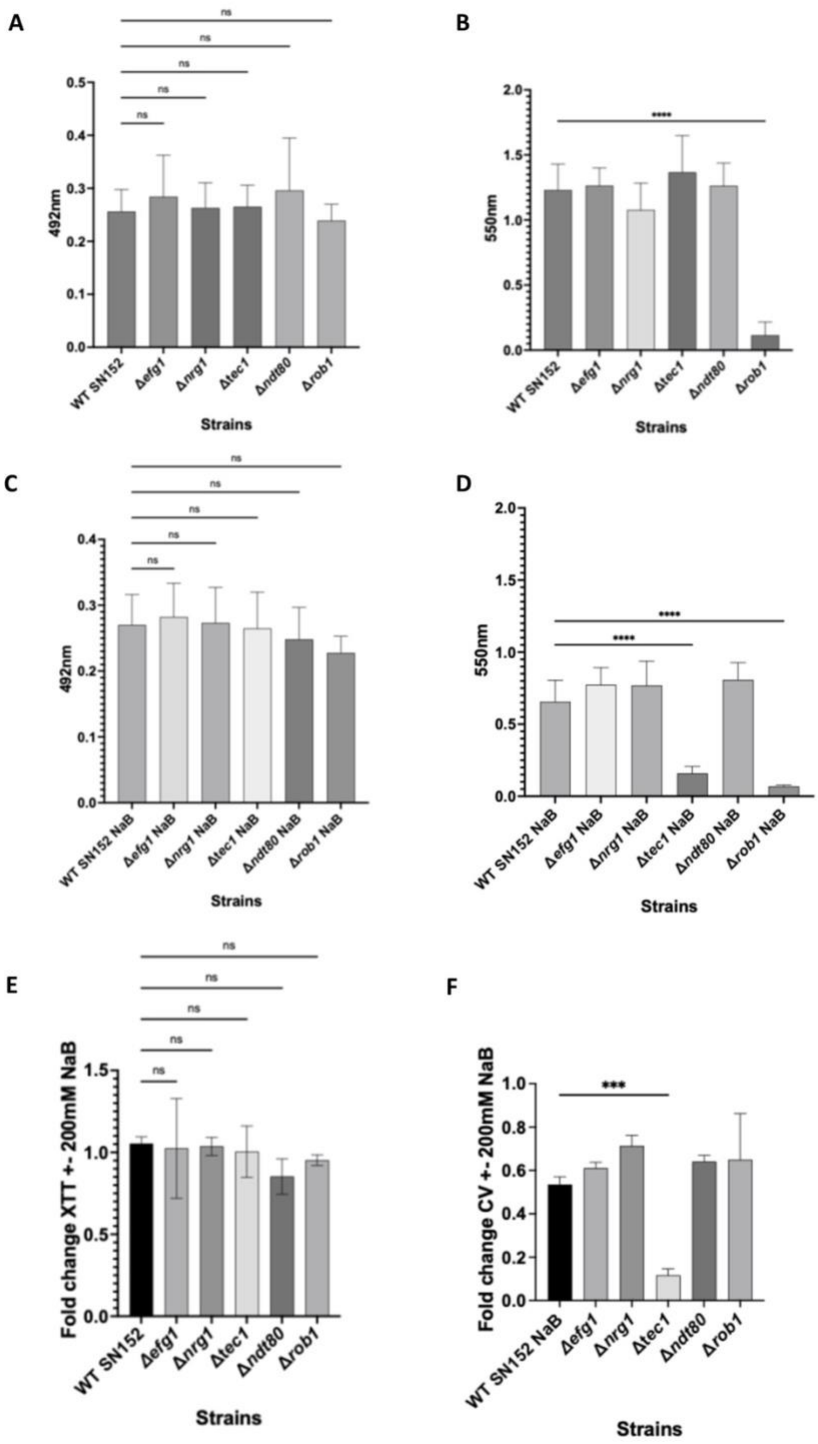


Figure 15 C. albicans of Sn152 and TF deletion strains 24 h biofilm quantification in RPMI with and without NaB using XTT and CV.
*Biofilms were grown in 96 well plates in RPMI media. 200 mM NaB was added to the media after the attachment phase. XTT (A,C) and CV (B, D) quantifications represent an average of three biological repeats. Fold changes (E, F) of NaB-treated/untreated biofilms were calculated for both XTT and CV data comparing to the fold change of the WT. The error bars display the standard deviation. A One-way ANOVA using a Tukey multiple comparison test was used to determine statistical significance. Non-significant = NS, * = adjusted p-value ≤ 0.05 and *** = adjusted p value ≤ 0.001.*

3.3.13 Effect of pH on NaB action in SC5314 *C. albicans*

SCFAs are produced in the colon through fermentation of dietary fibres and saccharides by bacteria causing weakly acidic conditions in the intestinal tract. The pH in the human gastrointestinal tract ranges from fairly acidic (pH 1.0 - 2.0) in the stomach to less acidic pHs in the duodenum (pH 6.1), small intestine (pH 7.1 - 7.5), and large intestine (pH 7.0) (Yamamura *et al.*, 2023). We were interested in investigating the effect of NaB in *C. albicans* at different pHs over a time period of 4 h. Widefield microscopy showed that NaB could prevent hyphae formation in *C. albicans* SC5314 grown in RPMI at the pHs of 8.0, 7.0, and 4.0. At pH 4.0 over a time period of 4 h, we also could observe misshapen cells in NaB-treated samples that we suspected may represent a dead cell population which was not detected in untreated and NaB-treated samples at pH 8.0 and 7.0 (Figure 16 A). In line with this, we could show that 200 mM NaB-treated *C. albicans* grown in RPMI at pH 4.0 had a reduced colony forming efficiency (CFU) of about 50 %, whilst untreated *C. albicans* grown in RPMI at pHs 8.0, 7.0, and 4.0 had a CFU of about 100 % (Figure 16 B). Flow cytometry analysis further revealed that high ROS levels, assessed by fluorescence output of the indicator dye H_2DCF-DA, were present in almost the entire population of *C. albicans* cells grown in RPMI at pH 4.0 in the presence of 200 mM NaB. However, cells grown in RPMI at pH 8.0 with or without NaB or untreated cells grown at pH 4.0 showed low ROS accumulation in almost 100 % of the population (Figure 16 C). The co-staining of cells with the propidium iodide showed that treatment of cells at either pH 8.0 or 4.0 was not associated with necrosis (Figure 16 C).

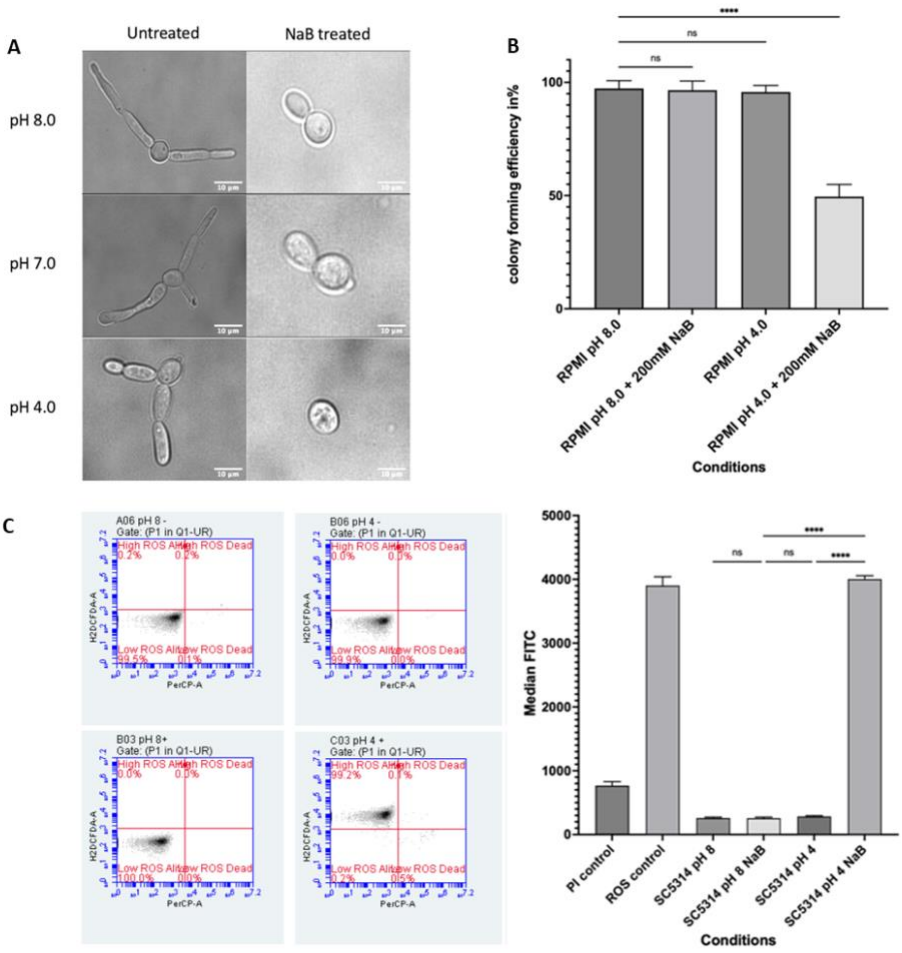


Figure 16 pH dependent effects of 200 mM NaB on C. albicans of SC5314.
*SC5314 cells were grown in standard RPMI until log phase before being grown in pH adjusted RPMI media in the presence or absence of 200 mM NaB for 4 h. The data sets represent an average of three biological repeats. The error bars display the standard deviation. A One-way ANOVA using a Tukey multiple comparison test was used to determine statistical significance. Non-significant = NS, * = adjusted p-value ≤ 0.05 and *** = adjusted p value ≤ 0.001.*
A) Widefield microscopy images of untreated and NaB-treated SC5314 cultured in pH 8.0, pH 7.0 or pH 4.0.
An Olympus 1X81 inverted microscope was used to visualise the cells and an Andor's Zyla 4.2 PLUS sCMOS camera was used to capture all images. An Olympus 100x objective lens (NA = 1.4) was used to visualise cells from the sample. A halogen light source was used to capture DIC images.
B) Colony forming efficiency (CFU) of untreated and NaB-treated SC5314 grown in pH 8.0 or pH 4.0 RPMI before being plated onto standard RPMI plates.
C) Flow cytometry analysis of ROS and viability of untreated and NaB-treated SC5314 at pH 8.0 and pH 4.0. Cells were gated allowing to select "singlet" cells rather than "doublets" or clumps of cells. On the X-axis PerCP-A indicates viability or cell death (PI stain), and the Y-axis was labelled H2DCFDA-A to detect ROS accumulation. FITC-A described the PI or H2DCFDA fluorescence detected via the FL1 detector (533/30).

Elevated levels of ROS have been linked to mitochondrial dysfunction and are a recognised marker for cell stress in yeast (Carmona-Gutierrez *et al.*, 2018). We therefore examined whether the addition of NaB at pH 4.0 and pH 8.0 led to effect on mitochondrial morphology using the mitochondrial stain Mitotracker Green FM. At pH 8.0 untreated dividing yeast cells displayed the expected mixture of tubular, fused, and fragmented mitochondria. A more fragmented appearance was observed over a time frame of 1 h upon 200 mM NaB treatment (Figure 17 A). At pH 4.0 mitochondrial fragmentation could be observed in untreated and NaB-treated cells (Figure 17 B). Surprisingly, after 1 h 200 mM NaB incubation the Mitotracker Green signal could no longer be visualised (Figure 17 B). As Mitotracker Green requires the presence of a membrane potential to accumulate fluoresce, the loss of signal may indicate that NaB treatment at 200 mM leads to a rapid depolarisation of mitochondrial inner membrane potential, which is commonly linked to the accumulation of ROS (Zhao *et al.*, 2019).

A sudden drop in the activity of the electron transport chain may result in the acidification of the mitochondrial matrix as protons are no longer pumped across the inner membrane to maintain a membrane potential. GFP fluorescence intensity can be used to indicate pH in living cells (Kneen *et al.*, 1998) and so we made use of a mitochondrial matrix targeted GFP (mtGFP) *C. albicans* to test whether matrix pH was affected by NaB addition at pH 4.0 and pH 8.0. Antimycin A is a complex III inhibitor that leads to loss of mitochondrial membrane potential and ROS accumulation, we used this inhibitor as a positive control. We observed a small drop in relative mtGFP intensity over time at pH 8.0 and this was increased with addition of 200 mM NaB. Treatment with antimycin A also led to a drop in relative mtGFP intensity indicating that inhibition of respiration is linked to an expected reduction in pH. Combined treatment of NaB and antimycin A showed a similar decrease in relative mtGFP

intensity when compared to antimycin A treatment alone (Figure 17 C). When we measured the relative mtGFP intensity in cells at pH 4.0, a decrease in GFP could be observed compared to the mtGFP intensity at pH 8.0 (Figure 17 C, D). When treated with 200 mM NaB at pH 4.0 the GFP intensity further decreased compared to that observed in NaB treated pH 8.0 samples (Figure 17 C). Treatment with antimycin A also caused a decrease in relative GFP intensity at pH 4.0, similar to the antimycin A pH 8.0 sample (Figure 17 C). When both NaB and antimycin A were added to *C. albicans* at pH 4.0 a further decrease in mtGFP intensity was observed (Figure 17 C).

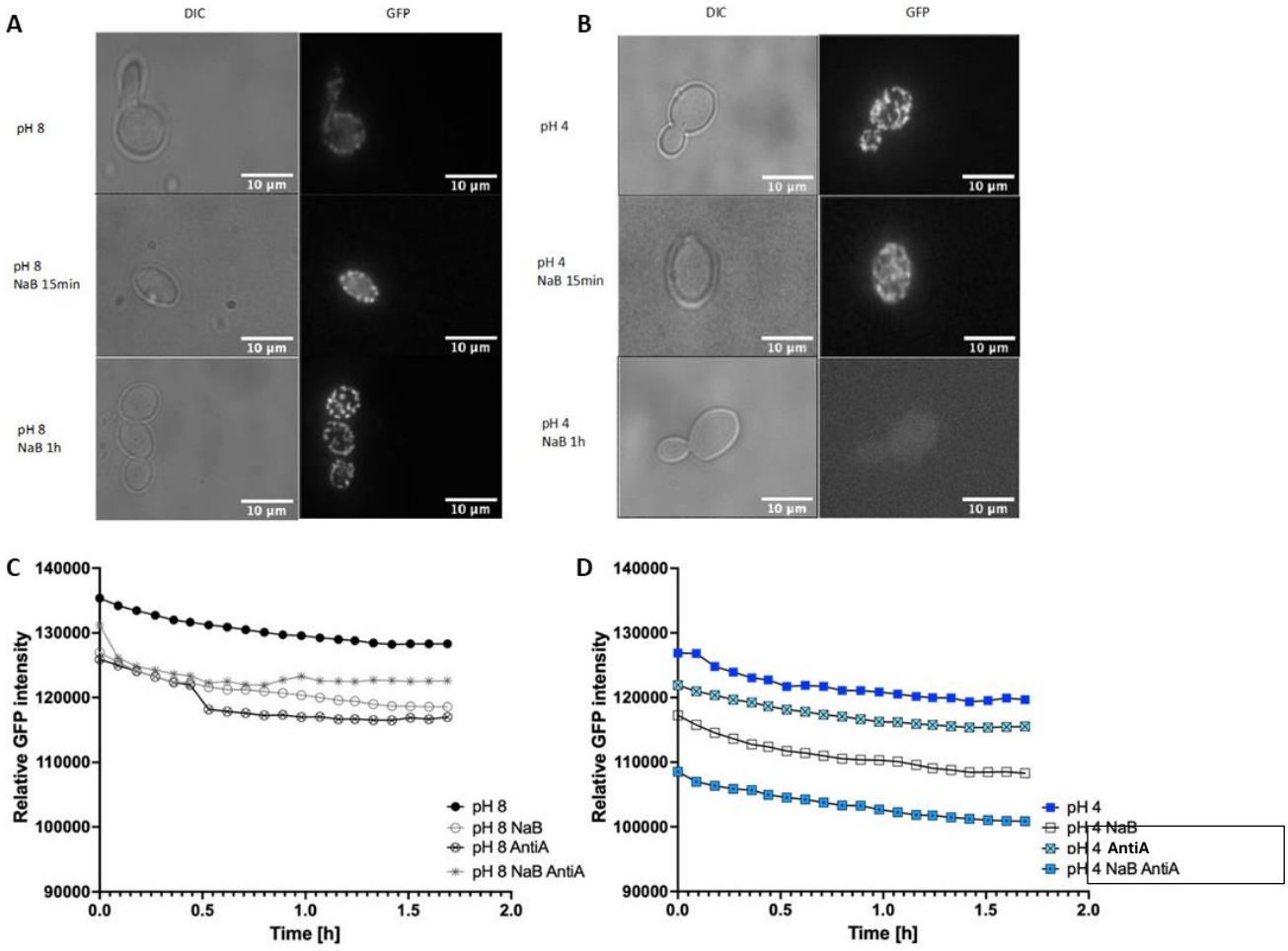


Figure 17 pH dependent effects of 200 mM NaB on mitochondria in C. albicans of SC5314. SC5314 cells were grown in standard RPMI until log phase before being grown in pH adjusted RPMI media in the presence or absence of 200 mM NaB for 15 min or 1 h. The mitotracker green FM (detection at 490/516 nm) was used to stain the inner mitochondrial membrane. The data sets represent an average of three biological repeats. The error bars display the standard deviation. A,B) DIC and GFP microscopy images of the inner mitochondrial membrane of untreated and NaB-treated SC5314 cultured in pH 8.0 (A) or pH 4.0 (B). Cells were visualised at x100 magnification under Bright field (BF) or GFP channel (Mitotracker green FM). The scale bar is 10 µm. The images represent three biological repeats.
C, D) Relative GFP intensity as an intracellular pH indicator of untreated, NaB or antimycin A (2 µM)-treated SC5314 cultured in pH 8.0 (C) or pH 4.0 (D).

As mitochondrial membrane potential is a direct consequence of electron transport chain activity, we sought to determine the effects of NaB addition on respiration in *C. albicans*. Following NaB addition we made use of Antimycin A addition to determine whether

electron transport chain activity remained after NaB addition. We assessed respiration levels of SC5314 *C. albicans* cell treated with 200 mM NaB over a 30-minute time period. Our data indicates that 200 mM treatment led to 74 % reduction in respiration within 30 mins of addition, which is consistent with a loss of membrane potential, matrix acidification and conditions that may lead to ROS production. The following addition of Antimycin A led a to a further decrease (16 %) indicating that some (10 %) electron transport chain function remained after 30 mins. (Figure 18 A, B). Interestingly, in contrast to the effects of acute addition at high levels, when we added 200 mM of NaB gradually (20 mM), an increase in respiration of 17 % could be observed after 40 min which continued until the final NaB concentration of 200 mM was reached. At this point an increase in respiration of 44 % was achieved compared to the starting point at time 1.06 h. The addition of Antimycin A led to a decrease in respiration of 129 % leaving only 15 % NMR (non-mitochondrial respiration) respiration (Figure 18 C, D).

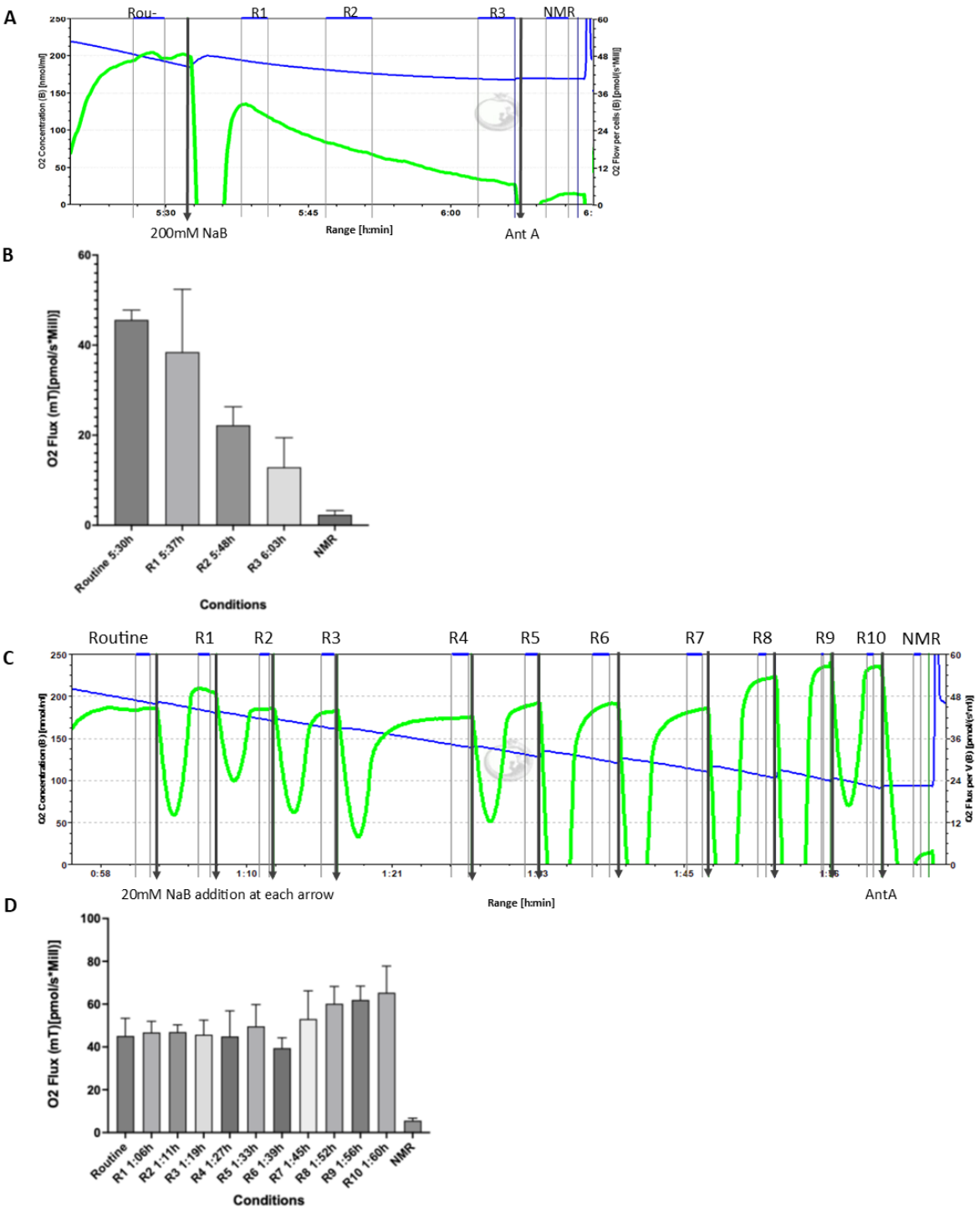


Figure 18 Respirometry profile of NaB-treated C. albicans.
*The oxygen flux per cell (pmol/s*Mill) is shown as the green line whereas the blue line represents the oxygen concentration. The "Routine" phase indicates the steady state oxygen flux. 200 mM NaB and 2 µM AntA were added to the chambers in order to analyse individual components of the respiratory chain. The data shown represents an average of three biological repeats and the error bars indicate the standard deviation.*
A, B) whole 200 mM NaB dosage administration.
C,D) gradual 20 mM NaB dosage administration until full 200 mM dosage was reached.

A loss of mitochondrial function has been linked to an increased sensitivity to oxidative stress in yeast (Grant, MacIver and Dawes, 1997; Bambach *et al.*, 2009) and the accumulation of ROS has been linked to a loss in calcium regulation and overload within the matrix (Brookes *et al.*, 2004).We therefore sought to investigate if NaB-treated cells at pH 4.0 are more sensitive to addition of additional oxidative stress and calcium. SC5314 *C. albicans* were exposed to 200 mM NaB for 15 min, 30 min, or 60 min prior 24 h growth in YPD (pH 4.0) containing 5 mM H_2O_2 or 50 mM $CaCl_2$.

No significant difference in the AUC could be observed upon treatment with 50 mM $CaCl_2$ condition when compared to the control, however, there was a significant decrease in growth when 5 mM H_2O_2 was added to the medium (Figure 19 A).

After 15 min NaB exposure prior to the growth assay, a significant decrease in growth could be observed in the NaB-treated sample compared to the pH 4.0 control (Figure 19 A).

When comparing the 15 min NaB-treated samples to their untreated 5 mM H_2O_2 or 50 mM $CaCl_2$ sample controls, no significant difference in growth could be observed for either (Figure 19 A).

A significant decrease in growth could be observed in SC5314 *C. albicans* when cells were treated with 200 mM NaB for 30 min prior to the growth assay at pH 4.0 compared to the untreated control at pH 4.0 (Figure 19 B). A significant decrease in growth occurred when 30 min NaB treated cells were grown in the presence of either 5 mM H_2O_2 or 50 mM $CaCl_2$ at pH 4.0 compared to their untreated 5 mM H_2O_2 or 50 mM $CaCl_2$ controls, respectively (Figure 19 B).

A significant decrease in growth and an increased lag phase could be observed in SC5314 *C. albicans* when cells were treated with 200 mM NaB for 60 min prior to the growth assay at pH 4.0 compared to the untreated control at pH 4.0 (Figure 19 C). Almost no growth could be observed in 60 min NaB treated cells grown in YPD medium containing either 5 mM H_2O_2 or 50 mM $CaCl_2$ at pH 4.0 compared to their untreated H_2O_2 or $CaCl_2$ controls, respectively (Figure 19 C).

In summary, we observed an increase in growth decline of SC5314 *C. albicans* the longer we incubated the cells in 200 mM NaB at pH 4.0. 200 mM NaB treated SC5314 *C. albicans* were also more stress sensitive the longer the NaB-exposure was (Figures 19 A-C).

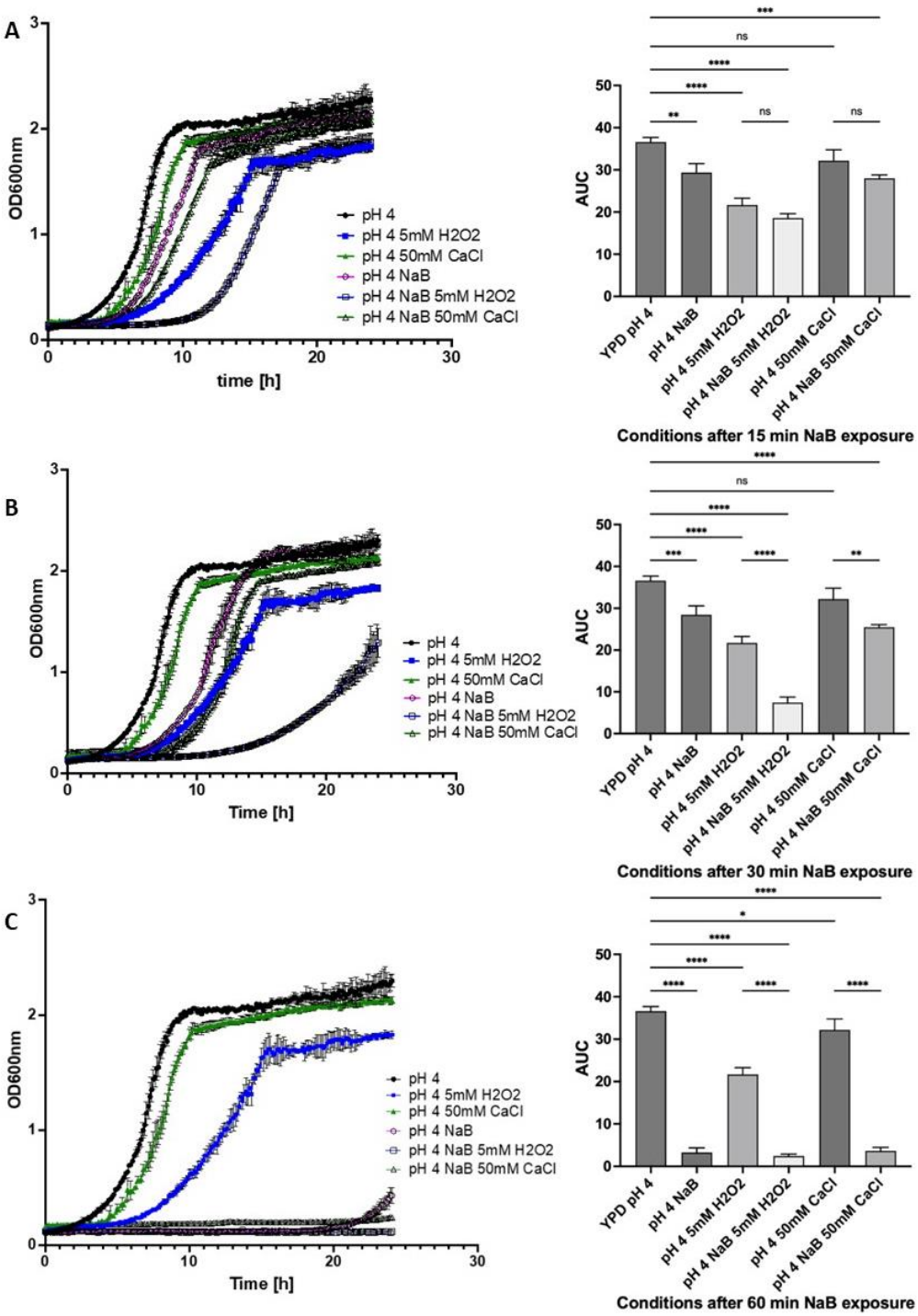


Figure 19 Growth analysis of C. albicans after 15, 30 or 60 min of 200 mM NaB-treatment at pH 4.0. C. albicans were incubated in YPD media containing 200 mM NaB for 15, 30 or 60 min prior the 24 h growth assay.

A) 24 h growth curve analysis at pH 4.0 after 15 min NaB-treatment and with or without the addition of 5 mM H_2O_2 or 50 mM $CaCl_2$.

B) 24 h growth curve analysis at pH 4.0 after 30 min NaB-treatment and with or without the addition of 5 mM H_2O_2 or 50 mM $CaCl_2$.

C) 24 h growth curve analysis at pH 4.0 after 60 min NaB-treatment and with or without the addition of 5 mM H_2O_2 or 50 mM $CaCl_2$.

*The data shown represent an average of three biological repeats. The error bars display the standard deviation. A One-way ANOVA using a Tukey multiple comparison test was used to determine statistical significance. Non-significant = NS, * = adjusted p-value ≤ 0.05 and *** = adjusted p value ≤ 0.001.*

The regulation of calcium homeostasis has been linked to mitochondrial function, ROS accumulation and viability. We therefore sought to investigate whether intracellular calcium homeostasis was perturbed in NaB-treated cells grown in RPMI at pH 8.0 and pH 4.0. To do this, we exploited the Aequorin system (Sanglard, 2021), which provides a fluorescence readout of cytosolic calcium levels in *C. albicans*. As a positive control 5 mM H_2O_2, which is reported to increase calcium levels detected by the Aequorin protein was used (Popa *et al.*, 2010).

As expected, a spike or increased intracellular calcium was observed when 5 mM H_2O_2 was added at both pH 8.0 and 4.0 (Figure 20 A, B).

However, this increase in intracellular calcium returned to baseline levels after a few minutes, indicating the cells activity to maintain cytosolic calcium levels (Figure 20 A, B). When 200 mM NaB was added at pH 8.0 a larger spike of increased intracellular calcium was observed than with 5 mM H_2O_2. This increase was also returned to baseline levels after a few minutes (Figure 20 A).

Interestingly, over the time course of 3 h a few smaller spikes could be identified which may indicate that the cells still experienced smaller bursts of increased intracellular calcium after NaB-treatment (Figure 20 A). When 200 mM NaB was added at pH 4.0 increased intracellular calcium could be measured. However, this time intracellular calcium levels were not returned to baseline levels over the course of the assay, indicating a loss of homeostasis (Figure 20 B).

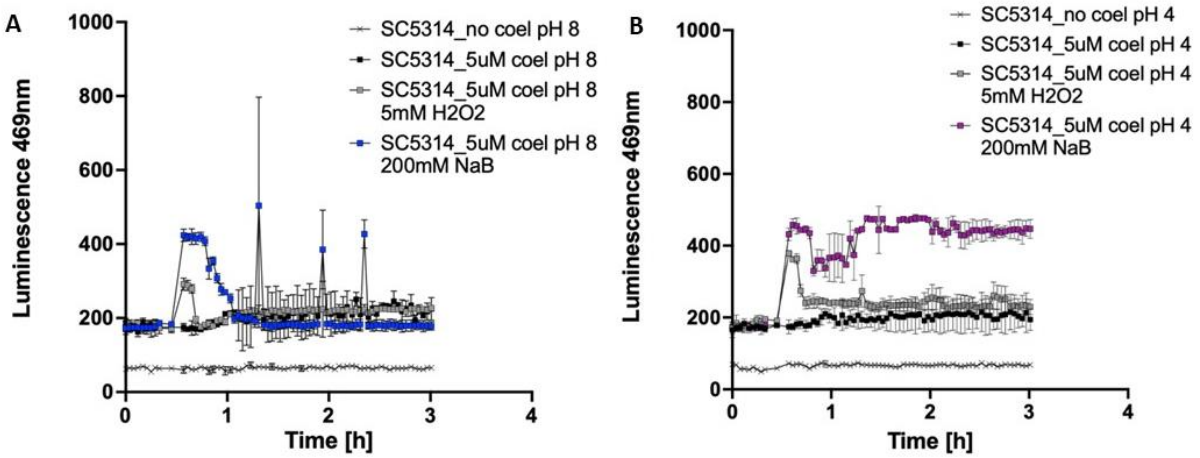


Figure 20 Effect of 200 mM NaB and other oxidative stresses on Calcium homeostasis in SC5314 C. albicans.
SC5314 cells were grown in appropriate media to mid log phase. Log- phase cells were then re-suspended at a density of ~108 cells/ml in fresh SD selective medium supplemented with 5 µM of the substrate Coelenterazine. Stresses were added after baseline reading were taken. The data sets represent an average of three biological repeats. The error bars display the standard deviation.
A) Aequorin luminescence curve at 469 nm measuring intracellular $CaCl_2$ levels at pH 8.0.
B) Aequorin luminescence curve at 469 nm measuring intracellular $CaCl_2$ levels at pH 4.0.

3.3.14 Calcium chelation or catalase overexpression prevents NaB induced cell death at pH 4

Our previous data suggested that 200 mM NaB may cause an imbalance of intracellular calcium at pH 4.0 but not at pH 8.0. We could observe high ROS accumulation and a decrease in CFUs at pH 4.0 and 200 mM NaB treatment (refer to Figure 16). We also observed lower relative GFP intensity indicative for lower intracellular pHs and generally a downward trend in intracellular pH after the addition of 200 mM NaB at pH 4.0 (refer to Figure 17). We, therefore, repeated flow cytometry, CFU and intracellular pH analysis using BAPTA-AM- a calcium chelator.

CFU analysis revealed that the observed decrease in CFUs at pH 4.0 when 200 mM NaB was added (Figures 16 B) could be restored to about 85 % with the addition of 50 µM BAPTA-AM in SC5314 cells (Figure 21 A).

We further repeated measuring intracellular pH through relative GFP intensity after the addition of BAPTA-AM: A clear downward trend in intracellular pH was observed after the addition of 200 mM NaB compared to the untreated pH 4.0 intracellular pH curve (Figures 17 D, 21 B). An even more pronounced downward trend in intracellular pH was observed after the addition of 2 µM Antimycin A and 200 mM NaB (Figures 17 D, 21 B). The addition of 50 µM BAPTA-AM was able to restore this downward trend in intracellular pH after NaB and/or Antimycin A treatment at pH 4.0 (Figure 21 B).

Previous flow cytometry analysis showed that, almost the entire population of *C. albicans* cells grown in RPMI at pH 4.0 in the presence of 200 mM NaB had high ROS levels (Figure 16 C). 50 µM BAPTA-AM was able to cancel ROS accumulation in NaB treated cells at pH 4.0 (Figure 21 C). This could also be seen in catalase CTA1 overexpression cells, but not in CAT1 deletions cells (Figure 21 C). In Figure 21 D we summarised the ROS and cell viability data obtained for pH 8.0 and pH 4.0 conditions in the absence or presence of 200 mM NaB and/or prior 50 µM BAPTA-AM treatment.

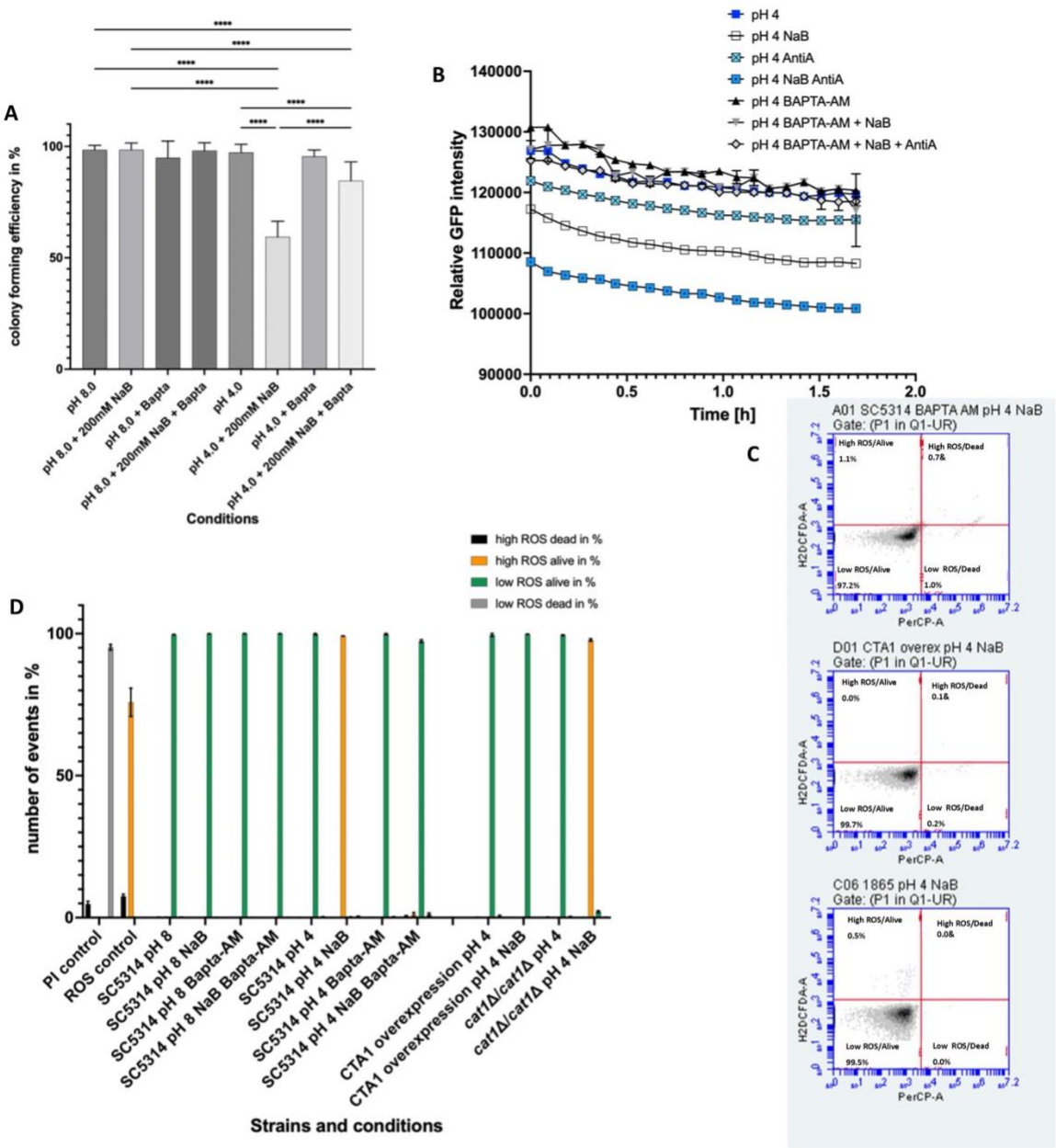


Figure 21 Effect of $CaCl_2$ chelation on pH dependent antifungal activities of NaB.
*SC5314 or CAT1 deletions cells were grown in standard RPMI until OD600 0.3 before being incubated with 50 µM BAPTA-AM for 3 h. Cells were then grown in pH adjusted RPMI media in the presence or absence of 200 mM NaB. The data sets represent an average of three biological repeats. The error bars display the standard deviation. A One-way ANOVA using a Tukey multiple comparison test was used to determine statistical significance. Non-significant = NS, * = adjusted p-value ≤ 0.05 and *** = adjusted p value ≤ 0.001.*
A) Colony forming efficiency (CFU) of untreated and NaB-treated SC5314 grown in pH 8.0 or pH 4.0 RPMI before being plated onto standard RPMI plates.
B) Relative GFP intensity as an intracellular pH indicator of untreated, NaB or antimycin A (2 µM)-treated SC5314 cultured in pH 4.0.
C) Flow cytometry analysis of ROS and viability of untreated and NaB-treated SC5314 at pH 8.0 and pH 4.0. Cells were gated allowing to select "singlet" cells rather than "doublets" or clumps of cells. On the X-axis PerCP-A indicates viability or cell death (PI stain), and the Y-axis was labelled H2DCFDA-A to detect ROS accumulation. FITC-A described the PI or H2DCFDA fluorescence detected via the FL1 detector (533/30).
D) Graphical depiction of ROS and cell viability flowcytometry data in %.

3.4 Discussion

ALS studies have shown that butyrate-producing bacteria, e.g. *Roseburia intestinalis* and *Eubacterium rectale* (Niccolai *et al.*, 2021), and enzymes involved in butyrate metabolism pathways are found at significantly lower levels in ALS patients when compared to healthy controls (Hertzberg *et al.*, 2022). Furthermore, evidence suggests that fungal infections may promote ALS disease as many fungi produce neurotoxins that can promote motor neuron degeneration (Castanedo-Vazquez *et al.*, 2019; French, Ludowyke and Guillemin, 2019). In the present study we sought to further investigate the pH-dependent mode of action of the antifungal effects of butyrate on *C. albicans* and considered this within the context of gut dysbiosis as an important feature of ALS pathology.

The human gastrointestinal tract is continuously exposed to the external environment through the ingestion of foods. Various pHs are distributed in the human gastrointestinal tract ranging from fairly acidic (pH 1.0-4.0) in the stomach to less acidic pHs in the duodenum (pH 6.1), small intestine (pH 7.1-7.5) and large intestine (pH 7.0) (Yamamura *et al.*, 2023). This pH gradient serves as a first-line of defence to supress pathogen overgrowth in the gut (Yamamura *et al.*, 2023), but also serves to partition microbial species within regions of the gut (Duncan *et al.*, 2009).

SCFAs are produced in the colon through fermentation of dietary fibres and saccharides by bacteria causing weakly acidic conditions in the intestinal tract. In acidic conditions butyrate is mainly found as its protonated form butyric acid whilst a small proportion will be present as butyrate ion (conjugated base).

We, therefore, tested antifungal effects of butyrate in both neutral (pH 8, butyrate ion form) and acidic (pH 4, protonated form butyric acid) conditions.

At pH 8 we found that butyrate supplementation can prevent growth of SC5314 *C. albicans* in both planktonic and biofilm modes of growth. In addition, NaB could prevent hyphae formation in SC5314 *C. albicans* as well as reduce biofilm mass in both primary biofilms and secondary biofilms in an HDAC inhibitory manner. Butyrate is known to act as an HDAC inhibitor (Davie, 2003; Sekhavat, Sun and Davie, 2007) and we were able to show that its application within our experimental approach led to rapid and sustained Histone H4 acetylation. HDAC inhibition has been shown to play a crucial role in the regulation of *C. albicans* pathogenicity. For example one study demonstrated that the HDACs *HOS1* and *RPD31* were not crucial in morphogenesis in *C. albicans*, whilst *HOS2* and *HDA1* were important in the yeast-to-hyphae switch (Zacchi, Schulz and Davis, 2010). Another study on *C. albicans* demonstrated that modulation of H3 acetylation may be used for antifungal treatment (Wurtele *et al.*, 2010). In line with the role that HDAC inhibition plays in *C. albicans* morphogenesis, we showed that filamentation was blocked upon its application. The yeast-to-hyphae switch in *C. albicans* is a well-known virulence trait (Mitchell, 1998) and has been proposed to be supressed by butyrate via inhibition of genes relevant for the switch (Hnisz *et al.*, 2010; Wurtele *et al.*, 2010; Zacchi, Schulz and Davis, 2010; Nguyen *et al.*, 2011). Here we attempted to determine the role of specific HDAC inhibition in growth, hyphal formation, biofilm formation and invasion.

Our data suggests a role for the Set3C complex in the action of butyrate as an HDAC inhibitor. A loss of HDAC *SET3* may lead to an insensitivity to NaB for growth, metabolic

activity, but not biomass. One possibility is that Set3 may be a target of NaB in its role as an HDAC inhibitor.

Set3, Hst1, and Hos2 are the HDACs that are found within the Set3C complex, a seven-member complex with Set3, Hos2, Snt1 and Sif2 forming part of the core and are crucial for the assembly of the complex, whilst Hos4, Hst1, and Cpr1 a peripheral member of the complex. In the absence of the core Set3C complex, NaB exposure did not increase H4 acetylation, suggesting the Set3C complex to be a putative target for NaB as an HDAC inhibitor.

The Set3C complex has been directly linked to the regulation of the biofilm regulatory network as it can control the activity of five of the six core biofilm regulatory transcription factors Nrg1, Brg1, Tec1, Ndt80, and Rob1 (Garnaud *et al.*, 2016). In addition, Set3C can control the expression of, Nrg1, which is involved in the regulation of cellular dispersion (Uppuluri, Pierce, *et al.*, 2010). The TEA/ATTS transcription factor Tec1 is crucial for hyphae formation (Schweizer *et al.*, 2000) and biofilm formation (Finkel and Mitchell, 2011; Nobile *et al.*, 2012; Pierce *et al.*, 2013). Additionally, inactivating the Tec1 and Efg1 genes influences matrix composition and deposition, and biofilm morphology (Daniels *et al.*, 2015; Panariello *et al.*, 2017). Interestingly, we showed that loss of Tec1 increased the efficacy of NaB in inhibiting biofilm matrix production. This synthetic interaction may suggest that NaB targets processes that are regulated by Tec1 within biofilm formation.

C. albicans biofilms are inherently resistant to azoles such as fluconazole (Al-Dhaheri and Douglas, 2010). Whilst some studies showed that butyrate enhanced fluconazole susceptibility in *C. albicans* biofilms (Nguyen *et al.*, 2011), our data suggested that butyrate did not have an additive effect. One explanation for this is that we showed that NaB

exposure significantly reduced biofilm metabolic activity and growth which is required for fluconazole, which inhibits ergosterol synthesis, to be effective (Spampinato and Leonardi, 2013). Another reason for our finding could be that drug pumps known to remove azole from the cell and contribute to resistance e.g. Cdr1 and Mdr1 are upregulated in the early phase of biofilm formation, in the first few hours after the cell attachment (Mukherjee *et al.*, 2003). Thus, in our experiments we would hypothesis that the upregulation of, drug efflux pumps is not affected by NaB addition and so does not lead to an increase in fluconazole efficacy.

Under acidic conditions NaB is mostly present in its protonated form, butyric acid. We discovered that exposure of *C. albicans* to butyric acid (pH 4.0) led to rapid cell death that was accompanied by loss of mitochondrial respiration, high ROS levels and a loss of Calcium regulation. Cell death could be prevented by adding a calcium chelator, BAPTA-AM, suggesting that loss of calcium homeostasis and its accumulation in the cytoplasm may underpin the loss of mitochondrial membrane potential and so pH which in turn drives ROS production from the mitochondria. In addition, the overexpression of catalase was able to prevent cell death, indicating that ROS production also plays a role in the demise of *C. albicans* cells treated with butyric acid. Importantly, necrosis was not seen at pH 4.0 suggesting that butyric acid induced cell death was triggered by a regulated form of cell death such as yeast apoptosis. Calcium signalling and ROS accumulation are also known to be involved in such pro-death signalling in higher eukaryotes (Cerella, Diederich and Ghibelli, 2010; Grosfeld *et al.*, 2021). In yeast, calcium regulation has been shown to be a crucial mediator of regulated cell death. For example, calcium has been shown to activate

the enzyme metacaspase which regulates yeast apoptotic processes, however the exact mechanism remains unknown (Wong, Yan and Shi, 2012). Studies have shown that calcium-depleted media can prevent cell death caused by carbon depletion (Yamagata, Obara and Kihara, 2013), and death caused by glutathione depletion could be prevented by adding of the calcium chelator BAPTA-AM (Chandel, Das and Bachhawat, 2016). Mitochondrial calcium uptake can be prevented through ruthenium red exposure and studies have shown this prevents cell death caused by toxic flavone compounds and lactoferrin derived peptides (van der Pal *et al.*, 1987; Lupetti *et al.*, 2004; Yun and Lee, 2016; Lee, Woo and Lee, 2019). A burst of cytosolic calcium could be observed after treatment with toxic peptides that lead to cell death (Lee, Hwang and Lee, 2016; Lee and Lee, 2018; Kim and Lee, 2019).

The major site of cellular energy metabolism is the mitochondrion comprising complexes I-IV which generate a H^+ gradient across the inner mitochondrial membrane. ATP synthesis is then driven by the electrochemical energy of the H^+ gradient and the reduction of O_2 to H_2O via ATP synthase (complex V) (Ferguson, 1997). In this process, several reactive oxygen species (ROS) are generated, which can damage cellular proteins, lipids, and DNA (Brookes *et al.*, 2004). Whilst being the main energy generator of the cell, mitochondria are also required for oxidative stress resistance in yeast (Grant, MacIver and Dawes, 1997). Mitochondrial ROS, however, may also act as an important regulator in redox cell signalling (Fleury, Mignotte and Vayssière, 2002; Ueda *et al.*, 2002) when its production is kept to the required amount for micro cell signalling (Inoue *et al.*, 1999; Brookes and Darley-Usmar, 2002; Brookes *et al.*, 2004).

Our data also showed that catalase overexpression prevented high ROS accumulation in the cells contributing to the idea that ROS accumulation at pH 4 after NaB addition occurs because ROS production exceeds the normal cell's ability to cope when mitochondrial membrane potential crashes. Our data also suggests that the pH drop observed after Antimycin A addition is dependent on loss of calcium homeostasis as it could be rescued with BAPTA-AM. As mentioned in the beginning, the mitochondria are also a significant source of ROS (respiratory chain) primarily in the form of superoxide ($O_2^{-}\cdot$) which is converted to H_2O_2 mostly by the enzyme superoxide dismutase (SOD). Thus, ROS production is dependent on the mitochondrial membrane potential (Starkov and Fiskum, 2003). Superoxide dismutase is not the only enzyme to counter stress induced ROS. Catalases such as CAT1 are essential antioxidants in *C. albicans* as well (Wysong *et al.*, 1998; Nakagawa, Kanbe and Mizuguchi, 2003). An important component of the inner mitochondrial membrane is cardiolipin, which can be oxidised by ROS promoting cytochrome c release (Vercesi *et al.*, 1997; Grijalba, Vercesi and Schreier, 1999; Ott *et al.*, 2002).

However, it is also important to mention that the apoptotic effect we observed at pH 4 after NaB addition may not be solemnly caused by NaB, but also by the acidic pH. It has been shown that acetic acid could induce cell death in yeast (Chaves *et al.*, 2021).

As described above low abundancy of butyrate-producing bacteria but also enzymes involved in butyrate metabolism pathways in ALS patients provide favourable conditions for *Candida* growth further contributing to motor neuron degeneration (Castanedo-Vazquez *et al.*, 2019; French, Ludowyke and Guillemin, 2019; Niccolai *et al.*, 2021; Hertzberg *et al.*, 2022). NaB treatment may be beneficial to combat this effect. However, inhibition of *C. albicans* growth is only achieved at high butyrate concentrations, as may be found upon

consumption of certain foods or under butyrate supplementation. This may suggest that the activity of butyrate producing bacteria does not have an impact on *Candida growth*, however conditions that promote transient high levels of production cannot be ruled out. Clinical research groups could identify potential therapeutic use of butyrate in a wide spectrum of gastroenterological disorders to exploit its effects on inflammation, proliferation of intestinal epithelial cells, and regulation of fluid and electrolyte uptake in disorders like irritable bowel syndrome (Vanhoutvin *et al.*, 2009), cholera (Rabbani *et al.*, 1999), congenital chloride diarrhoea (Berni Canani *et al.*, 2004; Wedenoja, Holmberg and Höglund, 2008), prevention of colorectal cancer (Scharlau *et al.*, 2009), and inflammatory bowel disease (Segain, 2000; Thibault *et al.*, 2010). In ALS clinical trials it could be demonstrated that patients receiving sodium phenylbutyrate– taurursodiol (related to butyrate) showed lower functional decline compared to the placebo controls (Paganoni *et al.*, 2020). However, effects on a wider scale are yet to be determined and the understanding of how beneficial butyrate administration is in ALS is still in its infancy. Compounds targeting HADCs are currently in the preclinical discovery phase of ALS treatment. HDAC6 inhibition restored axonal transport defects in human *FUS*-associated ALS cellular models (Kim *et al.*, 2010; W. Guo *et al.*, 2017). *Candida* growth could be inhibited by HDAC inhibitors such as TSA and fluconazole sensitivity could be enhanced (Smith and Edlind, 2002). The supplementation of the SCFA acetate but also butyrate could reduce levels of *C. albicans* in mice guts (D. Fan *et al.*, 2015; McCrory, Lenardon and Traven, 2024). Acetate-producing *Bifidobacteria* could also reduce *C. albican*s growth in human *in vitro* studies (Ricci *et al.*, 2022).

Chapter 4 New Roles and Interactions for Sod1 and Sod1^{A4V} under conditions of stress

Abstract

Amyotrophic lateral sclerosis (ALS) is a progressive neurodegenerative disease associated with protein misfolding and disruption of cellular homeostasis. Mutations in superoxide dismutase 1 (SOD1), including A4V, have been linked to defects in proteostasis, autophagy, vesicular trafficking, and calcium signalling. Using *Saccharomyces cerevisiae* expressing Sod1^{A4V}, this study investigated genetic interactions affecting vacuolar function and stress responses. Screening of a vacuolar deletion library under calcium, zinc, and calcineurin inhibition identified interactions involving vacuolar trafficking, autophagy, TORC1 and Ras signalling, metal homeostasis, and calcium regulation. Trehalose metabolism also emerged as a potential protective mechanism. Although no direct interaction between Sod1^{A4V} and the vATPase component Vma2 was detected, the findings highlighted an important role for vacuolar function in mutant SOD1 toxicity. Sod1^{A4V} also impaired calcineurin-dependent Crz1 nuclear translocation and calcium homeostasis. Overall, these findings demonstrate that Sod1^{A4V} disrupts interconnected pathways involved in proteostasis, metabolism, and ion regulation, providing insight into conserved mechanisms of SOD1-associated ALS pathology.

4.1 Introduction

4.1.1 Expression of single copy *SOD1* and mutant *sod1^{A4V}* alleles in *S. cerevisiae*

The enzyme superoxide dismutase 1 (Sod1) is responsible for converting superoxide into hydrogen peroxide and water. Mutations in the *SOD1* gene, which encodes Sod1, have been linked to familial amyotrophic lateral sclerosis (ALS), a neurodegenerative disease characterized by the progressive loss of motor neurons. While over 200 *SOD1* mutations

have been identified, the exact mechanism by which they contribute to ALS remains unclear. Various animal models of *SOD1*-associated ALS (*SOD1*-ALS), spanning organisms from baker's yeast (*Saccharomyces cerevisiae*) to mice (*Mus musculus*), have provided valuable insights into Sod1 function. Over the last few years, research has emphasized the development of stable single-copy ALS models to investigate mutant Sod1 isoforms under physiologically relevant low expression levels.

Previous work by Dr Kevin Doyle sought to develop a stable single-copy *SOD1*-ALS model in *S. cerevisiae* (Doyle, 2022). The Gateway cloning technique was applied to generate an integrated plasmid-based model, whereby wild type *SOD1* or *mutant sod1^{A4V}* were constitutively expressed from a single copy within the genome. The same technique was then used to integrate and generate *SOD1* or *mutant sod1^{A4V}* into a library of deletions of genes involved the control of the metabolic functions carried out by the vacuole in *S. cerevisiae*. This was carried out to investigate whether overexpression of *SOD1* or *mutant sod1^{A4V}* exhibited enhanced toxicity when vacuolar functions were disrupted as a means to identifying synthetic interactions. A control plate was generated that contains 72 knockouts from the MATa deletion library (Winzeler *et al.*, 1999) that contain an integrated control vector pAG306. The *sod1^{A4V}* expression plate tested in this chapter contains the same 72 knockouts but has the pAG306 chrI vector expressing *sod1^{A4V}* integrated into the genome. In general, the library contains a number of mutants lacking genes encoding amino acid, metal ion and other transporters located on the vacuole membrane. The pAG306 *sod1^{A4V}* vector was integrated into each knockout and confirmed by PCR by Dr Kevin Doyle (Doyle, 2022).

The interaction of another key player in ALS – the enzyme calcineurin (Cn)- with Sod1 was also explored: Previous data indicated that overexpressing mutant Sod1 isoforms in a Δ*sod1* background using 2µ plasmids led to growth defects, which were associated with vacuolar

and metabolic dysfunctions e.g. vacuolar acidification defects (Bastow *et al.*, 2016; Doyle, 2022). We wished to determine if the relatively lower expression of Sod1^{A4V} from an integration vector also caused vacuolar and metabolic defects. To test this the growth of the strains under various stresses aimed at challenging vacuole function, calcium and zinc stress and Cn inhibition using FK506 was assessed (Doyle, 2022).

4.1.2 Overexpression of ALS-linked mutant isoforms of Sod1 into *S. cerevisiae* causes cytotoxicity, metabolic dysfunction, and a vacuole acidification defect

The key findings of previous work by Dr Kevin Doyle (Doyle, 2022) showed that Sod1 is crucial for maintaining central homeostatic processes, particularly in vacuole function and calcineurin signalling. These findings also suggested that the overexpression level of ALS-linked Sod1 mutants in *S. cerevisiae* significantly influences the severity of observed phenotypes. As a brief summary of these findings, whilst Sod1 is not required for maintaining vacuole acidification, its absence comprises vacuole function. In addition, overexpression of ALS-linked Sod1 mutants from high-copy plasmids leads to vacuole acidification defects, whereas stable single-copy expression does not produce the same effect. Sod1 was shown to interact with Vma2 of the V-ATPase in an *in-vivo* DHFR reconstitution assay, though it did not regulate the reversible disassembly of the V-ATPase enzyme complex. A small but reproducible reduction in V-ATPase activity was observed in vacuole extractions incubated with recombinant bovine Sod1, suggesting a possible *in vitro* interaction. Furthermore, the study showed an interaction between Sod1 and calcineurin, playing an essential role in Cn activation in response to increased intracellular calcium.

These findings may contribute to a better understanding of ALS pathogenesis in patients with *SOD1* mutations, and if lysosomal dysfunction is an early defect in ALS motor neurons, it could serve as a potential target for future therapeutic strategies. A prominent feature of motor neurons compared to other cells is their vulnerability to calcium overload as calcium permeable AMPA receptors are highly expressed (Williams *et al.*, 1997; Shaw and Eggett, 2000; Van Den Bosch *et al.*, 2000; Guatteo *et al.*, 2007) while the endogenous expression of calcium buffering proteins (CaBPs), like parvalbumin and calbindin, is low (Alexianu *et al.*, 1994; Palecek, Lips and Keller, 1999; Jaiswal, 2013), even though EF-hand calcium binding proteins are present in motor neurons (Migheli *et al.*, 1999; M.-D. Zhang *et al.*, 2014). Several studies could detect intracellular calcium overload and a further decrease in calretinin and parvalbumin in motor neuron axons in ALS patients (Siklós *et al.*, 1996, 1998; Kruman *et al.*, 1999; Grosskreutz, Van Den Bosch and Keller, 2010; Kawamata and Manfredi, 2010; Hayashi, Amari and Okamoto, 2013). Another pathological pathway in ALS causing calcium overload is that mutated SOD1 was found to accumulate in the mitochondrial intermembrane space, which impairs normal mitochondrial function. This is interesting as mitochondria are supposedly crucial in buffering calcium in motor neurons (Jaarsma *et al.*, 2001; Liu *et al.*, 2004; Jaiswal and Keller, 2009; Lautenschläger *et al.*, 2013). Thus, SOD1 mutations can lead to disturbances in calcium homeostasis.

In this context, it was also shown that calcium can bind to immature SOD1 increasing its accumulation (Leal *et al.*, 2013; Estácio *et al.*, 2015). In agreement, overexpression of CaBPs and AMPA channel antagonists could decrease calcium overload, neurodegeneration, and abnormal SOD1 accumulation in ALS1 models (Van Damme *et al.*, 2003; Tateno *et al.*, 2004; Tortarolo *et al.*, 2006; Yin, Tang and Weiss, 2007; Beers *et al.*, 2008; Parone *et al.*, 2013). The activity of the protein phosphatase Cn is calcium dependent and regulated by

calmodulin. Being highly expressed in the CNS and playing a major part in many pathways involving modulation of immune responses and signal transduction in the nervous system through regulating neuronal excitability, the release of neurotransmitters and hormones, gene transcription and calcium-dependent apoptosis, Cn activity is thought to be pivotal in motor neuron diseases (Morioka *et al.*, 1999; Wang *et al.*, 1999; Rusnak and Mertz, 2000). Previous studies using human neuroblastoma cells expressing fALS-SOD1 and mice models expressing fALS SOD1 showed that the phosphatase activity of Cn is depressed when mutant antioxidant SOD1 is present (Ferri *et al.*, 2002) thus supporting evidence that Cn is redox regulated. This is further supported by showing that wild type SOD1 functions as a protective element for Cn (Wang, Culotta and Klee, 1996), and fALS-SOD1 can directly deactivate Cn (Ferri *et al.*, 2008). The target of such oxidation of Cn is supposedly the iron atom at its active site (Namgaladze, Hofer and Ullrich, 2002). Decreased Cn activity was directly found in ALS patients: a study reported significantly decreased Cn activity in lymphocytes in 37 sporadic and eight fALS patients with an increase in protein oxidation which was not found in the control subjects (Ferri *et al.*, 2004).

In this way the yeast model may prove useful in investigating how mutations in Sod1 affect calcium regulation and so contribute to the field.

4.1.3 Vacuolar functions

The break-down of proteins is performed by lysosomes – organelles containing hydrolytic enzymes. Lysosomes are also pivotal in protein sorting, ion storage, autophagy, and stress responses in the cell. Lysosomal defects have been strongly associated with neurodegenerative diseases involving protein misfolding, like Alzheimer's disease,

Parkinson's disease, Huntington's disease, and ALS (Fulceri *et al.*, 2011; Tashiro *et al.*, 2012b). In *S. cerevisiae*, the vacuole shares many functional similarities to the mammalian lysosome. Interestingly, a link has been found between overexpression of ALS-linked Sod1 and vacuole dysfunction in *S. cerevisiae*, such as defects in vacuole acidification and a decrease in autophagy (Bastow *et al.*, 2016). Constitutive functions of the yeast vacuole include degradation, storage, buffering, and detoxification.

Together with proteasomes vacuoles represent one of the two main degradation systems within the yeast cell. Hydrolytic enzymes, including soluble and membrane-bound proteases, which break down a wide range of proteins. These enzymes are transported to the vacuole in an inactive form and activated through a cascade of processing events, often at low pH (Zubenko, Park and Jones, 1983; Knop *et al.*, 1993; van den Hazel, Kielland-Brandt and Winther, 1996). Proteins are directed to the vacuole for degradation through multiple pathways. Plasma membrane proteins, including receptors like Ste2p and Ste3p, are degraded in a process involving ubiquitination and endocytosis, similar to how mammalian cells degrade the EGF receptor (Davis, Horecka and Sprague, 1993; Hicke and Riezman, 1996; Katzmann, Odorizzi and Emr, 2002). Certain nutrient transporters, such as Fur4p and Gap1p, are also sent to the vacuole for degradation depending on nutrient levels (Galan *et al.*, 1996; Séron *et al.*, 1999; Helliwell, Losko and Kaiser, 2001). Another process through which vacuoles degrade especially cytosolic and organellar proteins is autophagy (Mizushima and Klionsky, 2007). While yeast can compensate for autophagy defects under normal conditions, in mammals, basal autophagy is essential for development and protein quality control. When vacuolar protease activity is impaired, autophagic vesicles accumulate, highlighting the vacuole's critical role in cellular recycling and homeostasis (Takeshige *et al.*, 1992; Mizushima and Klionsky, 2007; Li and Kane, 2009).

In times of nutrient deprivation, the yeast vacuole also serves as the primary storage site for amino acids, phosphate, calcium, and metal ions allowing yeast to regulate cytosolic levels and mobilize reserves when needed (Klionsky, Herman and Emr, 1990; Van Ho, Ward and Kaplan, 2002). Yeast vacuoles can accumulate high levels of basic and neutral amino acids, while acidic amino acids are stored to a lesser extent. This process relies on a proton gradient and specific transporters. The Vba1p, Vba2p, and Vba3p transporters facilitate the uptake of lysine, arginine, and histidine, while Avt1p imports large neutral amino acids like tyrosine and leucine. Other Avt transporters (Avt3p, Avt4p, Avt6p) function in amino acid export, all depending on the proton gradient (Klionsky, Herman and Emr, 1990; Russnak, Konczal and McIntire, 2001; Shimazu *et al.*, 2005). Regulating free ionized calcium levels in yeast is also a function of the vacuole: Ca^{2+} in the cytosol can then be transported into vacuoles for storage via vacuole calcium ATPases Pmc1 and a vacuole Ca^{2+}/H^{+} exchanger Vcx1, or it can be transported to other organelles, such as the endoplasmic reticulum and the Golgi apparatus via calcium ATPase Pmr1 (Cui, Kaandorp, Ositelu, *et al.*, 2009). Under hypertonic conditions the Ca^{2+} channel Yvc1 – a distant homolog of the mammalian TRPC-type Ca^{2+} channels – will release vacuolar Ca^{2+} into the cytosol (Denis and Cyert, 2002). Vacuoles are also the primary storage site for zinc in yeast cells. When Zn^{2+} levels are high, the transporters Zrc1p and Cot1p facilitate its uptake into the vacuole. In contrast, when Zn^{2+} is scarce, the vacuolar exporter Zrt3p is activated to release stored zinc. This regulation allows yeast cells to accumulate over ten times more zinc when external levels are high and then use these reserves to sustain growth for multiple generations when external zinc is unavailable (MacDiarmid, 2000; MacDiarmid, Milanick and Eide, 2002; Simm *et al.*, 2007). Beyond storage, the vacuole plays a key role in detoxification by sequestering harmful substances away from the cytosol and other organelles. Some of these substances, like

redox-active heavy metals, are essential at normal levels but become toxic in excess. The vacuolar ABC transporters Ycf1p and Bpt1p help remove toxins by transporting them as glutathione conjugates. These transporters have overlapping functions but are regulated differently, and they help eliminate harmful metals like arsenite and cadmium, as well as metabolic byproducts in certain mutants (Rebbeor *et al.*, 1998; Ghosh, Shen and Rosen, 1999; Klein *et al.*, 2002; Sharma *et al.*, 2002).

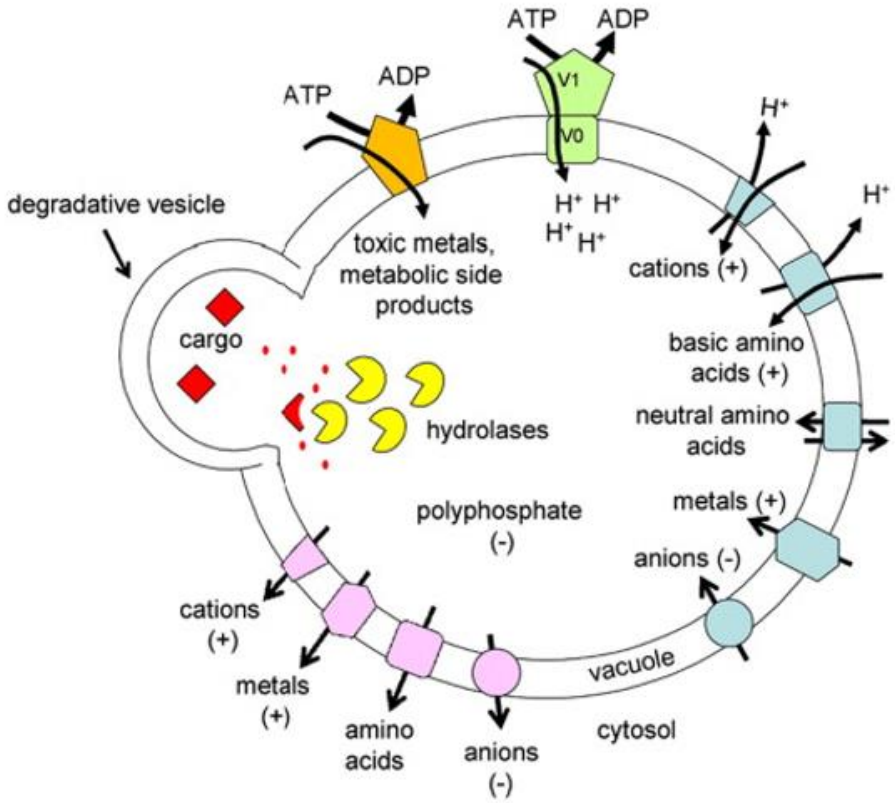


Figure 1 Constitutive functions of the yeast vacuole.
The four main constitutive functions of the yeast vacuole include degradation, storage, buffering, and detoxification. 1) Degradation is facilitated through enriched hydrolases present in vacuole. 2) Storage: amino acids, ions and metals are imported through multiple transporters in the vacuole. 3) buffering: ion homeostasis and amino acid recycling is achieved through vacuole transporters. 4) Detoxification: toxic metals or harmful metabolic bi-products are sequestered by vacuolar ABC-transporters.
Image from (Li and Kane, 2009)

4.1.4 Aims of this chapter

In the current study, we aimed to determine whether cell response to calcium, calcineurin, or zinc stress are affected by the expression of mutant Sod1^{A4V} as previously proposed by work by Dr Kevin Doyle (Doyle, 2022). Furthermore, we tried to characterise if Sod1^{A4V} interacts with the vATPase subunit VMA2. Lastly, we explored the nature of calcium sensitivity in cells expressing Sod1^{A4V}.

4.2 Materials and Methods

4.2.1 Media preparation and growth conditions for *Saccharomyces cerevisiae* and *Escherichia coli*

All components of the media were mixed in to deionised distilled water prior to autoclaving. All media were sterilised using a Prestige Medical bench-top autoclave at 121 °C, 15 Ib/sQ.in for 11 min. All *Escherichia coli* liquid cultures were incubated at 37 °C with constant rotation at 180 rpm. All liquid cultures of *Saccharomyces cerevisiae* were incubated at 30 °C with constant rotation at 180 rpm. 2 % w/v granulated agar (Oxoid technical agar No. 3) was added prior to autoclaving for solid medium and glucose, if required, was added after autoclaving.

4.2.1.1 Yeast growth media

4.2.1.2 Yeast extract, peptone, dextrose (YPD) growth medium

The YPD growth medium contained 2 % w/v glucose (Fisher), 1 % w/v yeast extract (BD) and 2 % w/v Bactopeptone (BD).

4.2.1.3 Synthetic complete (SC) drop-out medium

Ingredients for this medium included 2 % w/v glucose (Fisher), 0.77 % Yeast Nitrogen Base without amino acids (Kaiser, Formedium), yeast synthetic complete drop-out media supplement (Formedium). Ammonium sulphate is the source of nitrogen for the yeast cells grown in this media. Once yeast was transformed with plasmid DNA containing the selective marker (uracil, leucine, histidine), Yeast Synthetic Complete Drop-Out Media Supplement (Formedium) lacking the appropriate nutrient was used to select successfully transformed yeast.

4.2.1.4 *E. coli* growth and selection

The LB medium contained 1 % Yeast Extract (BD), 2 % Sodium Chloride (Fisher), 2 % Bactotryptone (BD), and if required 2 % agar (Oxoid). The appropriate antibiotics (Ampicillin stock concentration: 100 mg/ml in sterile deionised water, Sigma-Aldrich; Kanamycin stock solution 10 mg/ml in sterile deionised water, Sigma-Aldrich) were added for the selection of successfully transformed *E. coli* containing the plasmid of interest. To select for *E. coli* colonies containing plasmids with the *AmpR* gene, ampicillin was supplemented to the growth medium to a final concentration of 100 µg/ml after autoclaving. Kanamycin was added to the growth medium to a final concentration of 50 µg/ml after autoclaving to select for *E. coli* colonies containing the gene for kanamycin resistance.

4.2.2 Yeast and bacterial strains used in this project

4.2.2.1 *E. coli* strains

DH5α: The genotype of the competent *E. coli* cells used in this study is F- endA1 glnV44 thi-1 recA1 relA1 gyrA96 deoR nupG Φ80dlacZΔM15 Δ(lacZYA-argF) U169, hsdR17(rK- mK+), λ–.

4.2.2.2 *S. cerevisiae*

The knockout library contains 72 knockouts from the MATa deletion library with the genotype of *BY4741 MATa his3Δ1 leu2Δ0 met15Δ0 ura3Δ0* (Winzeler *et al.*, 1999). Each knockout has the pAG306 chrI vector expressing $sod1^{A4V}$ integrated into the genome.

4.2.3 Molecular Biology methods

4.2.3.1 Plasmids used in this project

TABLE 8 LIST OF PLASMIDS USED IN THIS STUDY

Plasmid	Description	Source
pAG306 empty vector	Gateway Destination Vector (Bacterial Resistance: Ampicillin; Selection marker: URA3 Chromosome integration: chr I)	**Addgene**
pAG306 Sod1A4V	$SOD1^{A4V}$ *in* Gateway Destination Vector (Bacterial Resistance: Ampicillin; Selection marker: URA3 Chromosome integration: chr I)	**Addgene**

pAMs366 4x-CDRE-GFP	Overexpression plasmid GFP reporter to monitor calcineurin activity via calcineurin-dependent response element (CDRE) in *S. cerevisiae.* (Bacterial Resistance: Ampicillin; Selection marker: URA3)	**Addgene**
pFa6 mcherry tagging plasmid	Overexpression plasmid VMA2 C-Terminally tagged with yeast optimised mCHERRY in a BY4741 background (Bacterial Resistance: Ampicillin; Selection marker: URA3)	**A kind gift from the Thorn lab** **Addgene**
pEVP11/AEQ	Overexpression plasmid Intracellular calcium reporter in *S. cerevisiae.* (Bacterial Resistance: Ampicillin; Selection marker: LEU2)	**A kind gift from Prof Anand K Bachhawat (Indian Institute of Science Education and Research)** (Chandel, Das and Bachhawat, 2016)
crz1-GFP (C terminal GFP tag)	*MAT* **a** *his3Δ1 leu2Δ0 met15Δ0 ura3Δ0 CRZ1-GFP ::HIS3*	**Isolated from the GFP collection generated published in** (Huh *et al.*, 2003) **the GFP collection was a mind gift from Dr Peter Thorpe (Queen Mary University of London)**

4.2.3.2 High efficiency yeast transformation using the LiAc/SS carrier DNA/PEG method for *S. cerevisiae*

A fresh colony of yeast was picked using a sterile inoculation loop and inoculated into 5 ml of appropriate medium and grown overnight at 30 °C with shaking at 180 rpm. The yeast strain was inoculated into 20 ml of YPD media to an OD of 0.1 and incubated at 30 °C with shaking at 180 rpm for 4 - 5 hours. 1 ml of the culture was transferred to a 1.5 ml microcentrifuge tube and harvested in a bench-top centrifuge at 4000 rpm for 5 minutes at room temperature. The supernatant was discarded, and the pellet resuspended in 400 µl of sterile water. 100 µl of this solution was transferred into a sterile Eppendorf tube and centrifuged at 10,000 g for 30 seconds. The supernatant was removed, and the following mixture was added to the pellet: 240 µl of 50% polyethylene glycol 3300 (PEG; Sigma), 36 µl of 10x (1M) LiAoc solution, 10 µl of 10 mg/ml single stranded DNA (boiled herring sperm DNA), 64 µl water and 10 µl of plasmid DNA. Once all the solutions were added the pellet was resuspended by vortexing and the tubes were placed into a 42 °C water bath for 40 minutes. After the 40 minutes heat shock the cells were centrifuged at 10,000 g for 30 seconds, the supernatant was removed, and the pellet was resuspended in 150 µl of sterile water. The cell suspension was spread onto agar plates with the appropriate selective media and incubated at 30 °C for at least two days to allow colony growth.

4.2.3.3 Quick genomic DNA extraction and PCR in *S. cerevisiae*

A small sample of a yeast colony was taken using a sterile pipette tip and mixed into 40 µl of 0.02 M NaOH. The sample was heated for 10 min at 95 °C and then iced for 10 min. The cells were then centrifuged at 2000 g for 5 min. 1 µl of the supernatant/DNA was used for the

PCR reaction and mixed with PCR reagents (Table 9). The mixture was made up to a final volume of 25 µl with sterile water. The samples were run on an 0.4 g agarose in 50 ml TAE (= 0.8 %) gel. Correct integration of the pAG306 vector was checked by PCR using the forward primer ChrIrev2, 5'-GAAGGATAGTTCGAAGCTCGC-3' which sits 500 bp upstream of the pAG306 integration site and the reverse primer, AmpR, 5'- ATAATACCGCGCCACATAGC-3' which amplifies from within AmpR gene within the linearised pAG306 plasmid. Successful integration of pAG306 at the correct integration locus will yield a single band of 850 bp.

TABLE 9 THE REAGENT MIXTURE FOR THE PCR REACTION USED FOR THE YEAST DNA EXTRACTION.

PCR reagents
10X PCR Buffer, -Mg 2.5 µl
50 mM MgCl2 0.75 µl
10 mM dNTP Mix 0.5 µl
10 µM forward primer AmpR 1.25 µl
10 µM reverse prime 503 Chr1rev2 1.25 µl
Template DNA 1 µl
Taq DNA Polymerase (5 U/µl) 0.1 µl

4.2.3.4 Restriction enzyme digest of DNA

Using restriction endonucleases from New England Biolabs (Not1), enzymatic scission of DNA at specific sequence points was carried out. The manufacturer's protocol was used, and the buffer was supplied by the manufacturer. The reagents listed below (Table 10) were added together to create a 20 µl reaction mix. The incubation time for the digests was at least 1 h (sometimes 4 h) at 37 °C. 10 µl of the samples was loaded onto an agarose gel to analyse the digested products.

TABLE 10 BASIC REACTION MIXTURE USED FOR THE RESTRICTION ENZYME DIGEST USED IN THIS STUDY.

Reagent	Volume	Concentrations
Sterile water	14.8 µl	
Plasmid DNA of interest	2 µl	2 µg/µl
BSA	0.2 µl	10 µg/µl
Buffer D	2 µl	10X
NOT1 (restriction enzyme)	1 µl	5 u/µl

4.2.3.5 Purification of plasmids from *E. coli*

A fresh colony of *E. coli* containing the plasmid of interest was picked using a sterile inoculation loop. The colony was inoculated into 5 ml of LB media supplemented with the appropriate antibiotic and placed overnight at 37 °C with constant rotation at 180 rpm for growth. The cells were harvested in a benchtop centrifuge at 8000 x g for 3 min at room temperature. The supernatant was removed, and the plasmid DNA of interest was extracted from the cell pellet using a Qiagen QIAprep Spin Miniprep Kit according to the manufactures' instructions.

4.2.3.6 Agarose gel electrophoresis

To analyse DNA fragments and plasmids, agarose gel electrophoresis was carried out. The agarose gels were generally composed of 0.8 % (w/v) agarose (Melford, MB12000) in TAE buffer (Table 11). TAE buffer was prepared at final concentrations of 40 mM Tris, 20 mM acetic acid, and 1 mM EDTA (pH 8.0).

0.4 g of agarose was dissolved in 50 ml 1x TAE by microwaving for 1 min until the solution became clear. The solution was left to cool for 5 min to around 60 °C before 3 µl of ethidium

bromide (10 mg/ml) was added to a final concentration of 0.5 µg/ml. The solution was poured into a gel cassette, and a comb was inserted. The gel was left to set for 30-60 min. The solidified gel was placed into an electrophoresis tank and 1x TAE buffer was poured over the gel to cover its surface by 2-3 mm. The comb was then removed. 10 µl of the Invitrogen Fisher 1 kb + gene ruler DNA ladder was transferred into the first well. 1 µl of 10x blue juice loading dye was mixed with the DNA samples in a 1 in 6 manner. 10 µl of sample was loaded into the wells. A voltage of 120 V was applied to the tank for 25 min until the DNA bands had migrated the desired distance.

4.2.3.7 Transformation of *E. coli* with plasmid DNA

A 50 µl aliquot of competent cell suspension was thawed on ice. To the solution of competent cells, a volume of plasmid DNA at a concentration of at least 50 ng/ml was added and mixed gently. The mixture was incubated on ice for 30 min and then incubated at 42 °C for 45 secs. The tubes were put back on ice for 2 min. 500 µl of appropriate medium (LB growth medium with appropriate antibiotics) was added to the cells and they were grown at 37 °C with shaking at 180 rpm for 45 min. The tubes containing the transformed bacteria were centrifuged at 5000 g for 3 min. Around 350 µl of the supernatant was removed and the pellet was resuspended. The suspension was then spread onto LB agar plates containing the appropriate antibiotic to select for transformants and incubated at 37 °C overnight. Plates were checked for colony growth the next morning.

4.2.3.8 *E. coli* competent cell preparation

E. coli cells (DH5α) were grown overnight in 10 ml of LB broth at 37 °C with constant shaking at 180 rpm in a flask with aeration. 8 µl of the overnight culture was sub-cultured and diluted in 28 ml of LB media to an OD_{600} of 0.5. A volume of 3.75 ml of sterile warm 100 % glycerol was added to the 28 ml flask. The cells were then chilled on ice for 10 min. The cells were pelleted at 4 °C for 10 min at 1789 g. The supernatant was removed carefully, and the cells resuspend in 3.75 ml of ice-cold 0.1 M $MgCl_2$ and 15 % glycerol (v/v). The cells were again pelleted at 4 °C for 8 min at 1614 g. The supernatant was removed, and the cells resuspend in 6.25 ml ice-cold T-salts containing 0.075 M CaCl2, 0.006 M $MgCl_2$, and 15 % glycerol (v/v). The suspension was incubated on ice for 20 min with occasional mixing. The cells were then centrifuged at 4 °C for 6 min at 1449 g and gently resuspended in 1.25 ml T-salts. The competent cells were then aliquot into pre-cooled tubes and stored immediately at - 80 °C for at least overnight before use.

4.2.3.9 Invitrogen Gateway cloning reaction

To generate the plasmids used in this study, the Invitrogen Gateway© cloning method was used. This cloning method uses the site-specific recombination of the *lambda bacteriophage*. The Gateway cloning system allows the recombination between the two types of recombination sites that were designed and the two ends of a source sequence and a host vector. This cloning system consists of two completely reversible recombination reactions, namely the BP reaction to create entry clones and the LR reaction to generate expression clones using the corresponding catalytic enzymes BP clonase II and LR clonase II, respectively. In the BP reaction the recombination sites attB and attP are recombined,

whereas the LR reaction recombines attL and attR sites. The transformation of the recombined sites occurs through swapping the opposites halves into the opposite set e.g. attL and attR become attB and attP and conversely attB and attP become attL and attR. The names for those engineered vectors are called Entry Clone, Expression Clone, Donor Vector, and Destination Vector.

4.2.3.9.1 BP cloning reaction

The Invitrogen Gateway BP cloning reaction was performed to generate the entry vectors used in this study. Prior to the BP reaction, plasmids containing the nucleotide sequences of interest were extracted and purified using the Qiagen Spin Miniprep Kit and sequenced by Eurofin. 1 µl of the purified episomal expression vector (50 ng/ml) was mixed with 1 µl of the pDONR221 entry vector (75 ng/ml) together with 2 µl of 1x TE buffer (pH 8.0). The reagents were mixed well while the BP clonase II enzyme was thawed on ice for around 2 minutes and then vortex for 2 seconds. 1 µl of the BP clonase II was then transferred into the reaction mixture and incubated at room temperature for 1 h. 0.5 µl of Proteinase K solution (2 mg/ml) was added to the solution to end the reaction. After briefly vortexing the reaction mixture, the tubes were incubated at 37 °C for 10 min. The samples were then stored at - 20 °C or transformed into bacteria. The pDONR221 entry clone used contained Kanamycin resistance genes. The samples were sent to GATC Eurofin for sanger sequencing with M13F or T7 promotor primers.

4.2.3.9.2 LR cloning reaction

To generate the expression clones used in this study, the Invitrogen Gateway LR cloning reaction was used. This reaction allows the recombination of the destination vector with the entry vector containing the gene of interest. Prior to the LR reaction, bacteria containing the destination vector pAG306 ccdB and pAG306 empty were grown and the plasmid was extracted and purified using the Qiagen Spin Miniprep Kit. The plasmids were checked using agarose gel electrophoresis. 2 µl of the entry clone (50-150 ng/ µl) was mixed with 2 µl of the destination vector (150 ng/ µl) together with 6 µl of 1x TE buffer (pH 8.0). The LR clonase II enzyme mix was thawed on ice for 2 min and vortexed for 2 secs. To each sample 2 µl of LR clonase II was added and well mixed by vortexing. The reaction was incubated at 25 °C for 1 h. 1 µl of Proteinase K solution (2 mg/ml) was added to each sample to terminate the reaction. The samples were vortexed briefly and incubated at 37 °C for 10 min before they were stored at - 20 °C or transformed into bacteria. The destination vector pAG306 ccdB contained an ampicillin resistance gene. The samples were sent GATC Eurofin for sanger sequencing with the GDPro-F primers.

4.2.4 Cell biology whole cell experimental procedures

4.2.4.1 Vacuole knockout library screen: Absorbance assays for growth rate analysis of *S. cerevisiae* cells

The vacuole knockout library was constructed by transforming the pAG306-GPD-*SOD1*-A4V-chrI integration vector into a library of MATa gene deletion mutants encoding proteins with functions related to the vacuole and metabolism in *S. cerevisiae*. The high efficiency transformation was used (5.2.3.2). Correct integration of pAG306-GPD-*SOD1*-A4V-chrI into

each mutant was confirmed by PCR and agarose gel electrophoresis analysis of the gDNA using the primers: chrIrev2, 5'- GAAGGATAGTTCGAAGCTCGC-3' and Amp-R, 5'-ATAATACCGCGCCACATAGC-3'.

The control and A4V 96-well plate were stamped out onto YPD agar using a sterile replicator and grown at 30 °C for 2 – 3 days. Once grown, cells from these plates were used to inoculate a 96-well plate with liquid YPD media, by stamping using the sterile replicator. Cells were grown overnight at 30 °C, 180 rpm shaking with parafilm around the edges of the 96-well plate to prevent evaporation. The following day, yeast cultures were diluted to an OD_{600} of 0.1 in 100 µl of appropriate medium with or without supplements (Table 12) into a sterile 96-well plate (Greiner). The 96-well plate was placed into a BMG LABTECH FLUOstar OPTIMA or a BMG LABTECH SPECTROstar Nano plate reader for 24 hours where the growth was measured (Table 13). The protocol setting used can be found in the table below. To analyse the generated data by the plate reader the data analysis software BMG LABTECH MARS was used. The data was then exported to Microsoft Excel to further analysing it. The area under the curve (AUC) was calculated using GraphPad Prism. Here, the trapezoidal method was applied where each connecting segment under the growth curve describes a trapezoid. The sum of each segmental trapezoid forms the total AUC.

TABLE 11 A LIST OF SUPPLEMENTS ADDED TO YPD MEDIA.

Supplement	**Concentration**
$ZnCl_2$ (Sigma Aldrich)	4 mM
$CaCl_2$ (Sigma Aldrich)	50 mM
FK506 (Sigma Aldrich)	100 µM

TABLE 12 THE PROTOCOL SETTING USED TO MEASURE GROWTH RATE

Cycle Time	**1800 seconds**
Flashes per Well	3
Excitation	600 nm
Shaking Frequency	400 nm
Shaking Mode	Double Orbital
Additional Shaking Time	30 seconds before each cycle
Temperature	30 °C
Positioning Delay	0.5 seconds

4.2.4.2 Quantification of calcineurin activity by flow cytometry

Desired strains were transformed with the pAMs366 4×-CDRE-GFP-URA3 reporter plasmid. Colonies were then streaked out onto SC media lacking uracil to maintain the reporter plasmid. For the flow cytometry experiment, 5 ml of SC-URA medium were inoculated with a colony of the desired yeast strain expressing pAMs366 4×-CDRE-GFP-URA3 and grown overnight at 30 °C with 180 rpm shaking. The next morning, this overnight culture was used to inoculate two 10 ml cultures of SC-URA to an OD_{600} of 0.1 per strain. This culture was grown at 30 °C with 180 rpm shaking for 7 h until an OD_{600} of 0.5–1 had been reached. A negative control was inoculated including BY4741 cells at an OD_{600} of 0.1 with 0.5 µM FK506, a calcineurin inhibitor. Once the cultures had reached an OD_{600} of 0.5–1, $CaCl_2$ was added to one of the 10 ml cultures to a final concentration of 50 mM. Cultures were placed back in the incubator at 30 °C for 1 h with 180 rpm shaking. After 1 h, all cultures were washed twice in sterile mqH_2O and diluted to an OD_{600} of 0.1 and then resuspended in sterile 1× PBS. Cells resuspended in 500 µl PBS were transferred to Eppendorf tubes.

Fluorescence intensity of cells expressing pAMs366 4×-CDRE-GFP-URA3 was analysed using the BD AccuriTM C6 Plus Personal Flow Cytometer (BD Biosciences). Measurement events were gated on the flow cytometer to ensure that singlet yeast cells were being recorded. The flow cytometer was equipped with a blue laser (488 nm) and a red laser (640 nm). The FL1 (533/30 nm) filter was used to detect the GFP fluorophore from cells expressing the 4×-CDRE-GFP reporter. Approximately 10,000 events were collected per sample and the data was acquired and analysed using the BD Accuri C6 Plus software.

4.2.4.3 Cytosolic Calcium concentration measurement using ApoAequorin luminescence

The Ca^{2+}-binding photoprotein aequorin is composed of an apoprotein (apoaequorin) that has a molecular weight of about 22 kDa and a prosthetic group, a luciferin molecule coelenterazine (MW 432). The functional holoprotein aequorin reconstitutes spontaneously when molecular oxygen is present. Three EF-hand Ca^{2+} binding site are present in the protein. Aequorin undergoes conformational change when Ca^{2+} binds and coelenterazine is converted into excited coelenteramide together with carbon dioxide. The excited coelenteramide relaxes to the ground state, and blue light (469 nm) is emitted which can be detected with a luminometer (Mithöfer and Mazars, 2002).

Desired yeast strains were transformed with the pEVP11/AEQ plasmid containing the apoaequorin gene and selected in appropriate SC media.

For luminescence assays, cells were grown overnight at 30 °C in Sc selection medium and sub-cultured to mid log-phase around OD 600 nm 0.5-0.7.

Log- phase cells were then re-suspended at a density of ~10^8 cells/ml in fresh SD selective medium. The substrate coelenterazine (Invitrogen) was added to a final concentration of 5 µM. As a negative control, cells were treated with the equivalent volume of solvent (methanol). The samples were incubated in the dark for 1 h at 30 °C before they were collected by centrifuging at 5000 rpm for 5 min. The samples were washed three times with PBS, resuspended in 200 µl of medium, and incubated for 30 min in the dark at 30 °C to reconstitute functional aequorin within the cells. After the incubation, cells were transferred into a 96 well microplate. Luminescence readings (469 nm) were taken every 1 min with 40 seconds shaking in between each read to keep cells in suspension. The gain was adjusted to 3600 to obtain a suitable reading. After 10 cycles to record the baseline luminescence, the plate was ejected and 100 mM $CaCl_2$ was added. The plate was then returned to the plate reader and readings were taken for further 2 h. Data sets were analysed using a two-way ANOVA. Post hoc comparisons were performed using Tukey's test for exploratory pairwise contrasts, except where only WT vs Δ was tested; in those cases, Sidak's correction was used as required by Prism.

4.2.5 Fluorescence microscopy of yeast cells

4.2.5.1 Sample preparation

A fresh colony of yeast was picked with a sterile inoculation loop. The colony was inoculated into 5 ml of appropriate media and grown overnight at 30 °C with shaking at 180 rpm. The $OD_{600\ nm}$ of this culture was measured using an Eppendorf Biophotometer plus. To analyse yeast cells in logarithmic phase of cell growth, cells were sub-cultured and grown to $OD_{600\ nm}$ 0.4-0.7 in fresh appropriate media. 2 µl of the culture was pipetted onto a

microscope slide and covered using a 20 mm by 20 mm cover slip. A single drop of Olympus Immoil-F30CC immersion oil was applied to the surface of the 100x (1.4 NA) objective lens prior to the examination under the microscope.

4.2.5.2 Fluorescence microscopy

An Olympus 1X81 inverted microscope was used to visualise fluorescent cells. A Cool LED pE4000 illumination system provided the light, and an Andor's Zyla 4.2 PLUS sCMOS camera was used to capture all images. The acquisition software Micro-Manager version 1.4.22 was used to obtain the images. An Olympus 100 x objective lens (NA = 1.4) was used to visualise cells from a sample. The GFP channel with excitation/emission wavelengths of 488/512 nm was used to observe Cells with GFP-tagged proteins. A halogen light source was used to capture DIC images. Each experiment was repeated in biological triplicates. The software ImageJ FIJI was used for the analysis and processing of the microscopy images.

4.2.5.3 FLIM/FRET microscopy

To complete FLIM/FRET we generated mCherry tagged Sod1 and Sod1^{A4V} strains using homologous recombination (Sod1^{A4V} was generated using CrispR Doyle 2022), mCherry was C-terminally tagged using a pFa6 mcherry tagging plasmid (a kind gift from the Thorn lab https://www.addgene.org/44643/) amplified using the following primers:

Sod1FwdMcherrytag

CGGTCGCAGGACACCCTGGTTGGTTCATTGGTTACACCAGCGTGACGGTGCTGGTTT

Sod1RevMcherrytag

ACTTACATACAGCGTTTTTTAACATGAATTAATCAATTAACACTGAATGAATTCGAGCTCG

Correct insertion of mCherry was confirmed the primers Sod1McherryFwdCheck 5'- GTG TCT CTG GTC GTC CTC AC -3' and Sod1McherryRevCheck 5'- GAC TAA GAA TGT CCC AGG CG -3'. VMA2 was tagged with GFP at the Nterminus using a gateway LR cloning reaction as per manufacturer's instructions using an N-terminal GFP tag destination vector (426-GPD-eGFP-ccdB) and a pDONR201-VMA2-KAN (entry clone). The GFP-VMA2 plasmid was introduced into Sod1-mCherry or Sod1^{A4V}-mCherry strains and maintained in -URA3 selective media. Cells were grown to log phase in -URA3 media containing 2 % glucose. FLIM data was collected using a one-photon time correlated single-photon counting (TCSPC) PC module (SPC830, Becker and Hickl GmbH) coupled to a Nikon confocal system (Eclipse EC2, running a EZ-C1 v.3.91 software, Nikon) attached to a Nikon Ti-E microscope The system is equipped with a SuperK EXTREME NKT-SC 470-2000 nm supercontinuum white light laser (NKT Photonics) which generates at 80 MHz repetition rate with 70 ps pulse width. The desired wavelengths were selected using a SuperK SELECT multi-line tuneable filter (NKT photonics). The FLIM platform was assembled and calibrated regularly using fluorescence probes in solution with known excited state lifetime such GFP, fluorescein at pH11 and 7-hydroxycoumarin carboxylic acid. Prior to FLIM acquisition, confocal imaging of GFP, mCherry, and transmitted light was carried out following excited at wavelengths of 488 nm and 561 nm respectively using a Nikon 60x VC (NA 1.20) with water immersion objective. Fluorescence emissions of GFP and mCherry were selected with a Nikon 520±35 and a Comar 633IU filters, respectively. Following confocal imaging to ensure the presence and expression of the chromophores, GFP lifetime was measured with HPM100-40 detector and raw FLIM data were generated by the TCSPC software v.9.77 (Becker and Hickl, GmbH). Raw

FLIM images were analysed with the SPCImage software v.6.9 (Becker and Hickl, GmbH) and exported as TIFF images. During the FLIM data analysis, an incomplete multiexponential fit model with a laser repetition time value of 25 ns was used for the decay curve fitting that do not decay to the base line. Lifetime values with χ^2 between 0.9 and 1.2 were taken as good exponential decay fit. GFP/RFP was used as the FRET pair with Sod1 or Sod1^{A4V} tagged in the genome with mCherry and VMA2 on a plasmid (URA selection).

4.3 Results

4.3.1 Interaction between Sod1 and parts of the vATPase (VMA2) using FLIM/FRET

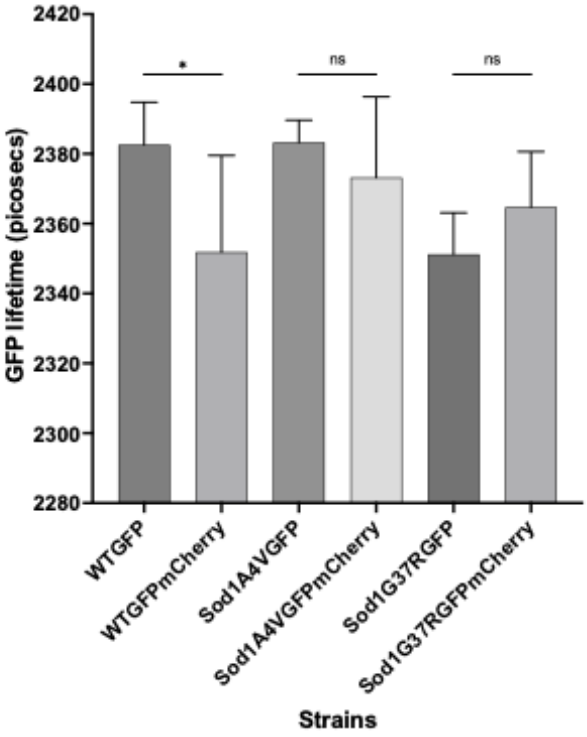
One of the key findings through previous work was the potential interaction between Sod1 and parts of the vATPase (VMA2). We therefore sought to explore this further using FLIM/FRET microscopy. The fluorescence microscopy tool FLIM/FRET is commonly used to study protein-protein interactions by measuring energy transfer between them. It uses changes in the fluorescence lifetime of the donor molecule to detect if energy is transferred to an acceptor. FLIM measures the fluorescence lifetime of a fluorophore which is the average time a light-absorbing molecule (fluorophore) remains excited after absorbing light before emitting a lower-energy photon and returning to its normal state. FLIM thus tracks changes in the donor's light emission time. FRET (Förster Resonance Energy Transfer) happens when energy from an excited molecule (the donor) transfers to a nearby molecule (the acceptor) without emitting light. The donor returns to its normal state, and the acceptor may emit light if it is fluorescent. FRET works over very short distances (less than

10 nm) and needs the donor and acceptor to be close, have overlapping light spectra, and be properly aligned (Liput et al., 2020).

Previous data by Dr Kevin Doyle showed an interaction between Sod1 and parts of the vATPase (Vma2, Vma4 and Vma8) (Doyle, 2022). This interaction between Sod1 and Vma2 was explored further using FLIM/FRET microscopy with GFP/RFP as the FRET pair, where Sod1 or $Sod1^{A4V}$ were tagged in the genome with mCherry and Vma2 tagged with GFP expressed from a high copy plasmid (URA selection). By overexpressing VMA2-GFP on a plasmid we reasoned the effects of an interaction may be observed given that Sod1 is a very abundant protein. The core idea is that if Sod1-mCherry interacted or was localised close enough to Vma2-GFP at the vacuole (putative interaction) then energy transferred from GFP upon excitation to mCherry would lead to a reduction in lifetime of GFP as measured by FLIM at the vacuole. The lifetime of Vma2-GFP was assessed in multiple cells and an average calculated in each cell from a number of points on the vacuole membrane that was clearly visible under GFP illumination (Figure 2 B). The raw data used to calculate the final averages is presented in supplementary appendix Figure 1.

A small but reproducible reduction in Vma2-GFP lifetime when Sod1-RFP (FRET acceptor) could be observed suggesting proximity but most likely at a distance that does not support a direct interaction between Sod1 and Vma2. No significant difference in Vma2-GFP lifetime could be observed when $Sod1^{A4V}$ – mCherry was co-expressed when compared to its control (Figure 2 A). A similar result could be observed when $Sod1^{G37R}$ was present (Figure 2 A).

A


2420
2400
2380
2360
2340
2320
2300
2280
GFP lifetime (picosecs)
*
ns
ns
WTGFP
WTGFPmCherry
Sod1A4VGFP
Sod1A4VGFPmCherry
Sod1G37RGFP
Sod1G37RGFPmCherry
Strains

B

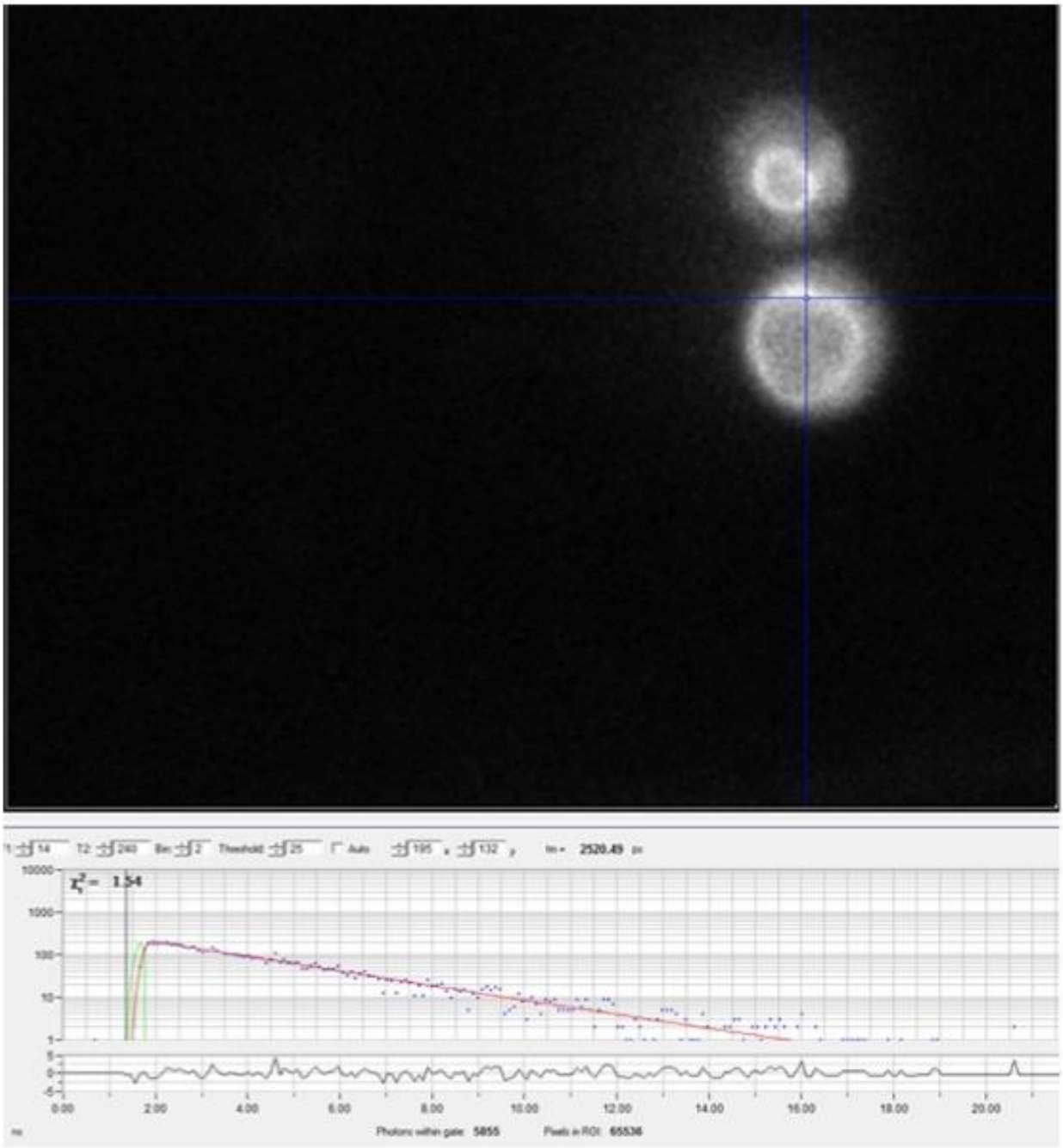


Figure 2 Interaction between SOD1 and VMA2 using FLIM/FRET microscopy.
A) Bar chart showing the GFP lifetime in picoseconds of the GFP tagged VMA2 when either wild type Sod1, mutant $Sod1^{A4V}$, or mutant $Sod1^{G37R}$ were expressed. Six cells per biological repeat were used to obtain the average. The data shown above represents three biological repeats. The error bars represent the standard deviation. A One-Way ANOVA using a Tukey multiple comparison test was used to determine statistical significance. (*) flags levels of significance compared to the WT/A4V, $p < 0.05$.
B) An example showing how GFP lifetime was obtained, the SPCImage software v.6.9 output is shown with the GFP lifetime plot obtained for a single point identified by the blue cross-section.

4.3.2 Generation of new strains to complete the knockout library

The FLIM/FRET observation that Sod1^{A4V} and Sod1^{G37R} do not interact directly with the vATPase led us to investigate other possibilities that may be responsible for the metabolic defects observed when mutated Sod1 is overexpressed in a Δ*sod1* background (Bastow et al., 2016). Kevin's Doyles work (Doyle, 2022) suggested that calcium stress, calcineurin signalling, and zinc addition may be linked to Sod1 mutant induced vacuole dysfunction. To investigate whether the presence of calcium or zinc stress or the inhibition of calcineurin signalling led to an increase in Sod1^{A4V} mediated vacuole dysfunction, we made use of and expanded a vacuole knockout library constructed by Dr Kevin Doyle. The layout for this vacuole knockout library is presented in Figure 3 A. The control plate contains 72 knockouts from the MATa deletion library (Doyle, 2022) selected as genes linked with the vacuole by annotation provided within the *S. cerevisiae* genome database. The vacuole KO library contains a number of mutants lacking genes encoding amino acid, metal ion and other transporters located on the vacuole membrane. The Sod1^{A4V} plate contains the same 72 knockout strains but have the pAG306 chr I vector expressing Sod1^{A4V} integrated into the genome (Doyle, 2022). For both the control and Sod1^{A4V} plate, the first six strains in wells A1–A6 contain the strains, WT EV (BY4741 pAG306 empty vector), WT SOD1 (BY4741 pAG306 WT SOD1), WT Sod1^{A4V} (BY4741 pAG306 Sod1^{A4V}, Δ*sod1* (Δ*sod1* pAG306 empty vector), Δ*sod1* SOD1 (pAG306 WT SOD1), Δ*sod1* Sod1^{A4V} (pAG306 Sod1^{A4V}).

The pAG306 SOD1^{A4V} vector was integrated into each knockout and confirmed by PCR by Dr Kevin Doyle (Doyle, 2022).

In addition, we expanded the library to include six additional strains that have gene ontology links to vacuole function; Δ*ypq1*, Δ*ypq2*, Δ*ypq3*, Δ*cnb1*, Δ*cna1*, and Δ*cmp2* that

were not included in the original library. Here, the pAG306 SOD1^{A4V} vector was integrated into each knockout, confirmed by PCR (Figure 3 B) and included in the library.

A

	1	2	3	4	5	6	7	8	9	10	11	12
A	WT Empty Vector	WT ySOD1	WT ySOD1-A4V	Δsod1 Empty Vector	Δsod1 ySOD1	Δsod1 ySOD1-A4V	Δtps2	Δvcx1	Δpfk2	Δras2	Δbpt1	Δyvc1
B	Δnth1	Δath1	Δvph1	Δmsn2	Δgpr1	Δycf1	Δvtc5	Δvma2	Δego2	Δrtg3	Δego3	Δtor1
C	Δgtr1	Δzrc1	Δmsn4	Δfth1	Δarf1	Δgpa2	NA	Δsnf1	Δtps3	Δpep4	Δphm5	Δstv1
D	Δcot1	Δvps30	Δatg5	Δtps1	Δnth2	Δrtg2	Δpmc1	Δyck2	Δego1	Δtsl1	Δptk2	Δdun1
E	Δvtc1	Δvba3	Δvba4	Δavt3	Δzrt3	Δvtc3	Δccc1	Δavt2	Δprb1	Δatg1	Δavt6	Δvps15
F	Δvps34	Δvtc2	Δatg22	Δatg17	Δavt1	Δavt7	Δfet5	Δatg18	Δvba1	Δyhc3	Δvba5	Δmon1
G	Δnhx1	Δatg8	Δatg32	Δatg11	Δccc2	Δsmf3	ΔYPQ1	ΔYPQ2	ΔYPQ3	ΔCNB1	ΔCNA1	ΔCMP2

B

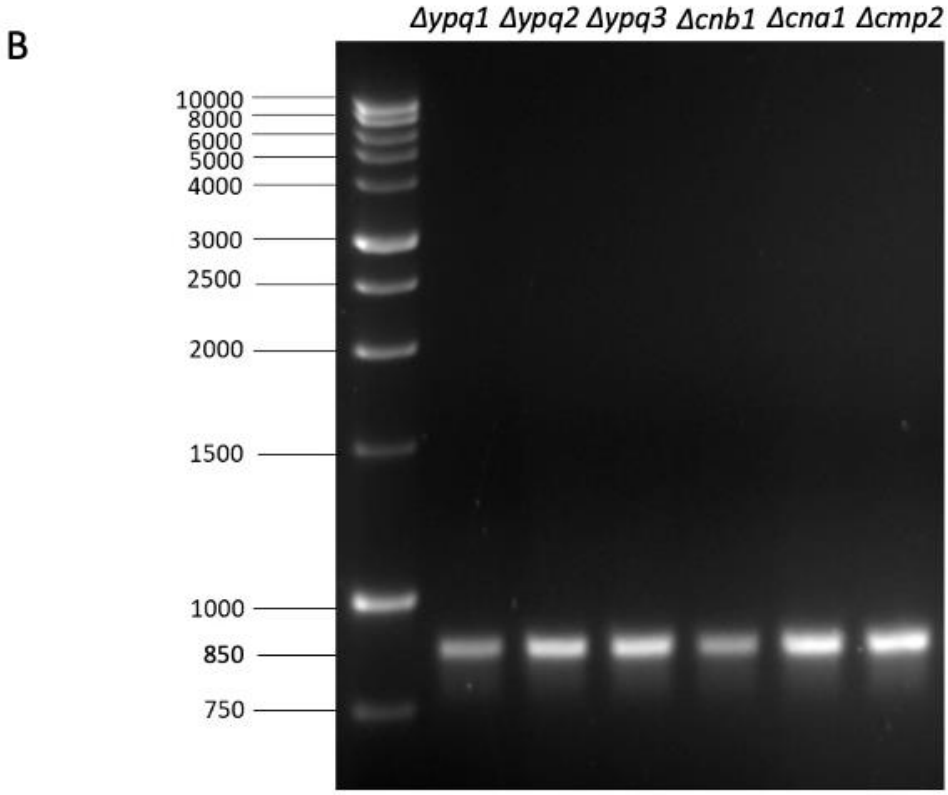


Figure 3 Expanded vacuole knockout library.
A) Layout of the vacuole KO library containing 72 knockouts from the MATa deletion library. The mutants lack genes encoding amino acid, metal ion and other transporters located on the vacuole membrane. For the control plate the pAG306 chr I empty vector and for the Sod1^{A4V} plate the pAG306 chr I vector expressing Sod1^{A4V} was integrated into the genome (Doyle, 2022).
B) Agarose gel confirming the integration (band size 850 bp) of pAG306 chr I vector expressing Sod1^{A4V} in Δypq1, Δypq2, Δypq3, Δcnb1, Δcna1, and Δcmp2. Refer to Materials and methods 5.2.3.3.

4.3.3 Assessment of effects of Sod1^{A4V} expression in vacuole KO library in YPD

From previous work we found that Sod1 may be important in regulating calcineurin (Cn) activity and thus be important in the calcium response (Doyle, 2022). We therefore sought to test the effects of several stresses when Sod1^{A4V} was expressed: 50 mM $CaCl_2$, Cn inhibitor FK506 and 4 mM $ZnCl_2$. To identify potential synthetic interactions between these stresses and Sod1^{A4V} with processes linked to vacuole function, we investigated the effects on growth in the vacuole KO library. From this, total AUC (area under the curve) values, which are a representation of total growth, were obtained and heatmaps generated (Figure 4 A, B). From the total AUC values, we then calculated the fold change of Sod1^{A4V} expressing strains over empty vector (EV) control vacuole KO library strains. Fold change analysis of strains grown in standard YPD medium without stresses revealed significant differences compared to the fold change of WT EV vs. Sod1^{A4V} in following vacuole KO library strains: Δ*ath1* EV vs. Δ*ath1* Sod1^{A4V} (increased), Δ*ego1* EV vs. Δ*ego1* Sod1^{A4V} (decreased), Δ*vtc1* EV vs. Δ*vtc1* Sod1^{A4V} (decreased), Δ*vps34* EV vs. Δ*vps34* Sod1^{A4V} (decreased), Δ*atg18* EV vs. Δ*atg18* Sod1^{A4V} (decreased), Δ*vba5* EV vs. Δ*vba5* Sod1^{A4V} (decreased), Δ*nhx1* EV vs. Δ*nhx1* Sod1^{A4V} (decreased), and Δ*atg8* EV vs. Δ*atg8* Sod1^{A4V} (decreased) (Figure 5 A). The functions of each vacuole KO library strain that showed significant differences in fold change values compared to the WT EV in YPD (see described above) are described in Figure 5 B.

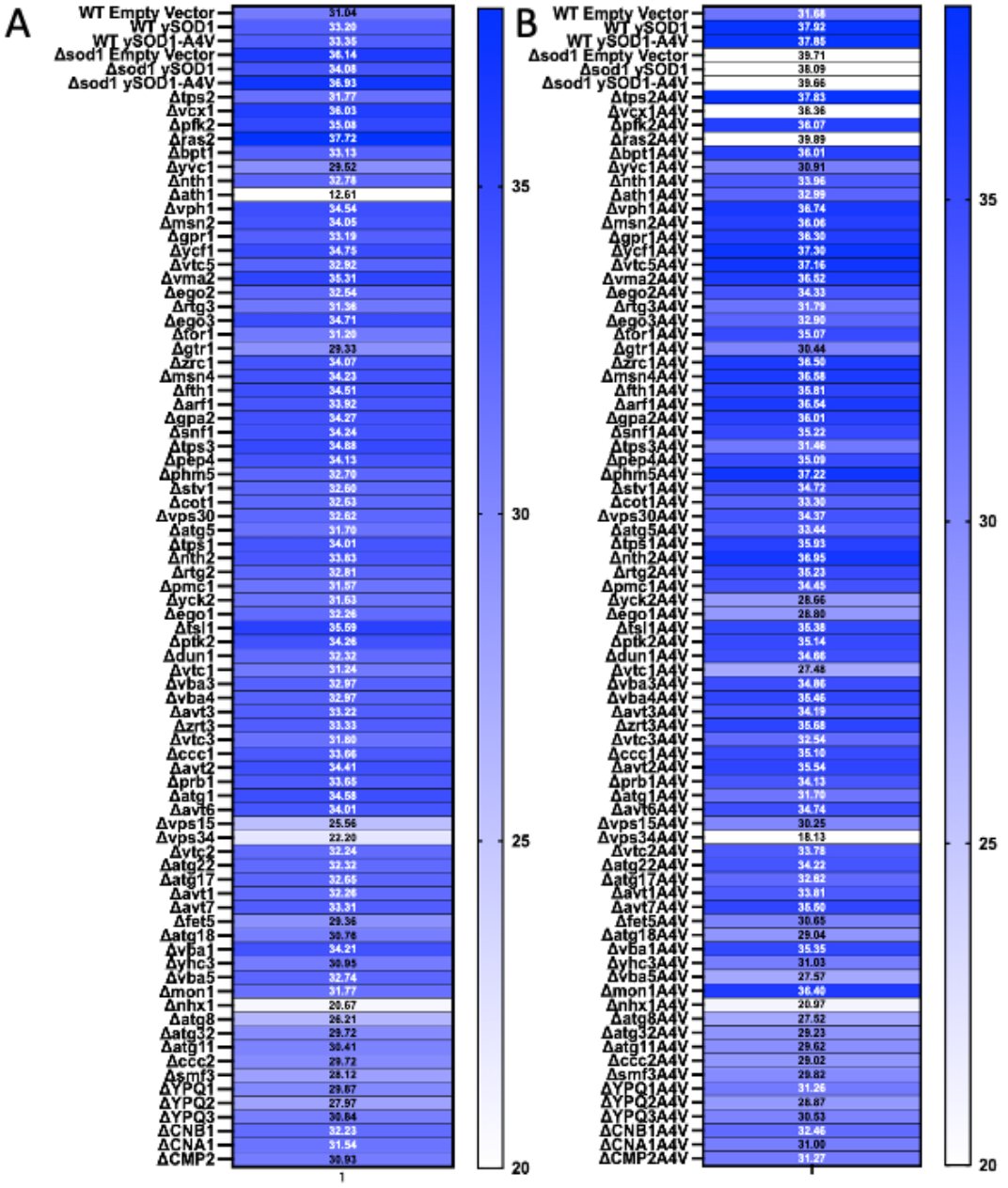
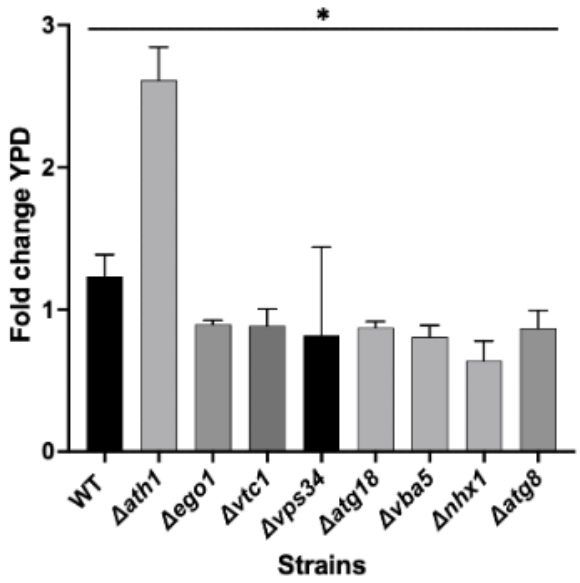


Figure 4 Potential synthetic interactions between expression of mutant Sod1^{A4V} and different gene deletions involved in metabolic functions of the vacuole in S. cerevisiae. A, B) Heatmaps generated from AUC values obtained from growth screen of the vacuole knockout library in standard YPD media.
Gene Knockouts expressing pAG306 EV (A) or pAG306 Sod1^{A4V} (B) are indicated. The AUC data was displayed as a blue gradient as shown in the key whereby the highest value set was 38 units and the lowest value set was 20 units. Values outside the set values are coloured white. The heatmaps represent the average AUC of three biological repeats for each strain.

A



B

Strain	Fold change	Function
Δego1	Decreased 0.89	Subunit of EGO/GSE complex; vacuolar/endosomal membrane-associated EGO/GSE complex regulates exit from rapamycin induced growth arrest, stimulating microautophagy and sorting of Gap1p from endosome to plasma membrane
Δvtc1	Decreased 0.88	Regulatory subunit of vacuolar transporter chaperone (VTC) complex; VTC complex is involved in membrane trafficking, vacuolar polyphosphate accumulation, microautophagy and non-autophagic vacuolar fusion
Δvps34	Decreased 0.81	Phosphatidylinositol (PI) 3-kinase that synthesize PI-3-phosphate; forms membrane-associated signal transduction complex with Vps15p to regulate protein sorting; activated by the GTP-bound form of Gpa1p
Δatg18	Decreased 0.87	Phosphoinositide binding protein; required for vesicle formation in autophagy and the cytoplasm-to-vacuole targeting (CVT) pathway
Δvba5	Decreased 0.80	Plasma membrane protein of the Major Facilitator Superfamily (MFS); involved in amino acid uptake and drug sensitivity
Δnhx1	Decreased 0.63	Na+/H+ and K+/H+ exchanger
Δatg8	Decreased 0.86	Ubiquitin-like protein conjugated to phosphatidylethanolamine (PE); role in membrane fusion and phagophore expansion during autophagosome formation; triggers its vacuolar degradation
Δath1	Increased 2.61	Acid trehalase involved in intracellular trehalose degradation during growth recovery after saline stress

Figure 5 Potential synthetic interactions between expression of mutant Sod1^{A4V} and different gene deletions involved in metabolic functions of the vacuole in S. cerevisiae.
A) Fold change comparison of growth of strains expressing the Sod1^{A4V} mutation versus the same strain containing an empty control vector when grown in YPD media. The graphs show the foldchange of strains containing the Sod1^{A4V} mutations vs. strains lacking the Sod1^{A4V} mutation. The fold changes were compared to the WT empty vector vs WT Sod1^{A4V} fold change. The error bars represent the standard deviation. A One-Way ANOVA using a Tukey multiple comparison test was used to determine statistical significance. (*) flags levels of significance compared to the WT/A4V, $p < 0.05$.
The graph represents three biological repeats.
B) List of KO strains and their gene function showing significant fold changes compared to the WT fold change under normal YPD conditions.

4.3.4 Assessment of effects of Sod1^{A4V} expression in vacuole KO library under 50 mM Calcium stress

After establishing potential synthetic interactions of strains from the vacuole knockout library in YPD medium without any additional stresses, we repeated the same experiment in the presence of 50 mM $CaCl_2$, a level that is well tolerated by *S. cerevisiae* cells. Fold change analysis of vacuole KO library strains grown in YPD medium supplemented with 50 mM $CaCl_2$ revealed significant differences compared to the fold change of WT EV vs. Sod1^{A4V} in following vacuole KO library strain combinations: Δ*ras2* EV vs. Δ*ras2*1 Sod1^{A4V} (decreased), Δ*yvc1* EV vs. Δ*yvc1* Sod1^{A4V} (decreased), Δ*nhx1* EV vs. Δ*nhx1* Sod1^{A4V} (decreased), Δ*ath1* EV vs. Δ*ath1* Sod1^{A4V} (increased), Δ*ccc1* EV vs. Δ*ccc1* Sod1^{A4V} (increased), and Δ*vps34* EV vs. Δ*vps34* Sod1^{A4V} (increased) (Figures 6, 7 A). The functions of each vacuole KO library strain that showed significant differences in fold change values compared to the WT in YPD supplemented with 50 mM $CaCl_2$ (see described above) were described in Figure 7 B.

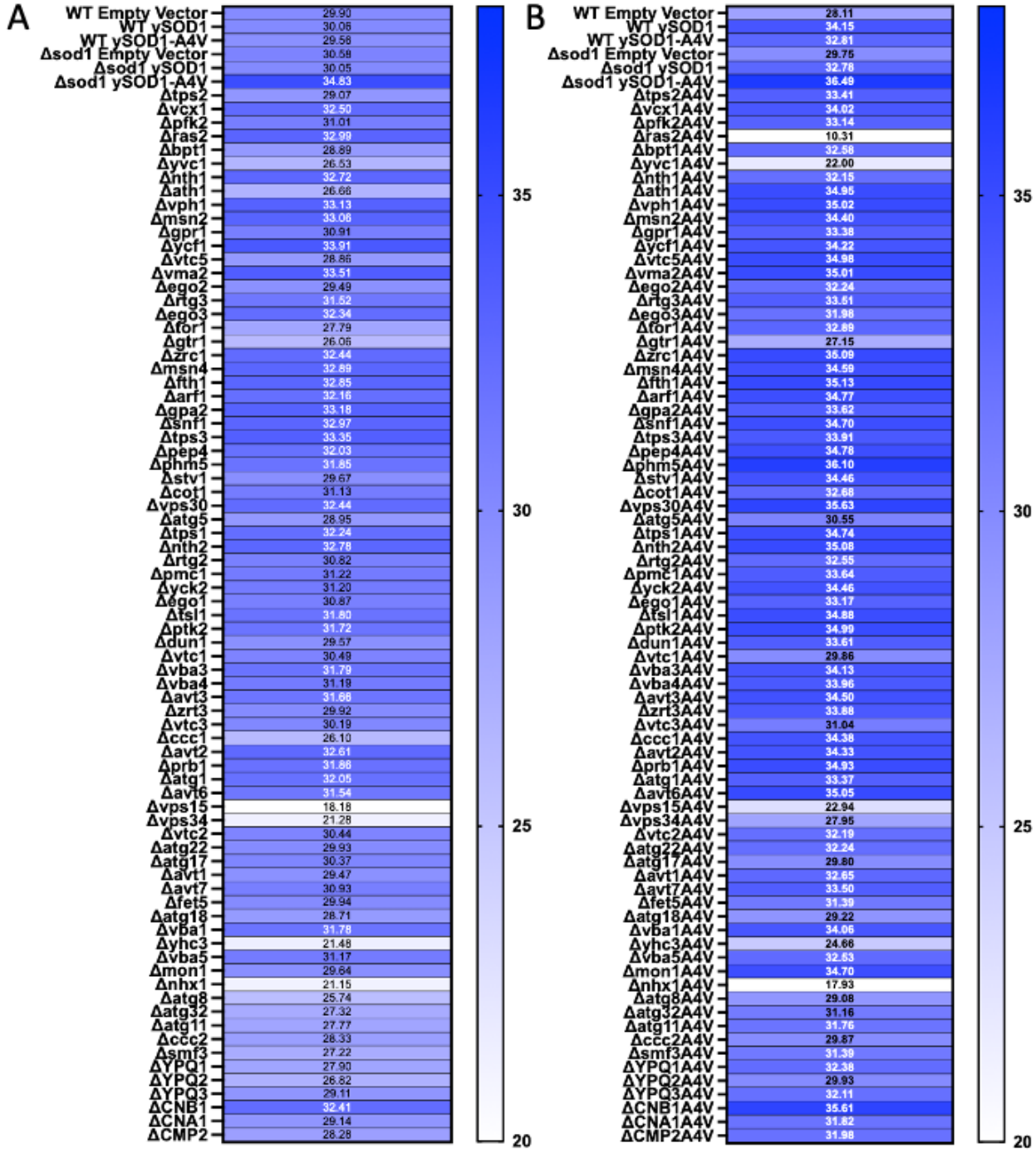
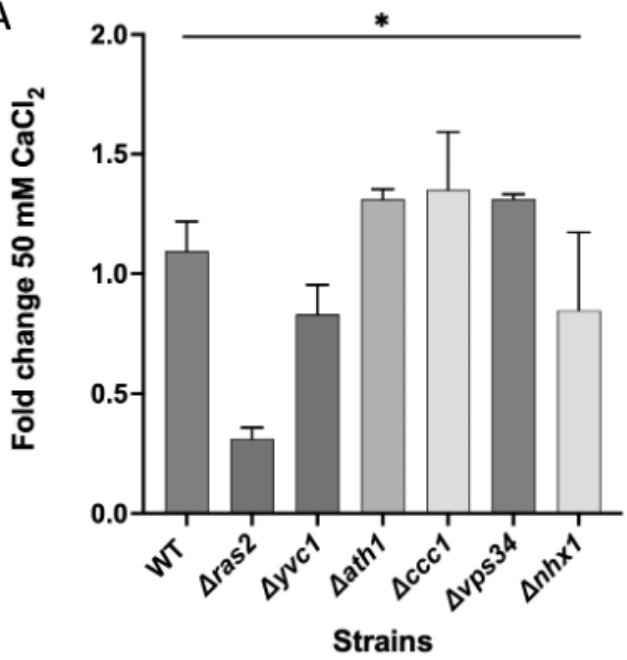


Figure 6 Potential synthetic interactions between expression of mutant Sod1^{A4V} and different gene deletions involved in metabolic functions of the vacuole in S. cerevisiae.
A, B) Heatmaps generated from AUC values obtained from growth screen of the vacuole knockout library in YPD media supplemented with 50 mM $CaCl_2$.
Knockouts expressing pAG306 EV (A) or pAG306 Sod1^{A4V} (B). The AUC data was displayed as a blue gradient as shown in the key whereby the highest value set was 38 units and the lowest value set was 20 units. Values outside the set values are coloured white. The heatmaps represent the average of three biological repeats.

A



B

Strain	Fold change	Function
Δras2	Decreased 0.31	GTP-binding protein; regulates nitrogen starvation response, sporulation, and filamentou growth; farnesylation and palmitoylation require for activity and localization to plasma membrane activated by increased levels of glycolysis intermediate fructose-1,6-bisphosphate; homolc of mammalian Ras proto-oncogenes
Δyvc1	Decreased 0.83	Vacuolar cation channel; mediates release of Ca (2+) from the vacuole in response to hyperosmotic shock
Δnhx1	Decreased 0.84	Na+/H+ and K+/H+ exchanger
Δvps34	Increased 1.31	Phosphatidylinositol (PI) 3-kinase that synthesize PI-3-phosphate; forms membrane-associated signal transduction complex with Vps15p to regulate protein sorting.
Δath1	Increased 1.31	Acid trehalase involved in intracellular trehalose degradation during growth recovery after saline stress
Δccc1	Increased 1.35	Vacuolar Fe2+/Mn2+ transporter

Figure 7 Potential synthetic interactions between expression of mutant Sod1^{A4V} and different gene deletions involved in metabolic functions of the vacuole in S. cerevisiae.
A) Fold change comparison of growth of strains expressing the Sod1^{A4V} mutation versus the same strain containing an empty control vector when grown in YPD media supplemented with 50 mM $CaCl_2$. The graphs show the foldchange of strains containing the Sod1^{A4V} mutations vs. strains lacking the Sod1^{A4V} mutation. The fold changes were compared to the WT empty vector vs WT Sod1^{A4V} fold change. The error bars represent the standard deviation. A One-Way ANOVA using a Tukey multiple comparison test was used to determine statistical significance. (*) flags levels of significance compared to the WT/A4V, $p < 0.05$.
The graphs represent three biological repeats.
B) Table 2 List of KO strains and their gene function showing significant fold changes compared to the WT fold change after 50 mM $CaCl_2$.

4.3.5 Assessment of effects of Sod1^{A4V} expression in vacuole KO library under Calcineurin inhibition (FK506)

We also investigated potential synthetic interactions of strains from the vacuole knockout library when calcineurin was inhibited by 100 µM FK506, a value that has been demonstrated to lead to Cn inhibition (Doyle, 2022). Fold change analysis of vacuole KO library strains grown in YPD medium supplemented with 100 µM FK506 revealed significant differences compared to the fold change of WT EV vs. Sod1^{A4V} in following vacuole KO library strains: Δ*vcx1* EV vs. Δ*vcx1* Sod1^{A4V} (decreased), Δ*pfk2* EV vs. Δ*pfk2* Sod1^{A4V} (decreased), Δ*ras2* EV vs. Δ*ras2* Sod1^{A4V} (decreased), Δ*yvc1* EV vs. Δ*yvc1* Sod1^{A4V} (decreased), Δ*rtg3* EV vs. Δ*rtg3* Sod1^{A4V} (decreased), Δ*ego3* EV vs. Δ*ego3* Sod1^{A4V} (decreased), Δ*gtr1* EV vs. Δ*gtr1* Sod1^{A4V} (decreased), Δ*zrc1* EV vs. Δ*zrc1* Sod1^{A4V} (decreased), Δ*tps3* EV vs. Δ*tps3* Sod1^{A4V} (decreased), Δ*tps1* EV vs. Δ*tps1* Sod1^{A4V} (decreased), Δ*nth2* EV vs. Δ*nth2* Sod1^{A4V} (decreased), Δ*yck2* EV vs. Δ*yck2* Sod1^{A4V} (decreased), Δ*ego1* EV vs. Δ*ego1* Sod1^{A4V} (decreased), Δ*ptk2* EV vs. Δ*ptk2* Sod1^{A4V} (decreased), Δ*vtc1* EV vs. Δ*vtc1* Sod1^{A4V} (decreased), Δ*vba3* EV vs. Δ*vba3* Sod1^{A4V} (decreased), Δ*vtc3* EV vs. Δ*vtc3* Sod1^{A4V} (decreased), Δ*atg1* EV vs. Δ*atg1* Sod1^{A4V} (decreased), Δ*vps15* EV vs. Δ*vps15* Sod1^{A4V} (decreased), Δ*fet5* EV vs. Δ*fet5* Sod1^{A4V} (decreased), Δ*vba5* EV vs. Δ*vba5* Sod1^{A4V} (decreased), Δ*ccc2* EV vs. Δ*ccc2* Sod1^{A4V} (decreased), and Δ*ath1* EV vs. Δ*ath1* Sod1^{A4V} (increased) (Figure 8, 9 A). The functions of each vacuole KO library strain that showed significant differences in fold change values compared to the WT in YPD supplemented with 100 µM FK506 (see described above) were described in Figure 9 B.

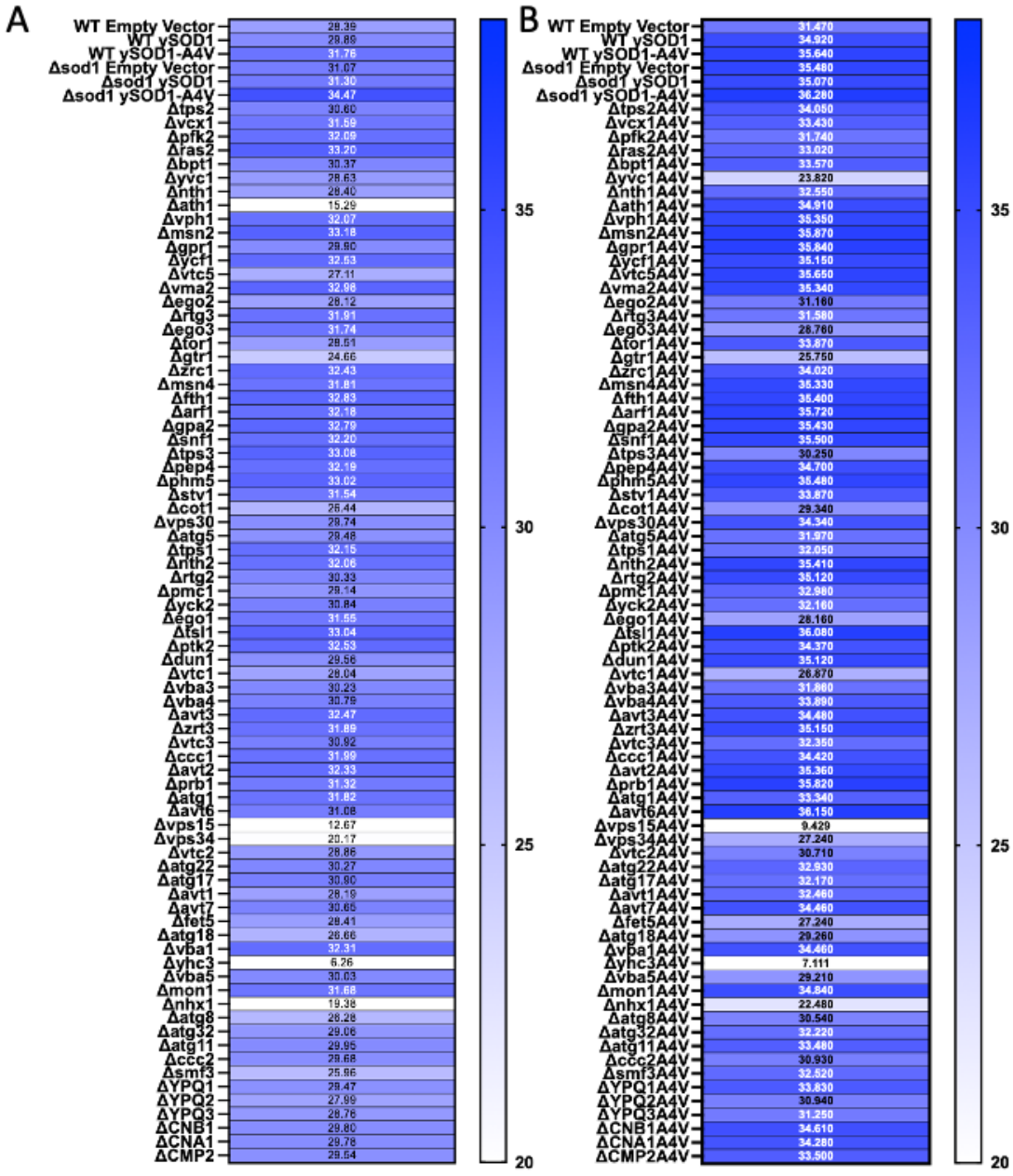
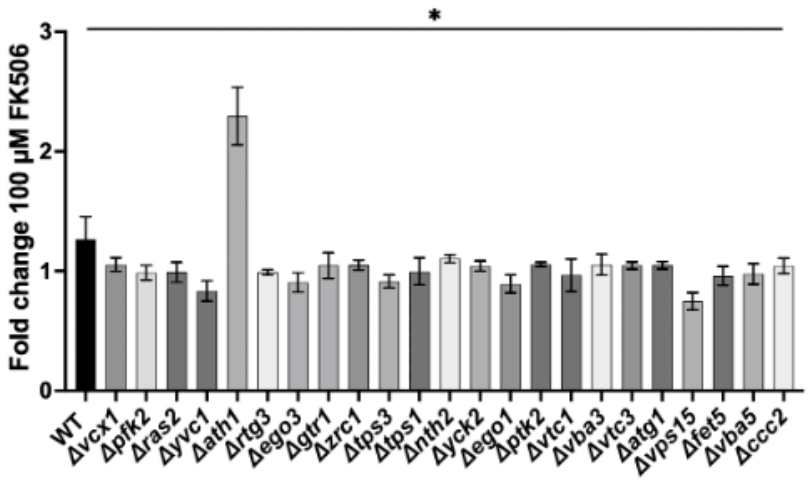


Figure 8 Potential synthetic interactions between expression of mutant Sod1^{A4V} and different gene deletions involved in metabolic functions of the vacuole in S. cerevisiae.
A) and B) Heatmaps generated from AUC values obtained from growth screen of the vacuole knockout library in YPD media supplemented with 100 µM FK506.
Knockouts expressing pAG306 EV (A) or pAG306 Sod1^{A4V} (B). The AUC data was displayed as a blue gradient as shown in the key whereby the highest value set was 38 units and the lowest value set was 20 units. Values outside the set values are coloured white. The heatmaps represent the average of three biological repeats.

A



B

Strain	Fold change	Function
Δvcx1	Decreased 1.05	Vacuolar membrane antiporter with Ca2+/H+ and K+/H+ exchange
Δpfk2	Decreased 0.98	Beta subunit of heterooctameric phosphofructokinase; involved in glycolysis; indispensable for anaerobic growth
Δras2	Decreased 0.99	GTP-binding protein; regulates nitrogen starvation response, sporulation, and filamentous growth; farnesylation and palmitoylation required for activity and localization to plasma membrane; activated by increased levels of glycolysis intermediate fructose-1,6-bisphosphate
Δyvc1	Decreased 0.83	Vacuolar cation channel; mediates release of Ca(2+) from the vacuole in response to hyperosmotic shock
Δrtg3	Decreased 0.99	bHLH/Zip transcription factor for retrograde (RTG) and TOR pathways
Δego3	Decreased 0.90	Subunit of EGO/GSE complex; vacuolar/endosomal membrane-associated EGO/GSE complex regulates exit from rapamycin-induced growth arrest, stimulating microautophagy and sorting of Gap1p from endosome to plasma membrane; essential for integrity and function of EGO; targeted to vacuole via AP-3 pathway; gene exhibits synthetic genetic interaction with MSS4
Δgtr1	Decreased 1.04	Subunit of TORC1-stimulating GTPase and EGO/GSE complex; subunit of Gtr1-Gtr2 GTPase that activates TORC1 in response to amino acid stimulation; subunit of EGO/GSE vacuolar membrane complex that regulates exit from rapamycin-induced growth arrest and sorting of Gap1p
Δzrc1	Decreased 1.04	Vacuolar membrane zinc transporter
Δtps3	Decreased 0.91	Regulatory subunit of trehalose-6-phosphate synthase/phosphatase
Δtps1	Decreased 0.99	Synthase subunit of trehalose-6-P synthase/phosphatase complex
Δnth2	Decreased 1.12	Putative neutral trehalase, required for thermotolerance
Δyck2	Decreased 1.04	Palmitoylated plasma membrane-bound casein kinase I
Δego1	Decreased 0.89	Subunit of EGO/GSE complex; vacuolar/endosomal membrane-associated EGO/GSE complex regulates exit from rapamycin-induced growth arrest, stimulating microautophagy and sorting of Gap1p from endosome to plasma membrane
Δptk2	Decreased 1.05	Serine/threonine protein kinase; involved in regulation of ion transport across plasma membrane
Δvtc1	Decreased 0.96	Regulatory subunit of vacuolar transporter chaperone (VTC) complex; VTC complex is involved in membrane trafficking, vacuolar polyphosphate accumulation, microautophagy and non-autophagic vacuolar fusion
Δvba3	Decreased 1.05	Permease of basic amino acids in the vacuolar membrane
Δvct3	Decreased 1.04	Regulatory subunit of vacuolar transporter chaperone (VTC) complex; involved in membrane trafficking, vacuolar polyphosphate accumulation, microautophagy and non-autophagic vacuolar fusion
Δatg1	Decreased 1.04	Protein serine/threonine kinase; required for vesicle formation in autophagy and the cytoplasm-to-vacuole targeting (Cvt) pathway; structurally required for phagophore assembly site formation; forms a complex with Atg13p and Atg17p during autophagy
Δvps15	Decreased 0.74	Serine/threonine protein kinase involved in vacuolar protein sorting; functions as a membrane-associated complex with Vps34p; active form recruits Vps34p to the Golgi membrane
Δfet5	Decreased 0.96	Multicopper oxidase
Δvba5	Decreased 0.97	Plasma membrane protein of the Major Facilitator Superfamily; involved in amino acid uptake and drug sensitivity
Δccc2	Decreased 1.04	Cu(+2)-transporting P-type ATPase
Δath1	Increased 2.29	Acid trehalase involved in intracellular trehalose degradation during growth recovery after saline stress

Figure 9 Potential synthetic interactions between expression of mutant Sod1^{A4V} and different gene deletions involved in metabolic functions of the vacuole in S. cerevisiae.
A)) Fold change comparison of growth of strains expressing the Sod1^{A4V} mutation versus the same strain containing an empty control vector when grown in YPD media supplemented with 100 µM FK506. The graphs show the foldchange of strains containing the Sod1^{A4V} mutations vs. strains lacking the Sod1^{A4V} mutation. The fold changes were compared to the WT empty vector vs WT Sod1^{A4V} fold change. The error bars represent the standard deviation. A One-Way ANOVA using a Tukey multiple comparison test was used to determine statistical significance. (*) flags levels of significance compared to the WT/A4V, $p < 0.05$.
The graphs represent three biological repeats.
B) List of KO strains and their gene function showing significant fold changes compared to the WT fold change under 100 µM FK506.

Gene ontology analysis using the *Saccharomyces* genome database SLIM Mapper function term analysis revealed: kinases (Atg1, Pfk26, Ptk2, Vps15, Yck2) and phosphatases (Tps1, Tps3) within the FK506 synthetic interaction hits. Transmembrane activity was also present as a GO term within the deletion strains tested (Ccc2, Vba3, Vcx1, Yvc1, Zrc1), with two hits being known calcium transporters (Yvc1 and Vcx1) as was the synthesis of trehalose (Figure 10).

GO Terms from the molecular function Ontology		
GO Term (GO ID)	**Genes Annotated to the GO Term**	**GO Term Usage in Gene List**
kinase activity (GO:0016301)	ATG1, PFK26, PTK2, VPS15, YCK2	5 of 22 genes, 22.73%
transmembrane transporter activity (GO:0022857)	CCC2, VBA3, VCX1, YVC1, ZRC1	5 of 22 genes, 22.73%
ion binding (GO:0043167)	CCC2, RAS2, ZRC1	3 of 22 genes, 13.64%
phosphatase activity (GO:0016791)	TPS1, TPS3	2 of 22 genes, 9.09%
hydrolase activity, acting on glycosyl bonds (GO:0016798)	ATH1, NTH2	2 of 22 genes, 9.09%
GTPase activity (GO:0003924)	GTR1, RAS2	2 of 22 genes, 9.09%
glycosyltransferase activity (GO:0016757)	TPS1, TPS3	2 of 22 genes, 9.09%
mRNA binding (GO:0003729)	VTC1	1 of 22 genes, 4.55%
enzyme regulator activity (GO:0030234)	TPS3	1 of 22 genes, 4.55%
transcription factor binding (GO:0008134)	RTG3	1 of 22 genes, 4.55%
oxidoreductase activity (GO:0016491)	FET5	1 of 22 genes, 4.55%
DNA binding (GO:0003677)	RTG3	1 of 22 genes, 4.55%
ubiquitin-like protein binding (GO:0032182)	VPS15	1 of 22 genes, 4.55%
DNA-binding transcription factor activity (GO:0003700)	RTG3	1 of 22 genes, 4.55%

Figure 10 Gene ontology analysis of hit gene set obtained for FK506.
The Gene Ontology Slim Term Mapper was used to obtain the functions and processes in which the gene hits obtained from Fold change comparison of growth of strains expressing the Sod1^{A4V} mutation versus the same strain containing an empty control vector when grown in YPD media supplemented with 100 µM FK506 (Figure 9).
https://www.yeastgenome.org/goSlimMapper

4.3.6 Assessment of effects of Sod1^{A4V} expression in vacuole KO library under 4 mM Zinc stress

Zinc stress was the last stress condition we sought to follow up based on preliminary findings presented from previous work by Dr Kevin Doyle (Doyle, 2022).

Generally lower AUC values for all vacuole KO library strains could be observed in the 4 mM $ZnCl_2$ screen (Figure 11 A, B) compared to the YPD (Figure 4), 50 mM $CaCl_2$ (Figure 6), and 100 µM FK506 screen (Figure 8). This suggests that 4 mM represents a significant stress to *S. cerevisiae* cells. Fold change analysis of vacuole KO library strains grown in YPD medium supplemented with 4 mM $ZnCl_2$ revealed significant differences compared to the fold

change of WT EV/ Sod1^{A4V} in following vacuole KO library strains: Δ*ath1* EV vs. Δ*ath1* Sod1^{A4V} (increased) (Figure 12 A). Only the fold change of Δ*ath1* EV vs Δ*ath1* Sod1^{A4V} showed significant differences compared to the WT EV in YPD supplemented with 4 mM $ZnCl_2$. Ath1 is an acid trehalase involved in intracellular trehalose degradation during growth recovery after saline stress (Figure 12 B).

The functions of each vacuole KO library strain that showed significant differences in fold change values compared to the WT EV in YPD supplemented with 4 mM $ZnCl_2$ (see described above) were described in Figure 12 B.

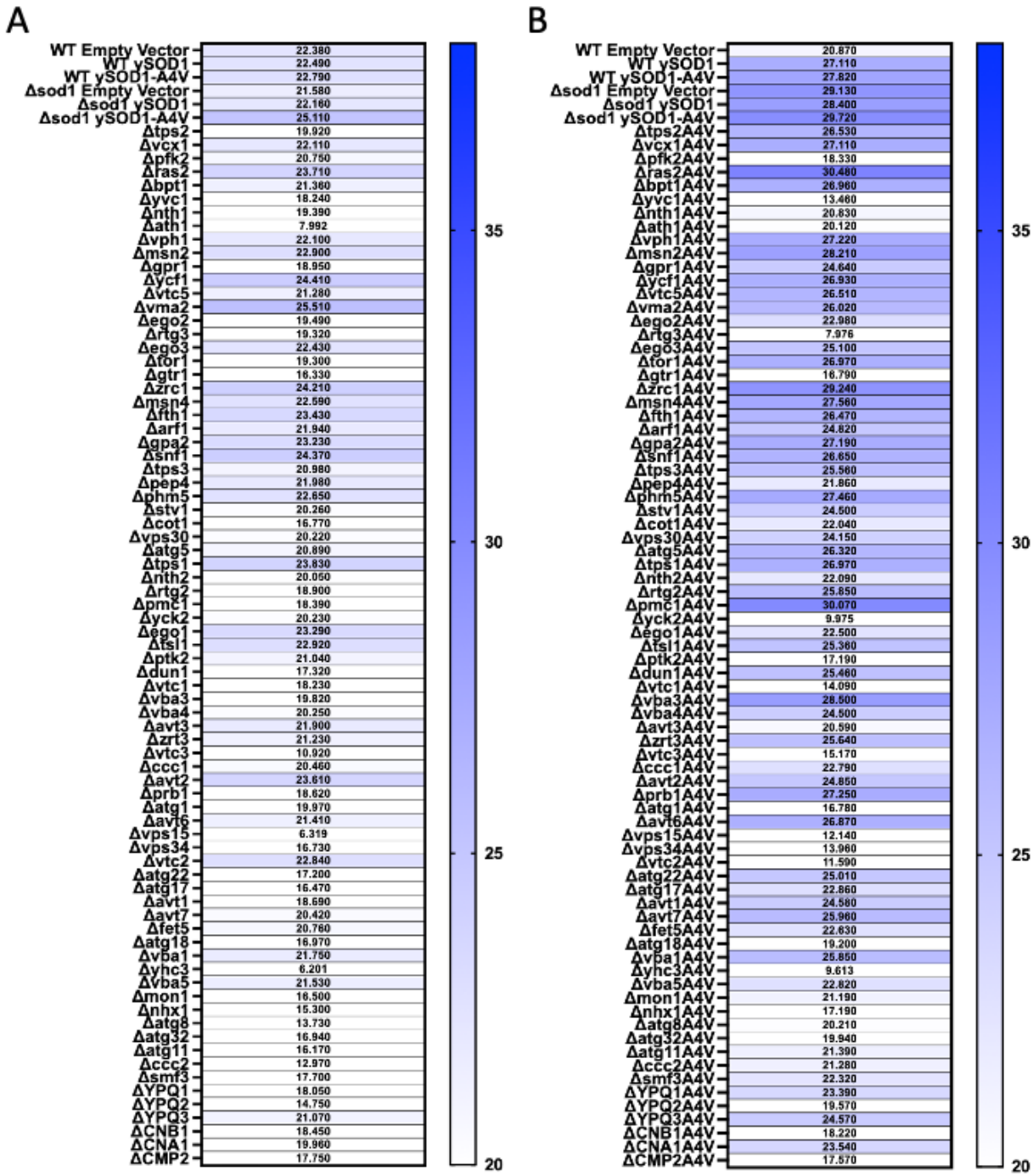
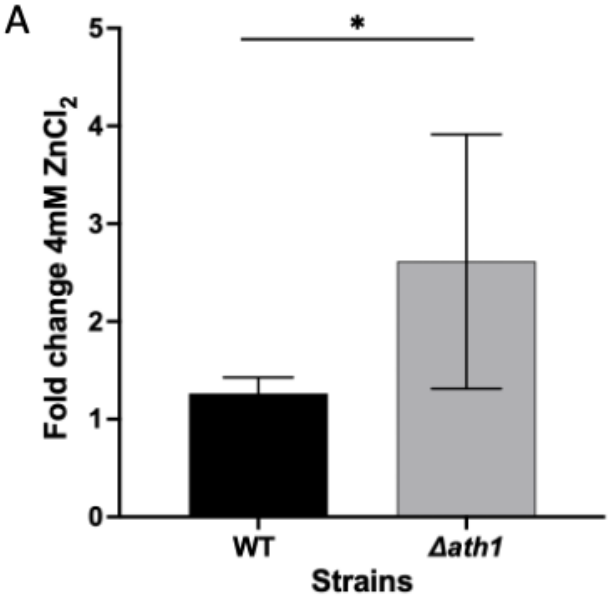


Figure 11 Potential synthetic interactions between expression of mutant Sod1^{A4V} and different gene deletions involved in metabolic functions of the vacuole in S. cerevisiae.
A, B) Fold change comparison of growth of strains expressing the Sod1^{A4V} mutation versus the same strain containing an empty control vector when grown in YPD media supplemented with 4 mM $ZnCl_2$. Knockouts expressing pAG306 EV (A) or pAG306 Sod1^{A4V} (B). The AUC data was displayed as a blue gradient as shown in the key whereby the highest value set was 38 units and the lowest value set was 20 units. Values outside the set values are coloured white. The heatmaps represent the average of three biological repeats.

A



B

Strain	Fold change	Function
Δath1	Increased 2.61	Acid trehalase involved in intracellular trehalose degradation during growth recovery after saline stress

Figure 12 Potential synthetic interactions between expression of mutant Sod1^{A4V} and different gene deletions involved in metabolic functions of the vacuole in S. cerevisiae.
A) Fold change comparison of growth of strains expressing the Sod1^{A4V} mutation versus the same strain containing an empty control vector when grown in YPD media supplemented with 4 mM $ZnCl_2$. The graphs show the foldchange of strains containing the Sod1^{A4V} mutations vs. strains lacking the Sod1^{A4V} mutation. The fold changes were compared to the WT empty vector vs WT Sod1^{A4V} fold change. The error bars represent the standard deviation. A One-Way ANOVA using a Tukey multiple comparison test was used to determine statistical significance. (*) flags levels of significance compared to the WT/A4V, $p < 0.05$.
The graph represents three biological repeats.
B) List of KO strains and their gene function showing significant fold changes compared to the WT fold change under 4 mM $ZnCl_2$.

4.3.7 Summary of reproducible potential synthetic interactions between Sod1^{A4V} and vacuole KO strains in YPD media and under 50 mM Calcium, calcineurin inhibition, and 4 mM Zinc stress

To identify whether there was any common vacuole KO deletion strain present in the four growth conditions used to conduct the screens; YPD, 50 mM $CaCl_2$, and 100 µM FK506 a Venn diagram was generated (Figure 13).

There were no common gene deletions showing reduced fold change values compared to the WT EV (Figure 13) between data sets generated to assess Sod1^{A4V} toxicity in YPD media (Figure 5) or YPD containing 50 mM $CaCl_2$ (Figure 7), or 100 µM FK506 (Figure 9). One gene deletion showing reduced fold change values compared to the WT could be found in YPD and 50 mM $CaCl_2$: Δ*nhx1* EV vs. Δ*nhx1* Sod1^{A4V}. Three common gene deletions showing reduced fold change values compared to the WT were identified in YPD and 100 µM FK506: Δ*ego1* EV vs. Δ*ego1* Sod1^{A4V}, Δ*vtc1* EV vs. Δ*vtc1* Sod1^{A4V}, Δ*vba5* EV vs. Δ*vba5* Sod1^{A4V}. Two gene deletions showing reduced fold change values compared to the WT were found between 50 mM $CaCl_2$ and 100 µM FK506: Δ*ras2* EV vs. Δ*ras2* Sod1^{A4V}, Δ*yvc1* EV vs. Δ*yvc1* Sod1^{A4V} (Figure 13).

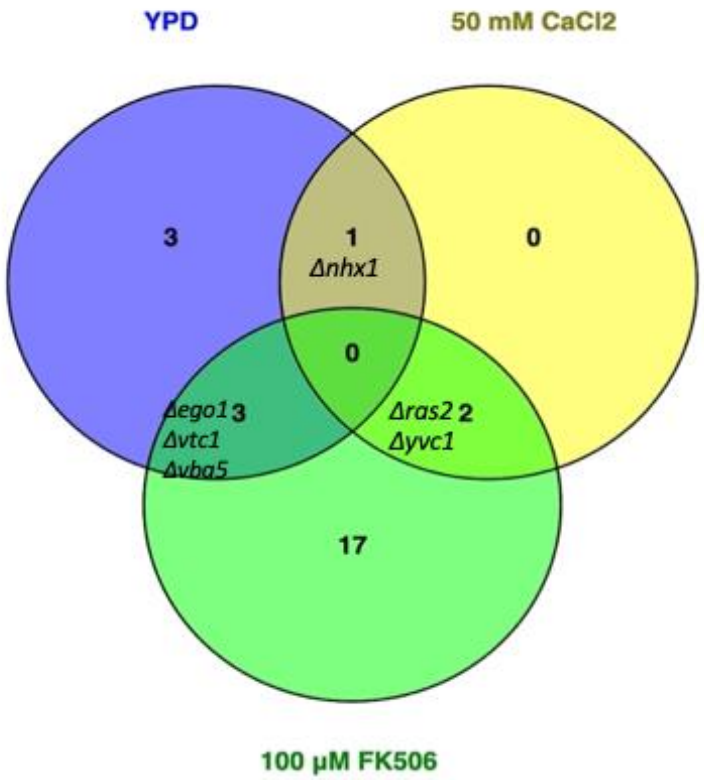


Figure 13 Venn diagram showing overlapping vacuole KO library strains of reduced fold change values compared to the WT between YPD, 50 mM $CaCl_2$, 100 µM FK506, and 4 mM $ZnCl_2$ conditions tested (Figures 5, 7, 9).
Oliveros, J.C. (2007-2015) Venny. An interactive tool for comparing lists with Venn's diagrams. https://bioinfogp.cnb.csic.es/tools/venny/index.html

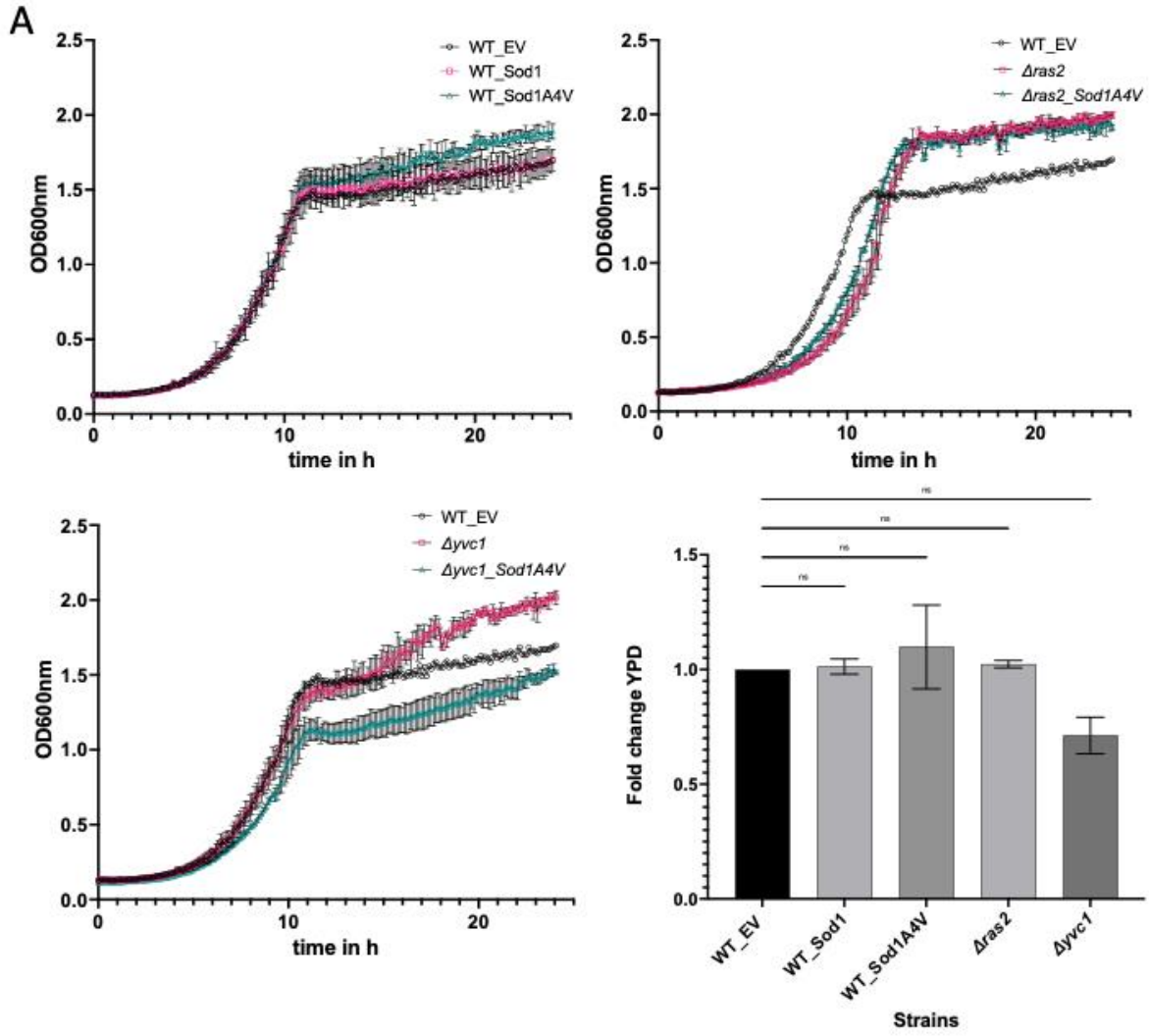
4.3.8 Sod1 and Sod1^{A4V} regulation of calcium response

The results from the vacuole knockout library screen described above suggested that the loss of *RAS2* or *YVC1* leads to an increase in toxicity when expressing Sod1^{A4V} when cells are grown under conditions of calcium stress or Cn inhibition. The screen itself relied on a transfer of cells from liquid to liquid without normalisation of cell number for practical reasons. We therefore sought to verify the effects of loss of *RAS2* or *YVC1* by repeating growth assays in a carefully controlled manner and at a higher concentration of 100 mM $CaCl_2$. Our rationale was that the elevated calcium stress level would return a larger difference in growth that would be useful for subsequent experiments.

In YPD medium, no significant difference in growth could be observed in WT EV, WT Sod1 and WT Sod1^{A4V}, whilst a slight increase in final OD_{600} could be observed for Δ*ras2* EV and Δ*ras2* Sod1^{A4V} compared to the WT EV control. Additionally, there was a slight increase in final OD_{600} in Δ*yvc1* EV and reduction in growth in Δ*yvc1* Sod1^{A4V} compared to the WT EV control (Figure 14 A). However, fold change analysis of Δ*ras2* EV vs. Δ*ras2* Sod1^{A4V} and Δ*yvc1* EV vs. Δ*yvc1* Sod1^{A4V} revealed no significant differences to WT EV vs. WT Sod1^{A4V} in YPD media (Figure 14 A).

In YPD media supplemented with 100 mM $CaCl_2$, a longer lag phase in WT Sod1^{A4V} compared to the WT EV control could be observed. Furthermore, when exposed to 100 mM $CaCl_2$, Δ*ras2* EV showed a significant extended lag phase and very little growth compared to

the WT EV control, whilst Δ*ras2* Sod1^{A4V} was not able to grow at all (Figure 14 B). Δ*yvc1* Sod1^{A4V} also showed an increased lag phase and a significantly reduced final OD_{600} compared to the WT EV control (Figure 14 B). Significantly reduced fold changes compared to the WT EV vs. WT Sod1^{A4V} could be observed in WT Sod1 vs. WT Sod1^{A4V}, Δ*ras2* EV vs. Δ*ras2* Sod1^{A4V}, and Δ*yvc1* EV vs. Δ*yvc1* Sod1^{A4V} (Figure 14 B). These experiments confirm the results of the larger screen.



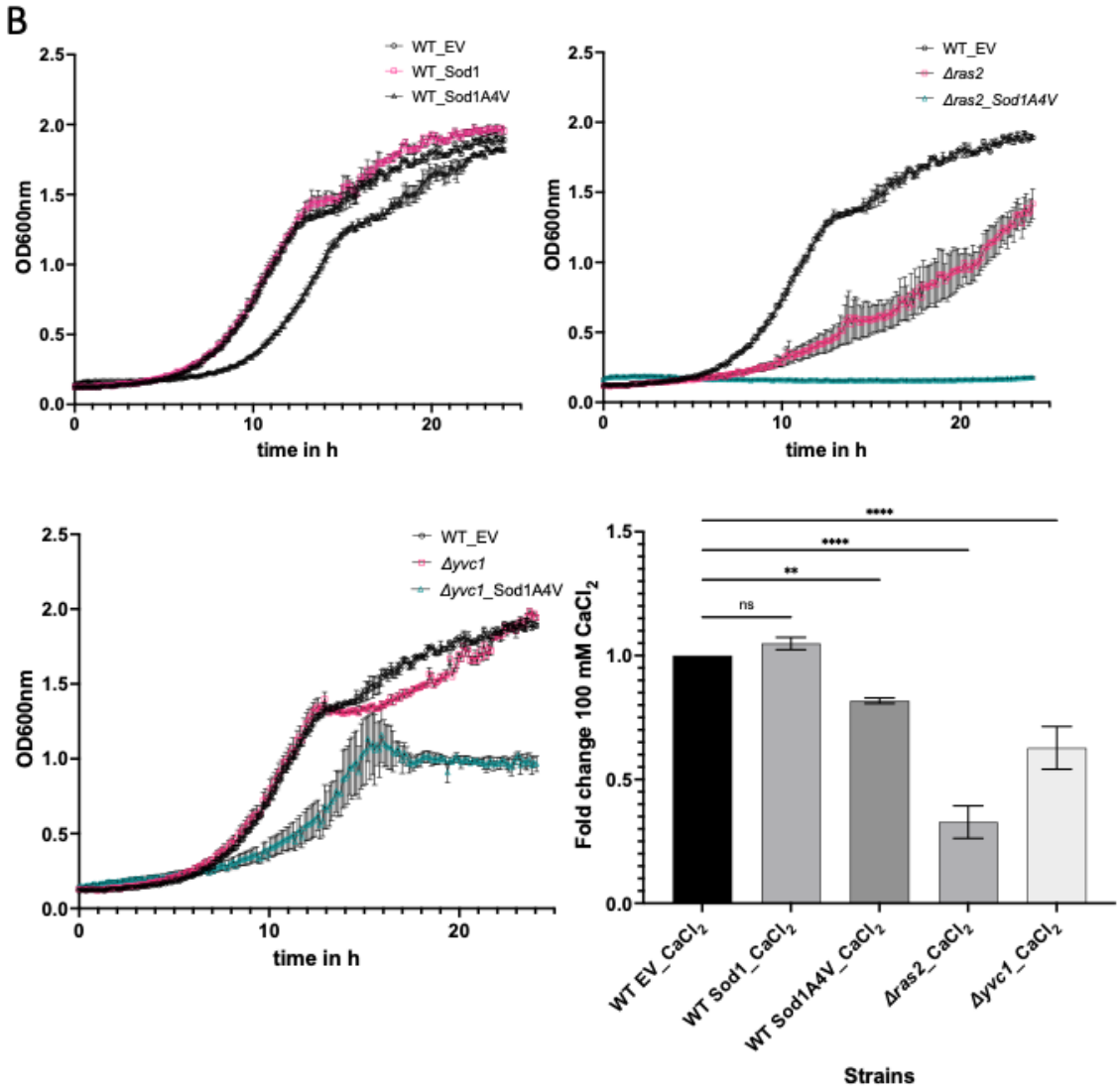


Figure 14 24 h Growth curve analysis of vacuole KO hits.
A) 24 h Growth curves of WT Sod1, WT Sod1^{A4V}, Δras2, Δras2 Sod1^{A4V}, Δyvc1, Δyvc1 Sod1^{A4V}. Fold change comparison of strains containing the Sod1^{A4V} mutation and strains lacking the Sod1^{A4V} mutation grown in YPD media.
B) Growth curves of WT Sod1, WT Sod1^{A4V}, Δras2, Δras2 Sod1^{A4V}, Δyvc1, Δyvc1 Sod1^{A4V}.Fold change comparison of strains containing the Sod1^{A4V} mutation and strains lacking the Sod1^{A4V} mutation grown in YPD media supplemented with 100 mM $CaCl_2$.
The graphs show the Fold change of three biological repeats of strains containing the Sod1^{A4V} mutations vs. strains lacking the Sod1^{A4V} mutation. The fold changes were compared to the WT empty vector vs WT Sod1^{A4V} fold change. The error bars represent the standard deviation. A One-Way ANOVA using a Tukey multiple comparison test was used to determine statistical significance. (*) flags levels of significance compared to the WT EV vs. WT Sod1^{A4V}, $p < 0.05$.

Given our findings that butyrate could reduce the effects of Sod1 mutant expression in *C. elegans* and cultured neuroblastoma cells we sought to investigate its effects at a

concentration that is not anti-fungal. Specifically, we investigated whether butyrate addition at 1 mM could rescue the effect of calcium toxicity in cells expressing Sod1^{A4V}.

In YPD media supplemented with 1 mM NaB and 100 mM $CaCl_2$, no changes in growth curve profiles could be observed in WT Sod1, and WT Sod1^{A4V} compared to the WT EV (Figure 15 A). The previously slightly increased lag phase observed in WT Sod1^{A4V} compared to the WT EV when 100 mM $CaCl_2$ was present (Figure 14 B) could be rescued when the WT Sod1^{A4V} was grown in 100 mM $CaCl_2$ along with 1 mM NaB (Figure 15 A).

In the presence of 100 mM $CaCl_2$ along with 1 mM NaB, partial growth rescue of Δ*ras2* Sod1^{A4V} and Δ*yvc1* Sod1^{A4V} could be observed (Figure 15 A): as described previously in Figure 14 B, 100 mM $CaCl_2$ could prevent growth of Δ*ras2* Sod1^{A4V} and significantly reduced growth of Δ*ras2* EV. In the presence of 1 mM NaB and 100 mM $CaCl_2$ Δ*ras2* Sod1^{A4V} showed growth again having almost an identical growth curve profile as Δ*ras2* EV. Interestingly, the growth curve profile of Δ*ras2* EV when grown in the presence of 100 mM $CaCl_2$ and 1 mM NaB compared to the growth curve profile in the presence of 100 mM $CaCl_2$ only, did not change (Figures 14 B, 15 A).

In the presence of 100 mM $CaCl_2$ Δ*yvc1* Sod1^{A4V} showed a significantly increased lag phase and reduced growth (Figure 14 B). However, when grown in 100 mM $CaCl_2$ along with 1 mM NaB this could also be partially rescued (Figure 15 A).

In the presence of 100 mM $CaCl_2$ and 1 mM NaB, no significantly changed fold changes compared to the fold change of WT EV vs. WT Sod1^{A4V} could be observed in WT EV vs. WT Sod1, WT Sod1 vs. WT Sod1^{A4V}, and Δ*yvc1* EV vs. Δ*yvc1* Sod1^{A4V} (Figure 15 B). There was a significant reduction in fold change in Δ*ras2* EV vs. Δ*ras2* Sod1^{A4V} compared to the fold change of WT EV vs. WT Sod1^{A4V} (Figure 15 B).

To examine whether the effects of NaB had an effect on viability a colony forming unit efficiency (CFU) analysis was conducted. Here, WT EV, WT Sod1, WT Sod1^{A4V}, Δ*ras2* EV*,* Δ*ras2* Sod1^{A4V}*,* Δ*yvc1* EV and Δ*yvc1* Sod1^{A4V} were exposed to 100 mM $CaCl_2$ for 4 h prior to another 4 h of NaB incubation at either 1 mM or 100 mM concentration. There was no significant difference in CFUs in the WT EV controls under YPD and 100 mM $CaCl_2$ exposure (Figure 15 C). A slight, but significant, change in CFU efficiency compared to the WT EV was observed for Δ*ras2* Sod1^{A4V} (~ 93 %) without any calcium or NaB exposure. Significantly reduced CFUs were observed for WT Sod1^{A4V} (~ 86 %), Δ*ras2* EV (~ 80 %)*,* and Δ*ras2* Sod1^{A4V} (~ 52 %) compared to the WT EV after 4 h of 100 mM $CaCl_2$ exposure (Figure 15 C). A 4 h exposure to 1 mM NaB after the 4 h 100 mM $CaCl_2$ incubation resulted in a 20 % reduction of CFUs in the WT EV (~ 65 %) compared to the YPD WT EV control (~ 100 %). Additionally, WT Sod1 (~ 45 %), WT Sod1^{A4V} (~ 47 %), Δ*ras2* EV (~ 37 %)*,* and Δ*ras2* Sod1^{A4V} (~ 36 %) showed severely decreased CFUs compared to the 1 mM NaB treated WT EV control (~ 65 %). Interestingly, whilst 1 mM NaB showed partial growth rescue in the Δ*ras2* Sod1^{A4V} strain, CFU efficiency was significantly reduced but not more than in the 1 mM NaB-treated Δ*ras2* EV strain (Figure 15 C). 100 mM NaB treatment resulted in even further CFU reduction as expected as this concentration has antifungal activity. Here, WT EV showed a CFU of 13 %, WT Sod1 12 %, WT Sod1^{A4V} 12 %, Δ*ras2* EV 10 %, and Δ*ras2* Sod1^{A4V} 9 % (Figure 15 C).

There were no significant changes in CFUs in Δ*yvc1* EV and Δ*yvc1* Sod1^{A4V} compared to the WT EV in YPD media. 4 h 100 mM $CaCl_2$ incubation resulted in reduced CFUs in WT Sod1^{A4V} (~ 86 %), Δ*yvc1* EV (~ 61 %) and Δ*yvc1* Sod1^{A4V} (~ 45 %) compared to the WT EV control (~ 95 %). A 4 h exposure to 1 mM NaB after the 4 h 100 mM $CaCl_2$ incubation resulted in a reduction of CFUs in WT EV (~ 65 %), WT Sod1 (~ 45 %), WT Sod1^{A4V} (~ 47 %), Δ*yvc1* EV (~ 32

%) and Δ*yvc1* Sod1^{A4V} (~ 36 %). 100 mM NaB treatment resulted in even further CFU reduction: WT EV (~ 13 %), WT Sod1 (~ 12 %), WT Sod1^{A4V} (~ 12 %), Δ*yvc1* EV (~ 15 %) and Δ*yvc1* Sod1^{A4V} (~ 5 %) (Figure 15 C).

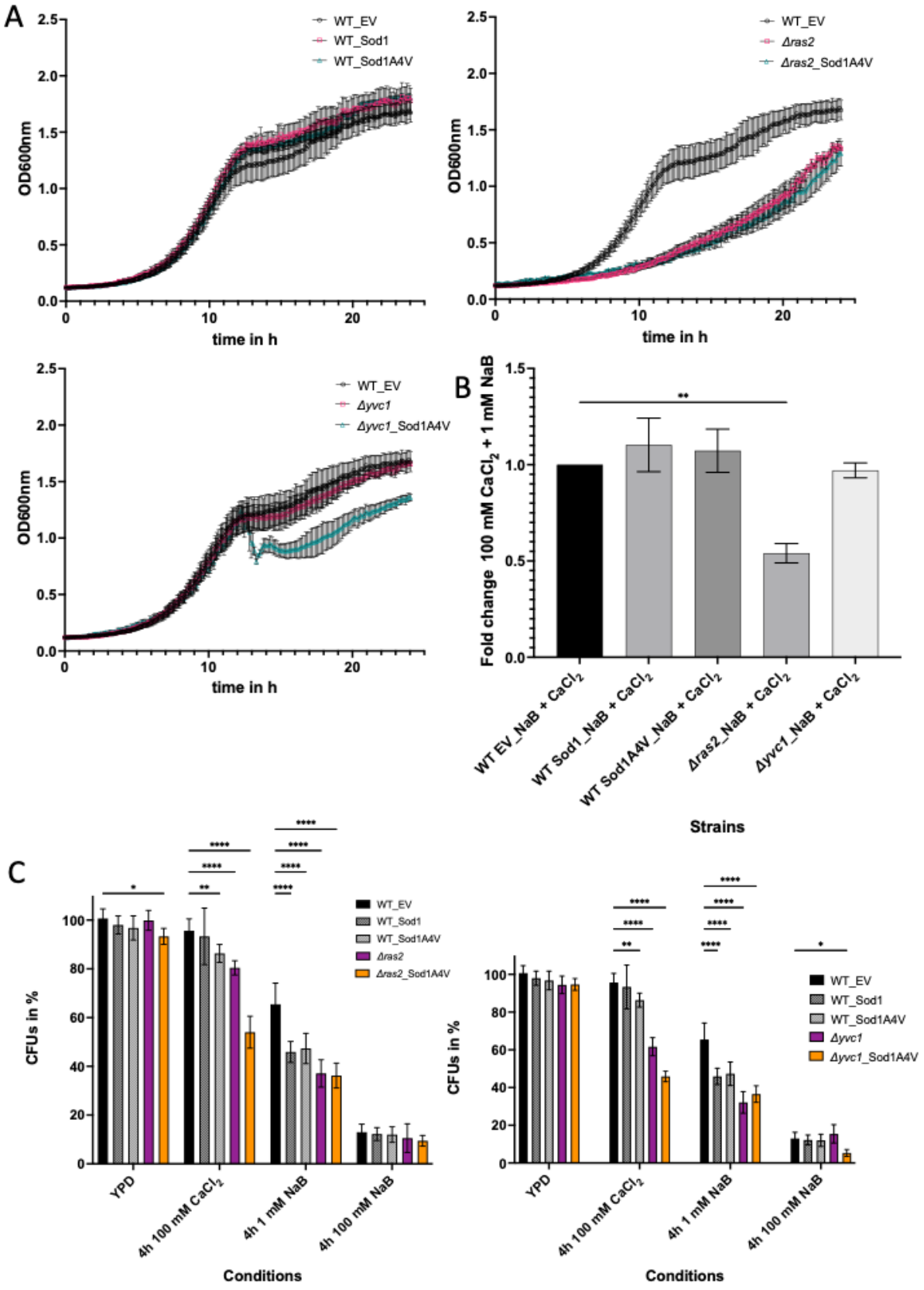

A
WT_EV
WT_Sod1
WT_Sod1A4V
OD600nm
time in h
WT_EV
Δras2
Δras2_Sod1A4V
OD600nm
time in h
WT_EV
Δyvc1
Δyvc1_Sod1A4V
OD600nm
time in h
B
Fold change 100 mM CaCl2 + 1 mM NaB
WT EV_NaB + CaCl2
WT Sod1_NaB + CaCl2
WT Sod1A4V_NaB + CaCl2
Δras2_NaB + CaCl2
Δyvc1_NaB + CaCl2
Strains
C
CFUs in %
WT_EV
WT_Sod1
WT_Sod1A4V
Δras2
Δras2_Sod1A4V
YPD
4h 100 mM CaCl2
4h 1 mM NaB
4h 100 mM NaB
Conditions
CFUs in %
WT_EV
WT_Sod1
WT_Sod1A4V
Δyvc1
Δyvc1_Sod1A4V
YPD
4h 100 mM CaCl2
4h 1 mM NaB
4h 100 mM NaB
Conditions

Figure 15 Effect of non-antifungal butyrate concentration on calcium toxicity in cells expressing Sod1^{A4V}.
A)24 h growth curves of WT EV, WT Sod1, WT Sod1^{A4V}, Δras2, Δras2 Sod1^{A4V}, Δyvc1, and Δyvc1 Sod1^{A4V} in YPD media supplemented with 1 mM NaB and 100 mM $CaCl_2$.
B) Fold change analysis of WT Sod1, WT Sod1^{A4V}, Δras2, Δras2 Sod1^{A4V}, Δyvc1, Δyvc1 Sod1^{A4V} comparing strains containing the Sod1^{A4V} mutation and strains lacking the Sod1^{A4V} mutation grown in YPD media supplemented with 1 mM NaB and 100 mM $CaCl_2$.
C) CFU analysis of Δras2, Δras2 Sod1^{A4V}, Δyvc1, and Δyvc1 Sod1^{A4V} after 100 mM $CaCl_2$ exposure prior 4 h of either 1 mM or 100 mM NaB treatment.
The data shown represents an average of three biological repeats. The error bars represent the standard deviation. A One-Way ANOVA using a Tukey multiple comparison test was used to determine statistical significance, $p < 0.05$.

4.3.9 Sod1^{A4V}-induced calcium toxicity is not linked to cell death in Δ*ras2* and Δ*yvc1*

Sod1^{A4V}-induced calcium toxicity was observed in growth curve and CFU analysis above in Δ*ras2* EV and Δ*yvc1* EV (Figure 15). We therefore sought to investigate whether calcium toxicity was linked to cell death or ROS accumulation through flow cytometry analysis. Here, high ROS levels, a common indicator of cell death in *S. cerevisiae* cells, were assessed by fluorescence output of the indicator dye H_2DCF-DA, and co-staining of cells with the propidium iodide (PI) was used to assess necrosis. The CGY638 (Δ*cox4*) mutant strain was used as positive ROS signal control (Leadsham *et al.*, 2013), and a heat-killed culture sample was used as a positive PI control. Measurement events were gated on the flow cytometer to ensure that singlet yeast cells were being recorded (Figure 16 A). The analysis revealed that there was no significant change in median FITC values in WT EV, Δ*ras2* EV, Δ*ras2* Sod1^{A4V} compared to the ROS and PI controls and compared to the WT EV under stress-free and 100 mM $CaCl_2$ stress conditions (Figure 16 B). This could also be visualised well in the flow cytometry profiles which show no necrosis or high ROS accumulation in WT EV, Δ*ras2* EV,

Δ*ras2* Sod1^{A4V}. There was only a very small population (10 %) of Δ*ras2* Sod1^{A4V} showing necrosis and high ROS (Figure 16 C). This suggests that the calcium toxicity observed in Figure 15 above is not linked to cell death when *RAS2* is deleted and SOD1^{A4V} present.

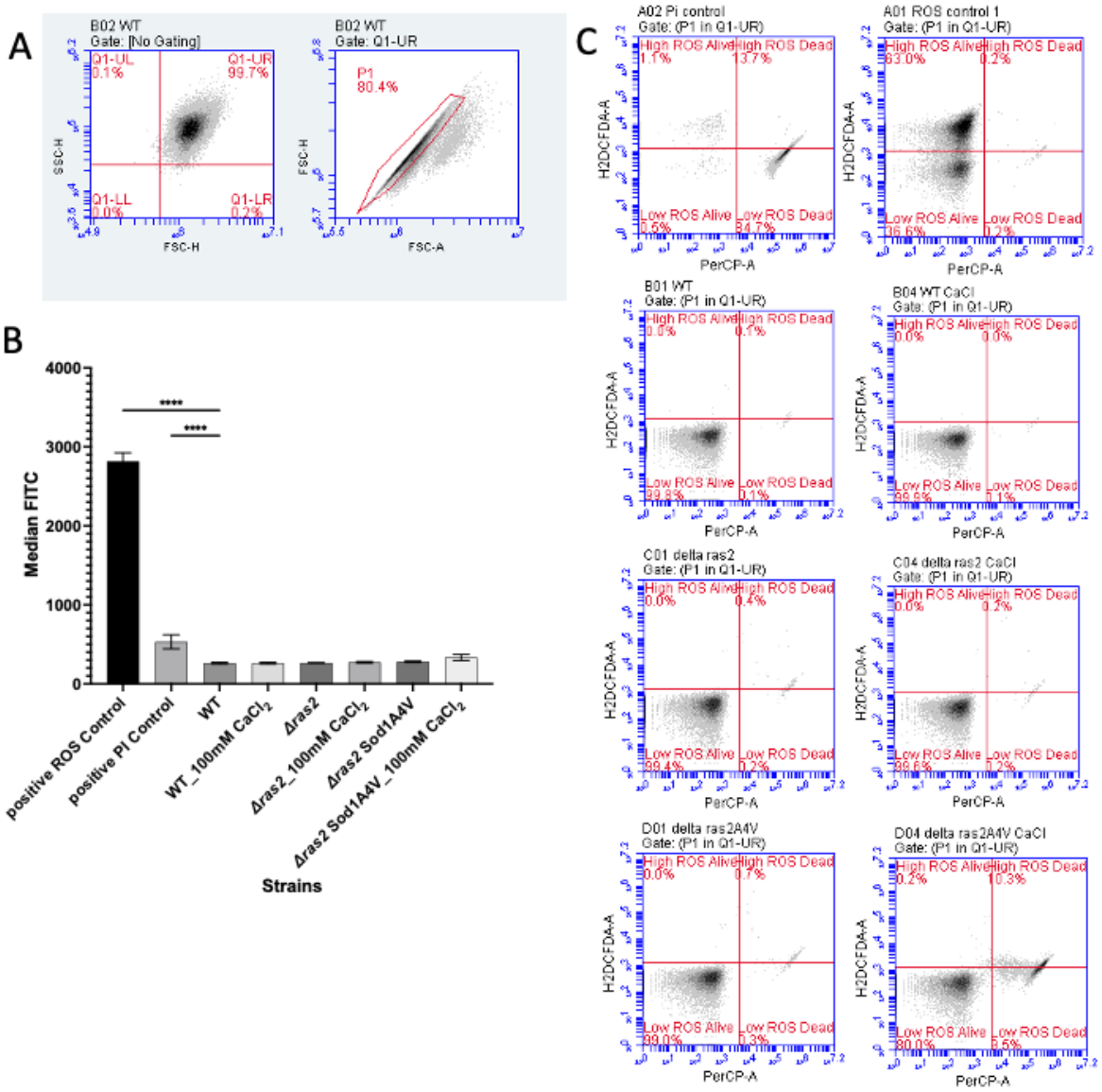


Figure 16 Flow cytometry analysis measuring ROS in cells lacking RAS2 in the presence or absence of $SOD1^{A4V}$ under 100 mM $CaCl_2$ addition.
A) showing gating used to select "singlet" cells rather than "doublets" or clumps of cells. On the X-axis PerCP-A indicates viability or cell death (PI stain), and the Y-axis was labelled H2DCFDA-A to detect ROS accumulation. A quadrant analysis was used to determine cells that contained either or both H2DCF-DA or PI signal.
B) Median FITC values of WT, Δras2, and Δras2 $Sod1^{A4V}$ with or without 100 mM $CaCl_2$ stress, the error bars represent the standard deviation. A One-Way ANOVA using a Tukey multiple comparison test was used to determine statistical significance, $p < 0.05$.
C) H2DCFDA and PerCP-A graphs of WT, Δras2, and Δras2 $Sod1^{A4V}$ with or without 100 mM $CaCl_2$ stress
The data shown represents an average of three biological repeats.

Whether Sod1^{A4V}-induced calcium toxicity was linked to cell death or ROS accumulation in Δ*yvc1* EV was also investigated via flow cytometry analysis revealing that there was no significant change in median FITC values in WT EV, Δ*yvc1* EV, Δ*yvc1* Sod1^{A4V} compared to the ROS and PI controls and compared to the WT EV under stress-free and 100 mM $CaCl_2$ stress conditions (Figure 17 A, B).

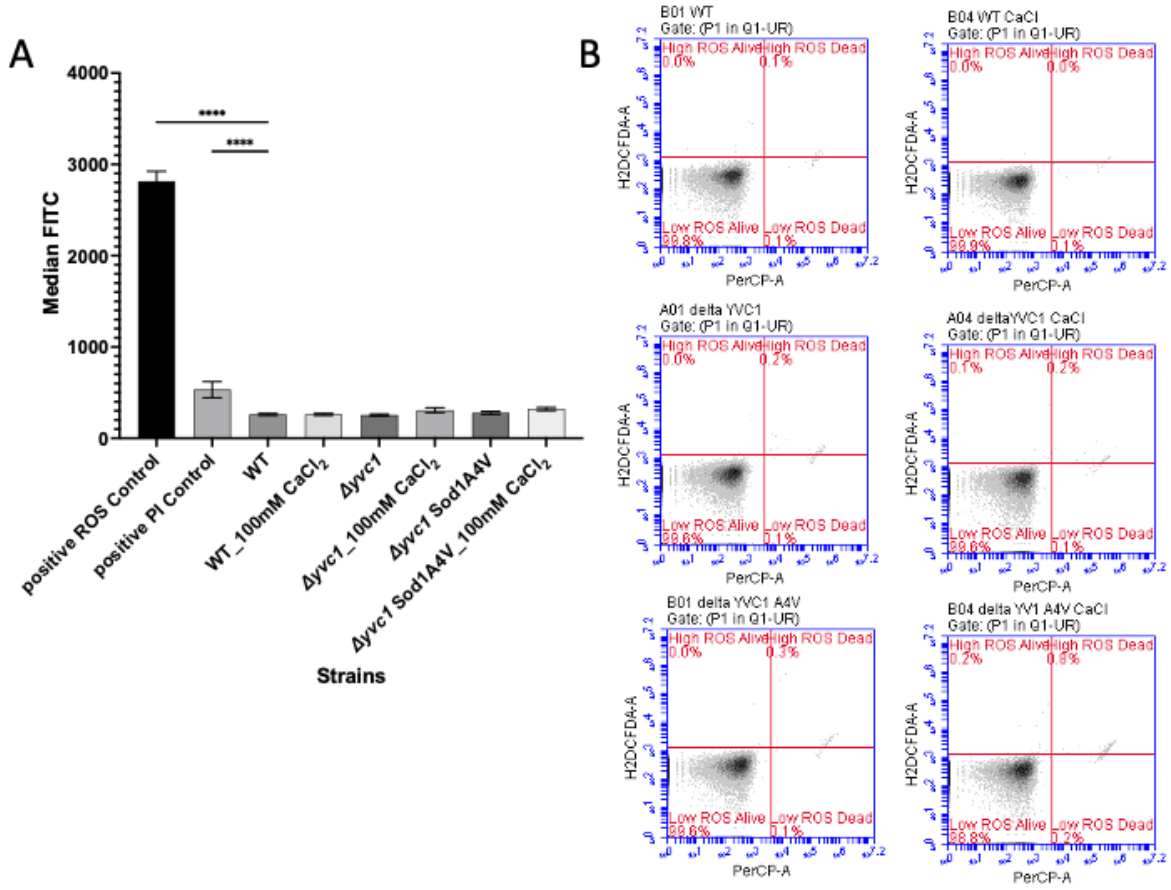


Figure 17 Flow cytometry analysis measuring ROS in cells lacking YVC1 in the presence or absence of SOD1^{A4V} under 100 mM $CaCl_2$ addition.
A) Quantification of median FITC values detecting ROS or non-viable cells in WT, Δyvc1, and Δyvc1 Sod1^{A4V} with or without 100 mM $CaCl_2$ stress. The data shown represents an average of three biological repeats. The error bars represent the standard deviation. A One-Way ANOVA using a Tukey multiple comparison test was used to determine statistical significance, $p < 0.05$.
B) A quadrant analysis was used to determine cells that contained either or both H2DCF-DA or PI signal, where PerCP-A indicates viability or cell death (PI stain), and H2DCFDA-A to indicates ROS accumulation.

4.3.10 Sod1^{A4V} expression induces calcium flux imbalance

To investigate whether Sod1^{A4V} induced intracellular calcium imbalance, we sought to measure intracellular calcium dynamics, utilising the calcium-sensitive aequorin system. Aequorin, a calcium-binding photoprotein, comprises an apoprotein and the luciferin molecule coelenterazine in the presence of oxygen. Upon calcium binding, aequorin undergoes a conformational change, converting coelenterazine into excited coelenteramide and carbon dioxide. As coelenteramide returns to its ground state, it emits blue light, which we detected using a luminometer at a wavelength of 469 nm (Mithöfer and Mazars, 2002) (Figure 18). Each deletion strain carried either an empty vector (EV) or the Sod1^{A4V} mutation integrated into the genome of the wild type *S. cerevisiae* strain. To investigate intracellular calcium responses under different conditions (e.g. no substrate, 5 µM coelenterazine (substrate), 100 mM $CaCl_2$), calcium curves were generated.

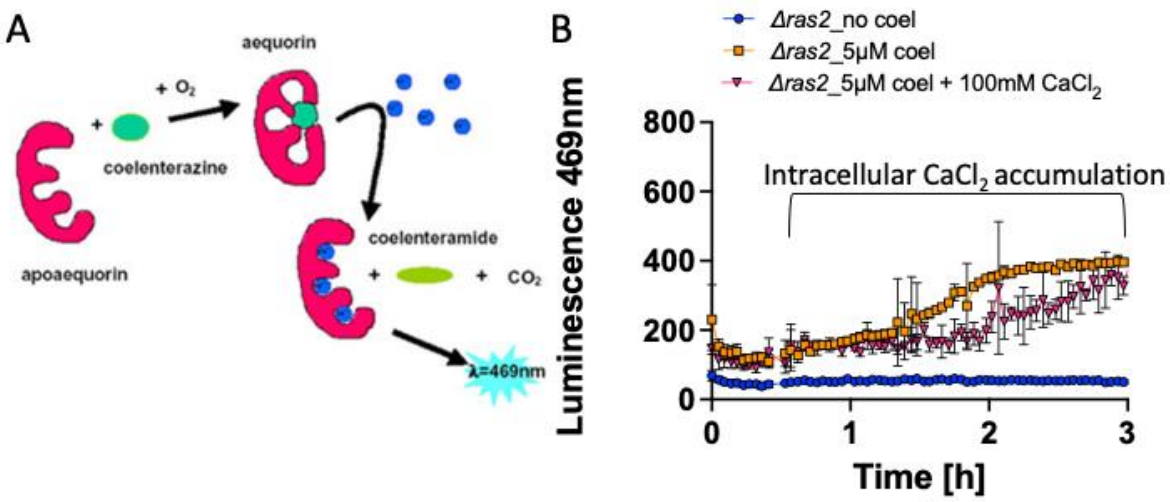


Figure 18 Graphical representation of the mechanism of light emission by aequorin upon calcium binding. A) Graphical representation of the mechanism of light emission by aequorin upon calcium binding. Image by (Mithöfer and Mazars, 2002).
B) Annotated graph of aequorin luminescence showing the intracellular calcium accumulation. Calcium accumulations were calculated as AUCs after the addition of 100 mM $CaCl_2$ starting at time point 0.57 h.

In the WT EV strain, the no substrate baseline appeared lower than the 5 µM coelenterazine (substrate) control. Subsequent comparisons of stress conditions were made relative to the substrate control, which represents the basal intracellular calcium level under assay conditions. Basal intracellular calcium levels in the WT EV remained consistently low throughout the assay period (Figure 19 A).

The addition of 100 mM $CaCl_2$ triggered a rapid increase in intracellular calcium, with levels peaking shortly after stress treatment and gradually returning to substrate/basal calcium levels within approximately 1 h (Figure 19 A). This pattern suggests a transient calcium influx followed by restoration of cytosolic calcium homeostasis (Figure 19 A).

Expression of $Sod1^{A4V}$ in the WT background appeared to lead to loss of calcium responses to 100 mM $CaCl_2$ addition (Figure 19 B) and to lower basal calcium levels compared to EV-expressing WT cells. Overall, the luminescence profiles suggest that expression of $Sod1^{A4V}$ in the WT background alteres intracellular calcium responses to calcium stress.

In Δ*ras2* EV cells, the no substrate baseline appeared lower than the 5 µM coelenterazine (substrate) control (Figure 19 A). However, the substrate control displayed a gradual increase in intracellular calcium levels over time, rather than a stable baseline. The upward trend resembled a sigmoidal pattern, suggesting a progressive accumulation of intracellular calcium during the assay under non-stressed conditions (Figure 19 A). Following the addition of 100 mM $CaCl_2$, intracellular calcium accumulation appeared elevated with a pattern similar to that observed in the substrate control (Figure 19 A). Thus, the calcium stress did not produce a clearly distinct transient response above the existing increase observed under basal conditions.

Expression of Sod1^{A4V} in the Δ*ras2* strain resulted in a lower no substrate baseline compared to the substrate control (Figure 19 B). Similar to Δ*ras2* EV cells, Δ*ras2* Sod1^{A4V} cells exhibited a gradual increase in intracellular calcium levels under basal conditions (substrate control). In this case, the increase appeared more linear over time, suggesting a steady accumulation of intracellular calcium throughout the assay in the absence of additional stress (Figure 19 B). Following the addition of 100 mM $CaCl_2$, intracellular calcium levels in Δ*ras2* Sod1^{A4V} cells followed a similar trend to the substrate control, with no clearly distinct transient response above the elevated basal levels (Figure 19 B).

Comparison of the Δ*ras2* EV and Δ*ras2* Sod1^{A4V} profiles showed that the Sod1^{A4V}-expressing cells displayed higher basal calcium levels and a more sustained increase in intracellular calcium following the addition of 100 mM $CaCl_2$. These profiles suggest that the expression of Sod1^{A4V} in the absence of *RAS2* is associated with altered calcium dynamics.

When comparing WT EV with Δ*ras2* EV cells, the luminescence profiles under no-substrate conditions appeared similar. However, the Δ*ras2* EV cells displayed a gradual increase in intracellular calcium under substrate conditions and following the additions of 100 mM $CaCl_2$, in contrast to the transient response observed in WT EV cells (Figure 19 A).

Visual inspection of the luminescence profiles showed that in WT EV cells, calcium levels remained low under basal conditions, and the calcium stress triggered a transient peak that returned to basal levels within about 1 h. In contrast, Δ*ras2* EV cells showed a sigmoidal increase in calcium levels under basal conditions and a similar, sustained pattern following $CaCl_2$ addition, rather than a transient response (Figure 19 A).

Lastly, comparison of WT Sod1^{A4V} and Δ*ras2* Sod1^{A4V} strains appeared to show higher basal calcium levels and higher calcium accumulations after 100 mM $CaCl_2$ treatment in Sod1^{A4V}-

expressing Δ*ras2* strain, indicating that the absence of *RAS2* further exacerbated calcium dysregulation in the presence of the Sod1^{A4V} mutation.

In the Δ*yvc1* EV strain, the no substrate baseline appeared lower than the 5 µM coelenterazine (substrate) control. Basal intracellular calcium levels in the Δ*yvc1* EV strain remained relatively low throughout the assay. The addition of 100 mM $CaCl_2$ triggered a rapid increase in intracellular calcium, with levels peaking shortly after stress treatment and gradually returning to basal levels after about 1 h (Figure 19 A). This pattern suggests a transient calcium influx followed by restoration of cytosolic calcium homeostasis.

In the Δ*yvc1* Sod1^{A4V} strain, the no substrate baseline also appeared lower than the 5 µM coelenterazine (substrate) control. Basal intracellular calcium levels in the Δ*yvc1* Sod1^{A4V} strain remained relatively low throughout the assay. The addition of 100 mM $CaCl_2$ triggered a rapid increase in intracellular calcium, with levels peaking shortly after stress treatment and gradually returning to basal levels after about 1 h (Figure 19 B). This profile similarly suggests a transient calcium influx followed by recovery towards basal levels.

Comparison of Δ*yvc1* EV and Δ*yvc1* Sod1^{A4V} cells showed broadly similar calcium profiles in the absence and presence of calcium stress. When comparing WT EV with Δ*yvc1* EV cells, the profiles under no-substrate and substrate conditions appeared broadly similar, although the rise in intracellular calcium following calcium stress appeared slightly less pronounced in the Δ*yvc1* EV strain compared to the WT EV (Figure 19 A).

Lastly, comparison of WT Sod1^{A4V} and Δ*yvc1* Sod1^{A4V} strain showed broadly similar basal calcium profiles. However, intracellular calcium accumulation following the 100 mM $CaCl_2$ addition seemed more pronounced in Δ*yvc1* Sod1^{A4V} cells than in WT Sod1^{A4V} (Figure 19 B).

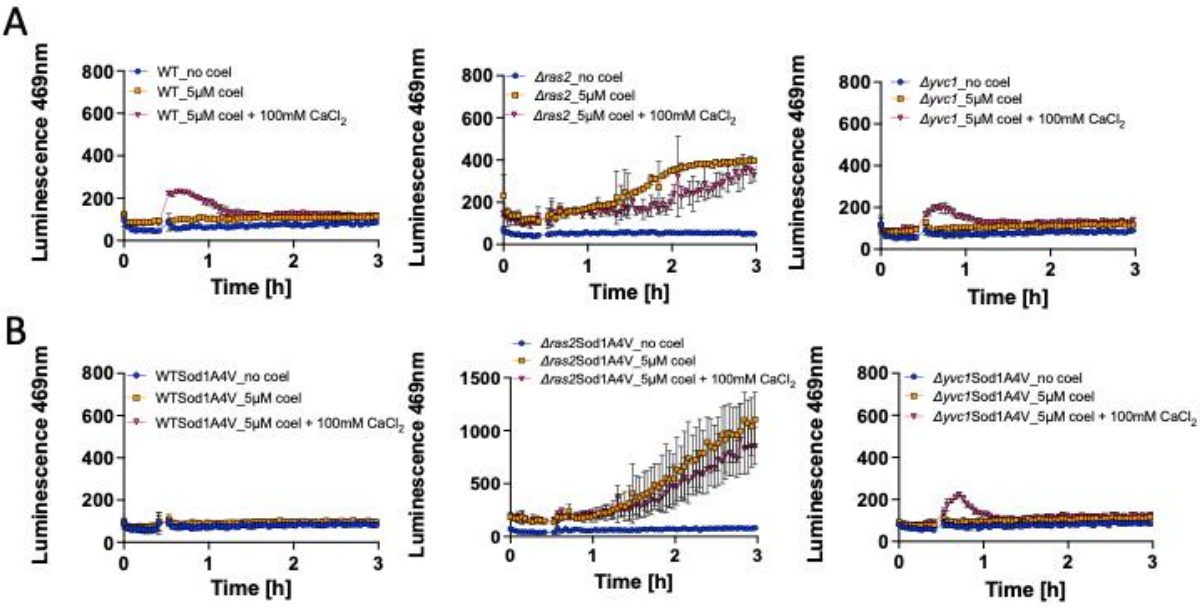


Figure 19 Effect of 100 mM $CaCl_2$ stress on calcium homeostasis in S. cerevisiae WT, Δras2, and Δyvc1 expressing the EV or Sod1^{A4V}.
Strains were grown in appropriate media to mid log phase. Log-phase cells were then re-suspended at a density of 10^8 cells/ml in fresh SD selective medium supplemented with 5 μM of the substrate Coelenterazine. After baseline readings were taken (about 30 min) 100 mM $CaCl_2$ was added . The data sets represent an average of three biological repeats. The error bars display the standard deviation.
A Two-Way ANOVA with post hoc tests: Tukey (within-strain comparisons); Sidak (WT vs. Δ) was used to determine statistical significance, $p < 0.05$ of AUCs.
A) Aequorin luminescence curve at 469 nm measuring intracellular calcium levels in EV-expressing S. cerevisiae WT, Δras2, and Δyvc1.
B) Aequorin luminescence curve at 469 nm measuring intracellular calcium levels in Sod1^{A4V}-expressing S. cerevisiae WT, Δras2, and Δyvc1.

Given that the expression of Sod1^{A4V} had clear effects on calcium regulation in WT, Δ*ras2* and Δ*yvc1* cells, we tested interactions between the Sod1^{A4V} mutation and intracellular calcium levels in more detail, focusing on the known calcium transporters and Cn regulators. Specifically, we tested deletion strains of Pmc1 (a vacuolar Ca^{2+} ATPase that removes Ca^{2+} from the cytosol), Pmr1 (a Ca^{2+} ATPase that transports Ca^{2+} into the Golgi), and Rcn2 (a Cn

regulator). Each deletion strain carried either an empty vector (EV) or the Sod1^{A4V} mutation integrated into the genome of the wild type *S. cerevisiae* strain.

In the Δ*pmc1* EV strain consistently low basal calcium levels under the substrate control were observed throughout the assay. The addition of 100 mM $CaCl_2$ triggered a rapid increase in intracellular calcium, with levels peaking shortly after stress treatment and gradually returning near-substrate/basal calcium levels within approximately 1 h (Figure 20 A).

In the Δ*pmc1* Sod1^{A4V} strain, basal calcium levels appeared elevated relative to the no substrate control but remained relatively low throughout the assay. The addition of 100 mM $CaCl_2$ triggered a rapid increase in intracellular calcium with levels returning to near-substrate levels a few minutes after stress treatment (Figure 20 A).

Comparison of the Δ*pmc1* EV and Δ*pmc1* Sod1^{A4V} profiles showed that basal calcium levels appeared higher in Δ*pmc1* Sod1^{A4V} cells, whereas the response to calcium stress appeared more pronounced in the Δ*pmc1* EV strain (Figure 20 A). Overall, the two strains displayed distinct calcium response profiles following the addition of 100 mM $CaCl_2$.

When comparing WT EV with Δ*pmc1* EV cells, basal calcium levels appeared higher in the WT EV cells. Following 100 mM $CaCl_2$ addition, the initial rise in intracellular calcium appeared more pronounced in Δ*pmc1* EV cells (Figures 19 A, 20 A). The luminescence profiles subsequently returned towards basal levels in both strains (Figures 19 A, 20 A).

Lastly, comparison of WT Sod1^{A4V} and Δ*pmc1* Sod1^{A4V} strains showed broadly similar basal calcium profiles. However, intracellular calcium accumulations after 100 mM $CaCl_2$ addition seemed more pronounced in the Δ*pmc1* Sod1^{A4V} than the WT Sod1^{A4V} (Figures 19 B, 20 A).

In the Δ*pmr1* EV strain, slightly elevated basal calcium levels were observed throughout the assay compared with the no-substrate control (Figure 20 B). Following 100 mM $CaCl_2$ addition, visual inspection of the luminescence profile revealed a rapid rise in intracellular calcium accumulation which returned to basal levels after about 1 h (Figure 20 B).

In the Δ*pmr1* $Sod1^{A4V}$ strain, slightly elevated basal calcium levels were also observed compared with the no-substrate control (Figure 20 B). Following 100 mM $CaCl_2$ addition, visual inspection of the luminescence profile revealed a slight rise in intracellular calcium accumulation which returned to basal levels after about 1 h (Figure 20 B).

Comparison of the Δ*pmr1* EV and Δ*pmr1* $Sod1^{A4V}$ profiles showed broadly similar basal calcium levels. However, the response to calcium stress appeared more pronounced in Δ*pmr1* EV (Figure 20 B).

When comparing WT EV with Δ*pmr1* EV, the basal calcium profiles appeared broadly similar. However, the response to calcium addition appeared more pronounced in the Δ*pmr1* EV (Figures 19 A, 20 B).

Lastly, comparison of WT $Sod1^{A4V}$ and Δ*pmr1* $Sod1^{A4V}$ showed broadly similar basal calcium levels(Figures 19 B, 20 B). However, visually Δ*pmr1* $Sod1^{A4V}$ appeared to have a slight response to calcium addition (Figures 19 B, 20 B).

In the Δ*rcn2* EV strain, consistently low basal (substrate control) calcium levels throughout the assay could be observed. The addition of 100 mM $CaCl_2$ triggered a rapid increase in intracellular calcium, with levels peaking shortly after stress treatment and gradually

returning to near substrate/basal calcium levels within a few minutes (Figure 20 C).

In Δ*rcn2* Sod1^{A4V} elevated basal calcium levels throughout the assay could be observed (Figure 20 C). Visual inspection of the luminescence profile of Δ*rcn2* Sod1^{A4V} showed that the addition of 100 mM $CaCl_2$ triggered a rapid increase in intracellular calcium with levels returning to substrate levels within a few minutes after stress treatment (Figure 20 C).

Comparing Δ*rcn2* EV and Δ*rcn2* Sod1^{A4V} Δ*rcn2* profiles showed that basal calcium levels appeared to be higher in Δ*rcn2* Sod1^{A4V}. However, following the 100 mM $CaCl_2$ treatment intracellular calcium accumulation appeared more pronounced in Δ*rcn2* EV (Figure 20 C).

When comparing WT EV and Δ*rcn2* EV, basal calcium levels appeared higher in the WT EV (Figures 19 A, 20 C). Following 100 mM $CaCl_2$ addition, the calcium response appeared broadly similar between the two strains, although calcium levels in the WT Ev strain appeared to take longer to return to basal levels (Figures 19 A, 20 C).

Lastly, comparison of WT Sod1^{A4V} and Δ*rcn2* Sod1^{A4V} showed higher basal calcium profiles in the Δ*rcn2* Sod1^{A4V} strain. Following the addition of 100 mM $CaCl_2$, the Δ*rcn2* Sod1^{A4V} strain also displayed a more pronounced increase in intracellular calcium compared to WT Sod1^{A4V} (Figure 20 B)

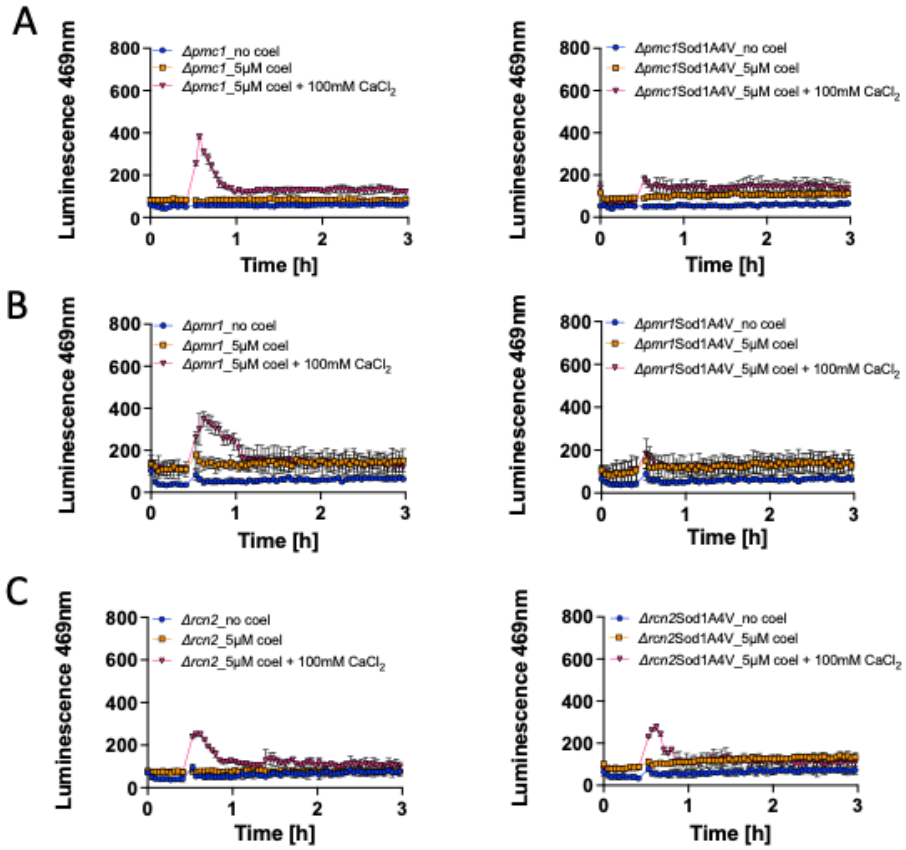


Figure 20 Effect of 100 mM $CaCl_2$ stress on calcium homeostasis in S. cerevisiae deletions of calcium transporters, Calcineurin (Cn) regulators, and Cn subunits.
Strains were grown in appropriate media to mid log phase. Log-phase cells were then re-suspended at a density of 10^8 cells/ml in fresh SD selective medium supplemented with 5 µM of the substrate Coelenterazine. 100 mM $CaCl_2$ were added after baseline readings were taken after about 30 min. The data sets represent an average of three biological repeats. The error bars display the standard deviation. A Two-Way ANOVA with post hoc tests: Tukey (within-strain comparisons); Sidak (WT vs. Δ) was used to determine statistical significance, $p < 0.05$ of AUCs.
A) Aequorin luminescence curve at 469 nm measuring intracellular calcium levels in Δpmc1 expressing either EV or $Sod1^{A4V}$.
B) Aequorin luminescence curve at 469 nm measuring intracellular calcium levels in Δpmr1 expressing either EV or $Sod1^{A4V}$.
C) Aequorin luminescence curve at 469 nm measuring intracellular calcium levels in Δrcn2 expressing either EV or $Sod1^{A4V}$.

Taken together, these results indicate that expression of $Sod1^{A4V}$ alters intracellular calcium regulation, although the effect varied depending on the genetic background. In WT cells, $Sod1^{A4V}$ expression was associated with reduced basal calcium levels and a loss of the transient calcium response following $CaCl_2$ addition, suggesting impaired calcium signalling. In contrast, $Sod1^{A4V}$ expression in the Δ*ras2* background was associated with elevated basal calcium levels and increased calcium accumulation following $CaCl_2$ exposure, indicating that

loss of *RAS2* further altered calcium regulation in the presence of Sod1^{A4V}. Deletion of *YVC1* did not significantly alter the calcium response to Sod1^{A4V}, although calcium accumulation following $CaCl_2$ addition remained higher in Δ*yvc1* Sod1^{A4V} compared with WT Sod1^{A4V} cells. Similarly, deletion of *PMC1* was associated with increased basal calcium levels in the presence of Sod1^{A4V}, whereas deletion of *PMR1* did not result in significant differences in calcium accumulation between EV and Sod1^{A4V}-expressing cells. In the Δ*rcn2* background, Sod1^{A4V} expression resulted in elevated basal calcium levels but did not increase calcium accumulation following $CaCl_2$ exposure. Overall, these findings suggest that Sod1^{A4V}-associated calcium dysregulation is influenced by the cellular mechanisms involved in calcium transport and regulation, with *RAS2* loss having the most pronounced effect on the calcium phenotype observed in this study.

4.3.11 The loss of Sod1 interacting proteins leads to the perturbation of Cn signalling

One possibility is that changes to Sod1 interactions leads to aberrant activity of one or more of its downstream targets and this in turn could lead to the loss of Cn signalling. Here we test this possibility by examining Cn activity in a number of strains lacking Sod1 effectors or signalling components. These include the loss of *SOD1*, *TOR1*, *AKR1*, *YCK1*, *YCK2*, *YPK1*, *YPK2*, *EGO3*, *YNO1*, and *YVC1*. Sod1 has been shown to regulate and stabilise the activity of the casein kinases Yck1 and Yck2. Yck1 and Yck2 are important mediators in glucose signalling and share redundant functions with each other. Akr1 encodes a palmitoyl transferase which prevents the palmitoylation of both Yck1 and Yck2 rendering them unable to function correctly as they will no longer be localised correctly to the plasma membrane (Feng and

Davis, 2000). Using Δ*akr1* essentially models a double deletion of *YCK1* and *YCK2*. In previous work Kevin Doyle reported a putative interaction between Sod1 and Ego3, which is part of the Ego complex that senses amino acid levels at the vacuole leading to the regulation of Tor1 signalling as a stop/signal for cell growth (Doyle, 2022). Sod1 has also been linked to the regulation of Tor signalling and its loss leads to perturbations in amino acid homeostasis (Tsang *et al.*, 2018). We therefore also measured Cn activity in cells lacking Ego3 or Tor1 as well as in strains lacking Ypk1 or Ypk2, kinases that have roles in regulation of TORC1 activity. Intracellular calcium release through the vacuole is regulated by the calcium channel Yvc1. As intracellular calcium levels affect calcineurin activation, we sought to include the mutant Δ*yvc1*.

To measure calcineurin activity a transcriptional GFP reporter plasmid was employed (Diessl *et al.*, 2020). It comprises of a GFP-tag that is C-terminally linked to a 4-fold repeat of the calcineurin-dependant response element (CDRE). The expression of CDRE is driven by the transcription factor Crz1 which becomes active upon dephosphorylation by calcineurin. Thus, increased calcineurin activity promotes the expression of 4×-CDRE-GFP. Using this reporter, calcineurin activity can be measured in live *S. cerevisiae* cells by flow cytometry.

The process for measuring calcineurin activity by flow cytometry using the 4×-CDRE-GFP reporter can be seen in Figure 21 A-C. The phosphatase activity of calcineurin is activated by calmodulin in a Ca^{2+} dependant manner. Treatment of the wild type (WT) cells with 50 mM $CaCl_2$ 1 h prior to measurement resulted in a 20- fold increase in calcineurin activity compared to the untreated control (Figure 21 D). The overlay plot shows the FITC-A value (log scale) of WT cells grown to mid-log phase, either treated with Ca^{2+} for 1 h prior to measurement or untreated. FITC-A described the GFP fluorescence detected via the FL1

detector which filters at 530/30. The addition of Ca^{2+} shifted the peak of FITC-A from between 10^2 and 10^3 to 10^4 indicating a large increase in fluorescence intensity of the 4×-CDRE-GFP reporter in response to calcium. The population of cells to be measured was gated by size, and then further gated to select the "singlet" population and avoid any "doublets" or clumps of cells. Using this method, the activity of calcineurin in response to calcium treatment was measured in WT and Δ*sod1* cells, and several deletion mutants representing the metabolic functions of the vacuole grown to mid-log phase.

Median FITC analysis revealed that without 50 mM $CaCl_2$ addition both WT and Δ*sod1* showed similar levels of median FITC of ~1000 units (Figure 21 E). However, upon addition of 50 mM $CaCl_2$ 1h prior to measurement, the median FITC value of WT was significantly higher at ~20,000 units than that of Δ*sod1* at ~3,800 units (Figure. 21 E). This suggests that calcineurin activity in response to calcium is reduced in cells lacking *SOD1*. Upon addition of 50 mM $CaCl_2$ 1 h prior to measurement, the median FITC value of Δ*tor1*, Δ*akr1*, Δ*yck1,* Δ*yck2*, and Δ*yno1* cells were significantly higher than their untreated cultures: Δ*tor1* CaCl ~6500, Δ*akr1* CaCl ~7500, Δ*yck1* CaCl ~20,000*,* Δ*yck2* CaCl ~20,000, Δ*yno1* CaCl ~10,000 units, and Δ*yvc1* CaCl ~ 16,000 units (Figure 21 E). There was no significant increase in the median FITC value upon calcium addition in Δ*ypk1*, Δ*ypk2*, and Δ*ego3* (Fig. 21 E).
The fold change increase in calcineurin activity in response to 50 mM $CaCl_2$ treatment was 22.6 for WT and ~3.6 for Δ*sod1* (Figure 21 E). The fold change increase in calcineurin activity in response to 50 mM $CaCl_2$ treatment for Δ*tor1,* Δ*akr1,* Δ*yck1,* Δ*yck2,* Δ*ypk1,* Δ*ypk2,* Δ*ego3,* Δ*yno1* included: Δ*tor1* (8.4), Δ*akr1* (8.3), Δ*yck1* (23.1)*,* Δ*yck2* (22.9)*,* Δ*ypk1* (0.9)*,* Δ*ego3* (0.9), Δ*ypk2* (1.06)*,* Δ*yno1* (6.6), and Δ*yvc1* (15.8) (Figure 21 E). These data demonstrate that impairment of process required for Sod1 activity (yno1 NADPH activity) or downstream

activity (Yck1/2 or akr1; Ego complex/Tor signalling) can lead to a loss of Cn signalling. These findings raise the possibility that Sod1 mutations may result in a range of signalling defects that feed in calcium signalling. This complexity will require further investigation within the context of Sod 1 mutations linked to ALS.

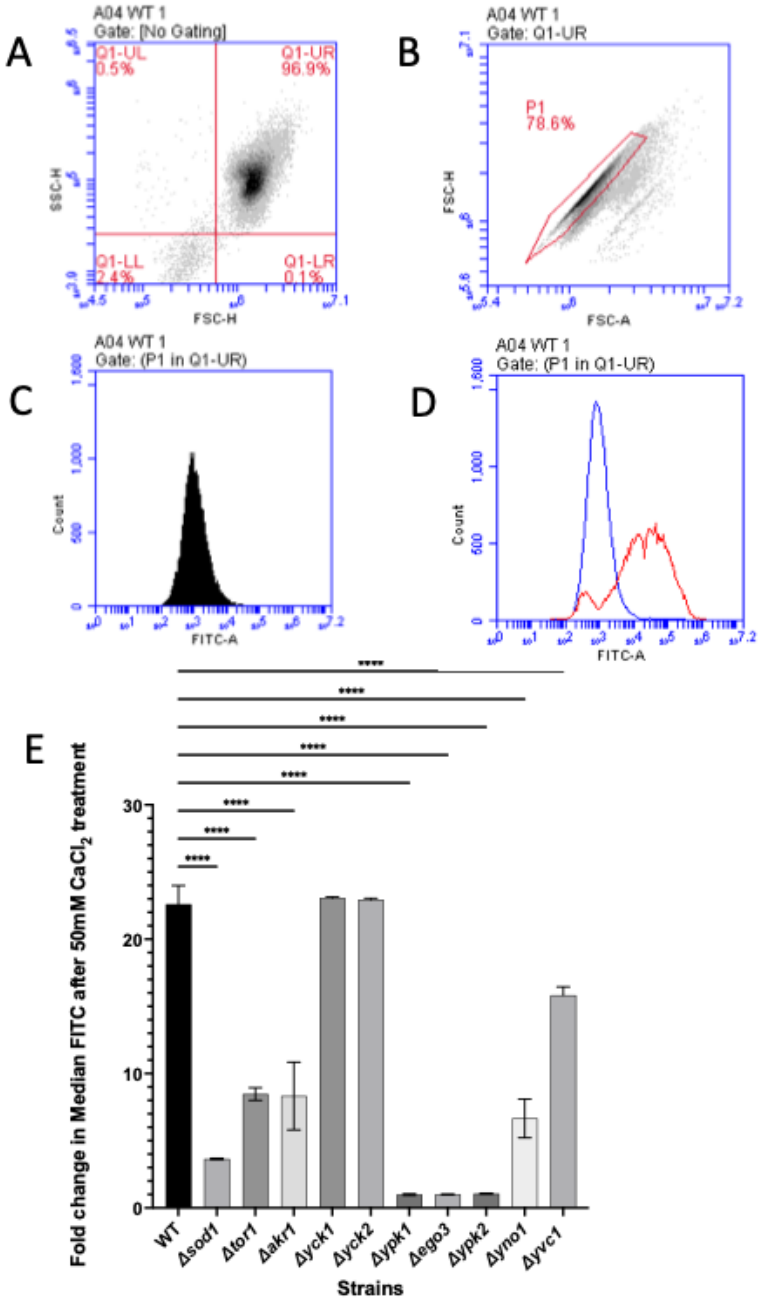


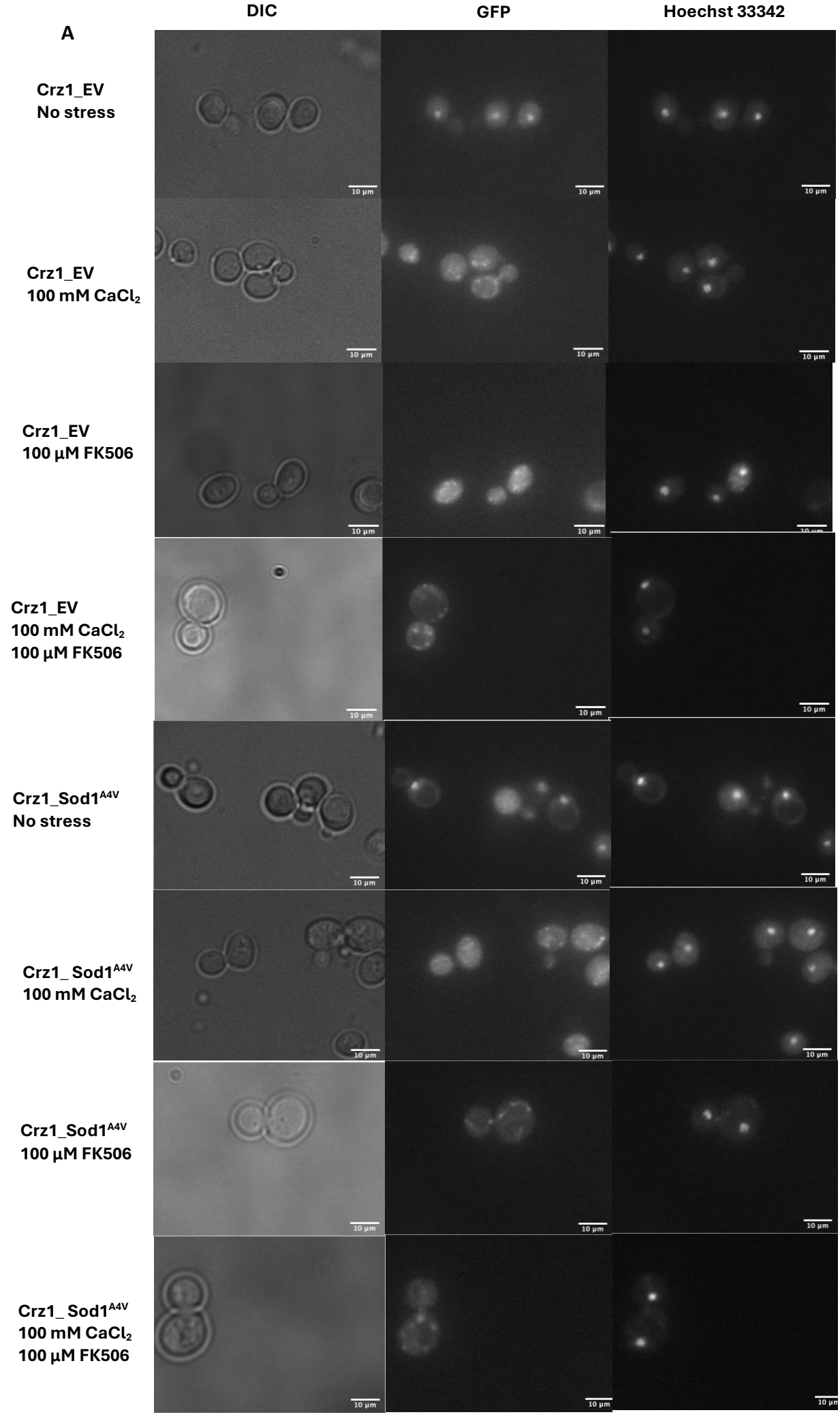
Figure 21 Potential synthetic interactions between Calcineurin and key regulatory proteins.
A-D) Flow cytometry of a transcriptional reporter for calcineurin activity of WT cells before and after 50 mM $CaCl_2$ treatment. Panels display the method of gating the cells for analysis of FITC fluorescence intensity by flow cytometry. A) has side-scatter height (SSC-H) on the y axis and forward-scatter height (FSC-H) on the x axis. Cells are in the upper right corner in the upper right quadrant. B) shows FSC-H on the y axis and forward-scatter area on the x axis (FSC-A). This plot allows to select 'singlet' cells, rather than "doublets" or clumps of cells. C) shows the count of cells on the y axis and the FITC-A reading of the gated 'singlet' cells from the middle plot. D) Displays an overlay plot of the FITC-A value of WT cells treated with Ca^{2+} (red) for 1 h prior to measurement or not (blue).
E) fold change in calcineurin activity after $CaCl_2$ + treatment in WT, Δsod1, Δtor1, Δego3, Δakr1, Δyck1, Δyck2, Δyno1, Δypk1, Δypk2 cells.
*The data shows the average of three biological repeats; each consists of three technical repeats. The error bars represent the standard deviation. A One-way ANOVA using a Tukey comparison test was used to determine statistical significance. Non-significant = NS, * = adjusted p-value ≤ 0.05, ** = adjusted p-value ≤ 0.01, **** = adjusted p-value ≤ 0.001.*

4.3.12 Sod1^{A4V}-induced Crz1 mislocalisation under calcium stress

The transcription factor Crz1 plays a crucial role in regulating the response to calcium signalling and stress adaptation within the cell. In actively budding cells, normal cytosolic calcium concentrations are held within 50-200 nM (Cui, Kaandorp, Sloot, *et al.*, 2009). When intracellular calcium concentrations rise, calmodulin – a calcium sensor protein- will bind to and activate the protein phosphatase Cn, which in turn will dephosphorylate Crz1 (Stathopoulos and Cyert, 1997). Crz1 will translocate from the cytosol to the nucleus binding to the calcineurin-dependent response element CDRE ultimately activating about 160 genes of e.g. calcium transporters involved in stress adaptation (Stathopoulos-Gerontides, Guo and Cyert, 1999; Yoshimoto *et al.*, 2002).

To see whether the lack of Cn response was due to Crz1 mislocalisation influenced by mutated Sod1^{A4V}, GFP-tagged Crz1 widefield microscopy was conducted. The pAG306 EV or pAG306 Sod1^{A4V} were integrated into a strain in which GFP had been fused to the genomic copy of Crz1. Cells were then grown to log phase in YPD medium following a 4 h incubation with 100 mM $CaCl_2$, and/or 100 µM FK506 Cn inhibitor. We observed that under no stress conditions stationary cells expressing the empty vector (EV) showed a split population in Crz1 localisation. Here, Crz1 GFP signal could be detected in the cytoplasm and the nucleus (Figure 22 A, B). Upon 100 mM $CaCl_2$ addition Crz1 localised into the nucleus and the mitochondria/ER or cytoplasmic foci. When Cn was inhibited most GFP signal was detected in the mitochondria/ER or cytoplasmic foci and only within the nucleus in a minority of cells (Figure 22 A, B). Under both, calcium addition and Cn inhibition, in wild type cells Crz1 was localised in the mitochondria/ER or foci with only few in the nucleus (Figure 22 A, B).

On the other hand, stationary cells expressing $Sod1^{A4V}$ without additional stress showed mostly a cytoplasmic/diffused Crz1 GFP signal (Figure 22 A, B). A third of the population of cells showed mitochondrial/foci Crz1 GFP localisation and only a very small population showed nuclear Crz1 GFP localisation had been observed in wild type cells (Figure 22 A, B). Under calcium stress, the majority of the Crz1 GFP signal could be detected either as a cytoplasmic/diffused signal or in the mitochondria/foci (Figure 22 A, B). A few cells showed nuclear Crz1 GFP localisation (Figure 22 A, B). When Cn was inhibited via 100 µM FK506 a split population could be detected whereby almost all cells showed a mitochondrial/foci Crz1 GFP localisation (Figure 22 A, B). When 100 mM $CaCl_2$ was added in combination with the Cn inhibitor FK506, all cells showed mitochondrial/foci Crz1 GFP localisation (Figure 22 A, B).


A
DIC
GFP
Hoechst 33342
Crz1_EV
No stress
Crz1_EV
100 mM CaCl2
Crz1_EV
100 µM FK506
Crz1_EV
100 mM CaCl2
100 µM FK506
Crz1_Sod1A4V
No stress
Crz1_ Sod1A4V
100 mM CaCl2
Crz1_Sod1A4V
100 µM FK506
Crz1_ Sod1A4V
100 mM CaCl2
100 µM FK506
10 µm

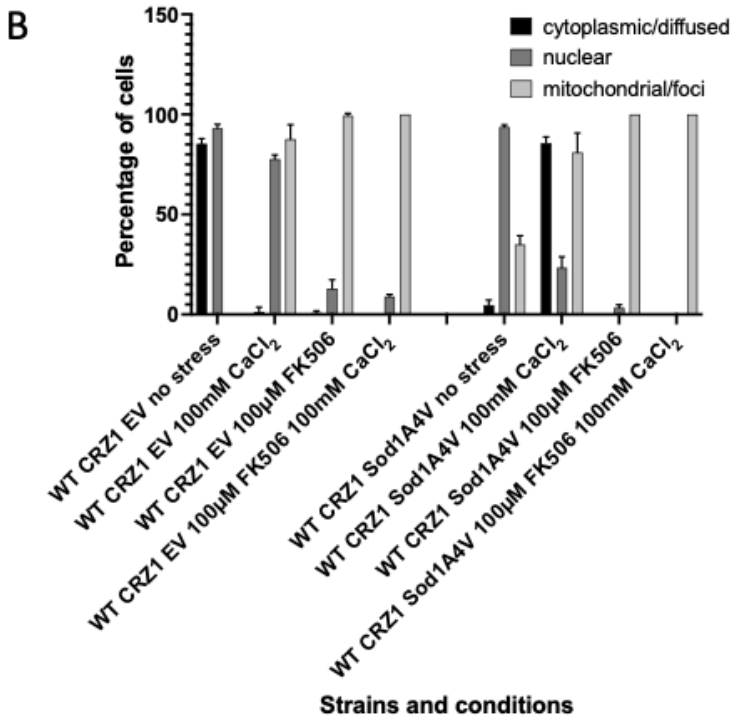


Figure 22 Sod1 and Sod1^{A4V} regulation of calcium response via Crz1 regulation.
A) Fluorescence microscopy images of active Crz1 in Crz1 GFP strains expressing an empty vector (EV) control or Sod1^{A4V} under standard conditions, 100 mM $CaCl_2$, and or 100 µM FK506 conditions during stationary phase. Crz1 was GFP tagged and FK506 is a calcineurin inhibitor. Stresses were added during log phase of growth following further incubation for 4 h. Fluorescence signal displays the presence of active Crz1 within the cells (GFP localisation). Cells were cultured in YPD growth media. This experiment was repeated three times, and a representative data set is shown. The scale bar is 10 µm.
B) Distribution of active Crz1 in Crz1 GFP strains expressing an empty vector (EV) control or SOD1^{A4V} under standard conditions, 100 mM $CaCl_2$, and or 100 µM FK506 conditions during stationary phase 100 cells for each strain were counted of samples taken on three separate days with a total 300 cells being counted. The number of cells represent the phenotypes seen and are represented and calculated as a percentage of the total number of cells counted. The error bars represent the standard deviation.

To determine whether the loss of *CRZ1* led to changes in intracellular calcium regulation, we performed an aequorin assay. To quantify intracellular calcium responses under different conditions (e.g. no substrate, 5 µM substrate, 100 mM $CaCl_2$), calcium curves were generated.

In the Δ*crz1* EV strain, the no substrate baseline appeared to be lower than the 5 µM coelenterazine (substrate) control. The basal intracellular calcium levels kept slightly increasing throughout the assay (Figure 23 A). The addition of 100 mM $CaCl_2$ triggered a rapid increase in intracellular calcium accumulation with levels peaking shortly after stress treatment and gradually returning after about 1 h (Figure 23 A).

In the Δ*crz1* $Sod1^{A4V}$ strain, the no substrate baseline appeared to be lower than the 5 µM coelenterazine (substrate) control. Basal intracellular calcium levels showed a slight upward trend throughout the assay under non-stressed conditions (Figure 23 B). Upon the addition of 100 mM $CaCl_2$, a rapid increase in intracellular calcium accumulation was observed, which returned to near-substrate levels after 1.2 h. However, calcium levels subsequently began to rise again, displaying a continuous upward trend for the remainder of the assay (Figure 23 B).

Comparing Δ*crz1* EV and Δ*crz1* $Sod1^{A4V}$ cells, it appeared that there were no significant differences between basal levels, but higher intracellular calcium levels seemed to appear after 100 mM $CaCl_2$ addition. When comparing WT EV with Δ*crz1* EV, no visual differences in basal intracellular calcium levels could be revealed. Visually, the calcium response following calcium stress appeared to last longer in WT EV cells. However, the intracellular calcium accumulation appeared higher in Δ*crz1* EV (Figures 19 A, 23 A). Lastly, comparison of WT $Sod1^{A4V}$ and Δ*crz1* $Sod1^{A4V}$ seemed to show higher intracellular calcium levels under basal conditions and following calcium addition in $Sod1^{A4V}$-expressing Δ*crz1* cells.

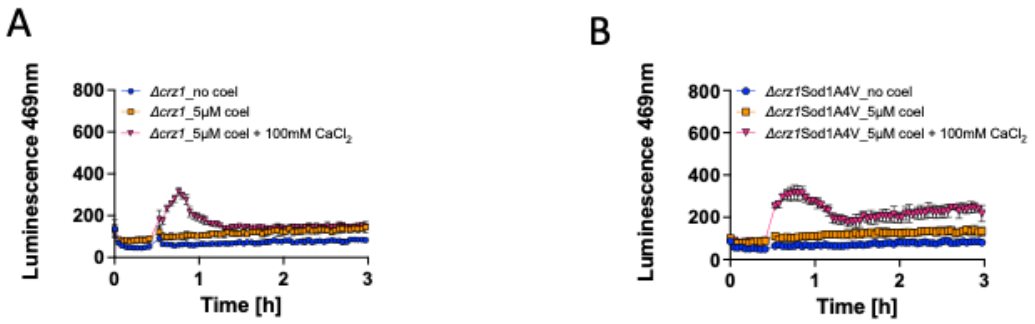


Figure 23 Sod1 and Sod1^{A4V} regulation of calcium response via Crz1 regulation.
The data sets represent an average of three biological repeats. The error bars display the standard deviation.
A, B) Aequorin luminescence curve at 469 nm measuring intracellular calcium levels in Δcrz1 expressing either EV or Sod1^{A4V}. A Two-Way ANOVA with post hoc tests: Tukey (within-strain comparisons); Sidak (WT vs. Δ) was used to determine statistical significance, $p < 0.05$ of AUCs.

Given that the expression of Sod1^{A4V} had clear effects on calcium regulation in not only WT cells but also in calcium transporters, cell cycle and calcineurin (Cn) regulators, we tested whether the expression of Sod1^{A4V} affects Cn function and intracellular calcium levels focusing on the Cn subunit Cnb1. We also sought to investigate whether the expression of Sod1^{A4V} affects Cn function through loss of Crz1 control leading to poor calcium stress response and viability reduction. Therefore, we conducted CFU assays, ROS accumulation and necrosis assays using flow cytometry, and intracellular calcium assays.

Regarding cell viability or colony forming efficiency (CFU), cells were exposed to 100 mM $CaCl_2$ for 4 h prior to another 4 h NaB incubation at either 1 mM or 100 mM concentration. Under no stress conditions (YPD media only), no significant changes in CFUs could be observed between WT EV, WT Sod^{A4V}, Δ*cnb1* EV, and Δ*cnb1* Sod1^{A4V}. All strains had a CFU of about 100 % (Figure 24 A). Compared to YPD, after the 4 h 100 mM $CaCl_2$ incubation, significantly reduced CFUs could be observed in the WT Sod1^{A4V} (~ 14 %) and Δ*cnb1* Sod1^{A4V}

(~ 26 %) compared to the WT EV control (~ 4 %). Exposure to 100 mM $CaCl_2$ did not lead to a reduction in CFUs in Δ*cnb1* EV (~ 102 %) compared to the WT EV control (Figure 24 A). Comparing Δ*cnb1* EV with Δ*cnb1* $Sod1^{A4V}$ a significant reduction in CFU (~ 26 %) could be observed in $Sod1^{A4V}$-expressing Δ*cnb1* cells (Figure 24 A).

Compared to YPD, 4 h exposure to 1 mM NaB after the 4 h 100 mM $CaCl_2$ incubation resulted in a significant reduction of CFUs in WT EV (~ 35 %), WT Sod1 (~ 55 %), WT $Sod1^{A4V}$ (~ 53 %), Δ*cnb1* EV (~ 68 %) and Δ*cnb1* $Sod1^{A4V}$ (~ 56 %). The decrease in CFUs in WT Sod1, WT $Sod1^{A4V}$, Δ*cnb1* EV, and Δ*cnb1* $Sod1^{A4V}$ differed significantly from the CFUs in WT EV (Figure 24 A). Interestingly, the reduction in CFU was more pronounced in Δ*cnb1* EV (~ 68 %) cells than in Δ*cnb1* $Sod1^{A4V}$ (~ 56 %) cells (Figure 24 A).

A 4 h 100 mM NaB treatment resulted in even further CFU reduction compared to YPD: WT EV (~ 87 %), WT Sod1 (~ 88 %), WT $Sod1^{A4V}$ (~ 88 %), Δ*cnb1* EV (~ 83 %) and Δ*cnb1* $Sod1^{A4V}$ (~ 87 %) (Figure 24 A). However, these reduction in CFUs were not significant compared to the WT EV within this condition. There was no significant difference in CFU between Δ*cnb1* EV (~ 83 %) and Δ*cnb1* $Sod1^{A4V}$ (~ 87 %) (Figure 24 A).

To see whether the reduction in CFUs in Δ*cnb1* EV and Δ*cnb1* $Sod1^{A4V}$ was a result of ROS accumulation or necrosis due to 100 mM $CaCl_2$ treatment, we conducted flow cytometry measuring ROS and necrosis. There was a significant difference in median FITC values in the positive ROS and PI (necrosis) controls compared to the WT (Figure 24 B). However, analysis of WT EV, Δ*cnb1* EV, and Δ*cnb1* $Sod1^{A4V}$ under 100 mM $CaCl_2$ stress or standard YPD conditions revealed no significant changed in median FITC values i.e. necrosis or ROS

accumulation (Figure 24 B) suggesting the reduction of CFUs previously seen (Figure 24 A) in Δ*cnb1* EV, and Δ*cnb1* Sod1^{A4V} under 100 mM $CaCl_2$ stress were not caused by ROS or necrosis.

We therefore hypothesised that reduction in CFU might be due to calcium dysregulation when *CNB1* is lost. We therefore performed an aequorin assay as described in Figure 18.

In the Δ*cnb1* EV strain, consistently low basal calcium levels throughout the assay could be observed, which were not significantly higher (p-value: 0.0630) to the no substrate control (Figure 24 C). Following 100 mM $CaCl_2$ addition, visual inspection of the luminescence profile revealed a slight rise in intracellular calcium accumulation which returned to basal levels after about 1 h (Figure 24 C). However, AUC analysis revealed no significant difference (p-value: 0.3293) in increased intracellular calcium accumulation between basal and calcium stress-induced calcium levels.

In the Δ*cnb1* Sod1^{A4V} strain, significantly elevated (p-value: <0.0001) basal calcium levels could be observed compared to the no substrate control. This gradual increase in intracellular calcium levels appeared to be linear over time, suggesting a steady accumulation of intracellular calcium throughout the assay in the absence of additional stress (Figure 24 C). Following 100 mM $CaCl_2$ addition, visual inspection of the luminescence profile revealed a slight increase in intracellular calcium accumulation which returned to basal levels after about 1 h (Figure 24 C). However, AUC analysis revealed no significant difference in increased intracellular calcium accumulation between basal and calcium stress-induced calcium levels. Comparing Δ*cnb1* EV and Δ*cnb1* Sod1^{A4V} strains, AUC analysis revealed significantly higher (p-value: <0.0001) basal calcium levels in Δ*cnb1* Sod1^{A4V}.

Furthermore, AUC analysis revealed significantly intracellular calcium accumulation after 100 mM $CaCl_2$ addition in Δ*cnb1* $Sod1^{A4V}$. Visual comparison of the luminescent profiles between Δ*cnb1* EV and Δ*cnb1* $Sod1^{A4V}$ strains confirmed this (Figure 24 C).

When comparing WT EV with Δ*cnb1* EV, AUC analysis revealed no significant differences between these strains under basal and stress conditions. However, visual comparison seemed to show a more pronounced calcium accumulation in WT EV cells (Figures 19 A, 24 C). Lastly, comparison of WT $Sod1^{A4V}$ and Δ*cnb1* $Sod1^{A4V}$ showed significantly higher basal (p-value: <0.0001) and calcium-induced (p-value: <0.0001) intracellular calcium levels in Δ*cnb1* $Sod1^{A4V}$. Visual comparison could confirm this (Figures 19 B, 24 C).

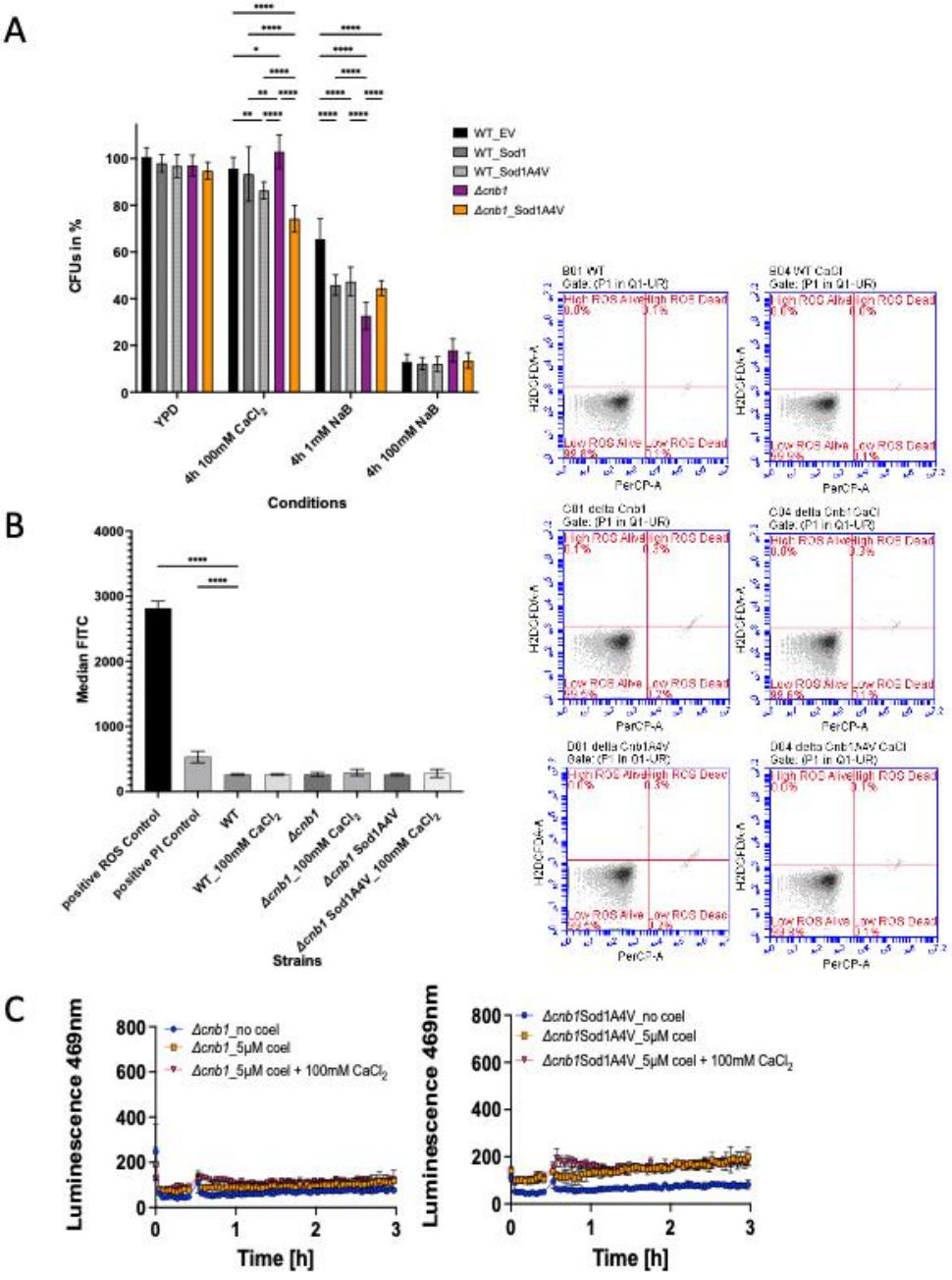


Figure 24 Effect of Sod1^{A4V} on Cn function and calcium homeostasis.
A) CFU analysis of WT EV, WT Sod1^{A4V}, Δcnb1, and Δcnb1 Sod1^{A4V} after 100 mM $CaCl_2$ exposure prior 4 h of either 1 mM or 100 mM NaB treatment. ***The data sets represent an average of three biological repeats. The error bars display the standard deviation.*** *A One-Way ANOVA using a Tukey multiple comparison test was used to determine statistical significance, $p < 0.05$.*
B) Median FITC values and H2DCFDA and PerCP-A graphs of WT, Δcnb1, and Δcnb1 Sod1^{A4V} with or without 100 mM $CaCl_2$ stress. ***The data sets represent an average of three biological repeats. The error bars display the standard deviation.*** *A One-Way ANOVA using a Tukey multiple comparison test was used to determine statistical significance, $p < 0.05$.*
C) Aequorin luminescence curve at 469 nm measuring intracellular calcium levels in Δcnb1 expressing either EV or Sod1^{A4V}. A Two-Way ANOVA with post hoc tests: Tukey (within-strain comparisons); Sidak (WT vs. Δ) was used to determine statistical significance, $p < 0.05$ of AUCs.

Taken together, these results indicate that expression of Sod1^{A4V} affects Crz1 localisation and intracellular calcium regulation under calcium stress. In WT cells, calcium exposure resulted in increased nuclear localisation of Crz1, whereas Sod1^{A4V}-expressing cells showed predominantly cytoplasmic or mitochondrial/foci localisation, with only a small proportion of cells displaying nuclear Crz1. This altered localisation was accompanied by changes in intracellular calcium regulation, particularly in the Δ*crz1* and Δ*cnb1* backgrounds, where Sod1^{A4V}expression was associated with increased basal calcium levels and altered calcium accumulation following $CaCl_2$ exposure. Loss of *CNB1* was also associated with reduced CFU following calcium stress in the presence of Sod1^{A4V}, although this reduction was not accompanied by increased ROS accumulation or necrosis. These findings suggest that Sod1^{A4V}expression interferes with calcium-responsive signalling involving the calcineurin-Crz1 pathway and that disruption of this pathway is associated with altered calcium homeostasis and reduced survival under calcium stress. However, the data do not establish whether the altered Crz1 localisation is a direct consequence of Sod1^{A4V}expression or is secondary to the changes in intracellular calcium regulation.

4.4 Discussion

4.4.1 Introduction

Previous work suggested that overexpression of ALS-linked mutations in the yeast SOD1 gene such as A4V, G37R, H48Q, G93A and S134N, which correspond to human mutations led to unstable and enzymatically inactive Sod1 proteins. It was reported that a loss of viability and acidification of the vacuole as well as defects in amino acid regulation (activation of the amino acid starvation response via Gcn4), and in autophagy were

identified when mutant Sod1 was expressed in *S. cerevisiae* cells. Rather than undergoing cell death a senescence-like state as well as the accumulation of trehalose could be observed in mutant cells. These phenotypes mark metabolic and autophagic dysfunction as key elements of SOD1 toxicity (Bastow *et al.*, 2016).

The loss in vacuole acidification suggested a defect in the activity of the vATPase that underpinned loss of regulation of vacuole function and to the phenotypes mentioned above. However, these data were obtained from a high overexpression system (Bastow *et al.*, 2016) and to test this more carefully a single copy integration model was constructed (Doyle, 2022). Work by (Doyle, 2022) suggested that there may be an interaction with parts of the vATPase complex. However, our FLIM/FRET results showed that there was not direct interaction between wild type or mutant Sod1 and VMA2. This finding is supported by results within Dr Kevin Doyles thesis in which an interaction between Vma2 and Sod1 could not be observed by immunoprecipitation. This may suggest that the mutations do affect the localisation or proximity of Sod1 to the vATPase (Doyle, 2022).

It was also found that the expression of Sod1 mutants from single copy system did not lead to growth defects or loss of vacuole acidification, suggesting that the level of protein leads to variable effects on cell function (Bastow *et al.*, 2016; Doyle, 2022).

However, relative expression levels of wild-type Sod1 and $Sod1^{A4V}$ were not directly assessed in this study. Therefore, phenotypic effects cannot be attributed solely to the A4V mutation, as differences in Sod1 expression could contribute to the observed effects.

A further limitation is the absence of an additional-copy Sod1WT control. Consequently, some phenotypes may reflect increased Sod1 dosage rather than mutation-specific effects.

Including an additional-copy Sod1WT control in future experiments would help distinguish these effects.

To determine more subtle genetic interactions within this model a vacuole deletion library created by Dr Kevin Doyle was generated (Doyle, 2022) and was expanded in this study with the intention that it may reveal which vacuole functions were vulnerable to the effects of lower Sod1^{A4V} expression when placed under additional stresses. We tested stresses like calcium, zinc, and FK506 (calcineurin inhibitor) as work by Dr Kevin Doyle had shown that loss of Sod1 generally sensitised cells to these stresses (Doyle, 2022), and the stresses have been implicated in ALS and are also linked to vacuole/lysosome function (Weiss, Sensi and Koh, 2000; Frederickson, Koh and Bush, 2005; Grosskreutz, Van Den Bosch and Keller, 2010; Hozumi *et al.*, 2011; Szewczyk, 2013; Sirabella *et al.*, 2018).

4.4.2 Vacuolar Function and Trafficking

Across all tested conditions, expression of the Sod1^{A4V} mutant revealed consistent synthetic interactions with genes involved in vacuolar trafficking, autophagy, and iron and calcium homeostasis, highlighting the centrality of vacuolar function in managing proteotoxic stress.

Malfunctions in vacuolar and endolysosomal trafficking has been increasingly recognised in ALS and other neurodegenerative diseases (Burk and Pasterkamp, 2019; Herman *et al.*, 2024). In ALS, particularly misfolded SOD1 has been shown to form aggregates in the neuronal tissue and accumulate in the endoplasmic reticulum (ER) and Golgi, which may interfere with vesicular transport and enhance ER stress (Urushitani *et al.*, 2008; Burk and

Pasterkamp, 2019; Berdyński *et al.*, 2022). A recent crucial genetic finding in ALS is an intronic GGGGCC repeat expansion mutation in chromosome 9 open reading frame 72 (C9ORF72) (Vance *et al.*, 2006; DeJesus-Hernandez *et al.*, 2011; Renton *et al.*, 2011). It was found that C9ORF72 is crucial for normal vesicle trafficking and lysosomal biogenesis in motor neurons and interaction with endosomes. Furthermore, *C9ORF72* repeat expansion led to impaired clearance of neurotoxic dipeptide repeat proteins derived from the repeat expansion. The study also showed that *C9ORF72* mutations led to aggregation and slower translocation of transmembrane receptors such as the Mannose-6-phosphate receptors (M6PRs) which have roles in targeting lysosomal enzymes to lysosomes for proper lysosomal degradation (Shi *et al.*, 2018; Burk and Pasterkamp, 2019). Another study demonstrated that M6PRs mislocalised to the cytosol in the presence of *C9ORF72* mutations (Aoki *et al.*, 2017). Mutations in SOD1 affect trafficking at the Golgi as well: It was found that ALS-associated mutations such as $SOD1^{A4V}$, $SOD1^{G85R}$, and $SOD1^{G93A}$ could cause defects in protein secretion and cause ER stress resulting in inclusions and apoptosis, esp. when $SOD1^{A4V}$ was present. This effect could be rescued by the overexpression of COPII vesicles (Atkin *et al.*, 2014). Another study found that SOD1 mutations such as the $SOD1^{G93A}$ inhibit protein transport from the ER to the ER-Golgi intermediate ERGIC compartment (Soo *et al.*, 2015). It could also be confirmed that Golgi fragmentation is associated with SOD1 mutations (Gonatas, Stieber and Gonatas, 2006; van Dis *et al.*, 2014). This aligns with our observation that deletion of genes essential for vacuolar fusion and trafficking, e.g. VTC1, EGO1, and VPS34, were affected by $SOD1^{A4V}$ expression, highlighting the importance of efficient vesicular degradation in proteostasis in ALS.

4.4.3 Autophagy

Autophagy, particularly macroautophagy, is a major degradative route for mutant SOD1 aggregates. Reduced autophagy degradation has been reported in ALS patient (LEIGH *et al.*, 1991; Arai *et al.*, 2006; Mizuno *et al.*, 2006; Neumann *et al.*, 2006) and animal models (Watanabe *et al.*, 2001). (Bastow, Gourlay and Tuite, 2011; Bastow *et al.*, 2016) did see a loss of autophagy in the high expression yeast model.

Studies found that abnormal mitochondria (Atsumi, 1981; Sasaki and Iwata, 1996; Siklós *et al.*, 1996; Wiedemann *et al.*, 1998; Chung and Suh, 2002; Napoli, 2011) and defective ERs (Ilieva *et al.*, 2007; Atkin *et al.*, 2008; Ito *et al.*, 2009; Tokuda *et al.*, 2016) accumulate in ALS which normally would be removed through autophagy (Johansen and Lamark, 2011). As one of the stress adaption pathways, autophagy can be over-induced through stressors such as damaged DNA, abnormal protein and organelle accumulation, and oxidative stress. This over-induction may impair the actual degradation process (Fujikake, Shin and Shimizu, 2018; Amin *et al.*, 2020) and may even lead to apoptosis (Boya *et al.*, 2005). To strengthen this assumption, studies could show that suppressing autophagosome formation may be beneficial in ALS mice (Hsueh *et al.*, 2016; Rudnick *et al.*, 2017; Zhou *et al.*, 2017). Consistent with this, our screen revealed synthetic interactions between Sod1A4V and multiple components of the autophagy pathway, including deletions in ATG8, ATG18, VPS34, and VTC1, all of which exacerbated $Sod1^{A4V}$ toxicity. These genes are essential for autophagosome formation and cargo recycling, highlighting the importance of intact degradation pathways in the presence of proteotoxic stress. Autophagy is triggered by the formation of the phagophore, a cup-shaped membrane assembled at the phagophore assembly site (PAS), which can be located at sites such as the ER, Golgi, or plasma

membrane. ATG proteins are recruited to the PAS and organize into five functional complexes, crucial for initiating this process (Glick, Barth and Macleod, 2010; Dikic and Elazar, 2018).

A central player is the class III PI3K complex, which includes VPS34, Beclin-1, ATG14, and p115. VPS34 converts PI into PI(3)P, promoting vesicle nucleation. This complex is regulated by SOD1. Mutant SOD1 can interfere with Beclin-1, destabilise the Beclin-1–Bcl-xL complex and impair autophagy initiation (Lee *et al.*, 2015; Stjepanovic *et al.*, 2017).

In our study, deletion of *ATH1*, encoding an acid trehalase, showed improved growth, suggesting a protective role for intracellular trehalose accumulation in opposing proteotoxic stress. Indeed, ALS mice studies have shown that trehalose - which is a MTOR-independent autophagic inducer- had a protective role in protein aggregation as it could stabilise proteins and promote autophagy (X. Zhang *et al.*, 2014). Recently, trehalose was trialled in individuals with ALS, but did not show any statistical benefits in ALS disease progression prevention (Macklin *et al.*, 2025).

4.4.4 Metabolic Signalling and Stress Response

Nutrient sensing pathways also emerged as a point of vulnerability in our results. Deletions of EGO complex components (EGO1, EGO3, GTR1) and vacuolar amino acid exporter (VBA5) sensitized $Sod1^{A4V}$-expressing cells to stresses, suggesting a broader impact on TORC1-mediated signalling. This pathway regulates growth and autophagy in response to amino acid availability (Noda, 2017) and has been implicated in ALS pathogenesis via mTOR hyperactivity and impaired cellular clearance (Zhang *et al.*, 2011; Ching and Weihl, 2013; Saxena *et al.*, 2013; Gomes *et al.*, 2023; Nogueira-Machado, Rocha-Silva and Gomes, 2025).

Our data also suggest the involvement of the trehalose pathway in protein stabilisation: We showed that loss of TPS1 and TPS3 led to decreased growth in Sod1^{A4V} strains under stress. Interestingly, the trehalose biosynthetic pathway, although absent in humans, has been shown to influence proteostasis and suppress aggregation in several neurodegeneration models (Mari *et al.*, 2020).

Moreover, loss of RAS2 significantly sensitised Sod1^{A4V}-expresssing yeast cells to stresses, supporting a protective role for Ras-cAMP-PKA signalling. In yeast, RAS2 controls cell cycle entry and modulates stress responses via cAMP and PKA (Tamanoi, 2011), whilst in mammalian cells cell stress response and other crucial cellular processes, such as cell proliferation, are controlled by Ras-MAPK signalling (ZHANG and LIU, 2002). It has been reported that Ras-MAPK signalling is altered in ALS (Kim and Choi, 2010; Ayala *et al.*, 2011; Sahana and Zhang, 2021) and linked to ROS regulation in both yeast and mammalian cells (Leadsham *et al.*, 2009; Hu *et al.*, 2012; Amigoni, Martegani and Colombo, 2013). This suggests that Sod1^{A4V} toxicity may be increased when cells are unable to induce a Ras-dependent metabolic response. Supporting this, we observed that 1 mM sodium butyrate — a known HDAC inhibitor — was able to rescue Sod1^{A4V}-expressing Δ*ras2* and Δ*yvc1* strains under calcium stress. This finding aligns with previous reports that butyrate can influence metabolism and elevate cAMP levels in fungi, effectively mimicking Ras–PKA activity (Zutz *et al.*, 2017) in cells lacking RAS2. These results strengthen the view of a potential link between HDAC regulation, Ras signalling, and calcium homeostasis in the context of ALS.

Under calcium stress, additional synthetic interactions were observed suggesting an interplay between ion signalling, metal homeostasis, and proteostasis: loss of *RAS2,* a key GTPase in the Ras-cAMP-PKA pathway elevated Sod1^{A4V} toxicity implying an important role

in the calcium-induced stress response. Similarly, deletion of the vacuolar calcium release channel Yvc1 led to reduced growth implicating that vacuolar calcium efflux is crucial for stress resistance. Similarly, *NHX1* deletion which encodes a vacuolar Na^+/H^+ exchanger, also showed reduced growth, strengthening the importance of vacuolar ion balance in stress resistance. In contrast, deletion of *ath1* resulted in increased growth suggesting that trehalose metabolism may be protective under calcium stress. Most likely, trehalose reduces aggregation or stimulates autophagy to clear unstable Sod1, and so the cells retain the stress response. Notably, deletion of *ccc1*, a vacuolar iron/manganese transporter, also showed growth advantage. Finally, deletions of *vps34* showed increased $Sod1^{A4V}$ fitness under calcium stress, potentially reflecting a protective remodelling of vesicle trafficking or autophagic flux that improves viability during calcium and proteotoxic stress.

Inhibition of calcineurin using FK506 revealed an extensive range of synthetic interactions. Multiple genes implicated in calcineurin signalling, TORC1 regulation, and autophagy were required for growth in the $Sod1^{A4V}$ background. Deletions of *vcx1* (vacuolar Ca^{2+}/H^+ exchanger), *yvc1*, and *ras2* all led to increased sensitivity. Several TORC1 regulators (*EGO1*, *EGO3*, *GTR1*) were also negatively affected by $Sod1^{A4V}$ toxicity, highlighting the importance of nutrient sensing in proteostasis when calcineurin is inactive. The retrograde (RTG) pathway was also negatively affected (Δ*rtg3*), which links mitochondrial function to nuclear gene expression suggesting a compensatory role of mitochondrial-nuclear communication in stress adaptation. Trehalose biosynthesis (Δ*tps1*, Δ*tps3*) and metal homeostasis (Δ*zrc1*, Δ*ccc2*, Δ*fet5*) were also affected by $Sod1^{A4V}$ in the presence of FK506, which may contribute to oxidative stress. Furthermore, multiple genes related to plasma membrane function and ion homeostasis (kinases Yck2, Ptk2) and autophagy and vesicle trafficking (*ATG1*, *VPS15*, *VTC1*, *VTC3*, *VBA3*, *VBA5*) emerged being negatively affected by $Sod1^{A4V}$.

.

Zinc exposure elicited a global reduction in AUC values across the vacuole KO library, suggesting it imposes a significant stress burden on yeast cells. In this stringent environment, only one vacuolar gene deletion showed a growth advantage: ATH1. This consistent phenotype across all tested conditions suggests a general role for intracellular trehalose accumulation in promoting $Sod1^{A4V}$-associated stress tolerance, maybe by stabilizing misfolded proteins under heavy metal stress. The absence of other differential hits may be because zinc toxicity overwhelms many compensatory pathways regardless of $Sod1^{A4V}$ expression and more hits may have been revealed at a lower zinc concentration.

4.4.5 Ionic homeostasis and Calcineurin Signalling

Lastly, our results demonstrated synthetic interaction between $Sod1^{A4V}$ and calcium homeostasis: Loss of YVC1 and VCX1, which regulate calcium flux across the vacuolar membrane (Cui, Kaandorp, Ositelu, *et al.*, 2009), led to increased growth deficits in $Sod1^{A4V}$-expressing yeast cells. Calcium dysregulation is another causative factor of ALS. A prominent feature of motor neurons compared to other cells is their vulnerability to calcium overload as calcium permeable AMPA receptors are highly expressed (Williams *et al.*, 1997; Shaw and Eggett, 2000; Van Den Bosch *et al.*, 2000; Guatteo *et al.*, 2007), while the endogenous expression of calcium buffering proteins (CaBPs), like parvalbumin and calbindin, is low (Alexianu *et al.*, 1994; Palecek, Lips and Keller, 1999; Jaiswal, 2013), even though EF-hand calcium binding proteins are present in motor neurons (Migheli *et al.*, 1999; M.-D. Zhang *et al.*, 2014). Several studies could detect intracellular calcium overload and a further decrease in calretinin and parvalbumin in motor neuron axons in ALS patients (Siklós *et al.*, 1996,

1998; Kruman *et al.*, 1999; Grosskreutz, Van Den Bosch and Keller, 2010; Kawamata and Manfredi, 2010; Hayashi, Amari and Okamoto, 2013). Another pathological pathway in ALS causing calcium overload is that mutated SOD1 was found to accumulate in the mitochondrial intermembrane space, which impairs normal mitochondrial function. This is interesting as mitochondria are supposedly crucial in buffering calcium in motor neurons (Jaarsma *et al.*, 2001; Liu *et al.*, 2004; Jaiswal and Keller, 2009; Lautenschläger *et al.*, 2013). Thus, SOD1 mutations can lead to disturbances in calcium homeostasis.

In this context, it was also shown that calcium can bind to immature SOD1 increasing its accumulation (Leal *et al.*, 2013; Estácio *et al.*, 2015). In agreement, overexpression of CaBPs and AMPA channel antagonists could decrease calcium overload, neurodegeneration, and abnormal SOD1 accumulation in ALS1 models (Van Damme *et al.*, 2003; Tateno *et al.*, 2004; Tortarolo *et al.*, 2006; Yin, Tang and Weiss, 2007; Beers *et al.*, 2008; Parone *et al.*, 2013).

Another key player in ALS is the protein phosphatase 2B calcineurin (Cn). The activity of Cn is calcium dependent and regulated by calmodulin. Being highly expressed in the CNS and playing a major part in many pathways involving modulation of immune responses and signal transduction in the nervous system through regulating neuronal excitability, the release of neurotransmitters and hormones, gene transcription and calcium-dependent apoptosis, Cn activity is thought to be pivotal in motor neuron diseases (Morioka *et al.*, 1999; Wang *et al.*, 1999; Rusnak and Mertz, 2000). Previous studies using human neuroblastoma cells expressing fALS-SOD1 and mouse models expressing fALS SOD1 showed that the phosphatase activity of Cn is repressed when mutant antioxidant SOD1 is present (Ferri *et al.*, 2002), thus supporting evidence that Cn is redox regulated. This is further supported by showing that wild type SOD1 functions as a protective element for Cn (Wang,

Culotta and Klee, 1996), and fALS-SOD1 can directly deactivate Cn (Ferri *et al.*, 2008). The target of such oxidation of Cn is supposedly the iron atom at its active site (Namgaladze, Hofer and Ullrich, 2002). Decreased Cn activity was directly found in ALS patients: a study reported significantly decreased Cn activity in lymphocytes in 37 sporadic and eight fALS patients with an increase in protein oxidation which was not found in the control subjects (Ferri *et al.*, 2004).

Sod1 is primarily known for its protective defence mechanism against antioxidants as it catalyses superoxide into peroxide and oxygen (McCord and Fridovich, 1969). As both proteins are zinc-containing metalloproteins (Rusnak and Mertz, 2000; Mera-Adasme *et al.*, 2016; Sirangelo and Iannuzzi, 2017), increased labile zinc accumulation causing motor neuron toxicity may be caused by aberrant SOD1-Cn interaction when SOD1 mutations are present (Tiwari and Hayward, 2005; Kim *et al.*, 2009). In mammalian neurons, direct physical interaction between SOD1 and Cn appears to be necessary for optimal Cn activation, and this relationship is disrupted by ALS-linked SOD1 mutations (Agbas *et al.*, 2007; Kim *et al.*, 2019). Our current study builds on previous work showing that *S. cerevisiae* cells lacking *SOD1* or overexpressing SOD1 mutants (*A4V*, *G37R*) (but not cell overexpressing wild type SOD1), display impaired Cn signalling in response to calcium stress. A drop in Cn activity was also seen when fragments of Sod1 were expressed, supporting the hypothesis that unstable or misfolded Sod1 disrupts Cn signalling (Doyle, 2022). Our results identified a set of deletions that significantly attenuated Cn activity under calcium stress: *TOR1*, *AKR1*, *YPK1*, *YPK2*, *EGO3*, *YNO1*, and *YVC1*. These genes are involved in several pathways, including nutrient sensing (TORC1), lipid metabolism and membrane composition (AKR1, YPK1/2), redox regulation (YNO1), and vacuolar calcium release (YVC1).

In yeast, Cn activation is largely triggered by cytosolic calcium influx (Billingsley *et al.*, 1990; Cyert *et al.*, 1991), with Yvc1 acting as a vacuolar calcium release channel (Palmer *et al.*, 2001; Denis and Cyert, 2002). The observed dependence on *YVC1* supports the critical role of internal calcium stores in modulating Cn response.

YNO1 encodes the NADPH oxidase in yeast and together with the mitochondrial respiration act as the main superoxide sources (Rinnerthaler *et al.*, 2012). Interestingly, studies have shown that in absence of YNO1, increased vacuole fragmentation occurs. Yno1p is also responsible for a burst of reactive oxygen species, which when exceeding the antioxidant capacity of the cell harmful events occur (Weber *et al.*, 2021). This could affect calcium channel regulation or Cn function through redox-sensitive modifications. Although mammalian cells contain a more complex NADPH oxidase system, increased ROS production and oxidative stress are hallmarks of ALS pathology (Shaw *et al.*, 1995; Ferrante *et al.*, 1997; Ihara *et al.*, 2005; Tam *et al.*, 2019), and Cn itself is susceptible to redox regulation (Ferri *et al.*, 2002).

The *TOR1* and *EGO3* deletions implicate the TORC1 signalling pathway as a key regulator of calcineurin (Cn) activity. TORC1 integrates amino acid availability and cellular energy status to control growth and autophagy (Loewith and Hall, 2011; González and Hall, 2017). In yeast, the EGO complex is essential for TORC1 activation in response to amino acids and vacuolar cues, linking nutrient sensing directly to autophagic control (Binda *et al.*, 2009). TOR may negatively control autophagy through TORC1. A study has shown that TOR may also operate independently to promote autophagy via TORC2 in response to amino acid starvation. This is mediated via the downstream target protein of TORC2, Ypk1. TORC2/Ypk1 may negatively regulate Cn in order to activate the amino acid-sensing eIF2α kinase, Gcn2,

and to promote autophagy (Vlahakis *et al.*, 2014). Studies using the mTORC1-dependent activator of autophagy, rapamycin, found that motor-neuron loss was increased and the survival of $Sod1^{G93A}$ mice was reduced. On the other hand, survival in immunodeficient ALS mouse models was increased (Zhang *et al.*, 2011; Staats *et al.*, 2013).

To further understand the mechanism underlying the impaired Cn response observed in cells expressing $Sod1^{A4V}$, we investigated the subcellular localization of the Cn-responsive transcription factor Crz1 using a GFP-tagged Crz1 fusion protein. We found that under basal conditions, Crz1-GFP in wild-type cells showed a signal distribution between the cytoplasm and the nucleus, consistent with low basal Cn activity during stationary phase. Upon exposure to 100 mM $CaCl_2$, Crz1 became predominantly nuclear or concentrated in mitochondrial/ER-like structures and cytoplasmic foci, suggesting active Cn signalling coupled with stress adaptation mechanisms. Inhibition of Cn using FK506 abrogated this nuclear translocation, with Crz1 accumulating in the cytoplasm or organelle-associated foci, confirming the dependence of nuclear import on Cn activity. The transcription factor Crz1 plays a crucial role in regulating the response to calcium signalling and stress adaptation within the cell. In actively budding cells normal cytosolic calcium concentrations are held within 50-200 nM (Cui, Kaandorp, Sloot, *et al.*, 2009). When intracellular calcium concentrations rise, calmodulin – a calcium sensor protein- will bind to and activate the protein phosphatase Cn, which in turn will dephosphorylate Crz1 (Stathopoulos and Cyert, 1997). Crz1 will translocate from the cytosol to the nucleus binding to the Cn-dependent response element CDRE, ultimately activating about 160 genes, including e.g. calcium transporters involved in stress adaptation (Stathopoulos-Gerontides, Guo and Cyert, 1999; Yoshimoto *et al.*, 2002).

In contrast, we showed that stationary cells expressing Sod1^{A4V} displayed a mislocalisation of Crz1-GFP to the cytoplasm, with only a minority of cells displaying nuclear or mitochondrial/foci signal. Upon calcium addition, Crz1 failed to efficiently translocate to the nucleus, and instead, remained cytoplasmic or accumulated in foci, suggesting impaired activation or trafficking. The combination of calcium and FK506 exacerbated this effect, with all Crz1 signal mislocalised to foci or organellar regions. We further identified that upon exposure to calcium intracellular calcium levels remained high in Sod1^{A4V} expressing Δ*crz1* cells, whilst intracellular calcium levels in EV expressing cells went back to normal. This mislocalisation of Crz1 is significant because its nuclear translocation is essential for activating transcriptional programs that mediate calcium homeostasis, ion transport, and stress resilience (Stathopoulos-Gerontides, Guo and Cyert, 1999; Yoshimoto *et al.*, 2002). Without this response, cells are unable to adequately adapt to calcium fluctuations, which may contribute to cellular vulnerability under stress. In the context of ALS, where calcium dysregulation and ER stress are prominent features, a failure to elicit effective Cn–Crz1 signalling could exacerbate neurodegenerative processes. The failure of Crz1 to enter the nucleus in Sod1^{A4V}-expressing cells complements our earlier findings that Cn activity is reduced in the presence of unstable SOD1 mutants (Doyle, 2022). These data suggest that Sod1^{A4V} impairs Cn-dependent transcriptional responses by interfering with Crz1 activation and nuclear translocation. The mislocalisation is backed up by the elevated calcium levels we observed in Δ*crz1* cells expressing Sod1^{A4V} when 100 mM $CaCl_2$ was added. This may occur through disrupted calcium homeostasis, altered redox signalling, or aberrant interactions between misfolded SOD1 and Cn, as previously proposed in mammalian models (Agbas *et al.*, 2007; Kim *et al.*, 2019).

4.4.6 Summary

In summary, our findings using *S. cerevisiae* as an ALS model illuminate how a single misfolded protein ($Sod1^{A4V}$) can perturb multiple, highly conserved cellular systems: vacuolar (lysosomal) function, autophagy, metabolic signalling, and Ca^{2+} homeostasis. Each of these systems has a counterpart in neurons that is implicated in ALS. The yeast model thereby provides a valuable mechanistic framework. It suggests that therapies for ALS might need to be multi-modal – for example, combining a proteostasis booster (to enhance autophagy/lysosomal clearance and stabilize proteins) with a metabolic modulator (to adjust TOR/Ras signalling or improve mitochondrial function) and a calcium regulator (to prevent calcineurin impairment and excitotoxic damage). Indeed, combination trials using interleukins to reduce inflammation and riluzole acting via sodium/calcium channel modulation are now underway e.g. (Bensimon *et al.*, 2025). Our work particularly highlights the centrality of the vacuole/lysosome: virtually every pathway we identified feeds into lysosomal health (trafficking of enzymes and receptors, autophagic flux, ion sequestration, signalling crosstalk). This reinforces the concept of ALS as a disorder of "endosomal–lysosomal dysfunction", in addition to proteopathy. Yeast, with its tractable genetics, allowed us to uncover these connections and will be a useful platform to screen for suppressors – for instance, small molecules that rescue yeast $Sod1^{A4V}$ phenotypes by enhancing vacuolar acidification or calcineurin activity could be candidates for further testing in animal models. In conclusion, the convergence of our yeast data with known ALS mechanisms underscores that simple eukaryotes can faithfully recapitulate complex neurodegenerative processes, and that preserving cellular homeostasis (in the face of misfolded protein stress) is a multi-faceted battle waged across metabolism, protein

clearance, and ion regulation. Insights from such models will guide us toward combinatorial therapeutic strategies to tackle ALS.

5. Final discussion

The neurodegenerative disease ALS and other neurodegenerative diseases such as Alzheimer's and Parkinson's, are more and more recognised as disorders where cellular homeostasis is disturbed due to imbalances in proteostasis, metabolism, cell signalling, and host-microbe interactions. These converge to drive neuronal vulnerability (Sheikh *et al.*, 2013; Gao *et al.*, 2025).

In this thesis, we used a combination of model systems, *C. elegans*, mammalian cell lines, *S. cerevisiae*, and *C. albicans*, to investigate how ALS-linked Sod1 mutations interfere with crucial biological processes, and how microbial metabolites such as butyrate may influence disease outcomes. In our *S. cerevisiae* model system, we were able to show that $Sod1^{A4V}$ expression interrupts multiple conserved cell signalling pathways including lysosomal/vacuolar function, autophagy, metabolic signalling, and calcium homeostasis. Together with our observations in the *C. elegans*, human neuroblastoma cells, and *C. albicans* models, our findings highlight that ALS pathology is likely linked to systemic influences such as the gut microbiome and microbial metabolites. Overall, our data supports the emerging picture that ALS is multifaceted and that simple model systems can play a role in dissecting the complex processes underlying its pathology.

5.1 Consistent themes across our model systems

Across all our model systems, Sod1 proteopathy emerged as a central driver of pathology. In *C. elegans* and human cells, Sod1 aggregation impaired neuromuscular function, whilst butyrate treatment reduced aggregation and rescued neuronal phenotypes. In yeast, $Sod1^{A4V}$ expression caused synthetic genetic interactions that revealed vulnerabilities in vacuolar trafficking, autophagy, Ras/TOR signalling, and calcineurin-dependent calcium homeostasis. In *C. albicans*, butyrate supressed key virulence traits, linking microbial metabolism to host health. Despite the diversity of these systems, the vacuole/lysosome signalling is consistently at the centre of $Sod1^{mut}$ disruption of proteostasis.

The vacuole/lysosome is not only a degradative organelle, but also a signalling hub integrating nutrient sensing, autophagy, metal ion sequestration, and calcium dynamics.

Almost every pathway identified in our yeast screens fed into vacuolar health, highlighting findings in ALS studies where lysosomal trafficking, autophagy, and ER/Golgi function are impaired (Urushitani *et al.*, 2008; Burk and Pasterkamp, 2019; Berdyński *et al.*, 2022; Herman *et al.*, 2024). Similarly, our microbiome work highlights that fungal dysbiosis and butyrate deficiency may indirectly weaken lysosomal resilience in neurons by increasing systemic metabolic stress. These findings reinforce the idea of ALS being a multifactorial disease with dysfunction in endosomal-lysosomal signalling inflicted by proteopathy (LEIGH *et al.*, 1991; Arai *et al.*, 2006; Mizuno *et al.*, 2006; Neumann *et al.*, 2006; Sheikh *et al.*, 2013).

5.2 Link between metabolism, ion signalling and microbial metabolites

A second key convergence is the interplay between metabolic signalling, ion homeostasis, and butyrate. In yeast, $Sod1^{A4V}$ expression sensitised cells to deletions in Ras/TOR signalling components, underscoring the importance of nutrient-sensing pathways in managing proteotoxic stress. Loss of *RAS2* was particularly detrimental, but its effects could be rescued by butyrate, maybe through elevating cAMP levels thus mimicking Ras/PKA activity (Tamanoi, 2011). This aligns with mammalian data showing altered Ras/MAPK signalling in ALS (Kim and Choi, 2010; Ayala *et al.*, 2011; Sahana and Zhang, 2021) and suggests that metabolic homeostasis is needed to buffer misfolded protein stress.

Calcium dysregulation also emerged as a recurring theme. Yeast expression of $Sod1^{A4V}$ showed impaired Crz1 nuclear translocation, reflecting defective calcineurin signalling. This resonates with ALS neurons which are vulnerable to calcium overload due to low buffering capacity and mitochondrial dysfunction (Williams *et al.*, 1997; Shaw and Eggett, 2000; Van Den Bosch *et al.*, 2000; Guatteo *et al.*, 2007). The ability of butyrate to modulate this signalling pathway indirectly in yeast further positions it as a metabolite that links the microbiome to calcineurin signalling homeostasis.

6. Implications

Collectively, this work placed Sod1^{A4V} toxicity within the broader context of ALS pathology. Four converging themes emerge: lysosomal/endosomal dysfunction, proteopathy, calcium stress, and microbiome contributions. Each provides a mechanistic foothold for future therapeutic development.

Lysosomal and endosomal dysfunction has repeatedly been identified as a central defect in ALS (Fulceri *et al.*, 2011; Tashiro *et al.*, 2012b). Our screens in our yeast model reinforce this as almost every pathway identified (vesicle trafficking, autophagy, ion sequestration) intersected with vacuolar health. In mammalian cells, these processes correspond to lysosomal clearance, receptor trafficking, and endosomal signalling (Staudt, Puissant and Boonen, 2016). Therapeutically, agents that restore lysosomal acidification or improve autophagic flux are of particular interest e.g. trehalose has shown promise as an mTOR-independent autophagy inducer (X. Zhang *et al.*, 2014; Wang and Ren, 2016), and more potent small molecule enhancers of lysosomal biogenesis are in development (Kuo *et al.*, 2015; Xue, Zhang and Li, 2023). These could be screened in yeast and *C. elegans* Sod1 models before moving to mammalian systems.

Proteopathy is a second major theme. Misfolded Sod1 can lead to aggregations that strain clearance systems and sequester cellular machinery (Fujikake, Shin and Shimizu, 2018; Amin *et al.*, 2020). Our finding that butyrate, a natural HDAC inhibitor, reduced Sod1 aggregation points to HDAC inhibition as viable route. Several HDAC inhibitors are already clinically approved (Vorinostat, Panobinostat, valproic acid (VPA)) or being trialled in neurodegeneration studies (Didonna and Opal, 2015; Markowicz-Piasecka *et al.*, 2025). These could be tested alone or in combination with dietary strategies that increase SCFAs,

e.g. high-fibre diets, fermented foods or supplementation with phenylbutyrate- which is already trialled in ALS, often in combination with taurursodiol (Paganoni *et al.*, 2020). Yeast models provide a platform to assess whether HDAC inhibition improves proteostasis, whilst worms and human cell systems can test effects on aggregation and survival.

Calcium stress represents another conserved vulnerability. In yeast, defective calcineurin signalling mirrored the calcium overload and impaired homeostasis present in ALS neurons (Williams *et al.*, 1997; Shaw and Eggett, 2000; Van Den Bosch *et al.*, 2000; Guatteo *et al.*, 2007). Pharmacological stabilisers of calcium handling like riluzole (which is already approved, partly acting via sodium/calcium channel modulation) (Hollingworth *et al.*, 2024), or more targeted agents like AMPA receptor antagonists (e.g. perampanel) (Akamatsu *et al.*, 2016, 2022; Patai *et al.*, 2017) or mitochondrial calcium uniporter modulators (Di Marco *et al.*, 2020; Rodríguez *et al.*, 2022) could be explored in parallel with strategies to restore calcineurin activity. Pre-clinically, yeast provides a screen for compounds that rescue calcineurin-Crz1 signalling, while mammalian models can investigate whether these compounds decrease excitotoxic injury seen in ALS neurons.

Finally, microbiome contributions add a systemic dimension. ALS patients show reduced abundance of butyrate-producing bacteria and evidence of fungal dysbiosis (Rowin *et al.*, 2017; Fournier *et al.*, 2020; Niccolai *et al.*, 2021). Our data suggest that loss of microbial butyrate not only deprives neurons of a metabolite that can supress aggregations, but also exacerbates vacuolar and calcineurin dysfunction. This opens two complementary therapeutic options: dietary/microbial interventions (prebiotics, probiotics, microbiota transfer) to restore SCFA levels (Kaul *et al.*, 2024; Noor Eddin *et al.*, 2024), and antifungal or microbiome-modulating approaches to correct gut mycobiome imbalance (T. Zhang *et al.*,

2025). For example, combining sodium phenylbutyrate (a systemic analogue already in ALS trials (see above)) with targeted probiotic consortia (Hong *et al.*, 2023) could provide a rational and translational pipeline.

Together, these findings emphasise that ALS should not be approached as a single-pathway disease. Instead, the future therapeutic impact likely lies in combinatorial strategies e.g. combining an HDAC inhibitor with a calcium stabiliser and a microbiome-directed therapy. The pre-clinical models developed here (yeast, nematodes, and human cell systems) offer a strong discovery pipeline for such interventions, providing a platform to test multi-agent strategies before they progress to mammalian models and ultimately to clinical trials.

7. Limitations

Whilst the yeast, worm, and cell-based models used here were instrumental in discovering conserved mechanisms relevant to ALS, several limitations remain. Yeast and worms are highly simplified compared to mammalian neurons, and controlled laboratory set-ups are too simple to mirror the complex and diverse microbial ecosystems in patients. Effects of butyrate on Candida virulence *in vitro* may not directly translate to the gut environment, where systemic outcomes are influenced by metabolite gradients and microbial competition. However, these models are highly genetically tractable and contain conserved core pathways allowing for exploring mechanisms in detail that can later be validated in more complex systems.

Looking forward, these limitations suggest some refinements. One improvement would be the use of advanced gut model systems for instance, co-culture platforms combining key bacterial species (e.g. *lactobacillus*), fungal communities, and epithelial cells expressing $Sod1^{A4V}$ or other ALS mutations. Such systems could replicate butyrate production and its roles under physiologically relevant conditions e.g. acidic vs. neutral pH and allow for direct readouts of cell responses like barrier integrity, energy metabolism and Sod1 aggregation. Similarly, mammalian organ models or gnotobiotic mouse systems could better capture the interplay between microbial metabolites, host signalling, and neurodegeneration. Finally, scaling from simple to complex models (from yeast screens to gut-cell systems to mammalian models) would provide a pipeline that improves translational relevance.

8. Concluding remarks

This thesis supports a model of ALS as a multi-system disorder of homeostasis. Misfolded Sod1 destabilises vacuolar/lysosomal function, autophagy, metabolic signalling, and calcium regulation, while microbiome disturbances deprive the host of protective metabolites such as butyrate and allows expansion of opportunistic fungi. Our findings highlight that preserving neuronal health in ALS requires a coordinated, multi-layered therapeutic approach. Insights from simple eukaryotes and microbial models are invaluable in guiding the design of combinatorial strategies that address both the neuronal and systemic dimensions of ALS pathology. The yeast model offers a powerful mechanistic framework and a platform for screening compounds that enhance vacuolar acidification or calcineurin activity, while the *C. elegans* and human cell systems validate butyrate as a modulator of protein aggregation, metabolism, and fungal virulence. Collectively, these results show that preserving cellular and microbial homeostasis in the face of misfolded protein stress is a multi-faceted challenge spanning metabolism, protein clearance, ion regulation, and host–microbe interactions. This integrative perspective points toward combinatorial therapeutic strategies that target both neuronal pathways and gut microbial imbalance in ALS. Previous ALS clinical trials highlight the limited efficacy of monotherapies but suggest promise for rational combinations. AMX0035 (sodium phenylbutyrate and taurursodiol) showed benefits in early studies (Paganoni *et al.*, 2020), although subsequent phase 3 results were negative (Höglinger *et al.*, 2024). Other combinations under investigation, such as immune-modulatory regimes (Thonhoff *et al.*, 2024; Bensimon *et al.*, 2025) or rational drug pairings identified by computational approaches (S. Y. Lee *et al.*, 2023; Salomon-Zimri *et al.*, 2023), underscore the current momentum towards multi-target interventions. Yet no trial to date

has deliberately paired HDAC inhibition with microbiome management. Given the dual identity of butyrate as both microbial metabolite and HDAC inhibitor, this represents a compelling opportunity. Pre-clinical evidence already suggests synergy between butyrate supplementation and riluzole (Y. Zhang *et al.*, 2025), raising the possibility that restoring microbial SCFA production alongside pharmacological HDAC inhibition could provide complementary benefits. Future work should test whether combining selective HDAC inhibitors e.g. HDAC6-targeted compounds with microbiome interventions or dietary strategies can enhance proteostasis, reduce calcium stress, and stabilise metabolic function (d'Ydewalle *et al.*, 2011; Paganoni *et al.*, 2021). Beyond HDAC-based strategies, two other mechanistic streams highlighted here deserve further exploration. First, calcium regulation and metabolic resilience remain central themes in ALS. The yeast findings of impaired calcineurin and calcium signalling match neuronal data, suggesting that agents which stabilise calcium homeostasis such as riluzole, perampanel or experimental mitochondrial calcium uniporter modulators should be considered in tandem with metabolic interventions (AMPK activators, NAD+ boosters, or autophagy enhancers). Such combinations could be screened in preclinical models for their ability to preserve mitochondrial function, support energy balance, and mitigate Sod1 aggregation. Second, the interplay between fungal and bacterial members of the microbiome requires deeper investigation. Our results indicate that fungal virulence is influenced by both butyrate availability and local pH, yet in the host this occurs within a complex ecosystem of competing bacteria. Future models should incorporate mixed microbial communities, epithelial barriers, and variable nutrient conditions to assess how bacterial-fungal interactions shape host proteostasis, barrier integrity, and immune activation.

In summary, this thesis emphasises that preserving cellular and microbial homeostasis in

ALS is a multifaceted challenge that required integrative strategies. By situating $Sod1^{A4V}$ toxcitiy within wider contexts of metabolism, calcium regulation and host-microbe interactions, these findings open paths for developing therapeutic combinations. The convergence of epigenetic modulation, metabolic balance, and microbiome management remains an underexplored but promising frontier for future ALS therapy.

References:

Agbas, A. *et al.* (2007) 'Activation of brain calcineurin (Cn) by Cu-Zn superoxide dismutase (SOD1) depends on direct SOD1–Cn protein interactions occurring in vitro and in vivo', *Biochemical Journal*, 405(1), pp. 51–59. doi: 10.1042/BJ20061202.

Agostinho, P. *et al.* (2008) 'Overactivation of calcineurin induced by amyloid-beta and prion proteins', *Neurochemistry International*, 52(6), pp. 1226–1233. doi: 10.1016/j.neuint.2008.01.005.

Ait-Belgnaoui, A. *et al.* (2012) 'Prevention of gut leakiness by a probiotic treatment leads to attenuated HPA response to an acute psychological stress in rats', *Psychoneuroendocrinology*, 37(11), pp. 1885–1895. doi: 10.1016/j.psyneuen.2012.03.024.

Akamatsu, M. *et al.* (2016) 'The AMPA receptor antagonist perampanel robustly rescues amyotrophic lateral sclerosis (ALS) pathology in sporadic ALS model mice', *Scientific Reports*, 6(1), p. 28649. doi: 10.1038/srep28649.

Akamatsu, M. *et al.* (2022) 'Testing of the therapeutic efficacy and safety of AMPA receptor RNA aptamers in an ALS mouse model', *Life Science Alliance*, 5(4), p. e202101193. doi: 10.26508/lsa.202101193.

Al-Chalabi, A. *et al.* (2014) 'Analysis of amyotrophic lateral sclerosis as a multistep process: a population-based modelling study', *The Lancet Neurology*, 13(11), pp. 1108–1113. doi: 10.1016/S1474-4422(14)70219-4.

Al-Dhaheri, R. S. and Douglas, L. J. (2010) 'Apoptosis in Candida biofilms exposed to amphotericin B', *Journal of Medical Microbiology*, 59(2), pp. 149–157. doi: 10.1099/jmm.0.015784-0.

Alexianu, M. E. *et al.* (1994) 'The role of calcium-binding proteins in selective motoneuron vulnerability in amyotrophic lateral sclerosis', *Annals of Neurology*, 36(6), pp. 846–858. doi: 10.1002/ana.410360608.

Alonso, R. *et al.* (2017) 'Fungal infection in neural tissue of patients with amyotrophic lateral sclerosis', *Neurobiology of Disease*, 108, pp. 249–260. doi: 10.1016/j.nbd.2017.09.001.

Alonso, R., Pisa, D. and Carrasco, L. (2019) 'Searching for Bacteria in Neural Tissue From Amyotrophic Lateral Sclerosis', *Frontiers in Neuroscience*, 13. doi: 10.3389/fnins.2019.00171.

Alshannaq, A. and Yu, J.-H. (2017) 'Occurrence, Toxicity, and Analysis of Major Mycotoxins in Food', *International Journal of Environmental Research and Public Health*, 14(6), p. 632. doi: 10.3390/ijerph14060632.

Altarejos, J. Y. and Montminy, M. (2011) 'CREB and the CRTC co-activators: sensors for hormonal and metabolic signals', *Nature Reviews Molecular Cell Biology*, 12(3), pp. 141–151. doi: 10.1038/nrm3072.

Amick, J., Roczniak-Ferguson, A. and Ferguson, S. M. (2016) 'C9orf72 binds SMCR8, localizes to lysosomes, and regulates mTORC1 signaling', *Molecular Biology of the Cell*. Edited by J. Brill, 27(20), pp. 3040–3051. doi: 10.1091/mbc.e16-01-0003.

Amigoni, L., Martegani, E. and Colombo, S. (2013) 'Lack of HXK2 Induces Localization of Active Ras in Mitochondria and Triggers Apoptosis in the Yeast Saccharomyces cerevisiae', *Oxidative Medicine and Cellular Longevity*, 2013, pp. 1–10. doi: 10.1155/2013/678473.

Amin, A. *et al.* (2020) 'Amyotrophic Lateral Sclerosis and Autophagy: Dysfunction and Therapeutic Targeting', *Cells*, 9(11), p. 2413. doi: 10.3390/cells9112413.

An, H. *et al.* (2019) 'ALS-linked FUS mutations confer loss and gain of function in the nucleus by promoting excessive formation of dysfunctional paraspeckles', *Acta Neuropathologica Communications*, 7(1), p. 7. doi: 10.1186/s40478-019-0658-x.

Andersen, P. M. (2006) 'Amyotrophic lateral sclerosis associated with mutations in the CuZn superoxide dismutase gene', *Current Neurology and Neuroscience Reports*, 6(1), pp. 37–46. doi: 10.1007/s11910-996-0008-9.

Andrusaite, A. *et al.* (2024) 'Microbiota-derived butyrate inhibits cDC development via HDAC inhibition, diminishing their ability to prime T cells', *Mucosal Immunology*. doi: 10.1016/j.mucimm.2024.08.003.

Aoki, Y. *et al.* (2017) 'C9orf72 and RAB7L1 regulate vesicle trafficking in amyotrophic lateral sclerosis and frontotemporal dementia', *Brain*, 140(4), pp. 887–897. doi:

10.1093/brain/awx024.

Arai, T. *et al.* (2006) 'TDP-43 is a component of ubiquitin-positive tau-negative inclusions in frontotemporal lobar degeneration and amyotrophic lateral sclerosis', *Biochemical and Biophysical Research Communications*, 351(3), pp. 602–611. doi: 10.1016/j.bbrc.2006.10.093.

Archer, S. *et al.* (1998) 'Butyrate inhibits colon carcinoma cell growth through two distinct pathways.', *Surgery*, 124(2), pp. 248–53. Available at: http://www.ncbi.nlm.nih.gov/pubmed/9706145.

Archer, S. Y. *et al.* (1998) 'p21 WAF1 is required for butyrate-mediated growth inhibition of human colon cancer cells', *Proceedings of the National Academy of Sciences*, 95(12), pp. 6791–6796. doi: 10.1073/pnas.95.12.6791.

Armstrong, D. L. (1989) 'Calcium channel regulation by calcineurin, a Ca2+-activated phosphatase in mammalian brain', *Trends in Neurosciences*, 12(3), pp. 117–122. doi: 10.1016/0166-2236(89)90168-9.

Arnesano, F. *et al.* (2004) 'The Unusually Stable Quaternary Structure of Human Cu,Zn-Superoxide Dismutase 1 Is Controlled by Both Metal Occupancy and Disulfide Status', *Journal of Biological Chemistry*, 279(46), pp. 47998–48003. doi: 10.1074/jbc.M406021200.

Arnold, F. J. *et al.* (2024) 'Revisiting Glutamate Excitotoxicity in Amyotrophic Lateral Sclerosis and Age-Related Neurodegeneration', *International Journal of Molecular Sciences*, 25(11), p. 5587. doi: 10.3390/ijms25115587.

Ash, P. E. A. *et al.* (2013) 'Unconventional Translation of C9ORF72 GGGGCC Expansion Generates Insoluble Polypeptides Specific to c9FTD/ALS', *Neuron*, 77(4), pp. 639–646. doi: 10.1016/j.neuron.2013.02.004.

Askwith, C. and Kaplan, J. (1998) 'Iron and copper transport in yeast and its relevance to human disease', *Trends in Biochemical Sciences*, 23(4), pp. 135–138. doi: 10.1016/S0968-0004(98)01192-X.

Atkin, J. D. *et al.* (2008) 'RETRACTED: Endoplasmic reticulum stress and induction of the unfolded protein response in human sporadic amyotrophic lateral sclerosis', *Neurobiology*

of Disease, 30(3), pp. 400–407. doi: 10.1016/j.nbd.2008.02.009.

Atkin, J. D. *et al.* (2014) 'Mutant <scp>SOD</scp> 1 inhibits <scp>ER</scp> -Golgi transport in amyotrophic lateral sclerosis', *Journal of Neurochemistry*, 129(1), pp. 190–204. doi: 10.1111/jnc.12493.

Atsumi, T. (1981) 'The ultrastructure of intramuscular nerves in amyotrophic lateral sclerosis', *Acta Neuropathologica*, 55(3), pp. 193–198. doi: 10.1007/BF00691318.

Ayala, V. *et al.* (2011) 'Cell stress induces TDP-43 pathological changes associated with ERK1/2 dysfunction: implications in ALS', *Acta Neuropathologica*, 122(3), pp. 259–270. doi: 10.1007/s00401-011-0850-y.

Balaban, R. S. (2002) 'Cardiac Energy Metabolism Homeostasis: Role of Cytosolic Calcium', *Journal of Molecular and Cellular Cardiology*, 34(10), pp. 1259–1271. doi: 10.1006/jmcc.2002.2082.

Ballan, R. *et al.* (2020) 'Interactions of probiotics and prebiotics with the gut microbiota', in, pp. 265–300. doi: 10.1016/bs.pmbts.2020.03.008.

Bambach, A. *et al.* (2009) 'Goa1p of Candida albicans Localizes to the Mitochondria during Stress and Is Required for Mitochondrial Function and Virulence', *Eukaryotic Cell*, 8(11), pp. 1706–1720. doi: 10.1128/EC.00066-09.

Banci, L. *et al.* (2002) 'The solution structure of reduced dimeric copper zinc superoxide dismutase', *European Journal of Biochemistry*, 269(7), pp. 1905–1915. doi: 10.1046/j.1432-1033.2002.02840.x.

Banerjee, R. *et al.* (eds) (2007) *Redox Biochemistry*. Wiley. doi: 10.1002/9780470177334.

Baskoylu, S. N. *et al.* (2018) 'Single copy/knock-in models of ALS SOD1 in C. elegans suggest loss and gain of function have different contributions to cholinergic and glutamatergic neurodegeneration', *PLOS Genetics*. Edited by G. S. Barsh, 14(10), p. e1007682. doi: 10.1371/journal.pgen.1007682.

Bastow, E. L. *et al.* (2016) 'New links between SOD1 and metabolic dysfunction from a yeast model of amyotrophic lateral sclerosis', *Journal of Cell Science*, 129(21), pp. 4118–4129. doi: 10.1242/jcs.190298.

Bastow, E. L., Gourlay, C. W. and Tuite, M. F. (2011) 'Using yeast models to probe the molecular basis of amyotrophic lateral sclerosis', *Biochemical Society Transactions*, 39(5), pp. 1482–1487. doi: 10.1042/BST0391482.

Batiza, A. F., Schulz, T. and Masson, P. H. (1996) 'Yeast Respond to Hypotonic Shock with a Calcium Pulse', *Journal of Biological Chemistry*, 271(38), pp. 23357–23362. doi: 10.1074/jbc.271.38.23357.

Beau, J. *et al.* (2012) 'Epigenetic Tailoring for the Production of Anti-Infective Cytosporones from the Marine Fungus Leucostoma persoonii', *Marine Drugs*, 10(12), pp. 762–774. doi: 10.3390/md10040762.

Beers, D. R. *et al.* (2008) 'Parvalbumin overexpression alters immune-mediated increases in intracellular calcium, and delays disease onset in a transgenic model of familial amyotrophic lateral sclerosis', *Journal of Neurochemistry*, 79(3), pp. 499–509. doi: 10.1046/j.1471-4159.2001.00582.x.

Bennett, S. A. *et al.* (2021) 'Trichostatin A Relieves Growth Suppression and Restores Histone Acetylation at Specific Sites in a FUS ALS/FTD Yeast Model', *Biochemistry*, 60(48), pp. 3671–3675. doi: 10.1021/acs.biochem.1c00455.

Bensimon, G. *et al.* (2025) 'Efficacy and safety of low-dose IL-2 as an add-on therapy to riluzole (MIROCALS): a phase 2b, double-blind, randomised, placebo-controlled trial', *The Lancet*, 405(10492), pp. 1837–1850. doi: 10.1016/S0140-6736(25)00262-4.

Berdyński, M. *et al.* (2022) 'SOD1 mutations associated with amyotrophic lateral sclerosis analysis of variant severity', *Scientific Reports*, 12(1), p. 103. doi: 10.1038/s41598-021-03891-8.

Berman, J. and Sudbery, P. E. (2002) 'Candida albicans: A molecular revolution built on lessons from budding yeast', *Nature Reviews Genetics*, 3(12), pp. 918–931. doi: 10.1038/nrg948.

Bernardi, P. and Petronilli, V. (1996) 'The permeability transition pore as a mitochondrial calcium release channel: A critical appraisal', *Journal of Bioenergetics and Biomembranes*, 28(2), pp. 131–138. doi: 10.1007/BF02110643.

Berni Canani, R. *et al.* (2004) 'Butyrate as an effective treatment of congenital chloride diarrhea', *Gastroenterology*, 127(2), pp. 630–634. doi: 10.1053/j.gastro.2004.03.071.

den Besten, G. *et al.* (2013) 'The role of short-chain fatty acids in the interplay between diet, gut microbiota, and host energy metabolism', *Journal of Lipid Research*, 54(9), pp. 2325–2340. doi: 10.1194/jlr.R036012.

Bhandari, R., Kuhad, A. and Kuhad, A. (2018) 'Edaravone: a new hope for deadly amyotrophic lateral sclerosis', *Drugs of Today*, 54(6), p. 349. doi: 10.1358/dot.2018.54.6.2828189.

Bianchi, V. E., Herrera, P. F. and Laura, R. (2021) 'Effect of nutrition on neurodegenerative diseases. A systematic review', *Nutritional Neuroscience*, 24(10), pp. 810–834. doi: 10.1080/1028415X.2019.1681088.

Biddle, A. *et al.* (2013) 'Untangling the Genetic Basis of Fibrolytic Specialization by Lachnospiraceae and Ruminococcaceae in Diverse Gut Communities', *Diversity*, 5(3), pp. 627–640. doi: 10.3390/d5030627.

Bienert, G. P., Schjoerring, J. K. and Jahn, T. P. (2006) 'Membrane transport of hydrogen peroxide', *Biochimica et Biophysica Acta (BBA) - Biomembranes*, 1758(8), pp. 994–1003. doi: 10.1016/j.bbamem.2006.02.015.

Billingsley, M. L. *et al.* (1990) '[53] Identification of calmodulin-binding proteins', in, pp. 451–467. doi: 10.1016/0076-6879(90)84307-3.

Binda, M. *et al.* (2009) 'The Vam6 GEF Controls TORC1 by Activating the EGO Complex', *Molecular Cell*, 35(5), pp. 563–573. doi: 10.1016/j.molcel.2009.06.033.

Biswas, S., Van Dijck, P. and Datta, A. (2007) 'Environmental Sensing and Signal Transduction Pathways Regulating Morphopathogenic Determinants of Candida albicans', *Microbiology and Molecular Biology Reviews*, 71(2), pp. 348–376. doi: 10.1128/MMBR.00009-06.

Bito, H., Deisseroth, K. and Tsien, R. W. (1996) 'CREB Phosphorylation and Dephosphorylation: A Ca2+- and Stimulus Duration–Dependent Switch for Hippocampal Gene Expression', *Cell*, 87(7), pp. 1203–1214. doi: 10.1016/S0092-8674(00)81816-4.

Blacher, E. *et al.* (2019) 'Potential roles of gut microbiome and metabolites in modulating

ALS in mice', *Nature*, 572(7770), pp. 474–480. doi: 10.1038/s41586-019-1443-5.

Bleackley, M. R. and MacGillivray, R. T. A. (2011) 'Transition metal homeostasis: from yeast to human disease', *BioMetals*, 24(5), pp. 785–809. doi: 10.1007/s10534-011-9451-4.

Block, K. *et al.* (2008) 'Nox4 NAD(P)H Oxidase Mediates Src-dependent Tyrosine Phosphorylation of PDK-1 in Response to Angiotensin II', *Journal of Biological Chemistry*, 283(35), pp. 24061–24076. doi: 10.1074/jbc.M803964200.

Boddy, S. L. *et al.* (2021) 'The gut microbiome: a key player in the complexity of amyotrophic lateral sclerosis (ALS)', *BMC Medicine*, 19(1), p. 13. doi: 10.1186/s12916-020-01885-3.

Boehning, D. *et al.* (2003) 'Cytochrome c binds to inositol (1,4,5) trisphosphate receptors, amplifying calcium-dependent apoptosis', *Nature Cell Biology*, 5(12), pp. 1051–1061. doi: 10.1038/ncb1063.

Boehning, D., Patterson, R. L. and Snyder, S. H. (2004) 'Apoptosis and calcium: new roles for cytochrome c and inositol 1,4,5-trisphosphate.', *Cell cycle (Georgetown, Tex.)*, 3(3), pp. 252–4. Available at: http://www.ncbi.nlm.nih.gov/pubmed/14726673.

Boll, M.-C. *et al.* (2022) 'A phase 2, double-blind, placebo-controlled trial of a valproate/lithium combination in ALS patients', *Neurología (English Edition)*. doi: 10.1016/j.nrleng.2022.07.003.

Bolognini, D. *et al.* (2016) 'The Pharmacology and Function of Receptors for Short-Chain Fatty Acids', *Molecular Pharmacology*, 89(3), pp. 388–398. doi: 10.1124/mol.115.102301.

Bonawitz, N. D. *et al.* (2007) 'Reduced TOR Signaling Extends Chronological Life Span via Increased Respiration and Upregulation of Mitochondrial Gene Expression', *Cell Metabolism*, 5(4), pp. 265–277. doi: 10.1016/j.cmet.2007.02.009.

Bonifacino, T. *et al.* (2021) 'Nearly 30 Years of Animal Models to Study Amyotrophic Lateral Sclerosis: A Historical Overview and Future Perspectives', *International Journal of Molecular Sciences*, 22(22), p. 12236. doi: 10.3390/ijms222212236.

Bonilla, M. (2002) 'Essential role of calcineurin in response to endoplasmic reticulum stress', *The EMBO Journal*, 21(10), pp. 2343–2353. doi: 10.1093/emboj/21.10.2343.

Van Den Bosch, L. *et al.* (2000) 'Ca2+-permeable AMPA receptors and selective vulnerability

of motor neurons', *Journal of the Neurological Sciences*, 180(1–2), pp. 29–34. doi: 10.1016/S0022-510X(00)00414-7.

Van Den Bosch, L. *et al.* (2006) 'The role of excitotoxicity in the pathogenesis of amyotrophic lateral sclerosis', *Biochimica et Biophysica Acta (BBA) - Molecular Basis of Disease*, 1762(11–12), pp. 1068–1082. doi: 10.1016/j.bbadis.2006.05.002.

Bosco, D. A. *et al.* (2010) 'Wild-type and mutant SOD1 share an aberrant conformation and a common pathogenic pathway in ALS', *Nature Neuroscience*, 13(11), pp. 1396–1403. doi: 10.1038/nn.2660.

Botstein, D. and Fink, G. R. (2011) 'Yeast: An Experimental Organism for 21st Century Biology', *Genetics*, 189(3), pp. 695–704. doi: 10.1534/genetics.111.130765.

Boustany, L. M. and Cyert, M. S. (2002) 'Calcineurin-dependent regulation of Crz1p nuclear export requires Msn5p and a conserved calcineurin docking site', *Genes & Development*, 16(5), pp. 608–619. doi: 10.1101/gad.967602.

Bouteloup, C. *et al.* (2009) 'Hypermetabolism in ALS patients: an early and persistent phenomenon', *Journal of Neurology*, 256(8), pp. 1236–1242. doi: 10.1007/s00415-009-5100-z.

Boya, P. *et al.* (2005) 'Inhibition of Macroautophagy Triggers Apoptosis', *Molecular and Cellular Biology*, 25(3), pp. 1025–1040. doi: 10.1128/MCB.25.3.1025-1040.2005.

Bradford, H. F., Norris, P. J. and Smith, C. C. (1990) 'Changes in transmitter release patterns in vitro induced by tremorgenic mycotoxins.', *Journal of environmental pathology, toxicology and oncology : official organ of the International Society for Environmental Toxicology and Cancer*, 10(1–2), pp. 17–30. Available at: http://www.ncbi.nlm.nih.gov/pubmed/1977902.

Brahe, L. K., Astrup, A. and Larsen, L. H. (2013) 'Is butyrate the link between diet, intestinal microbiota and obesity-related metabolic diseases?', *Obesity Reviews*, 14(12), pp. 950–959. doi: 10.1111/obr.12068.

Brasil, A. A. *et al.* (2013) 'The involvement of GSH in the activation of human Sod1 linked to FALS in chronologically aged yeast cells', *FEMS Yeast Research*, 13(5), pp. 433–440. doi:

10.1111/1567-1364.12045.

Bravo-Sagua, R. *et al.* (2017) 'Calcium Transport and Signaling in Mitochondria', in *Comprehensive Physiology*. Wiley, pp. 623–634. doi: 10.1002/cphy.c160013.

Brenner, S. (1974) 'THE GENETICS OF CAENORHABDITIS ELEGANS', *Genetics*, 77(1), pp. 71–94. doi: 10.1093/genetics/77.1.71.

Brody, H. (2020) 'The gut microbiome', *Nature*, 577(7792), pp. S5–S5. doi: 10.1038/d41586-020-00194-2.

Brookes, P. and Darley-Usmar, V. M. (2002) 'Hypothesis: the mitochondrial NO• signaling pathway, and the transduction of nitrosative to oxidative cell signals: an alternative function for cytochrome C oxidase', *Free Radical Biology and Medicine*, 32(4), pp. 370–374. doi: 10.1016/S0891-5849(01)00805-X.

Brookes, P. S. *et al.* (2004) 'Calcium, ATP, and ROS: a mitochondrial love-hate triangle', *American Journal of Physiology-Cell Physiology*, 287(4), pp. C817–C833. doi: 10.1152/ajpcell.00139.2004.

Broom, H. R. *et al.* (2015) 'Destabilization of the dimer interface is a common consequence of diverse ALS-associated mutations in metal free SOD1', *Protein Science*, 24(12), pp. 2081–2089. doi: 10.1002/pro.2803.

Broom, W. J. *et al.* (2006) 'Variants in candidate ALS modifier genes linked to Cu/Zn superoxide dismutase do not explain divergent survival phenotypes', *Neuroscience Letters*, 392(1–2), pp. 52–57. doi: 10.1016/j.neulet.2005.08.058.

Brown, R. H. and Al-Chalabi, A. (2017) 'Amyotrophic Lateral Sclerosis', *New England Journal of Medicine*. Edited by D. L. Longo, 377(2), pp. 162–172. doi: 10.1056/NEJMra1603471.

Browning, M. *et al.* (2006) 'Potential of butyric acid for control of soil-borne fungal pathogens and nematodes affecting strawberries', *Soil Biology and Biochemistry*, 38(2), pp. 401–404. doi: 10.1016/j.soilbio.2005.05.020.

Bui, T. P. N. *et al.* (2015) 'Production of butyrate from lysine and the Amadori product fructoselysine by a human gut commensal', *Nature Communications*, 6(1), p. 10062. doi: 10.1038/ncomms10062.

Burberry, A. *et al.* (2020) 'C9orf72 suppresses systemic and neural inflammation induced by gut bacteria', *Nature*, 582(7810), pp. 89–94. doi: 10.1038/s41586-020-2288-7.

Burk, K. and Pasterkamp, R. J. (2019) 'Disrupted neuronal trafficking in amyotrophic lateral sclerosis', *Acta Neuropathologica*, 137(6), pp. 859–877. doi: 10.1007/s00401-019-01964-7.

Burley, J. R. and Sihra, T. S. (2000) 'A modulatory role for protein phosphatase 2B (calcineurin) in the regulation of Ca 2+ entry', *European Journal of Neuroscience*, 12(8), pp. 2881–2891. doi: 10.1046/j.1460-9568.2000.00178.x.

Byrne, C. S. *et al.* (2015) 'The role of short chain fatty acids in appetite regulation and energy homeostasis', *International Journal of Obesity*, 39(9), pp. 1331–1338. doi: 10.1038/ijo.2015.84.

Caetano-Silva, M. E. *et al.* (2023) 'Inhibition of inflammatory microglia by dietary fiber and short-chain fatty acids', *Scientific Reports*, 13(1), p. 2819. doi: 10.1038/s41598-022-27086-x.

Cai, L., Dalal, C. K. and Elowitz, M. B. (2008) 'Frequency-modulated nuclear localization bursts coordinate gene regulation', *Nature*, 455(7212), pp. 485–490. doi: 10.1038/nature07292.

Canani, R. B. (2011) 'Potential beneficial effects of butyrate in intestinal and extraintestinal diseases', *World Journal of Gastroenterology*, 17(12), p. 1519. doi: 10.3748/wjg.v17.i12.1519.

Candido, E. (1978) 'Sodium butyrate inhibits histone deacetylation in cultured cells', *Cell*, 14(1), pp. 105–113. doi: 10.1016/0092-8674(78)90305-7.

Carabotti, M. *et al.* (2015) 'The gut-brain axis: Interactions between enteric microbiota, central and enteric nervous systems', *Annals of Gastroenterology*, 28(2), pp. 203–209. Available at: http://www.ncbi.nlm.nih.gov/pubmed/25830558.

Carafoli, E. (1974) 'The release of calcium from heart mitochondria by sodium', *Journal of Molecular and Cellular Cardiology*, 6(4), pp. 361–371. doi: 10.1016/0022-2828(74)90077-7.

Carafoli, E. and Lehninger, A. L. (1971) 'A survey of the interaction of calcium ions with mitochondria from different tissues and species', *Biochemical Journal*, 122(5), pp. 681–690. doi: 10.1042/bj1220681.

Carmona-Gutierrez, D. *et al.* (2018) 'Guidelines and recommendations on yeast cell death nomenclature', *Microbial Cell*, 5(1), pp. 4–31. doi: 10.15698/mic2018.01.607.

Carraro, M. and Bernardi, P. (2016) 'Calcium and reactive oxygen species in regulation of the mitochondrial permeability transition and of programmed cell death in yeast', *Cell Calcium*, 60(2), pp. 102–107. doi: 10.1016/j.ceca.2016.03.005.

Castanedo-Vazquez, D. *et al.* (2019) 'Infectious agents and amyotrophic lateral sclerosis: another piece of the puzzle of motor neuron degeneration', *Journal of Neurology*, 266(1), pp. 27–36. doi: 10.1007/s00415-018-8919-3.

Cavalheiro, M. and Teixeira, M. C. (2018) 'Candida Biofilms: Threats, Challenges, and Promising Strategies', *Frontiers in Medicine*, 5. doi: 10.3389/fmed.2018.00028.

Cerella, C., Diederich, M. and Ghibelli, L. (2010) 'The Dual Role of Calcium as Messenger and Stressor in Cell Damage, Death, and Survival', *International Journal of Cell Biology*, 2010, pp. 1–14. doi: 10.1155/2010/546163.

Chandel, A., Das, K. K. and Bachhawat, A. K. (2016) 'Glutathione depletion activates the yeast vacuolar transient receptor potential channel, Yvc1p, by reversible glutathionylation of specific cysteines', *Molecular Biology of the Cell*. Edited by C. Boone, 27(24), pp. 3913–3925. doi: 10.1091/mbc.E16-05-0281.

Chaves, S. R. *et al.* (2021) 'Regulation of Cell Death Induced by Acetic Acid in Yeasts', *Frontiers in Cell and Developmental Biology*, 9. doi: 10.3389/fcell.2021.642375.

Chawla, S. *et al.* (2023) 'Calcineurin stimulation by Cnb1p overproduction mitigates protein aggregation and α-synuclein toxicity in a yeast model of synucleinopathy', *Cell Communication and Signaling*, 21(1), p. 220. doi: 10.1186/s12964-023-01242-w.

Chen, J.-H. *et al.* (2023) 'Reduced lysosomal density in neuronal dendrites mediates deficits in synaptic plasticity in Huntington's disease', *Cell Reports*, 42(12), p. 113573. doi: 10.1016/j.celrep.2023.113573.

Chen, J., Zhao, K.-N. and Vitetta, L. (2019) 'Effects of Intestinal Microbial–Elaborated Butyrate on Oncogenic Signaling Pathways', *Nutrients*, 11(5), p. 1026. doi: 10.3390/nu11051026.

Chen, S. *et al.* (2012) 'Autophagy Dysregulation in Amyotrophic Lateral Sclerosis', *Brain Pathology*, 22(1), pp. 110–116. doi: 10.1111/j.1750-3639.2011.00546.x.

Chen, T. *et al.* (2002) 'Histone acetylation is involved in hsp70 gene transcription regulation in Drosophila melanogaster', *Archives of Biochemistry and Biophysics*, 408(2), pp. 171–176. doi: 10.1016/S0003-9861(02)00564-7.

Chen, Y. and Klionsky, D. J. (2011) 'The regulation of autophagy – unanswered questions', *Journal of Cell Science*, 124(2), pp. 161–170. doi: 10.1242/jcs.064576.

Chen, Y., Scarcelli, V. and Legouis, R. (2017) 'Approaches for Studying Autophagy in Caenorhabditis elegans', *Cells*, 6(3), p. 27. doi: 10.3390/cells6030027.

Chew, Y. L. *et al.* (2017) 'Recordings of Caenorhabditis elegans locomotor behaviour following targeted ablation of single motorneurons', *Scientific Data*, 4(1), p. 170156. doi: 10.1038/sdata.2017.156.

Ching, J. K. and Weihl, C. C. (2013) 'Rapamycin-induced autophagy aggravates pathology and weakness in a mouse model of VCP-associated myopathy', *Autophagy*, 9(5), pp. 799–800. doi: 10.4161/auto.23958.

Choi, S. Y. *et al.* (2019) 'C9ORF72-ALS/FTD-associated poly(GR) binds Atp5a1 and compromises mitochondrial function in vivo', *Nature Neuroscience*, 22(6), pp. 851–862. doi: 10.1038/s41593-019-0397-0.

Chua, J. P. *et al.* (2022) 'Autophagy and ALS: mechanistic insights and therapeutic implications', *Autophagy*, 18(2), pp. 254–282. doi: 10.1080/15548627.2021.1926656.

Chung, M. J. and Suh, Y.-L. (2002) 'Ultrastructural Changes of Mitochondria in the Skeletal Muscle of Patients with Amyotrophic Lateral Sclerosis', *Ultrastructural Pathology*, 26(1), pp. 3–7. doi: 10.1080/01913120252934260.

Coffey, E. E. *et al.* (2014) 'Lysosomal alkalization and dysfunction in human fibroblasts with the Alzheimer's disease-linked presenilin 1 A246E mutation can be reversed with cAMP', *Neuroscience*, 263, pp. 111–124. doi: 10.1016/j.neuroscience.2014.01.001.

Conlon, M. and Bird, A. (2014) 'The Impact of Diet and Lifestyle on Gut Microbiota and Human Health', *Nutrients*, 7(1), pp. 17–44. doi: 10.3390/nu7010017.

Connolly, S. *et al.* (2018) 'Calcineurin Regulatory Subunit Calcium-Binding Domains Differentially Contribute to Calcineurin Signaling in Saccharomyces cerevisiae', *Genetics*, 209(3), pp. 801–813. doi: 10.1534/genetics.118.300911.

Conway, J. and A Duggal, N. (2021) 'Ageing of the gut microbiome: Potential influences on immune senescence and inflammageing', *Ageing Research Reviews*, 68, p. 101323. doi: 10.1016/j.arr.2021.101323.

Corcia, P. *et al.* (2008) 'Causes of death in a post-mortem series of ALS patients', *Amyotrophic Lateral Sclerosis*, 9(1), pp. 59–62. doi: 10.1080/17482960701656940.

Cordeiro, R. de A. *et al.* (2019) 'Sodium butyrate inhibits planktonic cells and biofilms of Trichosporon spp.', *Microbial Pathogenesis*, 130, pp. 219–225. doi: 10.1016/j.micpath.2019.03.013.

Cottier, F. and Hall, R. A. (2020) 'Face/Off: The Interchangeable Side of Candida Albicans', *Frontiers in Cellular and Infection Microbiology*, 9. doi: 10.3389/fcimb.2019.00471.

Cox, G. M. *et al.* (2003) 'Superoxide Dismutase Influences the Virulence of Cryptococcus neoformans by Affecting Growth within Macrophages', *Infection and Immunity*, 71(1), pp. 173–180. doi: 10.1128/IAI.71.1.173-180.2003.

Cox, L. M. *et al.* (2022) 'The microbiota restrains neurodegenerative microglia in a model of amyotrophic lateral sclerosis', *Microbiome*, 10(1), p. 47. doi: 10.1186/s40168-022-01232-z.

Cox, P. A., Banack, S. A. and Murch, S. J. (2003) 'Biomagnification of cyanobacterial neurotoxins and neurodegenerative disease among the Chamorro people of Guam', *Proceedings of the National Academy of Sciences*, 100(23), pp. 13380–13383. doi: 10.1073/pnas.2235808100.

Cozzolino, M. and Carrì, M. T. (2012) 'Mitochondrial dysfunction in ALS', *Progress in Neurobiology*, 97(2), pp. 54–66. doi: 10.1016/j.pneurobio.2011.06.003.

Crozat, A. *et al.* (1993) 'Fusion of CHOP to a novel RNA-binding protein in human myxoid liposarcoma', *Nature*, 363(6430), pp. 640–644. doi: 10.1038/363640a0.

Crugnola, V. *et al.* (2010) 'Mitochondrial Respiratory Chain Dysfunction in Muscle From Patients With Amyotrophic Lateral Sclerosis', *Archives of Neurology*, 67(7). doi:

10.1001/archneurol.2010.128.

Csordas, A. (1996) 'Butyrate, aspirin and colorectal cancer', *European Journal of Cancer Prevention*, 5(4), pp. 221–231. doi: 10.1097/00008469-199608000-00002.

Cuajungco, M. P. and Lees, G. J. (1997) 'Zinc Metabolism in the Brain: Relevance to Human Neurodegenerative Disorders', *Neurobiology of Disease*, 4(3–4), pp. 137–169. doi: 10.1006/nbdi.1997.0163.

Cui, J., Kaandorp, J. A., Sloot, P. M. A., *et al.* (2009) 'Calcium homeostasis and signaling in yeast cells and cardiac myocytes', *FEMS Yeast Research*, 9(8), pp. 1137–1147. doi: 10.1111/j.1567-1364.2009.00552.x.

Cui, J., Kaandorp, J. A., Ositelu, O. O., *et al.* (2009) 'Simulating calcium influx and free calcium concentrations in yeast', *Cell Calcium*, 45(2), pp. 123–132. doi: 10.1016/j.ceca.2008.07.005.

Cunningham, K. and Fink, G. (1994) 'Calcineurin-dependent growth control in Saccharomyces cerevisiae mutants lacking PMC1, a homolog of plasma membrane Ca2+ ATPases', *The Journal of cell biology*, 124(3), pp. 351–363. doi: 10.1083/jcb.124.3.351.

Cunningham, K. W. and Fink, G. R. (1994) 'Ca2+ Transport in Saccharomyces Cerevisiae', *Journal of Experimental Biology*, 196(1), pp. 157–166. doi: 10.1242/jeb.196.1.157.

Cyert, M. S. *et al.* (1991) 'Yeast has homologs (CNA1 and CNA2 gene products) of mammalian calcineurin, a calmodulin-regulated phosphoprotein phosphatase.', *Proceedings of the National Academy of Sciences*, 88(16), pp. 7376–7380. doi: 10.1073/pnas.88.16.7376.

Cyert, M. S. and Philpott, C. C. (2013) 'Regulation of Cation Balance in Saccharomyces cerevisiae', *Genetics*, 193(3), pp. 677–713. doi: 10.1534/genetics.112.147207.

Cyert, M. S. and Thorner, J. (1992) 'Regulatory subunit (CNB1 gene product) of yeast Ca2+/calmodulin-dependent phosphoprotein phosphatases is required for adaptation to pheromone.', *Molecular and Cellular Biology*, 12(8), pp. 3460–3469. doi: 10.1128/MCB.12.8.3460.

D'hooge, P. *et al.* (2015) 'Ca 2+ homeostasis in the budding yeast Saccharomyces cerevisiae : Impact of ER/Golgi Ca 2+ storage', *Cell Calcium*, 58(2), pp. 226–235. doi:

10.1016/j.ceca.2015.05.004.

d'Ydewalle, C. *et al.* (2011) 'HDAC6 inhibitors reverse axonal loss in a mouse model of mutant HSPB1–induced Charcot-Marie-Tooth disease', *Nature Medicine*, 17(8), pp. 968–974. doi: 10.1038/nm.2396.

Dafinca, R. *et al.* (2016) 'C9orf72 Hexanucleotide Expansions Are Associated with Altered Endoplasmic Reticulum Calcium Homeostasis and Stress Granule Formation in Induced Pluripotent Stem Cell-Derived Neurons from Patients with Amyotrophic Lateral Sclerosis and Frontotemporal Demen', *Stem Cells*, 34(8), pp. 2063–2078. doi: 10.1002/stem.2388.

Van Damme, P. *et al.* (2003) 'The AMPA receptor antagonist NBQX prolongs survival in a transgenic mouse model of amyotrophic lateral sclerosis', *Neuroscience Letters*, 343(2), pp. 81–84. doi: 10.1016/S0304-3940(03)00314-8.

Daniels, K. J. *et al.* (2015) 'Role of Tec1 in the development, architecture, and integrity of sexual biofilms of Candida albicans.', *Eukaryotic cell*, 14(3), pp. 228–40. doi: 10.1128/EC.00224-14.

Daulatzai, M. (2015) 'Non-Celiac Gluten Sensitivity Triggers Gut Dysbiosis, Neuroinflammation, Gut-Brain Axis Dysfunction, and Vulnerability for Dementia', *CNS & Neurological Disorders - Drug Targets*, 14(1), pp. 110–131. doi: 10.2174/1871527314666150202152436.

Davie, J. R. (2003) 'Inhibition of Histone Deacetylase Activity by Butyrate', *The Journal of Nutrition*, 133(7), pp. 2485S-2493S. doi: 10.1093/jn/133.7.2485S.

Davis, N., Horecka, J. and Sprague, G. (1993) 'Cis- and trans-acting functions required for endocytosis of the yeast pheromone receptors', *The Journal of cell biology*, 122(1), pp. 53–65. doi: 10.1083/jcb.122.1.53.

Davis, S. A. *et al.* (2018) 'TDP-43 interacts with mitochondrial proteins critical for mitophagy and mitochondrial dynamics', *Neuroscience Letters*, 678, pp. 8–15. doi: 10.1016/j.neulet.2018.04.053.

Day, M. *et al.* (2002) 'Stimulation of 5-HT 2 Receptors in Prefrontal Pyramidal Neurons Inhibits Ca v 1.2 L-Type Ca 2+ Currents Via a PLCβ/IP3/Calcineurin Signaling Cascade',

Journal of Neurophysiology, 87(5), pp. 2490–2504. doi: 10.1152/jn.00843.2001.

DeJesus-Hernandez, M. *et al.* (2011) 'Expanded GGGGCC Hexanucleotide Repeat in Noncoding Region of C9ORF72 Causes Chromosome 9p-Linked FTD and ALS', *Neuron*, 72(2), pp. 245–256. doi: 10.1016/j.neuron.2011.09.011.

Denis, V. and Cyert, M. S. (2002) 'Internal Ca2+ release in yeast is triggered by hypertonic shock and mediated by a TRP channel homologue', *Journal of Cell Biology*, 156(1), pp. 29–34. doi: 10.1083/jcb.200111004.

Desai, J. V (2018) 'Candida albicans Hyphae: From Growth Initiation to Invasion.', *Journal of fungi (Basel, Switzerland)*, 4(1). doi: 10.3390/jof4010010.

Desport, J. C. *et al.* (2001) 'Factors correlated with hypermetabolism in patients with amyotrophic lateral sclerosis', *The American Journal of Clinical Nutrition*, 74(3), pp. 328–334. doi: 10.1093/ajcn/74.3.328.

Dethlefsen, L. *et al.* (2008) 'The Pervasive Effects of an Antibiotic on the Human Gut Microbiota, as Revealed by Deep 16S rRNA Sequencing', *PLoS Biology*. Edited by J. A. Eisen, 6(11), p. e280. doi: 10.1371/journal.pbio.0060280.

Devaney, E. (2006) 'Thermoregulation in the life cycle of nematodes', *International Journal for Parasitology*, 36(6), pp. 641–649. doi: 10.1016/j.ijpara.2006.02.006.

DiDonato, M. *et al.* (2003) 'ALS Mutants of Human Superoxide Dismutase Form Fibrous Aggregates Via Framework Destabilization', *Journal of Molecular Biology*, 332(3), pp. 601–615. doi: 10.1016/S0022-2836(03)00889-1.

Didonna, A. and Opal, P. (2015) 'The promise and perils of <scp>HDAC</scp> inhibitors in neurodegeneration', *Annals of Clinical and Translational Neurology*, 2(1), pp. 79–101. doi: 10.1002/acn3.147.

Diessl, J. *et al.* (2020) 'Stable and destabilized GFP reporters to monitor calcineurin activity in Saccharomyces cerevisiae', *Microbial Cell*, 7(4), pp. 106–114. doi: 10.15698/mic2020.04.713.

Dikic, I. and Elazar, Z. (2018) 'Mechanism and medical implications of mammalian autophagy', *Nature Reviews Molecular Cell Biology*, 19(6), pp. 349–364. doi:

10.1038/s41580-018-0003-4.

van Dis, V. *et al.* (2014) 'Golgi fragmentation precedes neuromuscular denervation and is associated with endosome abnormalities in SOD1-ALS mouse motor neurons', *Acta Neuropathologica Communications*, 2(1), p. 38. doi: 10.1186/2051-5960-2-38.

Doble, A. (1996) 'The pharmacology and mechanism of action of riluzole', *Neurology*, 47(6_suppl_4). doi: 10.1212/WNL.47.6_Suppl_4.233S.

Dominy, S. S. *et al.* (2019) 'Porphyromonas gingivalis in Alzheimer's disease brains: Evidence for disease causation and treatment with small-molecule inhibitors', *Science Advances*, 5(1). doi: 10.1126/sciadv.aau3333.

Donohoe, D. R. *et al.* (2011) 'The Microbiome and Butyrate Regulate Energy Metabolism and Autophagy in the Mammalian Colon', *Cell Metabolism*, 13(5), pp. 517–526. doi: 10.1016/j.cmet.2011.02.018.

Donohoe, D. R. *et al.* (2014) 'A Gnotobiotic Mouse Model Demonstrates That Dietary Fiber Protects against Colorectal Tumorigenesis in a Microbiota- and Butyrate-Dependent Manner', *Cancer Discovery*, 4(12), pp. 1387–1397. doi: 10.1158/2159-8290.CD-14-0501.

Douglas, L. J. (2003) 'Candida biofilms and their role in infection', *Trends in Microbiology*, 11(1), pp. 30–36. doi: 10.1016/S0966-842X(02)00002-1.

Doyle, K. (2022) *Investigating metabolic dysfunction in a Saccharomyces cerevisiae model of SOD1-associated amyotrophic lateral sclerosis*. University of Kent. doi: 10.22024/UniKent/01.02.95966.

Duncan, S. H. *et al.* (2009) 'The role of pH in determining the species composition of the human colonic microbiota', *Environmental Microbiology*, 11(8), pp. 2112–2122. doi: 10.1111/j.1462-2920.2009.01931.x.

Dupuis, L. *et al.* (2004) 'Evidence for defective energy homeostasis in amyotrophic lateral sclerosis: Benefit of a high-energy diet in a transgenic mouse model', *Proceedings of the National Academy of Sciences*, 101(30), pp. 11159–11164. doi: 10.1073/pnas.0402026101.

Dupuis, L. *et al.* (2011) 'Energy metabolism in amyotrophic lateral sclerosis', *The Lancet Neurology*, 10(1), pp. 75–82. doi: 10.1016/S1474-4422(10)70224-6.

Durães, F., Pinto, M. and Sousa, E. (2018) 'Old Drugs as New Treatments for Neurodegenerative Diseases', *Pharmaceuticals*, 11(2), p. 44. doi: 10.3390/ph11020044.

Duvenage, L. *et al.* (2019) 'An analysis of respiratory function and mitochondrial morphology in Candida albicans'. doi: 10.1101/697516.

Echaniz-Laguna, A. *et al.* (2006) 'Muscular mitochondrial function in amyotrophic lateral sclerosis is progressively altered as the disease develops: A temporal study in man', *Experimental Neurology*, 198(1), pp. 25–30. doi: 10.1016/j.expneurol.2005.07.020.

Eleutherio, E. C. A. *et al.* (2021) 'SOD1, more than just an antioxidant', *Archives of Biochemistry and Biophysics*, 697, p. 108701. doi: 10.1016/j.abb.2020.108701.

Esch, T. *et al.* (2002) 'The role of stress in neurodegenerative diseases and mental disorders.', *Neuro endocrinology letters*, 23(3), pp. 199–208. Available at: http://www.ncbi.nlm.nih.gov/pubmed/12080279.

Esquivel-Elizondo, S. *et al.* (2017) 'Insights into Butyrate Production in a Controlled Fermentation System via Gene Predictions', *mSystems*. Edited by R. G. Beiko, 2(4). doi: 10.1128/mSystems.00051-17.

Estácio, S. G. *et al.* (2015) 'Calcium binding to gatekeeper residues flanking aggregation-prone segments underlies non-fibrillar amyloid traits in superoxide dismutase 1 (SOD1)', *Biochimica et Biophysica Acta (BBA) - Proteins and Proteomics*, 1854(2), pp. 118–126. doi: 10.1016/j.bbapap.2014.11.005.

Fallani, M. *et al.* (2011) 'Determinants of the human infant intestinal microbiota after the introduction of first complementary foods in infant samples from five European centres', *Microbiology*, 157(5), pp. 1385–1392. doi: 10.1099/mic.0.042143-0.

Fan, D. *et al.* (2015) 'Activation of HIF-1α and LL-37 by commensal bacteria inhibits Candida albicans colonization', *Nature Medicine*, 21(7), pp. 808–814. doi: 10.1038/nm.3871.

Fan, P. *et al.* (2015) 'Metabolites of Dietary Protein and Peptides by Intestinal Microbes and their Impacts on Gut', *Current Protein & Peptide Science*, 16(7), pp. 646–654. doi: 10.2174/1389203716666150630133657.

Fang, F. *et al.* (2009) 'Familial aggregation of amyotrophic lateral sclerosis', *Annals of*

Neurology, 66(1), pp. 94–99. doi: 10.1002/ana.21580.

Fang, F. *et al.* (2015) 'Risk factors for amyotrophic lateral sclerosis', *Clinical Epidemiology*, p. 181. doi: 10.2147/CLEP.S37505.

Fang, X. *et al.* (2016) 'Evaluation of the Microbial Diversity in Amyotrophic Lateral Sclerosis Using High-Throughput Sequencing', *Frontiers in Microbiology*, 7. doi: 10.3389/fmicb.2016.01479.

Farcasanu, I. C. *et al.* (1995) 'Protein Phosphatase 2B of Saccharomyces Cerevisiae is Required for Tolerance to Manganese, in Blocking the Entry of ions into the Cells', *European Journal of Biochemistry*, 232(3), pp. 712–717. doi: 10.1111/j.1432-1033.1995.712zz.x.

Farg, Manal A *et al.* (2014) 'C9ORF72, implicated in amytrophic lateral sclerosis and frontotemporal dementia, regulates endosomal trafficking.', *Human molecular genetics*, 23(13), pp. 3579–95. doi: 10.1093/hmg/ddu068.

Farg, Manal A. *et al.* (2014) 'C9ORF72, implicated in amytrophic lateral sclerosis and frontotemporal dementia, regulates endosomal trafficking', *Human Molecular Genetics*, 23(13), pp. 3579–3595. doi: 10.1093/hmg/ddu068.

Feng, Y. and Davis, N. G. (2000) 'Akr1p and the type I casein kinases act prior to the ubiquitination step of yeast endocytosis: Akr1p is required for kinase localization to the plasma membrane.', *Molecular and cellular biology*, 20(14), pp. 5350–9. doi: 10.1128/MCB.20.14.5350-5359.2000.

Ferguson, S. J. (1997) 'Chapter 2 Bioenergetics after 1960', in, pp. 3–22. doi: 10.1016/S1874-5660(97)80004-4.

Ferraiuolo, L. *et al.* (2011) 'Molecular pathways of motor neuron injury in amyotrophic lateral sclerosis', *Nature Reviews Neurology*, 7(11), pp. 616–630. doi: 10.1038/nrneurol.2011.152.

Ferrante, R. J. *et al.* (1997) 'Evidence of Increased Oxidative Damage in Both Sporadic and Familial Amyotrophic Lateral Sclerosis', *Journal of Neurochemistry*, 69(5), pp. 2064–2074. doi: 10.1046/j.1471-4159.1997.69052064.x.

Ferri, A. *et al.* (2002) 'Calcineurin Activity Is Regulated Both by Redox Compounds and by

Mutant Familial Amyotrophic Lateral Sclerosis-Superoxide Dismutase', *Journal of Neurochemistry*, 75(2), pp. 606–613. doi: 10.1046/j.1471-4159.2000.0750606.x.

Ferri, A. *et al.* (2004) 'Activity of protein phosphatase calcineurin is decreased in sporadic and familial amyotrophic lateral sclerosispatients', *Journal of Neurochemistry*, 90(5), pp. 1237–1242. doi: 10.1111/j.1471-4159.2004.02588.x.

Ferri, A. *et al.* (2008) 'Oxidative inactivation of calcineurin by Cu,Zn superoxide dismutase G93A, a mutant typical of familial amyotrophic lateral sclerosis', *Journal of Neurochemistry*, 79(3), pp. 531–538. doi: 10.1046/j.1471-4159.2001.00558.x.

Ferri, A. and Coccurello, R. (2017) 'What is "Hyper" in the ALS Hypermetabolism?', *Mediators of Inflammation*, 2017, pp. 1–11. doi: 10.1155/2017/7821672.

Figueroa-Romero, C. *et al.* (2019) 'Temporal evolution of the microbiome, immune system, and epigenome with disease progression in ALS mice', *Disease Models & Mechanisms*. doi: 10.1242/dmm.041947.

Finkel, J. S. and Mitchell, A. P. (2011) 'Genetic control of Candida albicans biofilm development', *Nature Reviews Microbiology*, 9(2), pp. 109–118. doi: 10.1038/nrmicro2475.

Fischer, L. R. *et al.* (2004) 'Amyotrophic lateral sclerosis is a distal axonopathy: evidence in mice and man', *Experimental Neurology*, 185(2), pp. 232–240. doi: 10.1016/j.expneurol.2003.10.004.

Fischer, M. *et al.* (1997) 'The Saccharomyces cerevisiae CCH1 gene is involved in calcium influx and mating', *FEBS Letters*, 419(2–3), pp. 259–262. doi: 10.1016/S0014-5793(97)01466-X.

Fleury, C., Mignotte, B. and Vayssière, J.-L. (2002) 'Mitochondrial reactive oxygen species in cell death signaling', *Biochimie*, 84(2–3), pp. 131–141. doi: 10.1016/S0300-9084(02)01369-X.

Fornai, F. *et al.* (2008) 'Lithium delays progression of amyotrophic lateral sclerosis', *Proceedings of the National Academy of Sciences*, 105(6), pp. 2052–2057. doi: 10.1073/pnas.0708022105.

Forsyth, C. B. *et al.* (2011) 'Increased Intestinal Permeability Correlates with Sigmoid Mucosa alpha-Synuclein Staining and Endotoxin Exposure Markers in Early Parkinson's

Disease', *PLoS ONE*. Edited by C. Oreja-Guevara, 6(12), p. e28032. doi: 10.1371/journal.pone.0028032.

Foster, J. and Zhou, L. (Linda) (2015) 'Psychobiotics and the gut–brain axis: in the pursuit of happiness', *Neuropsychiatric Disease and Treatment*, p. 715. doi: 10.2147/NDT.S61997.

Fournier, C. N. *et al.* (2020) 'The gut microbiome and neuroinflammation in amyotrophic lateral sclerosis? Emerging clinical evidence', *Neurobiology of Disease*, 135, p. 104300. doi: 10.1016/j.nbd.2018.10.007.

Foury, F. (1997) 'Human genetic diseases: a cross-talk between man and yeast', *Gene*, 195(1), pp. 1–10. doi: 10.1016/S0378-1119(97)00140-6.

Fraga, M. F. *et al.* (2005) 'Loss of acetylation at Lys16 and trimethylation at Lys20 of histone H4 is a common hallmark of human cancer', *Nature Genetics*, 37(4), pp. 391–400. doi: 10.1038/ng1531.

Fratta, P. *et al.* (2012) 'C9orf72 hexanucleotide repeat associated with amyotrophic lateral sclerosis and frontotemporal dementia forms RNA G-quadruplexes', *Scientific Reports*, 2(1), p. 1016. doi: 10.1038/srep01016.

Frederickson, C. J., Koh, J.-Y. and Bush, A. I. (2005) 'The neurobiology of zinc in health and disease', *Nature Reviews Neuroscience*, 6(6), pp. 449–462. doi: 10.1038/nrn1671.

Freibaum, B. D. *et al.* (2010) 'Global Analysis of TDP-43 Interacting Proteins Reveals Strong Association with RNA Splicing and Translation Machinery', *Journal of Proteome Research*, 9(2), pp. 1104–1120. doi: 10.1021/pr901076y.

French, P. W., Ludowyke, R. and Guillemin, G. J. (2019) 'Fungal Neurotoxins and Sporadic Amyotrophic Lateral Sclerosis', *Neurotoxicity Research*, 35(4), pp. 969–980. doi: 10.1007/s12640-018-9980-5.

Fujikake, N., Shin, M. and Shimizu, S. (2018) 'Association Between Autophagy and Neurodegenerative Diseases', *Frontiers in Neuroscience*, 12. doi: 10.3389/fnins.2018.00255.

Fulceri, F. *et al.* (2011) 'Autophagy activation in glutamate-induced motor neuron loss.', *Archives italiennes de biologie*, 149(1), pp. 101–11. doi: 10.4449/aib.v149i1.1259.

Furukawa, Y., Torres, A. S. and O'Halloran, T. V (2004) 'Oxygen-induced maturation of SOD1: a key role for disulfide formation by the copper chaperone CCS', *The EMBO Journal*, 23(14), pp. 2872–2881. doi: 10.1038/sj.emboj.7600276.

Fusco, W. *et al.* (2023) 'Short-Chain Fatty-Acid-Producing Bacteria: Key Components of the Human Gut Microbiota', *Nutrients*, 15(9), p. 2211. doi: 10.3390/nu15092211.

Gal, J. *et al.* (2013) 'HDAC6 Regulates Mutant SOD1 Aggregation through Two SMIR Motifs and Tubulin Acetylation', *Journal of Biological Chemistry*, 288(21), pp. 15035–15045. doi: 10.1074/jbc.M112.431957.

Galan, J. M. *et al.* (1996) 'Ubiquitination Mediated by the Npi1p/Rsp5p Ubiquitin-protein Ligase Is Required for Endocytosis of the Yeast Uracil Permease', *Journal of Biological Chemistry*, 271(18), pp. 10946–10952. doi: 10.1074/jbc.271.18.10946.

Ganguly, S. and Mitchell, A. P. (2011) 'Mucosal biofilms of Candida albicans', *Current Opinion in Microbiology*, 14(4), pp. 380–385. doi: 10.1016/j.mib.2011.06.001.

Ganley, I. G. *et al.* (2009) 'ULK1·ATG13·FIP200 Complex Mediates mTOR Signaling and Is Essential for Autophagy', *Journal of Biological Chemistry*, 284(18), pp. 12297–12305. doi: 10.1074/jbc.M900573200.

Gao, W. *et al.* (2025) 'Advancements in neurodegenerative diseases: Pathogenesis and novel neurorestorative interventions', *Journal of Neurorestoratology*, 13(2), p. 100176. doi: 10.1016/j.jnrt.2024.100176.

Garbe, E. *et al.* (2023) 'Functional analysis of the Candida albicans ECE1 Promoter', *Microbiology Spectrum*. Edited by R. S. Shapiro, 11(2). doi: 10.1128/spectrum.00253-23.

Garnaud, C. *et al.* (2016) 'Histone Deacetylases and Their Inhibition in Candida Species', *Frontiers in Microbiology*, 7. doi: 10.3389/fmicb.2016.01238.

Geng, J. and Klionsky, D. J. (2008) 'The Atg8 and Atg12 ubiquitin-like conjugation systems in macroautophagy', *EMBO reports*, 9(9), pp. 859–864. doi: 10.1038/embor.2008.163.

Gerhardt, S. and Mohajeri, M. (2018) 'Changes of Colonic Bacterial Composition in Parkinson's Disease and Other Neurodegenerative Diseases', *Nutrients*, 10(6), p. 708. doi: 10.3390/nu10060708.

Ghosh, M., Shen, J. and Rosen, B. P. (1999) 'Pathways of As(III) detoxification in Saccharomyces cerevisiae', *Proceedings of the National Academy of Sciences*, 96(9), pp. 5001–5006. doi: 10.1073/pnas.96.9.5001.

Ghrenassia, E. *et al.* (2019) 'Candidemia in critically ill immunocompromised patients: report of a retrospective multicenter cohort study', *Annals of Intensive Care*, 9(1), p. 62. doi: 10.1186/s13613-019-0539-2.

Gidalevitz, T. *et al.* (2009) 'Destabilizing Protein Polymorphisms in the Genetic Background Direct Phenotypic Expression of Mutant SOD1 Toxicity', *PLoS Genetics*. Edited by H. Orr, 5(3), p. e1000399. doi: 10.1371/journal.pgen.1000399.

Gincel, D., Zaid, H. and Shoshan-Barmatz, V. (2001) 'Calcium binding and translocation by the voltage-dependent anion channel: a possible regulatory mechanism in mitochondrial function.', *The Biochemical journal*, 358(Pt 1), pp. 147–55. doi: 10.1042/0264-6021:3580147.

Di Gioia, D. *et al.* (2020) 'A prospective longitudinal study on the microbiota composition in amyotrophic lateral sclerosis', *BMC Medicine*, 18(1), p. 153. doi: 10.1186/s12916-020-01607-9.

De Giorgi, F. *et al.* (2002) 'The permeability transition pore signals apoptosis by directing Bax translocation and multimerization', *The FASEB Journal*, 16(6), pp. 607–609. doi: 10.1096/fj.01-0269fje.

Giorgio, M. *et al.* (2007) 'Hydrogen peroxide: a metabolic by-product or a common mediator of ageing signals?', *Nature Reviews Molecular Cell Biology*, 8(9), pp. 722–728. doi: 10.1038/nrm2240.

Gitler, A. D. (2008) 'Beer and Bread to Brains and Beyond: Can Yeast Cells Teach Us about Neurodegenerative Disease?', *Neurosignals*, 16(1), pp. 52–62. doi: 10.1159/000109759.

Glick, D., Barth, S. and Macleod, K. F. (2010) 'Autophagy: cellular and molecular mechanisms', *The Journal of Pathology*, 221(1), pp. 3–12. doi: 10.1002/path.2697.

Goffeau, A. *et al.* (1996) 'Life with 6000 Genes', *Science*, 274(5287), pp. 546–567. doi: 10.1126/science.274.5287.546.

Gogvadze, V. *et al.* (2001) 'Cytochrome c Release Occurs via Ca2+-dependent and Ca2+-independent Mechanisms That Are Regulated by Bax', *Journal of Biological Chemistry*, 276(22), pp. 19066–19071. doi: 10.1074/jbc.M100614200.

Golden, T. (2007) 'Gene expression changes associated with aging in C. elegans-revision1', *WormBook*. doi: 10.1895/wormbook.1.127.2.

Goldman, A. *et al.* (2014) 'The Calcineurin Signaling Network Evolves via Conserved Kinase-Phosphatase Modules that Transcend Substrate Identity', *Molecular Cell*, 55(3), pp. 422–435. doi: 10.1016/j.molcel.2014.05.012.

Gomes, N. A. *et al.* (2023) 'Overexpression of mTOR in Leukocytes from ALS8 Patients', *Current Neuropharmacology*, 21(3), pp. 482–490. doi: 10.2174/1570159X21666230201151016.

Gonatas, N. K., Stieber, A. and Gonatas, J. O. (2006) 'Fragmentation of the Golgi apparatus in neurodegenerative diseases and cell death', *Journal of the Neurological Sciences*, 246(1–2), pp. 21–30. doi: 10.1016/j.jns.2006.01.019.

González, A. and Hall, M. N. (2017) 'Nutrient sensing and <scp>TOR</scp> signaling in yeast and mammals', *The EMBO Journal*, 36(4), pp. 397–408. doi: 10.15252/embj.201696010.

Gottlicher, M. (2001) 'Valproic acid defines a novel class of HDAC inhibitors inducing differentiation of transformed cells', *The EMBO Journal*, 20(24), pp. 6969–6978. doi: 10.1093/emboj/20.24.6969.

Goutman, S. A. *et al.* (2022) 'Metabolomics identifies shared lipid pathways in independent amyotrophic lateral sclerosis cohorts', *Brain*, 145(12), pp. 4425–4439. doi: 10.1093/brain/awac025.

Graef, I. A. *et al.* (2003) 'Neurotrophins and Netrins Require Calcineurin/NFAT Signaling to Stimulate Outgrowth of Embryonic Axons', *Cell*, 113(5), pp. 657–670. doi: 10.1016/S0092-8674(03)00390-8.

Grant, C. M., MacIver, F. H. and Dawes, I. W. (1997) 'Mitochondrial function is required for resistance to oxidative stress in the yeast Saccharomyces cerevisiae', *FEBS Letters*, 410(2–3), pp. 219–222. doi: 10.1016/S0014-5793(97)00592-9.

Grijalba, M. T., Vercesi, A. E. and Schreier, S. (1999) 'Ca 2+ -Induced Increased Lipid Packing and Domain Formation in Submitochondrial Particles. A Possible Early Step in the Mechanism of Ca 2+ -Stimulated Generation of Reactive Oxygen Species by the Respiratory Chain', *Biochemistry*, 38(40), pp. 13279–13287. doi: 10.1021/bi9828674.

Grosfeld, E. V. *et al.* (2021) 'A Systematic Survey of Characteristic Features of Yeast Cell Death Triggered by External Factors', *Journal of Fungi*, 7(11), p. 886. doi: 10.3390/jof7110886.

Grosskreutz, J., Van Den Bosch, L. and Keller, B. U. (2010) 'Calcium dysregulation in amyotrophic lateral sclerosis', *Cell Calcium*, 47(2), pp. 165–174. doi: 10.1016/j.ceca.2009.12.002.

Groth, R. D. and Mermelstein, P. G. (2003) 'Brain-Derived Neurotrophic Factor Activation of NFAT (Nuclear Factor of Activated T-Cells)-Dependent Transcription: A Role for the Transcription Factor NFATc4 in Neurotrophin-Mediated Gene Expression', *The Journal of Neuroscience*, 23(22), pp. 8125–8134. doi: 10.1523/JNEUROSCI.23-22-08125.2003.

Guaragnella, N. *et al.* (2014) 'The expanding role of yeast in cancer research and diagnosis: insights into the function of the oncosuppressors p53 and BRCA1/2', *FEMS Yeast Research*, 14(1), pp. 2–16. doi: 10.1111/1567-1364.12094.

Guatteo, E. *et al.* (2007) 'Altered calcium homeostasis in motor neurons following AMPA receptor but not voltage-dependent calcium channels' activation in a genetic model of amyotrophic lateral sclerosis', *Neurobiology of Disease*, 28(1), pp. 90–100. doi: 10.1016/j.nbd.2007.07.002.

Gunter, T. E. *et al.* (2000) 'Mitochondrial calcium transport: mechanisms and functions', *Cell Calcium*, 28(5–6), pp. 285–296. doi: 10.1054/ceca.2000.0168.

Gunter, T. E. *et al.* (2004) 'Calcium and mitochondria', *FEBS Letters*, 567(1), pp. 96–102. doi: 10.1016/j.febslet.2004.03.071.

Guo, K. *et al.* (2024) 'Gut microbiome correlates with plasma lipids in amyotrophic lateral sclerosis', *Brain*, 147(2), pp. 665–679. doi: 10.1093/brain/awad306.

Guo, W. *et al.* (2017) 'HDAC6 inhibition reverses axonal transport defects in motor neurons

derived from FUS-ALS patients', *Nature Communications*, 8(1), p. 861. doi: 10.1038/s41467-017-00911-y.

Guo, X. *et al.* (2017) 'Amyloid β-Induced Redistribution of Transcriptional Factor EB and Lysosomal Dysfunction in Primary Microglial Cells', *Frontiers in Aging Neuroscience*, 9. doi: 10.3389/fnagi.2017.00228.

Gurney, M. E. *et al.* (1994) 'Motor Neuron Degeneration in Mice that Express a Human Cu,Zn Superoxide Dismutase Mutation', *Science*, 264(5166), pp. 1772–1775. doi: 10.1126/science.8209258.

Halestrap, A. and Brenner, C. (2003) 'The Adenine Nucleotide Translocase: A Central Component of the Mitochondrial Permeability Transition Pore and Key Player in Cell Death', *Current Medicinal Chemistry*, 10(16), pp. 1507–1525. doi: 10.2174/0929867033457278.

Hall, D., Herndon, L. and Altun, Z. (2017) *WormAtlas Embryo Handbook - Introduction to C. elegans Embryo Anatomy.*, *WormAtlas*. Available at: https://www.wormatlas.org/hermaphrodite/introduction/mainframe.htm.

Hamer, H. M. *et al.* (2010) 'Effect of butyrate enemas on inflammation and antioxidant status in the colonic mucosa of patients with ulcerative colitis in remission', *Clinical Nutrition*, 29(6), pp. 738–744. doi: 10.1016/j.clnu.2010.04.002.

HAMER, H. M. *et al.* (2007) 'Review article: the role of butyrate on colonic function', *Alimentary Pharmacology & Therapeutics*, 27(2), pp. 104–119. doi: 10.1111/j.1365-2036.2007.03562.x.

Han, H. *et al.* (2015) 'Autophagy-linked FYVE protein (Alfy) promotes autophagic removal of misfolded proteins involved in amyotrophic lateral sclerosis (ALS)', *In Vitro Cellular & Developmental Biology - Animal*, 51(3), pp. 249–263. doi: 10.1007/s11626-014-9832-4.

Hansford, R. G. and Zorov, D. (1998) 'Role of mitochondrial calcium transport in the control of substrate oxidation.', *Molecular and cellular biochemistry*, 184(1–2), pp. 359–69. Available at: http://www.ncbi.nlm.nih.gov/pubmed/9746330.

Hanson, K. *et al.* (2018) 'The HDAC6 Inhibitor Trichostatin A Acetylates Microtubules and Protects Axons From Excitotoxin-Induced Degeneration in a Compartmented Culture

Model', *Frontiers in Neuroscience*, 12. doi: 10.3389/fnins.2018.00872.

Hayashi, S., Amari, M. and Okamoto, K. (2013) 'Loss of calretinin- and parvalbumin-immunoreactive axons in anterolateral columns beyond the corticospinal tracts of amyotrophic lateral sclerosis spinal cords', *Journal of the Neurological Sciences*, 331(1–2), pp. 61–66. doi: 10.1016/j.jns.2013.05.008.

van den Hazel, H. B., Kielland-Brandt, M. C. and Winther, J. R. (1996) 'Review: Biosynthesis and function of yeast vacuolar proteases', *Yeast*, 12(1), pp. 1–16. doi: 10.1002/(SICI)1097-0061(199601)12:1<1::AID-YEA902>3.0.CO;2-N.

Heijtz, R. D. *et al.* (2011) 'Normal gut microbiota modulates brain development and behavior', *Proceedings of the National Academy of Sciences*, 108(7), pp. 3047–3052. doi: 10.1073/pnas.1010529108.

Helliwell, S. B., Losko, S. and Kaiser, C. A. (2001) 'Components of a Ubiquitin Ligase Complex Specify Polyubiquitination and Intracellular Trafficking of the General Amino Acid Permease', *The Journal of Cell Biology*, 153(4), pp. 649–662. doi: 10.1083/jcb.153.4.649.

Hemmings, S. M. J. *et al.* (2017) 'The Microbiome in Posttraumatic Stress Disorder and Trauma-Exposed Controls: An Exploratory Study', *Psychosomatic Medicine*, 79(8), pp. 936–946. doi: 10.1097/PSY.0000000000000512.

Herman, M. *et al.* (2024) 'Endo-lysosomal dysfunction in neurodegenerative diseases: opinion on current progress and future direction in the use of exosomes as biomarkers', *Philosophical Transactions of the Royal Society B: Biological Sciences*, 379(1899). doi: 10.1098/rstb.2022.0387.

Hertweck, M. (2003) 'C. elegans, a model for aging with high-throughput capacity', *Experimental Gerontology*, 38(3), pp. 345–346. doi: 10.1016/S0531-5565(02)00208-5.

Hertzberg, V. S. *et al.* (2022) 'Gut microbiome differences between amyotrophic lateral sclerosis patients and spouse controls', *Amyotrophic Lateral Sclerosis and Frontotemporal Degeneration*, 23(1–2), pp. 91–99. doi: 10.1080/21678421.2021.1904994.

Hicke, L. and Riezman, H. (1996) 'Ubiquitination of a Yeast Plasma Membrane Receptor Signals Its Ligand-Stimulated Endocytosis', *Cell*, 84(2), pp. 277–287. doi: 10.1016/S0092-

8674(00)80982-4.

Higgins, C. M., Jung, C. and Xu, Z. (2003) 'ALS-associated mutant SOD1G93A causes mitochondrial vacuolation by expansion of the intermembrane space and by involvement of SOD1 aggregation and peroxisomes', *BMC Neuroscience*, 4(1), p. 16. doi: 10.1186/1471-2202-4-16.

Hilgers, A. R., Conradi, R. A. and Burton, P. S. (1990) 'Caco-2 cell monolayers as a model for drug transport across the intestinal mucosa.', *Pharmaceutical research*, 7(9), pp. 902–10. doi: 10.1023/a:1015937605100.

Hnisz, D. *et al.* (2010) 'The Set3/Hos2 Histone Deacetylase Complex Attenuates cAMP/PKA Signaling to Regulate Morphogenesis and Virulence of Candida albicans', *PLoS Pathogens*. Edited by L. E. Cowen, 6(5), p. e1000889. doi: 10.1371/journal.ppat.1000889.

Hnisz, D. *et al.* (2012) 'A Histone Deacetylase Adjusts Transcription Kinetics at Coding Sequences during Candida albicans Morphogenesis', *PLoS Genetics*. Edited by H. D. Madhani, 8(12), p. e1003118. doi: 10.1371/journal.pgen.1003118.

Van Ho, A., Ward, D. M. and Kaplan, J. (2002) 'Transition Metal Transport in Yeast', *Annual Review of Microbiology*, 56(1), pp. 237–261. doi: 10.1146/annurev.micro.56.012302.160847.

Hodin, R. A. *et al.* (1996) 'Cellular growth state differentially regulates enterocyte gene expression in butyrate-treated HT-29 cells.', *Cell growth & differentiation : the molecular biology journal of the American Association for Cancer Research*, 7(5), pp. 647–53. Available at: http://www.ncbi.nlm.nih.gov/pubmed/8732674.

Hoffmann, L. *et al.* (2023) 'Neural regeneration research model to be explored: SH-SY5Y human neuroblastoma cells', *Neural Regeneration Research*, 18(6), p. 1265. doi: 10.4103/1673-5374.358621.

Höglinger, G. *et al.* (2024) 'ORION : A Global , Phase 3 , Randomized , Double-Blind , Placebo-Controlled Trial of AMX0035 in Progressive Supranuclear Palsy', pp. 1–19.

Hollingworth, D. *et al.* (2024) 'Structural basis for the rescue of hyperexcitable cells by the amyotrophic lateral sclerosis drug Riluzole', *Nature Communications*, 15(1), p. 8426. doi:

10.1038/s41467-024-52539-4.

Hom, J. *et al.* (2010) 'Regulation of mitochondrial fission by intracellular Ca2+ in rat ventricular myocytes', *Biochimica et Biophysica Acta (BBA) - Bioenergetics*, 1797(6–7), pp. 913–921. doi: 10.1016/j.bbabio.2010.03.018.

Hong, D. *et al.* (2023) 'Modulation of the gut–brain axis via the gut microbiota: a new era in treatment of amyotrophic lateral sclerosis', *Frontiers in Neurology*, 14. doi: 10.3389/fneur.2023.1133546.

Honjo, K., Reekum, R. and Verhoeff, N. P. L. G. (2009) 'Alzheimer's disease and infection: Do infectious agents contribute to progression of Alzheimer's disease?', *Alzheimer's & Dementia*, 5(4), pp. 348–360. doi: 10.1016/j.jalz.2008.12.001.

Hosokawa, N. *et al.* (2009) 'Nutrient-dependent mTORC1 Association with the ULK1–Atg13–FIP200 Complex Required for Autophagy', *Molecular Biology of the Cell*. Edited by S. L. Schmid, 20(7), pp. 1981–1991. doi: 10.1091/mbc.e08-12-1248.

Hough, M. A. *et al.* (2004) 'Dimer destabilization in superoxide dismutase may result in disease-causing properties: Structures of motor neuron disease mutants', *Proceedings of the National Academy of Sciences*, 101(16), pp. 5976–5981. doi: 10.1073/pnas.0305143101.

Hozumi, I. *et al.* (2011) 'Patterns of levels of biological metals in CSF differ among neurodegenerative diseases', *Journal of the Neurological Sciences*, 303(1–2), pp. 95–99. doi: 10.1016/j.jns.2011.01.003.

Hsiao, E. Y. *et al.* (2013) 'Microbiota Modulate Behavioral and Physiological Abnormalities Associated with Neurodevelopmental Disorders', *Cell*, 155(7), pp. 1451–1463. doi: 10.1016/j.cell.2013.11.024.

Hsu, F.-S. *et al.* (2019) 'Histone Deacetylase Inhibitor, Trichostatin A, Synergistically Enhances Paclitaxel-Induced Cytotoxicity in Urothelial Carcinoma Cells by Suppressing the ERK Pathway', *International Journal of Molecular Sciences*, 20(5), p. 1162. doi: 10.3390/ijms20051162.

Hsueh, K.-W. *et al.* (2016) 'Autophagic down-regulation in motor neurons remarkably prolongs the survival of ALS mice', *Neuropharmacology*, 108, pp. 152–160. doi:

10.1016/j.neuropharm.2016.03.035.

Hu, Y. *et al.* (2012) 'K-rasG12V transformation leads to mitochondrial dysfunction and a metabolic switch from oxidative phosphorylation to glycolysis', *Cell Research*, 22(2), pp. 399–412. doi: 10.1038/cr.2011.145.

Huang, C.-H., Kuo, W.-Y. and Jinn, T.-L. (2012) 'Models for the mechanism for activating copper-zinc superoxide dismutase in the absence of the CCS Cu chaperone in Arabidopsis', *Plant Signaling & Behavior*, 7(3), pp. 428–430. doi: 10.4161/psb.19192.

Huang, M. *et al.* (2024) 'Variability in SOD1-associated amyotrophic lateral sclerosis: geographic patterns, clinical heterogeneity, molecular alterations, and therapeutic implications', *Translational Neurodegeneration*, 13(1), p. 28. doi: 10.1186/s40035-024-00416-x.

Hubbard, M. J. and Klee, C. B. (1987) 'Calmodulin binding by calcineurin. Ligand-induced renaturation of protein immobilized on nitrocellulose.', *The Journal of biological chemistry*, 262(31), pp. 15062–70. Available at: http://www.ncbi.nlm.nih.gov/pubmed/2822712.

Huh, G. *et al.* (2002) 'Salt causes ion disequilibrium-induced programmed cell death in yeast and plants', *The Plant Journal*, 29(5), pp. 649–659. doi: 10.1046/j.0960-7412.2001.01247.x.

Huh, W.-K. *et al.* (2003) 'Global analysis of protein localization in budding yeast.', *Nature*, 425(6959), pp. 686–91. doi: 10.1038/nature02026.

Icardi, L., De Bosscher, K. and Tavernier, J. (2012) 'The HAT/HDAC interplay: Multilevel control of STAT signaling', *Cytokine & Growth Factor Reviews*, 23(6), pp. 283–291. doi: 10.1016/j.cytogfr.2012.08.002.

Ihara, Y. *et al.* (2005) 'Oxidative stress and metal content in blood and cerebrospinal fluid of amyotrophic lateral sclerosis patients with and without a Cu, Zn-superoxide dismutase mutation', *Neurological Research*, 27(1), pp. 105–108. doi: 10.1179/016164105X18430.

Iida, H. *et al.* (1994) 'MID1, a novel Saccharomyces cerevisiae gene encoding a plasma membrane protein, is required for Ca2+ influx and mating.', *Molecular and Cellular Biology*, 14(12), pp. 8259–8271. doi: 10.1128/MCB.14.12.8259.

Ilieva, E. V. *et al.* (2007) 'Oxidative and endoplasmic reticulum stress interplay in sporadic

amyotrophic lateral sclerosis', *Brain*, 130(12), pp. 3111–3123. doi: 10.1093/brain/awm190.

Inoue, M. *et al.* (1999) 'Cross-talk of NO, superoxide and molecular oxygen, a majesty of aerobic life', *Free Radical Research*, 31(4), pp. 251–260. doi: 10.1080/10715769900300831.

Islinger, M. *et al.* (2009) 'Hitchhiking of Cu/Zn Superoxide Dismutase to Peroxisomes – Evidence for a Natural Piggyback Import Mechanism in Mammals', *Traffic*, 10(11), pp. 1711–1721. doi: 10.1111/j.1600-0854.2009.00966.x.

Israelson, A. *et al.* (2010) 'Misfolded Mutant SOD1 Directly Inhibits VDAC1 Conductance in a Mouse Model of Inherited ALS', *Neuron*, 67(4), pp. 575–587. doi: 10.1016/j.neuron.2010.07.019.

Itakura, E. *et al.* (2008) 'Beclin 1 Forms Two Distinct Phosphatidylinositol 3-Kinase Complexes with Mammalian Atg14 and UVRAG', *Molecular Biology of the Cell*. Edited by S. Subramani, 19(12), pp. 5360–5372. doi: 10.1091/mbc.e08-01-0080.

Itakura, E. and Mizushima, N. (2010) 'Characterization of autophagosome formation site by a hierarchical analysis of mammalian Atg proteins', *Autophagy*, 6(6), pp. 764–776. doi: 10.4161/auto.6.6.12709.

Ito, Y. *et al.* (2009) 'Involvement of CHOP, an ER-stress apoptotic mediator, in both human sporadic ALS and ALS model mice', *Neurobiology of Disease*, 36(3), pp. 470–476. doi: 10.1016/j.nbd.2009.08.013.

Jaarsma, D. *et al.* (2001) 'CuZn superoxide dismutase (SOD1) accumulates in vacuolated mitochondria in transgenic mice expressing amyotrophic lateral sclerosis-linked SOD1 mutations', *Acta Neuropathologica*, 102(4), pp. 293–305. doi: 10.1007/s004010100399.

Jaiswal, M. K. (2013) 'Calcium, mitochondria, and the pathogenesis of ALS: the good, the bad, and the ugly', *Frontiers in Cellular Neuroscience*, 7. doi: 10.3389/fncel.2013.00199.

Jaiswal, M. K. and Keller, B. U. (2009) 'Cu/Zn Superoxide Dismutase Typical for Familial Amyotrophic Lateral Sclerosis Increases the Vulnerability of Mitochondria and Perturbs Ca 2+ Homeostasis in SOD1 G93A Mice', *Molecular Pharmacology*, 75(3), pp. 478–489. doi: 10.1124/mol.108.050831.

Jiminez, J. A. *et al.* (2017) 'Butyrate Supplementation at High Concentrations Alters Enteric

Bacterial Communities and Reduces Intestinal Inflammation in Mice Infected with Citrobacter rodentium.', *mSphere*, 2(4). doi: 10.1128/mSphere.00243-17.

Jin, Y. *et al.* (2017) 'Effects of environmental pollutants on gut microbiota', *Environmental Pollution*, 222, pp. 1–9. doi: 10.1016/j.envpol.2016.11.045.

Johansen, T. and Lamark, T. (2011) 'Selective autophagy mediated by autophagic adapter proteins', *Autophagy*, 7(3), pp. 279–296. doi: 10.4161/auto.7.3.14487.

Johnson, B. S. *et al.* (2009) 'TDP-43 Is Intrinsically Aggregation-prone, and Amyotrophic Lateral Sclerosis-linked Mutations Accelerate Aggregation and Increase Toxicity', *Journal of Biological Chemistry*, 284(30), pp. 20329–20339. doi: 10.1074/jbc.M109.010264.

Jung, C. H. *et al.* (2009) 'ULK-Atg13-FIP200 Complexes Mediate mTOR Signaling to the Autophagy Machinery', *Molecular Biology of the Cell*. Edited by S. L. Schmid, 20(7), pp. 1992–2003. doi: 10.1091/mbc.e08-12-1249.

Kajiwara, K. *et al.* (2012) 'Perturbation of sphingolipid metabolism induces endoplasmic reticulum stress-mediated mitochondrial apoptosis in budding yeast', *Molecular Microbiology*, 86(5), pp. 1246–1261. doi: 10.1111/mmi.12056.

Kato, S. *et al.* (2000) 'Advanced glycation endproduct-modified superoxide dismutase-1 (SOD1)-positive inclusions are common to familial amyotrophic lateral sclerosis patients with SOD1 gene mutations and transgenic mice expressing human SOD1 with a G85R mutation', *Acta Neuropathologica*, 100(5), pp. 490–505. doi: 10.1007/s004010000226.

Katzmann, D. J., Odorizzi, G. and Emr, S. D. (2002) 'Receptor downregulation and multivesicular-body sorting', *Nature Reviews Molecular Cell Biology*, 3(12), pp. 893–905. doi: 10.1038/nrm973.

Kaul, M. *et al.* (2024) 'Gut microbiota immune cross-talk in amyotrophic lateral sclerosis', *Neurotherapeutics*, 21(6), p. e00469. doi: 10.1016/j.neurot.2024.e00469.

Kaur, J. and Nobile, C. J. (2023) 'Antifungal drug-resistance mechanisms in Candida biofilms', *Current Opinion in Microbiology*, 71, p. 102237. doi: 10.1016/j.mib.2022.102237.

Kausar, S., Wang, F. and Cui, H. (2018) 'The Role of Mitochondria in Reactive Oxygen Species Generation and Its Implications for Neurodegenerative Diseases', *Cells*, 7(12), p. 274. doi:

10.3390/cells7120274.

Kavanagh, N. I., Ainscow, E. K. and Brand, M. D. (2000) 'Calcium regulation of oxidative phosphorylation in rat skeletal muscle mitochondria', *Biochimica et Biophysica Acta (BBA) - Bioenergetics*, 1457(1–2), pp. 57–70. doi: 10.1016/S0005-2728(00)00054-2.

Kawamata, H. and Manfredi, G. (2010) 'Mitochondrial dysfunction and intracellular calcium dysregulation in ALS', *Mechanisms of Ageing and Development*, 131(7–8), pp. 517–526. doi: 10.1016/j.mad.2010.05.003.

Keenan, M. J. *et al.* (2015) 'Role of Resistant Starch in Improving Gut Health, Adiposity, and Insulin Resistance', *Advances in Nutrition*, 6(2), pp. 198–205. doi: 10.3945/an.114.007419.

El Khoury, A. and Atoui, A. (2010) 'Ochratoxin A: General Overview and Actual Molecular Status', *Toxins*, 2(4), pp. 461–493. doi: 10.3390/toxins2040461.

Kien, C. L. *et al.* (2008) 'Effects of the In Vivo Supply of Butyrate on Histone Acetylation of Cecum in Piglets', *Journal of Parenteral and Enteral Nutrition*, 32(1), pp. 51–56. doi: 10.1177/0148607108032001S1.

Kim, E. K. and Choi, E.-J. (2010) 'Pathological roles of MAPK signaling pathways in human diseases', *Biochimica et Biophysica Acta (BBA) - Molecular Basis of Disease*, 1802(4), pp. 396–405. doi: 10.1016/j.bbadis.2009.12.009.

Kim, H.-J. and Bae, S.-C. (2011) 'Histone deacetylase inhibitors: molecular mechanisms of action and clinical trials as anti-cancer drugs.', *American journal of translational research*, 3(2), pp. 166–79. Available at: http://www.ncbi.nlm.nih.gov/pubmed/21416059.

Kim, J. *et al.* (2009) 'Accumulation of labile zinc in neurons and astrocytes in the spinal cords of G93A SOD-1 transgenic mice', *Neurobiology of Disease*, 34(2), pp. 221–229. doi: 10.1016/j.nbd.2009.01.004.

Kim, J., Lee, J.-E. and Lee, J.-S. (2015) 'Histone deacetylase-mediated morphological transition in Candida albicans', *Journal of Microbiology*, 53(12), pp. 805–811. doi: 10.1007/s12275-015-5488-3.

Kim, J. M. *et al.* (2019) 'Impaired Cu–Zn Superoxide Dismutase (SOD1) and Calcineurin (Cn) Interaction in ALS: A Presumed Consequence for TDP-43 and Zinc Aggregation in Tg

SOD1G93A Rodent Spinal Cord Tissue', *Neurochemical Research*, 44(1), pp. 228–233. doi: 10.1007/s11064-017-2461-z.

Kim, S. H. *et al.* (2010) 'Amyotrophic lateral sclerosis-associated proteins TDP-43 and FUS/TLS function in a common biochemical complex to co-regulate HDAC6 mRNA.', *The Journal of biological chemistry*, 285(44), pp. 34097–105. doi: 10.1074/jbc.M110.154831.

Kim, S. and Lee, D. G. (2019) 'Role of calcium in reactive oxygen species-induced apoptosis in Candida albicans : an antifungal mechanism of antimicrobial peptide, PMAP-23', *Free Radical Research*, 53(1), pp. 8–17. doi: 10.1080/10715762.2018.1511052.

Kimura, I. *et al.* (2011) 'Short-chain fatty acids and ketones directly regulate sympathetic nervous system via G protein-coupled receptor 41 (GPR41)', *Proceedings of the National Academy of Sciences*, 108(19), pp. 8030–8035. doi: 10.1073/pnas.1016088108.

King, I. N. *et al.* (2014) 'The RNA-binding Protein TDP-43 Selectively Disrupts MicroRNA-1/206 Incorporation into the RNA-induced Silencing Complex', *Journal of Biological Chemistry*, 289(20), pp. 14263–14271. doi: 10.1074/jbc.M114.561902.

King, M. M. and Huang, C. Y. (1984) 'The calmodulin-dependent activation and deactivation of the phosphoprotein phosphatase, calcineurin, and the effect of nucleotides, pyrophosphate, and divalent metal ions. Identification of calcineurin as a Zn and Fe metalloenzyme.', *The Journal of biological chemistry*, 259(14), pp. 8847–56. Available at: http://www.ncbi.nlm.nih.gov/pubmed/6086614.

Kissinger, C. R. *et al.* (1995) 'Crystal structures of human calcineurin and the human FKBP12–FK506–calcineurin complex', *Nature*, 378(6557), pp. 641–644. doi: 10.1038/378641a0.

Kitagaki, H. *et al.* (2007) 'Ethanol-induced death in yeast exhibits features of apoptosis mediated by mitochondrial fission pathway', *FEBS Letters*, 581(16), pp. 2935–2942. doi: 10.1016/j.febslet.2007.05.048.

Klee, C. B., Crouch, T. H. and Krinks, M. H. (1979) 'Calcineurin: a calcium- and calmodulin-binding protein of the nervous system.', *Proceedings of the National Academy of Sciences*, 76(12), pp. 6270–6273. doi: 10.1073/pnas.76.12.6270.

Klein, M. *et al.* (2002) 'The ATP-binding cassette (ABC) transporter Bpt1p mediates vacuolar sequestration of glutathione conjugates in yeast', *FEBS Letters*, 520(1–3), pp. 63–67. doi: 10.1016/S0014-5793(02)02767-9.

Klingl, Y. E., Pakravan, D. and Van Den Bosch, L. (2021) 'Opportunities for histone deacetylase inhibition in amyotrophic lateral sclerosis', *British Journal of Pharmacology*, 178(6), pp. 1353–1372. doi: 10.1111/bph.15217.

Klionsky, D. J. (2008) 'Autophagy revisited: A conversation with Christian de Duve', *Autophagy*, 4(6), pp. 740–743. doi: 10.4161/auto.6398.

Klionsky, D. J., Herman, P. K. and Emr, S. D. (1990) 'The fungal vacuole: composition, function, and biogenesis', *Microbiological Reviews*, 54(3), pp. 266–292. doi: 10.1128/mr.54.3.266-292.1990.

Kneen, M. *et al.* (1998) 'Green Fluorescent Protein as a Noninvasive Intracellular pH Indicator', *Biophysical Journal*, 74(3), pp. 1591–1599. doi: 10.1016/S0006-3495(98)77870-1.

Knop, M. *et al.* (1993) 'Vacuolar/lysosomal proteolysis: proteases, substrates mechanisms', *Current Opinion in Cell Biology*, 5(6), pp. 990–996. doi: 10.1016/0955-0674(93)90082-2.

Koh, J.-Y. *et al.* (2019) 'Lysosomal dysfunction in proteinopathic neurodegenerative disorders: possible therapeutic roles of cAMP and zinc', *Molecular Brain*, 12(1), p. 18. doi: 10.1186/s13041-019-0439-2.

Koike, A. *et al.* (2012) 'Genetic Screening for Regulators of Prz1, a Transcriptional Factor Acting Downstream of Calcineurin in Fission Yeast', *Journal of Biological Chemistry*, 287(23), pp. 19294–19303. doi: 10.1074/jbc.M111.310615.

Kovalevich, J. and Langford, D. (2013) 'Considerations for the Use of SH-SY5Y Neuroblastoma Cells in Neurobiology', in, pp. 9–21. doi: 10.1007/978-1-62703-640-5_2.

Krasnianski, A. *et al.* (2005) 'Mitochondrial changes in skeletal muscle in amyotrophic lateral sclerosis and other neurogenic atrophies', *Brain*, 128(8), pp. 1870–1876. doi: 10.1093/brain/awh540.

Kreilaus, F. *et al.* (2020) 'Novel behavioural characteristics of the superoxide dismutase 1 G93A (SOD1 G93A) mouse model of amyotrophic lateral sclerosis include sex-dependent

phenotypes', *Genes, Brain and Behavior*, 19(2). doi: 10.1111/gbb.12604.

Kruman, I. I. *et al.* (1999) 'ALS-Linked Cu/Zn–SOD Mutation Increases Vulnerability of Motor Neurons to Excitotoxicity by a Mechanism Involving Increased Oxidative Stress and Perturbed Calcium Homeostasis', *Experimental Neurology*, 160(1), pp. 28–39. doi: 10.1006/exnr.1999.7190.

Kumamoto, C. A. (2005) 'A contact-activated kinase signals Candida albicans invasive growth and biofilm development', *Proceedings of the National Academy of Sciences*, 102(15), pp. 5576–5581. doi: 10.1073/pnas.0407097102.

Kuo, S.-Y. *et al.* (2015) 'Small-molecule enhancers of autophagy modulate cellular disease phenotypes suggested by human genetics', *Proceedings of the National Academy of Sciences*, 112(31). doi: 10.1073/pnas.1512289112.

Kuwahara, T. *et al.* (2008) 'A systematic RNAi screen reveals involvement of endocytic pathway in neuronal dysfunction in α-synuclein transgenic C . elegans', *Human Molecular Genetics*, 17(19), pp. 2997–3009. doi: 10.1093/hmg/ddn198.

Kwon, S. (2003) 'H2O2 regulates cardiac myocyte phenotype via concentration-dependent activation of distinct kinase pathways', *Journal of Molecular and Cellular Cardiology*, 35(6), pp. 615–621. doi: 10.1016/S0022-2828(03)00084-1.

Lacomblez, L. *et al.* (1996) 'Dose-ranging study of riluzole in amyotrophic lateral sclerosis', *The Lancet*, 347(9013), pp. 1425–1431. doi: 10.1016/S0140-6736(96)91680-3.

LaFayette, S. L. *et al.* (2010) 'PKC Signaling Regulates Drug Resistance of the Fungal Pathogen Candida albicans via Circuitry Comprised of Mkc1, Calcineurin, and Hsp90', *PLoS Pathogens*. Edited by A. P. Mitchell, 6(8), p. e1001069. doi: 10.1371/journal.ppat.1001069.

LaFleur, M. D. *et al.* (2011) 'Novel high-throughput screen against Candida albicans identifies antifungal potentiators and agents effective against biofilms', *Journal of Antimicrobial Chemotherapy*, 66(4), pp. 820–826. doi: 10.1093/jac/dkq530.

Lamb, C. A., Yoshimori, T. and Tooze, S. A. (2013) 'The autophagosome: origins unknown, biogenesis complex', *Nature Reviews Molecular Cell Biology*, 14(12), pp. 759–774. doi: 10.1038/nrm3696.

Lasiene, J. and Yamanaka, K. (2011) 'Glial Cells in Amyotrophic Lateral Sclerosis', *Neurology Research International*, 2011, pp. 1–7. doi: 10.1155/2011/718987.

St. Laurent, R., O'Brien, L. M. and Ahmad, S. T. (2013) 'Sodium butyrate improves locomotor impairment and early mortality in a rotenone-induced Drosophila model of Parkinson's disease', *Neuroscience*, 246, pp. 382–390. doi: 10.1016/j.neuroscience.2013.04.037.

Lautenschläger, J. *et al.* (2013) 'Overexpression of human mutated G93A SOD1 changes dynamics of the ER mitochondria calcium cycle specifically in mouse embryonic motor neurons', *Experimental Neurology*, 247, pp. 91–100. doi: 10.1016/j.expneurol.2013.03.027.

Leadsham, J. E. *et al.* (2009) 'Whi2p links nutritional sensing to actin-dependent Ras-cAMP-PKA regulation and apoptosis in yeast', *Journal of Cell Science*, 122(5), pp. 706–715. doi: 10.1242/jcs.042424.

Leadsham, J. E. *et al.* (2013) 'Loss of Cytochrome c Oxidase Promotes RAS-Dependent ROS Production from the ER Resident NADPH Oxidase, Yno1p, in Yeast', *Cell Metabolism*, 18(2), pp. 279–286. doi: 10.1016/j.cmet.2013.07.005.

Leal, S. S. *et al.* (2013) 'Calcium Ions Promote Superoxide Dismutase 1 (SOD1) Aggregation into Non-fibrillar Amyloid', *Journal of Biological Chemistry*, 288(35), pp. 25219–25228. doi: 10.1074/jbc.M113.470740.

LeBlanc, J. G. *et al.* (2017) 'Beneficial effects on host energy metabolism of short-chain fatty acids and vitamins produced by commensal and probiotic bacteria', *Microbial Cell Factories*, 16(1), p. 79. doi: 10.1186/s12934-017-0691-z.

Lee, G. M. *et al.* (2023) 'The Ycx1 protein encoded by the yeast YDL206W gene plays a role in calcium and calcineurin signaling', *Journal of Biological Chemistry*, 299(5), p. 104647. doi: 10.1016/j.jbc.2023.104647.

Lee, H., Hwang, J.-S. and Lee, D. G. (2016) 'Scolopendin 2 leads to cellular stress response in Candida albicans', *Apoptosis*, 21(7), pp. 856–865. doi: 10.1007/s10495-016-1254-1.

Lee, J.-H. *et al.* (2010) 'Lysosomal Proteolysis and Autophagy Require Presenilin 1 and Are Disrupted by Alzheimer-Related PS1 Mutations', *Cell*, 141(7), pp. 1146–1158. doi: 10.1016/j.cell.2010.05.008.

Lee, J. K. *et al.* (2015) 'Role of autophagy in the pathogenesis of amyotrophic lateral sclerosis', *Biochimica et Biophysica Acta (BBA) - Molecular Basis of Disease*, 1852(11), pp. 2517–2524. doi: 10.1016/j.bbadis.2015.08.005.

Lee, S. Y. *et al.* (2023) 'Therapeutic Effects of Combination of Nebivolol and Donepezil: Targeting Multifactorial Mechanisms in ALS', *Neurotherapeutics*, 20(6), pp. 1779–1795. doi: 10.1007/s13311-023-01444-7.

Lee, W. and Lee, D. G. (2018) 'Reactive oxygen species modulate itraconazole-induced apoptosis via mitochondrial disruption in Candida albicans', *Free Radical Research*, 52(1), pp. 39–50. doi: 10.1080/10715762.2017.1407412.

Lee, W., Woo, E.-R. and Lee, D. G. (2019) 'Effect of apigenin isolated from Aster yomena against Candida albicans: apigenin-triggered apoptotic pathway regulated by mitochondrial calcium signaling', *Journal of Ethnopharmacology*, 231, pp. 19–28. doi: 10.1016/j.jep.2018.11.005.

Lee, Y. *et al.* (2023) 'Functional genomic analysis of Candida albicans protein kinases reveals modulators of morphogenesis in diverse environments', *iScience*, 26(3), p. 106145. doi: 10.1016/j.isci.2023.106145.

LEIGH, P. N. *et al.* (1991) 'UBIQUITIN-IMMUNOREACTIVE INTRANEURONAL INCLUSIONS IN AMYOTROPHIC LATERAL SCLEROSIS', *Brain*, 114(2), pp. 775–788. doi: 10.1093/brain/114.2.775.

Li, C. *et al.* (2013) 'Cupric Ions Induce the Oxidation and Trigger the Aggregation of Human Superoxide Dismutase 1', *PLoS ONE*. Edited by J. M. Sanchez-Ruiz, 8(6), p. e65287. doi: 10.1371/journal.pone.0065287.

Li, J. *et al.* (2014) 'Human superoxide dismutase 1 overexpression in motor neurons of Caenorhabditis elegans causes axon guidance defect and neurodegeneration', *Neurobiology of Aging*, 35(4), pp. 837–846. doi: 10.1016/j.neurobiolaging.2013.09.003.

Li, J., Huang, K. and Le, W. (2013) 'Establishing a novel C. elegans model to investigate the role of autophagy in amyotrophic lateral sclerosis', *Acta Pharmacologica Sinica*, 34(5), pp. 644–650. doi: 10.1038/aps.2012.190.

Li, S. *et al.* (2020) 'Quality-control mechanisms targeting translationally stalled and C-terminally extended poly(GR) associated with ALS/FTD', *Proceedings of the National Academy of Sciences*, 117(40), pp. 25104–25115. doi: 10.1073/pnas.2005506117.

Li, S. C. and Kane, P. M. (2009) 'The yeast lysosome-like vacuole: endpoint and crossroads.', *Biochimica et biophysica acta*, 1793(4), pp. 650–63. doi: 10.1016/j.bbamcr.2008.08.003.

Li, W. *et al.* (2017) 'Structural changes of gut microbiota in Parkinson's disease and its correlation with clinical features', *Science China Life Sciences*, 60(11), pp. 1223–1233. doi: 10.1007/s11427-016-9001-4.

Li, W., Li, J. and Bao, J. (2012) 'Microautophagy: lesser-known self-eating', *Cellular and Molecular Life Sciences*, 69(7), pp. 1125–1136. doi: 10.1007/s00018-011-0865-5.

Li, X. *et al.* (2017) 'Extensive functional redundancy in the regulation of <scp> *C* </scp> *andida albicans* drug resistance and morphogenesis by lysine deacetylases <scp>H</scp> os2, <scp>H</scp> da1, <scp>R</scp> pd3 and <scp>R</scp> pd31', *Molecular Microbiology*, 103(4), pp. 635–656. doi: 10.1111/mmi.13578.

Lin, J. and Filler, S. G. (2025) 'Host targets of candidalysin', *PLOS Pathogens*. Edited by M. A. Jabra-Rizk, 21(6), p. e1013284. doi: 10.1371/journal.ppat.1013284.

Liput, D. J. *et al.* (2020) 'A Guide to Fluorescence Lifetime Microscopy and Förster's Resonance Energy Transfer in Neuroscience.', *Current protocols in neuroscience*, 94(1), p. e108. doi: 10.1002/cpns.108.

Liu, H. *et al.* (2018) 'Butyrate: A Double-Edged Sword for Health?', *Advances in Nutrition*, 9(1), pp. 21–29. doi: 10.1093/advances/nmx009.

Liu, J. *et al.* (1991) 'Calcineurin is a common target of cyclophilin-cyclosporin A and FKBP-FK506 complexes', *Cell*, 66(4), pp. 807–815. doi: 10.1016/0092-8674(91)90124-H.

Liu, J. *et al.* (2004) 'Toxicity of Familial ALS-Linked SOD1 Mutants from Selective Recruitment to Spinal Mitochondria', *Neuron*, 43(1), pp. 5–17. doi: 10.1016/j.neuron.2004.06.016.

Liu, J. *et al.* (2017) 'Sodium butyrate exerts protective effect against Parkinson's disease in mice via stimulation of glucagon like peptide-1', *Journal of the Neurological Sciences*, 381, pp. 176–181. doi: 10.1016/j.jns.2017.08.3235.

Liu, X. *et al.* (2015) 'Reliable cell cycle commitment in budding yeast is ensured by signal integration', *eLife*, 4. doi: 10.7554/eLife.03977.

Loeffler, M. and Kroemer, G. (2000) 'The Mitochondrion in Cell Death Control: Certainties and Incognita', *Experimental Cell Research*, 256(1), pp. 19–26. doi: 10.1006/excr.2000.4833.

Loewith, R. and Hall, M. N. (2011) 'Target of Rapamycin (TOR) in Nutrient Signaling and Growth Control', *Genetics*, 189(4), pp. 1177–1201. doi: 10.1534/genetics.111.133363.

Logroscino, G. *et al.* (2008) 'Descriptive epidemiology of amyotrophic lateral sclerosis: new evidence and unsolved issues', *Journal of Neurology, Neurosurgery & Psychiatry*, 79(1), pp. 6–11. doi: 10.1136/jnnp.2006.104828.

Lopes da Rosa, J. and Kaufman, P. D. (2012) 'Chromatin-mediated Candida albicans virulence', *Biochimica et Biophysica Acta (BBA) - Gene Regulatory Mechanisms*, 1819(3–4), pp. 349–355. doi: 10.1016/j.bbagrm.2011.08.007.

Lopez-Gonzalez, R. *et al.* (2016) 'Poly(GR) in C9ORF72 -Related ALS/FTD Compromises Mitochondrial Function and Increases Oxidative Stress and DNA Damage in iPSC-Derived Motor Neurons', *Neuron*, 92(2), pp. 383–391. doi: 10.1016/j.neuron.2016.09.015.

Louis, P. and Flint, H. J. (2017) 'Formation of propionate and butyrate by the human colonic microbiota', *Environmental Microbiology*, 19(1), pp. 29–41. doi: 10.1111/1462-2920.13589.

Lu, Y., Su, C. and Liu, H. (2012) 'A GATA Transcription Factor Recruits Hda1 in Response to Reduced Tor1 Signaling to Establish a Hyphal Chromatin State in Candida albicans', *PLoS Pathogens*. Edited by A. P. Mitchell, 8(4), p. e1002663. doi: 10.1371/journal.ppat.1002663.

Luger, K. *et al.* (1997) 'Crystal structure of the nucleosome core particle at 2.8 Å resolution', *Nature*, 389(6648), pp. 251–260. doi: 10.1038/38444.

Lührs, H. *et al.* (2002) 'Butyrate Inhibits NF-κB Activation in Lamina Propria Macrophages of Patients with Ulcerative Colitis', *Scandinavian Journal of Gastroenterology*, 37(4), pp. 458–466. doi: 10.1080/003655202317316105.

Luigetti, M. *et al.* (2009) 'Heterozygous SOD1 D90A mutation presenting as slowly progressive predominant upper motor neuron amyotrophic lateral sclerosis', *Neurological Sciences*, 30(6), pp. 517–520. doi: 10.1007/s10072-009-0125-8.

Lupetti, A. *et al.* (2004) 'Release of calcium from intracellular stores and subsequent uptake by mitochondria are essential for the candidacidal activity of an N-terminal peptide of human lactoferrin', *Journal of Antimicrobial Chemotherapy*, 54(3), pp. 603–608. doi: 10.1093/jac/dkh385.

Luther, C. H. *et al.* (2023) 'Integrated analysis of SR-like protein kinases Sky1 and Sky2 links signaling networks with transcriptional regulation in Candida albicans', *Frontiers in Cellular and Infection Microbiology*, 13. doi: 10.3389/fcimb.2023.1108235.

Ma, N. *et al.* (2017) 'Contributions of the Interaction Between Dietary Protein and Gut Microbiota to Intestinal Health', *Current Protein & Peptide Science*, 18(8). doi: 10.2174/1389203718666170216153505.

Ma, Q. *et al.* (2019) 'Impact of microbiota on central nervous system and neurological diseases: the gut-brain axis', *Journal of Neuroinflammation*, 16(1), p. 53. doi: 10.1186/s12974-019-1434-3.

Ma, X. *et al.* (2021) 'The Regulatory Role of RNA Metabolism Regulator TDP-43 in Human Cancer', *Frontiers in Oncology*, 11. doi: 10.3389/fonc.2021.755096.

Ma, Y. *et al.* (2024) 'Intratumor microbiome-derived butyrate promotes lung cancer metastasis', *Cell Reports Medicine*, 5(4), p. 101488. doi: 10.1016/j.xcrm.2024.101488.

MacDiarmid, C. W. (2000) 'Zinc transporters that regulate vacuolar zinc storage in Saccharomyces cerevisiae', *The EMBO Journal*, 19(12), pp. 2845–2855. doi: 10.1093/emboj/19.12.2845.

MacDiarmid, C. W., Milanick, M. A. and Eide, D. J. (2002) 'Biochemical Properties of Vacuolar Zinc Transport Systems ofSaccharomyces cerevisiae', *Journal of Biological Chemistry*, 277(42), pp. 39187–39194. doi: 10.1074/jbc.M205052200.

Macklin, E. *et al.* (2025) 'Safety and efficacy of trehalose in amyotrophic lateral sclerosis (HEALEY ALS Platform Trial): an adaptive, phase 2/3, double-blind, randomised, placebo-controlled trial', *The Lancet Neurology*, 24(6), pp. 500–511. doi: 10.1016/S1474-4422(25)00173-5.

Madeo, F. *et al.* (1999) 'Oxygen Stress: A Regulator of Apoptosis in Yeast', *The Journal of Cell*

Biology, 145(4), pp. 757–767. doi: 10.1083/jcb.145.4.757.

Madrid, M. *et al.* (2016) 'Multiple crosstalk between TOR and the cell integrity MAPK signaling pathway in fission yeast', *Scientific Reports*, 6(1), p. 37515. doi: 10.1038/srep37515.

Magner, M. *et al.* (2015) 'Clinical manifestation of mitochondrial diseases.', *Developmental period medicine*, 19(4), pp. 441–9. Available at: http://www.ncbi.nlm.nih.gov/pubmed/26982751.

Magrané, J. *et al.* (2014) 'Abnormal mitochondrial transport and morphology are common pathological denominators in SOD1 and TDP43 ALS mouse models', *Human Molecular Genetics*, 23(6), pp. 1413–1424. doi: 10.1093/hmg/ddt528.

Mannarino, S. C. *et al.* (2011) 'Requirement of glutathione for Sod1 activation during lifespan extension', *Yeast*, 28(1), pp. 19–25. doi: 10.1002/yea.1817.

Mannella, C. A. *et al.* (1998) 'Electron microscopic tomography of rat-liver mitochondria and their interactions with the endoplasmic reticulum', *BioFactors*, 8(3–4), pp. 225–228. doi: 10.1002/biof.5520080309.

Marangi, G. and Traynor, B. J. (2015) 'Genetic causes of amyotrophic lateral sclerosis: New genetic analysis methodologies entailing new opportunities and challenges', *Brain Research*, 1607, pp. 75–93. doi: 10.1016/j.brainres.2014.10.009.

Di Marco, G. *et al.* (2020) 'A High-Throughput Screening Identifies MICU1 Targeting Compounds', *Cell Reports*, 30(7), pp. 2321-2331.e6. doi: 10.1016/j.celrep.2020.01.081.

Mari, E. *et al.* (2020) 'Trehalose Effect on The Aggregation of Model Proteins into Amyloid Fibrils', *Life*, 10(5), p. 60. doi: 10.3390/life10050060.

Markowicz-Piasecka, M. *et al.* (2025) 'Beyond epilepsy: The expanding role of valproic acid in Alzheimer disease therapy – a review', *The Journal of Pharmacology and Experimental Therapeutics*, 392(9), p. 103658. doi: 10.1016/j.jpet.2025.103658.

Matamala, J. M. and Kiernan, M. C. (2017) 'Natural history and the dawning of a new era for familial ALS', *Journal of Neurology, Neurosurgery & Psychiatry*, 88(2), pp. 95–96. doi: 10.1136/jnnp-2016-313898.

Maza, P. K. *et al.* (2017) 'Candida albicans: The Ability to Invade Epithelial Cells and Survive under Oxidative Stress Is Unlinked to Hyphal Length', *Frontiers in Microbiology*, 8. doi: 10.3389/fmicb.2017.01235.

Mazzini, L. *et al.* (2018) 'Potential Role of Gut Microbiota in ALS Pathogenesis and Possible Novel Therapeutic Strategies', *Journal of Clinical Gastroenterology*, 52(Supplement 1), pp. S68–S70. doi: 10.1097/MCG.0000000000001042.

McCord, J. M. and Fridovich, I. (1969) 'Superoxide dismutase. An enzymic function for erythrocuprein (hemocuprein).', *The Journal of biological chemistry*, 244(22), pp. 6049–55. Available at: http://www.ncbi.nlm.nih.gov/pubmed/5389100.

McCormack, J. G. and Denton, R. M. (1993) 'Mitochondrial Ca2+ Transport and the Role of Intramitochondrial Ca2+ in the Regulation of Energy Metabolism', *Developmental Neuroscience*, 15(3–5), pp. 165–173. doi: 10.1159/000111332.

McCormack, J. G., Halestrap, A. P. and Denton, R. M. (1990) 'Role of calcium ions in regulation of mammalian intramitochondrial metabolism', *Physiological Reviews*, 70(2), pp. 391–425. doi: 10.1152/physrev.1990.70.2.391.

McCrory, C., Lenardon, M. and Traven, A. (2024) 'Bacteria-derived short-chain fatty acids as potential regulators of fungal commensalism and pathogenesis', *Trends in Microbiology*, 32(11), pp. 1106–1118. doi: 10.1016/j.tim.2024.04.004.

Medina, D. L. *et al.* (2015) 'Lysosomal calcium signalling regulates autophagy through calcineurin and TFEB', *Nature Cell Biology*, 17(3), pp. 288–299. doi: 10.1038/ncb3114.

Mehta, P. *et al.* (2023) 'Prevalence of amyotrophic lateral sclerosis in the United States using established and novel methodologies, 2017', *Amyotrophic Lateral Sclerosis and Frontotemporal Degeneration*, 24(1–2), pp. 108–116. doi: 10.1080/21678421.2022.2059380.

Mendoza, I. *et al.* (1994) 'The protein phosphatase calcineurin is essential for NaCl tolerance of Saccharomyces cerevisiae.', *The Journal of biological chemistry*, 269(12), pp. 8792–6. Available at: http://www.ncbi.nlm.nih.gov/pubmed/8132612.

Mera-Adasme, R. *et al.* (2016) 'Destabilization of the metal site as a hub for the pathogenic

mechanism of five ALS-linked mutants of copper, zinc superoxide dismutase', *Metallomics*, 8(10), pp. 1141–1150. doi: 10.1039/C6MT00085A.

Mertsalmi, T. H., Pekkonen, E. and Scheperjans, F. (2020) 'Antibiotic Exposure and Risk of Parkinson's Disease in Finland: A Nationwide Case-Control Study', *Movement Disorders*, 35(3), pp. 431–442. doi: 10.1002/mds.27924.

Michan, S. and Sinclair, D. (2007) 'Sirtuins in mammals: insights into their biological function', *Biochemical Journal*, 404(1), pp. 1–13. doi: 10.1042/BJ20070140.

Migheli, A. *et al.* (1999) 'S-100β protein is upregulated in astrocytes and motor neurons in the spinal cord of patients with amyotrophic lateral sclerosis', *Neuroscience Letters*, 261(1–2), pp. 25–28. doi: 10.1016/S0304-3940(98)01001-5.

Miletta, M. C. *et al.* (2014) 'Butyrate Increases Intracellular Calcium Levels and Enhances Growth Hormone Release from Rat Anterior Pituitary Cells via the G-Protein-Coupled Receptors GPR41 and 43', *PLoS ONE*. Edited by F. Blachier, 9(10), p. e107388. doi: 10.1371/journal.pone.0107388.

Miseta, A. *et al.* (1999) 'The vacuolar Ca 2+ /H + exchanger Vcx1p/Hum1p tightly controls cytosolic Ca 2+ levels in S. cerevisiae', *FEBS Letters*, 451(2), pp. 132–136. doi: 10.1016/S0014-5793(99)00519-0.

Mishra, J. *et al.* (2017) 'The Mitochondrial Ca2+ Uniporter: Structure, Function, and Pharmacology', in, pp. 129–156. doi: 10.1007/164_2017_1.

Mitchell, A. P. (1998) 'Dimorphism and virulence in Candida albicans', *Current Opinion in Microbiology*, 1(6), pp. 687–692. doi: 10.1016/S1369-5274(98)80116-1.

Mithöfer, A. and Mazars, C. (2002) 'Aequorin-based measurements of intracellular Ca2+-signatures in plant cells', *Biological Procedures Online*, 4(1), pp. 105–118. doi: 10.1251/bpo40.

Mizuno, Y. *et al.* (2006) 'Immunoreactivities of p62, an ubiqutin-binding protein, in the spinal anterior horn cells of patients with amyotrophic lateral sclerosis', *Journal of the Neurological Sciences*, 249(1), pp. 13–18. doi: 10.1016/j.jns.2006.05.060.

Mizushima, N. and Klionsky, D. J. (2007) 'Protein Turnover Via Autophagy: Implications for

Metabolism', *Annual Review of Nutrition*, 27(1), pp. 19–40. doi: 10.1146/annurev.nutr.27.061406.093749.

Mizushima, N. and Komatsu, M. (2011) 'Autophagy: Renovation of Cells and Tissues', *Cell*, 147(4), pp. 728–741. doi: 10.1016/j.cell.2011.10.026.

Mohajeri, M. H. *et al.* (2018) 'The role of the microbiome for human health: from basic science to clinical applications', *European Journal of Nutrition*, 57(S1), pp. 1–14. doi: 10.1007/s00394-018-1703-4.

Mohammadi, S. *et al.* (2015) 'Scope and limitations of yeast as a model organism for studying human tissue-specific pathways', *BMC Systems Biology*. BMC Systems Biology, 9(1). doi: 10.1186/s12918-015-0253-0.

Moors, T. E. *et al.* (2017) 'Therapeutic potential of autophagy-enhancing agents in Parkinson's disease', *Molecular Neurodegeneration*, 12(1), p. 11. doi: 10.1186/s13024-017-0154-3.

Moreno-Arriola, E. *et al.* (2014) 'Caenorhabditis elegans : A Useful Model for Studying Metabolic Disorders in Which Oxidative Stress Is a Contributing Factor', *Oxidative Medicine and Cellular Longevity*, 2014, pp. 1–9. doi: 10.1155/2014/705253.

Moreno-Ruiz, E. *et al.* (2009) 'Candida albicans internalization by host cells is mediated by a clathrin-dependent mechanism', *Cellular Microbiology*, 11(8), pp. 1179–1189. doi: 10.1111/j.1462-5822.2009.01319.x.

Mori, K. *et al.* (2013) 'The C9orf72 GGGGCC Repeat Is Translated into Aggregating Dipeptide-Repeat Proteins in FTLD/ALS', *Science*, 339(6125), pp. 1335–1338. doi: 10.1126/science.1232927.

Morioka, M. *et al.* (1999) 'Potential role of calcineurin for brain ischemia and traumatic injury', *Progress in Neurobiology*, 58(1), pp. 1–30. doi: 10.1016/S0301-0082(98)00073-2.

Moser, M. J., Geiser, J. R. and Davis, T. N. (1996) 'Ca2+-calmodulin promotes survival of pheromone-induced growth arrest by activation of calcineurin and Ca2+-calmodulin-dependent protein kinase', *Molecular and Cellular Biology*, 16(9), pp. 4824–4831. doi: 10.1128/MCB.16.9.4824.

Mosmann, T. (1983) ‘Rapid colorimetric assay for cellular growth and survival: Application to proliferation and cytotoxicity assays’, *Journal of Immunological Methods*, 65(1–2), pp. 55–63. doi: 10.1016/0022-1759(83)90303-4.

Mukherjee, A. *et al.* (2010) ‘Calcineurin Inhibition at the Clinical Phase of Prion Disease Reduces Neurodegeneration, Improves Behavioral Alterations and Increases Animal Survival’, *PLoS Pathogens*. Edited by N. Mabbott, 6(10), p. e1001138. doi: 10.1371/journal.ppat.1001138.

Mukherjee, A. and Soto, C. (2011) ‘Role of calcineurin in neurodegeneration produced by misfolded proteins and endoplasmic reticulum stress’, *Current Opinion in Cell Biology*, 23(2), pp. 223–230. doi: 10.1016/j.ceb.2010.12.006.

Mukherjee, P. K. *et al.* (2003) ‘Mechanism of Fluconazole Resistance in Candida albicans Biofilms: Phase-Specific Role of Efflux Pumps and Membrane Sterols’, *Infection and Immunity*, 71(8), pp. 4333–4340. doi: 10.1128/IAI.71.8.4333-4340.2003.

Münch, C., O’Brien, J. and Bertolotti, A. (2011) ‘Prion-like propagation of mutant superoxide dismutase-1 misfolding in neuronal cells’, *Proceedings of the National Academy of Sciences*, 108(9), pp. 3548–3553. doi: 10.1073/pnas.1017275108.

Nagpal, R. *et al.* (2018) ‘Gut microbiome and aging: Physiological and mechanistic insights’, *Nutrition and Healthy Aging*, 4(4), pp. 267–285. doi: 10.3233/NHA-170030.

Nakagawa, Y., Kanbe, T. and Mizuguchi, I. (2003) ‘Disruption of the Human Pathogenic Yeast Candida albicans Catalase Gene Decreases Survival in Mouse-Model Infection and Elevates Susceptibility to Higher Temperature and to Detergents’, *Microbiology and Immunology*, 47(6), pp. 395–403. doi: 10.1111/j.1348-0421.2003.tb03376.x.

Namgaladze, D., Hofer, H. W. and Ullrich, V. (2002) ‘Redox Control of Calcineurin by Targeting the Binuclear Fe2+-Zn2+ Center at the Enzyme Active Site’, *Journal of Biological Chemistry*, 277(8), pp. 5962–5969. doi: 10.1074/jbc.M111268200.

Napoli, L. (2011) ‘Ultrastructural Mitochondrial Abnormalities in Patients With Sporadic Amyotrophic Lateral Sclerosis’, *Archives of Neurology*, 68(12), p. 1612. doi: 10.1001/archneur.68.12.1612.

Narita, M. *et al.* (1998) 'Bax interacts with the permeability transition pore to induce permeability transition and cytochrome c release in isolated mitochondria.', *Proceedings of the National Academy of Sciences of the United States of America*, 95(25), pp. 14681–6. doi: 10.1073/pnas.95.25.14681.

Nau, H., Hauck, R. and Ehlers, K. (1991) 'Valproic Acid-Induced Neural Tube Defects in Mouse and Human: Aspects of Chirality, Alternative Drug Development, Pharmacokinetics and Possible Mechanisms', *Pharmacology & Toxicology*, 69(5), pp. 310–321. doi: 10.1111/j.1600-0773.1991.tb01303.x.

Neufeld, K. M. *et al.* (2011) 'Reduced anxiety-like behavior and central neurochemical change in germ-free mice', *Neurogastroenterology & Motility*, 23(3), pp. 255-e119. doi: 10.1111/j.1365-2982.2010.01620.x.

Neumann, M. *et al.* (2006) 'Ubiquitinated TDP-43 in Frontotemporal Lobar Degeneration and Amyotrophic Lateral Sclerosis', *Science*, 314(5796), pp. 130–133. doi: 10.1126/science.1134108.

Nguyen, L. N. *et al.* (2011) 'Sodium butyrate inhibits pathogenic yeast growth and enhances the functions of macrophages', *Journal of Antimicrobial Chemotherapy*, 66(11), pp. 2573–2580. doi: 10.1093/jac/dkr358.

Niccolai, E. *et al.* (2021) 'The Gut Microbiota-Immunity Axis in ALS: A Role in Deciphering Disease Heterogeneity?', *Biomedicines*, 9(7), p. 753. doi: 10.3390/biomedicines9070753.

Nicholson, K. *et al.* (2021) 'The human gut microbiota in people with amyotrophic lateral sclerosis', *Amyotrophic Lateral Sclerosis and Frontotemporal Degeneration*, 22(3–4), pp. 186–194. doi: 10.1080/21678421.2020.1828475.

Niethammer, P. *et al.* (2009) 'A tissue-scale gradient of hydrogen peroxide mediates rapid wound detection in zebrafish', *Nature*, 459(7249), pp. 996–999. doi: 10.1038/nature08119.

Nijs, M. and Van Damme, P. (2024) 'The genetics of amyotrophic lateral sclerosis', *Current Opinion in Neurology*, 37(5), pp. 560–569. doi: 10.1097/WCO.0000000000001294.

Nobile, C. J. *et al.* (2008) 'Complementary Adhesin Function in C. albicans Biofilm Formation', *Current Biology*, 18(14), pp. 1017–1024. doi: 10.1016/j.cub.2008.06.034.

Nobile, C. J. *et al.* (2012) 'A Recently Evolved Transcriptional Network Controls Biofilm Development in Candida albicans', *Cell*, 148(1–2), pp. 126–138. doi: 10.1016/j.cell.2011.10.048.

Noda, T. (2017) 'Regulation of Autophagy through TORC1 and mTORC1', *Biomolecules*, 7(3), p. 52. doi: 10.3390/biom7030052.

Nogueira-Machado, J. A., Rocha-Silva, F. and Gomes, N. A. (2025) 'The Role of mTOR in Amyotrophic Lateral Sclerosis', *Biomedicines*, 13(4), p. 952. doi: 10.3390/biomedicines13040952.

Noor Eddin, A. *et al.* (2024) 'Gut-Modulating Agents and Amyotrophic Lateral Sclerosis: Current Evidence and Future Perspectives', *Nutrients*, 16(5), p. 590. doi: 10.3390/nu16050590.

Nordlund, A. *et al.* (2009) 'Functional features cause misfolding of the ALS-provoking enzyme SOD1', *Proceedings of the National Academy of Sciences*, 106(24), pp. 9667–9672. doi: 10.1073/pnas.0812046106.

Norris, P. J. *et al.* (1980) 'Actions of Tremorgenic Fungal Toxins on Neurotransmitter Release', *Journal of Neurochemistry*, 34(1), pp. 33–42. doi: 10.1111/j.1471-4159.1980.tb04618.x.

Oeda, T. (2001) 'Oxidative stress causes abnormal accumulation of familial amyotrophic lateral sclerosis-related mutant SOD1 in transgenic Caenorhabditis elegans', *Human Molecular Genetics*, 10(19), pp. 2013–2023. doi: 10.1093/hmg/10.19.2013.

Ogbu, D. *et al.* (2022) 'Dietary butyrate treatment enhances healthy metabolites by longitudinal untargeted metabolomic analysis in amyotrophic lateral sclerosis mice', *bioRxiv*, p. 2022.01.15.476456. doi: 10.1101/2022.01.15.476456.

Olanow, C. W. (1993) 'A radical hypothesis for neurodegeneration', *Trends in Neurosciences*, 16(11), pp. 439–444. doi: 10.1016/0166-2236(93)90070-3.

Onafuye, H. *et al.* (2019) 'Doxorubicin-loaded human serum albumin nanoparticles overcome transporter-mediated drug resistance in drug-adapted cancer cells.', *Beilstein journal of nanotechnology*, 10, pp. 1707–1715. doi: 10.3762/bjnano.10.166.

Onesto, E. *et al.* (2016) 'Gene-specific mitochondria dysfunctions in human TARDBP and C9ORF72 fibroblasts', *Acta Neuropathologica Communications*, 4(1), p. 47. doi: 10.1186/s40478-016-0316-5.

Ott, M. *et al.* (2002) 'Cytochrome c release from mitochondria proceeds by a two-step process', *Proceedings of the National Academy of Sciences*, 99(3), pp. 1259–1263. doi: 10.1073/pnas.241655498.

Paganoni, S. *et al.* (2020) 'Trial of Sodium Phenylbutyrate–Taurursodiol for Amyotrophic Lateral Sclerosis', *New England Journal of Medicine*, 383(10), pp. 919–930. doi: 10.1056/NEJMoa1916945.

Paganoni, S. *et al.* (2021) 'Long-term survival of participants in the <scp>CENTAUR</scp> trial of sodium phenylbutyrate-taurursodiol in <scp>amyotrophic lateral sclerosis</scp>', *Muscle & Nerve*, 63(1), pp. 31–39. doi: 10.1002/mus.27091.

Paiva, I. *et al.* (2017) 'Sodium butyrate rescues dopaminergic cells from alpha-synuclein-induced transcriptional deregulation and DNA damage', *Human Molecular Genetics*, 26(12), pp. 2231–2246. doi: 10.1093/hmg/ddx114.

van der Pal, R. H. M. *et al.* (1987) 'Effect of ruthenium red upon Ca2+ and Mn2+ uptake in Saccharomyces cerevisiae. Comparison with the effect of La3+', *Biochimica et Biophysica Acta (BBA) - Biomembranes*, 902(1), pp. 19–23. doi: 10.1016/0005-2736(87)90131-3.

Palecek, J., Lips, M. B. and Keller, B. U. (1999) 'Calcium dynamics and buffering in motoneurones of the mouse spinal cord', *The Journal of Physiology*, 520(2), pp. 485–502. doi: 10.1111/j.1469-7793.1999.00485.x.

Palmer, C. *et al.* (2007) 'Development of the Human Infant Intestinal Microbiota', *PLoS Biology*. Edited by Y. Ruan, 5(7), p. e177. doi: 10.1371/journal.pbio.0050177.

Palmer, C. P. *et al.* (2001) 'A TRP homolog in Saccharomyces cerevisiae forms an intracellular Ca 2+ -permeable channel in the yeast vacuolar membrane', *Proceedings of the National Academy of Sciences*, 98(14), pp. 7801–7805. doi: 10.1073/pnas.141036198.

Panariello, B. H. D. *et al.* (2017) 'Inactivation of genes TEC1 and EFG1 in Candida albicans influences extracellular matrix composition and biofilm morphology', *Journal of Oral*

Microbiology, 9(1), p. 1385372. doi: 10.1080/20002297.2017.1385372.

Panda, S. *et al.* (2021) 'Endoplasmic reticulum & mitochondrial calcium homeostasis: The interplay with viruses.', *Mitochondrion*, 58, pp. 227–242. doi: 10.1016/j.mito.2021.03.008.

Pansarasa, O. *et al.* (2018) 'SOD1 in Amyotrophic Lateral Sclerosis: "Ambivalent" Behavior Connected to the Disease', *International Journal of Molecular Sciences*, 19(5), p. 1345. doi: 10.3390/ijms19051345.

Pant, K. *et al.* (2023) 'The Role of Gut Microbiome-Derived Short-Chain Fatty Acid Butyrate in Hepatobiliary Diseases', *The American Journal of Pathology*, 193(10), pp. 1455–1467. doi: 10.1016/j.ajpath.2023.06.007.

Parada Venegas, D. *et al.* (2019) 'Short Chain Fatty Acids (SCFAs)-Mediated Gut Epithelial and Immune Regulation and Its Relevance for Inflammatory Bowel Diseases', *Frontiers in Immunology*, 10. doi: 10.3389/fimmu.2019.00277.

Park, H.-S. *et al.* (2019) 'Calcium-Calmodulin-Calcineurin Signaling: A Globally Conserved Virulence Cascade in Eukaryotic Microbial Pathogens', *Cell Host & Microbe*, 26(4), pp. 453–462. doi: 10.1016/j.chom.2019.08.004.

Parone, P. A. *et al.* (2013) 'Enhancing Mitochondrial Calcium Buffering Capacity Reduces Aggregation of Misfolded SOD1 and Motor Neuron Cell Death without Extending Survival in Mouse Models of Inherited Amyotrophic Lateral Sclerosis', *Journal of Neuroscience*, 33(11), pp. 4657–4671. doi: 10.1523/JNEUROSCI.1119-12.2013.

Parra-Cantu, C. *et al.* (2021) 'Prevalence of Gastrointestinal Symptoms, Severity of Dysphagia, and Their Correlation with Severity of Amyotrophic Lateral Sclerosis in a Mexican Cohort', *Neurodegenerative Diseases*, 21(1–2), pp. 42–47. doi: 10.1159/000517613.

Parton, M. J. *et al.* (2002) 'D90A-SOD1 mediated amyotrophic lateral sclerosis: A single founder for all cases with evidence for aCis-acting disease modifier in the recessive haplotype', *Human Mutation*, 20(6), pp. 473–473. doi: 10.1002/humu.9081.

Parzych, K. R. and Klionsky, D. J. (2014) 'An Overview of Autophagy: Morphology, Mechanism, and Regulation', *Antioxidants & Redox Signaling*, 20(3), pp. 460–473. doi: 10.1089/ars.2013.5371.

Pascale, A. *et al.* (2018) 'Microbiota and metabolic diseases', *Endocrine*, 61(3), pp. 357–371. doi: 10.1007/s12020-018-1605-5.

Patai, R. *et al.* (2017) 'Presymptomatically applied AMPA receptor antagonist prevents calcium increase in vulnerable type of motor axon terminals of mice modeling amyotrophic lateral sclerosis', *Biochimica et Biophysica Acta (BBA) - Molecular Basis of Disease*, 1863(7), pp. 1739–1748. doi: 10.1016/j.bbadis.2017.05.016.

Patnala, R. *et al.* (2017) 'HDAC Inhibitor Sodium Butyrate-Mediated Epigenetic Regulation Enhances Neuroprotective Function of Microglia During Ischemic Stroke', *Molecular Neurobiology*, 54(8), pp. 6391–6411. doi: 10.1007/s12035-016-0149-z.

Paulsen, C. E. and Carroll, K. S. (2010) 'Orchestrating Redox Signaling Networks through Regulatory Cysteine Switches', *ACS Chemical Biology*, 5(1), pp. 47–62. doi: 10.1021/cb900258z.

Pedrini, S. *et al.* (2010) 'ALS-linked mutant SOD1 damages mitochondria by promoting conformational changes in Bcl-2', *Human Molecular Genetics*, 19(15), pp. 2974–2986. doi: 10.1093/hmg/ddq202.

Peleg, A. Y., Hogan, D. A. and Mylonakis, E. (2010) 'Medically important bacterial–fungal interactions', *Nature Reviews Microbiology*, 8(5), pp. 340–349. doi: 10.1038/nrmicro2313.

Pereira, C., Bessa, C., *et al.* (2012) 'Contribution of Yeast Models to Neurodegeneration Research', *Journal of Biomedicine and Biotechnology*, 2012, pp. 1–12. doi: 10.1155/2012/941232.

Pereira, C., Coutinho, I., *et al.* (2012) 'New insights into cancer-related proteins provided by the yeast model', *FEBS Journal*, 279(5), pp. 697–712. doi: 10.1111/j.1742-4658.2012.08477.x.

Perrett, R. M., Alexopoulou, Z. and Tofaris, G. K. (2015) 'The endosomal pathway in Parkinson's disease', *Molecular and Cellular Neuroscience*, 66, pp. 21–28. doi: 10.1016/j.mcn.2015.02.009.

Peterson, D. W. *et al.* (1982) 'A comparative study of sheep and pigs given the tremorgenic mycotoxins verruculogen and penitrem A.', *Research in veterinary science*, 33(2), pp. 183–7.

Available at: http://www.ncbi.nlm.nih.gov/pubmed/7146626.

Petranovic, D. *et al.* (2010) 'Prospects of yeast systems biology for human health: integrating lipid, protein and energy metabolism', *FEMS Yeast Research*, 10(8), pp. 1046–1059. doi: 10.1111/j.1567-1364.2010.00689.x.

Phan, Q. T. *et al.* (2007) 'Als3 Is a Candida albicans Invasin That Binds to Cadherins and Induces Endocytosis by Host Cells', *PLoS Biology*. Edited by J. Heitman, 5(3), p. e64. doi: 10.1371/journal.pbio.0050064.

Phiel, C. J. *et al.* (2001) 'Histone deacetylase is a direct target of valproic acid, a potent anticonvulsant, mood stabilizer, and teratogen.', *The Journal of biological chemistry*, 276(39), pp. 36734–41. doi: 10.1074/jbc.M101287200.

Phipps, A. J. *et al.* (2024) 'HDAC6 inhibition as a mechanism to prevent neurodegeneration in the mSOD1G93A mouse model of ALS', *Heliyon*, 10(14), p. e34587. doi: 10.1016/j.heliyon.2024.e34587.

Pickles, S. *et al.* (2013) 'Mitochondrial damage revealed by immunoselection for ALS-linked misfolded SOD1', *Human Molecular Genetics*, 22(19), pp. 3947–3959. doi: 10.1093/hmg/ddt249.

Piepers, S. *et al.* (2009) 'Randomized sequential trial of valproic acid in amyotrophic lateral sclerosis', *Annals of Neurology*, 66(2), pp. 227–234. doi: 10.1002/ana.21620.

Pierce, J. V. *et al.* (2013) 'Normal Adaptation of Candida albicans to the Murine Gastrointestinal Tract Requires Efg1p-Dependent Regulation of Metabolic and Host Defense Genes', *Eukaryotic Cell*, 12(1), pp. 37–49. doi: 10.1128/EC.00236-12.

Pineda, J. R. *et al.* (2009) 'Genetic and pharmacological inhibition of calcineurin corrects the BDNF transport defect in Huntington's disease', *Molecular Brain*, 2(1), p. 33. doi: 10.1186/1756-6606-2-33.

Pircs, K. *et al.* (2018) 'Huntingtin Aggregation Impairs Autophagy, Leading to Argonaute-2 Accumulation and Global MicroRNA Dysregulation', *Cell Reports*, 24(6), pp. 1397–1406. doi: 10.1016/j.celrep.2018.07.017.

Polizotto, R. S. and Cyert, M. S. (2001) 'Calcineurin-dependent nuclear import of the

transcription factor Crz1p requires Nmd5p', *The Journal of Cell Biology*, 154(5), pp. 951–960. doi: 10.1083/jcb.200104078.

Popa, C. *et al.* (2010) 'Exogenous oxidative stress induces Ca 2+ release in the yeast Saccharomyces cerevisiae', *The FEBS Journal*, 277(19), pp. 4027–4038. doi: 10.1111/j.1742-4658.2010.07794.x.

Le Poul, E. *et al.* (2003) 'Functional Characterization of Human Receptors for Short Chain Fatty Acids and Their Role in Polymorphonuclear Cell Activation', *Journal of Biological Chemistry*, 278(28), pp. 25481–25489. doi: 10.1074/jbc.M301403200.

Prudencio, M. *et al.* (2009) 'Variation in aggregation propensities among ALS-associated variants of SOD1: correlation to human disease.', *Human molecular genetics*, 18(17), pp. 3217–26. doi: 10.1093/hmg/ddp260.

Prudencio, M. and Borchelt, D. R. (2011) 'Superoxide dismutase 1 encoding mutations linked to ALS adopts a spectrum of misfolded states', *Molecular Neurodegeneration*, 6(1), p. 77. doi: 10.1186/1750-1326-6-77.

Puig, S. and Thiele, D. J. (2002) 'Molecular mechanisms of copper uptake and distribution', *Current Opinion in Chemical Biology*, 6(2), pp. 171–180. doi: 10.1016/S1367-5931(02)00298-3.

Quesada-Vázquez, S. *et al.* (2020) 'Diet, Gut Microbiota and Non-Alcoholic Fatty Liver Disease: Three Parts of the Same Axis', *Cells*, 9(1), p. 176. doi: 10.3390/cells9010176.

Rabbani, G. H. *et al.* (1999) 'Short-chain fatty acids inhibit fluid and electrolyte loss induced by cholera toxin in proximal colon of rabbit in vivo.', *Digestive diseases and sciences*, 44(8), pp. 1547–53. doi: 10.1023/a:1026650624193.

Rabbitts, T. H. *et al.* (1993) 'Fusion of the dominant negative transcription regulator CHOP with a novel gene FUS by translocation t(12;16) in malignant liposarcoma', *Nature Genetics*, 4(2), pp. 175–180. doi: 10.1038/ng0693-175.

Rahman, M. A. and Rhim, H. (2017) 'Therapeutic implication of autophagy in neurodegenerative diseases', *BMB Reports*, 50(7), pp. 345–354. doi: 10.5483/BMBRep.2017.50.7.069.

Rakhit, R. *et al.* (2002) 'Oxidation-induced Misfolding and Aggregation of Superoxide Dismutase and Its Implications for Amyotrophic Lateral Sclerosis', *Journal of Biological Chemistry*, 277(49), pp. 47551–47556. doi: 10.1074/jbc.M207356200.

Rand, J. B. (2007) 'Acetylcholine.', *WormBook : the online review of C. elegans biology*, pp. 1–21. doi: 10.1895/wormbook.1.131.1.

Rasconi, S. *et al.* (2009) 'Use of calcofluor white for detection, identification, and quantification of phytoplanktonic fungal parasites.', *Applied and environmental microbiology*, 75(8), pp. 2545–53. doi: 10.1128/AEM.02211-08.

Rebbeor, J. F. *et al.* (1998) 'ATP-dependent Transport of Reduced Glutathione on YCF1, the Yeast Orthologue of Mammalian Multidrug Resistance Associated Proteins', *Journal of Biological Chemistry*, 273(50), pp. 33449–33454. doi: 10.1074/jbc.273.50.33449.

Reddy, D. S. *et al.* (2018) 'Measuring Histone Deacetylase Inhibition in the Brain', *Current Protocols in Pharmacology*, 81(1). doi: 10.1002/cpph.41.

Redler, R. L. and Dokholyan, N. V. (2012) 'The Complex Molecular Biology of Amyotrophic Lateral Sclerosis (ALS)', in, pp. 215–262. doi: 10.1016/B978-0-12-385883-2.00002-3.

Reese, L. C. *et al.* (2008) 'Selective induction of calcineurin activity and signaling by oligomeric amyloid beta', *Aging Cell*, 7(6), pp. 824–835. doi: 10.1111/j.1474-9726.2008.00434.x.

Renton, A. E. *et al.* (2011) 'A Hexanucleotide Repeat Expansion in C9ORF72 Is the Cause of Chromosome 9p21-Linked ALS-FTD', *Neuron*, 72(2), pp. 257–268. doi: 10.1016/j.neuron.2011.09.010.

Renton, A. E., Chiò, A. and Traynor, B. J. (2014) 'State of play in amyotrophic lateral sclerosis genetics', *Nature Neuroscience*, 17(1), pp. 17–23. doi: 10.1038/nn.3584.

Ricci, L. *et al.* (2022) 'Human gut bifidobacteria inhibit the growth of the opportunistic fungal pathogen Candida albicans', *FEMS Microbiology Ecology*, 98(10). doi: 10.1093/femsec/fiac095.

Richmond, J. E. and Jorgensen, E. M. (1999) 'One GABA and two acetylcholine receptors function at the C. elegans neuromuscular junction', *Nature Neuroscience*, 2(9), pp. 791–797.

doi: 10.1038/12160.

Rinnerthaler, M. *et al.* (2012) 'Yno1p/Aim14p, a NADPH-oxidase ortholog, controls extramitochondrial reactive oxygen species generation, apoptosis, and actin cable formation in yeast', *Proceedings of the National Academy of Sciences*, 109(22), pp. 8658–8663. doi: 10.1073/pnas.1201629109.

Rivière, A. *et al.* (2016) 'Bifidobacteria and Butyrate-Producing Colon Bacteria: Importance and Strategies for Their Stimulation in the Human Gut', *Frontiers in Microbiology*, 7. doi: 10.3389/fmicb.2016.00979.

Rizzuto, R., Duchen, M. R. and Pozzan, T. (2004) 'Flirting in Little Space: The ER/Mitochondria Ca 2+ Liaison', *Science's STKE*, 2004(215). doi: 10.1126/stke.2152004re1.

Robbins, N. *et al.* (2011) 'Hsp90 Governs Dispersion and Drug Resistance of Fungal Biofilms', *PLoS Pathogens*. Edited by R. C. May, 7(9), p. e1002257. doi: 10.1371/journal.ppat.1002257.

Robbins, N., Caplan, T. and Cowen, L. E. (2017) 'Molecular Evolution of Antifungal Drug Resistance', *Annual Review of Microbiology*, 71(1), pp. 753–775. doi: 10.1146/annurev-micro-030117-020345.

Rodriguez, J. A. *et al.* (2005) 'Destabilization of apoprotein is insufficient to explain Cu,Zn-superoxide dismutase-linked ALS pathogenesis', *Proceedings of the National Academy of Sciences*, 102(30), pp. 10516–10521. doi: 10.1073/pnas.0502515102.

Rodríguez, L. R. *et al.* (2022) 'Therapeutic Strategies Targeting Mitochondrial Calcium Signaling: A New Hope for Neurological Diseases?', *Antioxidants*, 11(1), p. 165. doi: 10.3390/antiox11010165.

Rosen, D. R. *et al.* (1993) 'Mutations in Cu/Zn superoxide dismutase gene are associated with familial amyotrophic lateral sclerosis', *Nature*, 362(6415), pp. 59–62. doi: 10.1038/362059a0.

Rouaux, C. (2003) 'Critical loss of CBP/p300 histone acetylase activity by caspase-6 during neurodegeneration', *The EMBO Journal*, 22(24), pp. 6537–6549. doi: 10.1093/emboj/cdg615.

Rousseaux, S. and Khochbin, S. (2015) 'Histone Acylation beyond Acetylation: Terra

Incognita in Chromatin Biology.', *Cell journal*, 17(1), pp. 1–6. doi: 10.22074/cellj.2015.506.

Rowin, J. *et al.* (2017) 'Gut inflammation and dysbiosis in human motor neuron disease', *Physiological Reports*, 5(18), p. e13443. doi: 10.14814/phy2.13443.

Roy, J. *et al.* (1998) 'Glutamate Potentiates the Toxicity of Mutant Cu/Zn-Superoxide Dismutase in Motor Neurons by Postsynaptic Calcium-Dependent Mechanisms', *The Journal of Neuroscience*, 18(23), pp. 9673–9684. doi: 10.1523/JNEUROSCI.18-23-09673.1998.

Roy, J. and Cyert, M. S. (2009) 'Cracking the phosphatase code: docking interactions determine substrate specificity.', *Science signaling*, 2(100), p. re9. doi: 10.1126/scisignal.2100re9.

Rudnick, N. D. *et al.* (2017) 'Distinct roles for motor neuron autophagy early and late in the SOD1 G93A mouse model of ALS', *Proceedings of the National Academy of Sciences*, 114(39). doi: 10.1073/pnas.1704294114.

Rusnak, F. and Mertz, P. (2000) 'Calcineurin: Form and Function', *Physiological Reviews*, 80(4), pp. 1483–1521. doi: 10.1152/physrev.2000.80.4.1483.

Russnak, R., Konczal, D. and McIntire, S. L. (2001) 'A Family of Yeast Proteins Mediating Bidirectional Vacuolar Amino Acid Transport', *Journal of Biological Chemistry*, 276(26), pp. 23849–23857. doi: 10.1074/jbc.M008028200.

Russo, A. *et al.* (2017) 'Increased cytoplasmic TDP-43 reduces global protein synthesis by interacting with RACK1 on polyribosomes', *Human Molecular Genetics*, 26(8), pp. 1407–1418. doi: 10.1093/hmg/ddx035.

Ryman, S. *et al.* (2023) 'Microbiome–gut–brain dysfunction in prodromal and symptomatic Lewy body diseases', *Journal of Neurology*, 270(2), pp. 746–758. doi: 10.1007/s00415-022-11461-9.

Ryu, H. *et al.* (2005) 'Sodium phenylbutyrate prolongs survival and regulates expression of anti-apoptotic genes in transgenic amyotrophic lateral sclerosis mice', *Journal of Neurochemistry*, 93(5), pp. 1087–1098. doi: 10.1111/j.1471-4159.2005.03077.x.

Saccon, R. A. *et al.* (2013) 'Is SOD1 loss of function involved in amyotrophic lateral sclerosis?', *Brain*, 136(8), pp. 2342–2358. doi: 10.1093/brain/awt097.

Saha, R. N. and Pahan, K. (2006) 'HATs and HDACs in neurodegeneration: a tale of disconcerted acetylation homeostasis', *Cell Death & Differentiation*, 13(4), pp. 539–550. doi: 10.1038/sj.cdd.4401769.

Sahana, T. and Zhang, K. (2021) 'Mitogen-Activated Protein Kinase Pathway in Amyotrophic Lateral Sclerosis', *Biomedicines*, 9(8), p. 969. doi: 10.3390/biomedicines9080969.

Salazar, N. *et al.* (2019) 'Age-Associated Changes in Gut Microbiota and Dietary Components Related with the Immune System in Adulthood and Old Age: A Cross-Sectional Study', *Nutrients*, 11(8), p. 1765. doi: 10.3390/nu11081765.

Salomon-Zimri, S. *et al.* (2023) 'Combination of ciprofloxacin/celecoxib as a novel therapeutic strategy for ALS', *Amyotrophic Lateral Sclerosis and Frontotemporal Degeneration*, 24(3–4), pp. 263–271. doi: 10.1080/21678421.2022.2119868.

Salowe, S. P. and Hermes, J. D. (1998) 'Competitive and Slow-Binding Inhibition of Calcineurin by Drug · Immunophilin Complexes', *Archives of Biochemistry and Biophysics*, 355(2), pp. 165–174. doi: 10.1006/abbi.1998.0739.

Samara, V. C. *et al.* (2021) 'Bowel, bladder, and sudomotor symptoms in ALS patients', *Journal of the Neurological Sciences*, 427, p. 117543. doi: 10.1016/j.jns.2021.117543.

Sampson, T. R. *et al.* (2016) 'Gut Microbiota Regulate Motor Deficits and Neuroinflammation in a Model of Parkinson's Disease', *Cell*, 167(6), pp. 1469-1480.e12. doi: 10.1016/j.cell.2016.11.018.

Sanglard, D. (2021) 'Aequorin as a Useful Calcium-Sensing Reporter in Candida albicans', *Journal of Fungi*, 7(4), p. 319. doi: 10.3390/jof7040319.

Sasaki, S. and Iwata, M. (1996) 'Ultrastructural study of synapses in the anterior horn neurons of patients with amyotrophic lateral sclerosis', *Neuroscience Letters*, 204(1–2), pp. 53–56. doi: 10.1016/0304-3940(96)12314-4.

Sava, V. *et al.* (2006) 'Can low level exposure to ochratoxin-A cause parkinsonism?', *Journal of the Neurological Sciences*, 249(1), pp. 68–75. doi: 10.1016/j.jns.2006.06.006.

Saxena, S. *et al.* (2013) 'Neuroprotection through Excitability and mTOR Required in ALS Motoneurons to Delay Disease and Extend Survival', *Neuron*, 80(1), pp. 80–96. doi:

10.1016/j.neuron.2013.07.027.

Schaffitzel, E. and Hertweck, M. (2006) 'Recent aging research in Caenorhabditis elegans', *Experimental Gerontology*, 41(6), pp. 557–563. doi: 10.1016/j.exger.2006.02.008.

Scharlau, D. *et al.* (2009) 'Mechanisms of primary cancer prevention by butyrate and other products formed during gut flora-mediated fermentation of dietary fibre', *Mutation Research/Reviews in Mutation Research*, 682(1), pp. 39–53. doi: 10.1016/j.mrrev.2009.04.001.

Scheperjans, F. *et al.* (2015) 'Gut microbiota are related to Parkinson's disease and clinical phenotype', *Movement Disorders*, 30(3), pp. 350–358. doi: 10.1002/mds.26069.

Scheppach, W. *et al.* (1992) 'Effect of butyrate enemas on the colonic mucosa in distal ulcerative colitis', *Gastroenterology*, 103(1), pp. 51–56. doi: 10.1016/0016-5085(92)91094-K.

Schweizer, A. *et al.* (2000) 'The TEA/ATTS transcription factor CaTec1p regulates hyphal development and virulence in Candida albicans', *Molecular Microbiology*, 38(3), pp. 435–445. doi: 10.1046/j.1365-2958.2000.02132.x.

Scofield, M. D. *et al.* (2012) 'Nucleus Accumbens 1, a Pox virus and Zinc finger/Bric-a-brac Tramtrack Broad protein binds to TAR DNA-binding protein 43 and has a potential role in Amyotrophic Lateral Sclerosis', *Neuroscience*, 227, pp. 44–54. doi: 10.1016/j.neuroscience.2012.09.043.

Sea, K. *et al.* (2015) 'Insights into the Role of the Unusual Disulfide Bond in Copper-Zinc Superoxide Dismutase', *Journal of Biological Chemistry*, 290(4), pp. 2405–2418. doi: 10.1074/jbc.M114.588798.

Segain, J.-P. (2000) 'Butyrate inhibits inflammatory responses through NFkappa B inhibition: implications for Crohn's disease', *Gut*, 47(3), pp. 397–403. doi: 10.1136/gut.47.3.397.

Sekhavat, A., Sun, J.-M. and Davie, J. R. (2007) 'Competitive inhibition of histone deacetylase activity by trichostatin A and butyrate', *Biochemistry and Cell Biology*, 85(6), pp. 751–758. doi: 10.1139/O07-145.

Sengupta, S., Muir, J. G. and Gibson, P. R. (2006) 'Does butyrate protect from colorectal

cancer?', *Journal of Gastroenterology and Hepatology*, 21(1), pp. 209–218. doi: 10.1111/j.1440-1746.2006.04213.x.

Séron, K. *et al.* (1999) 'Uracil-Induced Down-Regulation of the Yeast Uracil Permease', *Journal of Bacteriology*, 181(6), pp. 1793–1800. doi: 10.1128/JB.181.6.1793-1800.1999.

Serrano, R. *et al.* (2002) 'The transcriptional response to alkaline pH in Saccharomyces cerevisiae : evidence for calcium-mediated signalling', *Molecular Microbiology*, 46(5), pp. 1319–1333. doi: 10.1046/j.1365-2958.2002.03246.x.

Severin, F. F. and Hyman, A. A. (2002) 'Pheromone Induces Programmed Cell Death in S. cerevisiae', *Current Biology*, 12(7), pp. R233–R235. doi: 10.1016/S0960-9822(02)00776-5.

Shan, X. *et al.* (2010) 'Altered distributions of Gemini of coiled bodies and mitochondria in motor neurons of TDP-43 transgenic mice', *Proceedings of the National Academy of Sciences*, 107(37), pp. 16325–16330. doi: 10.1073/pnas.1003459107.

Sharma, K. G. *et al.* (2002) 'Localization, Regulation, and Substrate Transport Properties of Bpt1p, a Saccharomyces cerevisiae MRP-Type ABC Transporter', *Eukaryotic Cell*, 1(3), pp. 391–400. doi: 10.1128/EC.1.3.391-400.2002.

Sharma, S., Taliyan, R. and Singh, S. (2015) 'Beneficial effects of sodium butyrate in 6-OHDA induced neurotoxicity and behavioral abnormalities: Modulation of histone deacetylase activity', *Behavioural Brain Research*, 291, pp. 306–314. doi: 10.1016/j.bbr.2015.05.052.

Shaw, P. and Eggett, C. J. (2000) 'Molecular factors underlying selective vulnerability of motor neurons to neurodegeneration in amyotrophic lateral sclerosis', *Journal of Neurology*, 247(S1), pp. I17–I27. doi: 10.1007/BF03161151.

Shaw, P. J. *et al.* (1995) 'Oxidative damage to protein in sporadic motor neuron disease spinal cord', *Annals of Neurology*, 38(4), pp. 691–695. doi: 10.1002/ana.410380424.

Sheikh, S. *et al.* (2013) 'Neurodegenerative Diseases: Multifactorial Conformational Diseases and Their Therapeutic Interventions.', *Journal of neurodegenerative diseases*, 2013, p. 563481. doi: 10.1155/2013/563481.

Shi, Y. *et al.* (2018) 'Haploinsufficiency leads to neurodegeneration in C9ORF72 ALS/FTD human induced motor neurons', *Nature Medicine*, 24(3), pp. 313–325. doi:

10.1038/nm.4490.

Shibasaki, F., Hallin, U. and Uchino, H. (2002) 'Calcineurin as a Multifunctional Regulator', *Journal of Biochemistry*, 131(1), pp. 1–15. doi: 10.1093/oxfordjournals.jbchem.a003063.

Shimazu, M. *et al.* (2005) 'A Family of Basic Amino Acid Transporters of the Vacuolar Membrane from Saccharomyces cerevisiae', *Journal of Biological Chemistry*, 280(6), pp. 4851–4857. doi: 10.1074/jbc.M412617200.

Shimizu, S. *et al.* (1999) 'Bcl-2 family proteins regulate the release of apoptogenic cytochrome c by the mitochondrial channel VDAC', *Nature*, 399(6735), pp. 483–487. doi: 10.1038/20959.

SHOU, Y. *et al.* (2004) 'Calcineurin-mediated Bad translocation regulates cyanide-induced neuronal apoptosis', *Biochemical Journal*, 379(3), pp. 805–813. doi: 10.1042/bj20031107.

Siklós, L. *et al.* (1996) 'Ultrastructural evidence for altered calcium in motor nerve terminals in amyotrophc lateral sclerosis', *Annals of Neurology*, 39(2), pp. 203–216. doi: 10.1002/ana.410390210.

Siklós, L. *et al.* (1998) 'Intracellular Calcium Parallels Motoneuron Degeneration in SOD-1 Mutant Mice', *Journal of Neuropathology & Experimental Neurology*, 57(6), pp. 571–587. doi: 10.1097/00005072-199806000-00005.

Silva, Y. P., Bernardi, A. and Frozza, R. L. (2020) 'The Role of Short-Chain Fatty Acids From Gut Microbiota in Gut-Brain Communication', *Frontiers in Endocrinology*, 11. doi: 10.3389/fendo.2020.00025.

Simm, C. *et al.* (2007) 'Saccharomyces cerevisiae Vacuole in Zinc Storage and Intracellular Zinc Distribution', *Eukaryotic Cell*, 6(7), pp. 1166–1177. doi: 10.1128/EC.00077-07.

Simonetti, G. *et al.* (2007) 'Histone deacetylase inhibitors may reduce pathogenicity and virulence in Candida albicans', *FEMS Yeast Research*, 7(8), pp. 1371–1380. doi: 10.1111/j.1567-1364.2007.00276.x.

Singh, N. *et al.* (2014) 'Activation of Gpr109a, Receptor for Niacin and the Commensal Metabolite Butyrate, Suppresses Colonic Inflammation and Carcinogenesis', *Immunity*, 40(1), pp. 128–139. doi: 10.1016/j.immuni.2013.12.007.

Sirabella, R. *et al.* (2018) 'Ionic Homeostasis Maintenance in ALS: Focus on New Therapeutic Targets', *Frontiers in Neuroscience*, 12. doi: 10.3389/fnins.2018.00510.

Sirangelo, I. and Iannuzzi, C. (2017) 'The Role of Metal Binding in the Amyotrophic Lateral Sclerosis-Related Aggregation of Copper-Zinc Superoxide Dismutase', *Molecules*, 22(9), p. 1429. doi: 10.3390/molecules22091429.

Slavin, J. (2013) 'Fiber and Prebiotics: Mechanisms and Health Benefits', *Nutrients*, 5(4), pp. 1417–1435. doi: 10.3390/nu5041417.

Smith, E. . and Macfarlane, G. . (1997) 'Dissimilatory Amino Acid Metabolism in Human Colonic Bacteria', *Anaerobe*, 3(5), pp. 327–337. doi: 10.1006/anae.1997.0121.

Smith, W. L. and Edlind, T. D. (2002) 'Histone deacetylase inhibitors enhance Candida albicans sensitivity to azoles and related antifungals: correlation with reduction in CDR and ERG upregulation.', *Antimicrobial agents and chemotherapy*, 46(11), pp. 3532–9. doi: 10.1128/AAC.46.11.3532-3539.2002.

Soo, K. Y. *et al.* (2015) 'Rab1-dependent ER–Golgi transport dysfunction is a common pathogenic mechanism in SOD1, TDP-43 and FUS-associated ALS', *Acta Neuropathologica*, 130(5), pp. 679–697. doi: 10.1007/s00401-015-1468-2.

Soto, C. (2003) 'Unfolding the role of protein misfolding in neurodegenerative diseases', *Nature Reviews Neuroscience*, 4(1), pp. 49–60. doi: 10.1038/nrn1007.

Spampinato, C. and Leonardi, D. (2013) 'Candida infections, causes, targets, and resistance mechanisms: traditional and alternative antifungal agents.', *BioMed research international*, 2013, p. 204237. doi: 10.1155/2013/204237.

Staats, K. A. *et al.* (2013) 'Rapamycin increases survival in ALS mice lacking mature lymphocytes', *Molecular Neurodegeneration*, 8(1), p. 31. doi: 10.1186/1750-1326-8-31.

Starkov, A. A. and Fiskum, G. (2003) 'Regulation of brain mitochondrial H 2 O 2 production by membrane potential and NAD(P)H redox state', *Journal of Neurochemistry*, 86(5), pp. 1101–1107. doi: 10.1046/j.1471-4159.2003.01908.x.

Stathopoulos-Gerontides, A., Guo, J. J. and Cyert, M. S. (1999) 'Yeast calcineurin regulates nuclear localization of the Crz1p transcription factor through dephosphorylation', *Genes &*

Development, 13(7), pp. 798–803. doi: 10.1101/gad.13.7.798.

Stathopoulos, A. M. and Cyert, M. S. (1997) 'Calcineurin acts through the CRZ1/TCN1-encoded transcription factor to regulate gene expression in yeast.', *Genes & development*, 11(24), pp. 3432–44. doi: 10.1101/gad.11.24.3432.

Stathopulos, P. B. *et al.* (2003) 'Cu/Zn superoxide dismutase mutants associated with amyotrophic lateral sclerosis show enhanced formation of aggregates in vitro', *Proceedings of the National Academy of Sciences*, 100(12), pp. 7021–7026. doi: 10.1073/pnas.1237797100.

Staudt, C., Puissant, E. and Boonen, M. (2016) 'Subcellular Trafficking of Mammalian Lysosomal Proteins: An Extended View', *International Journal of Molecular Sciences*, 18(1), p. 47. doi: 10.3390/ijms18010047.

Steyn, F. J. *et al.* (2018) 'Hypermetabolism in ALS is associated with greater functional decline and shorter survival', *Journal of Neurology, Neurosurgery & Psychiatry*, 89(10), pp. 1016–1023. doi: 10.1136/jnnp-2017-317887.

Stilling, R. M. *et al.* (2016) 'The neuropharmacology of butyrate: The bread and butter of the microbiota-gut-brain axis?', *Neurochemistry International*, 99, pp. 110–132. doi: 10.1016/j.neuint.2016.06.011.

Stilling, R. M., Dinan, T. G. and Cryan, J. F. (2014) 'Microbial genes, brain & behaviour - epigenetic regulation of the gut-brain axis', *Genes, Brain and Behavior*, 13(1), pp. 69–86. doi: 10.1111/gbb.12109.

Stjepanovic, G. *et al.* (2017) 'Vps34 Kinase Domain Dynamics Regulate the Autophagic PI 3-Kinase Complex', *Molecular Cell*, 67(3), pp. 528-534.e3. doi: 10.1016/j.molcel.2017.07.003.

Strahl, B. D. and Allis, C. D. (2000) 'The language of covalent histone modifications', *Nature*, 403(6765), pp. 41–45. doi: 10.1038/47412.

Strasser, A., O'Connor, L. and Dixit, V. M. (2000) 'Apoptosis Signaling', *Annual Review of Biochemistry*, 69(1), pp. 217–245. doi: 10.1146/annurev.biochem.69.1.217.

Stull, J. T. (2001) 'Ca2+-dependent Cell Signaling through Calmodulin-activated Protein Phosphatase and Protein Kinases Minireview Series', *Journal of Biological Chemistry*, 276(4),

pp. 2311–2312. doi: 10.1074/jbc.R000030200.

Sturtz, L. A. *et al.* (2001) 'A Fraction of Yeast Cu,Zn-Superoxide Dismutase and Its Metallochaperone, CCS, Localize to the Intermembrane Space of Mitochondria', *Journal of Biological Chemistry*, 276(41), pp. 38084–38089. doi: 10.1074/jbc.M105296200.

Su, S. *et al.* (2020) 'Histone Acetylation/Deacetylation in Candida Albicans and their Potential as Antifungal Targets', *Future Microbiology*, 15(11), pp. 1075–1090. doi: 10.2217/fmb-2019-0343.

Sudo, N. *et al.* (2004) 'Postnatal microbial colonization programs the hypothalamic-pituitary-adrenal system for stress response in mice', *The Journal of Physiology*, 558(1), pp. 263–275. doi: 10.1113/jphysiol.2004.063388.

Sun, J. *et al.* (2019) 'Antibiotics use and risk of amyotrophic lateral sclerosis in Sweden', *European Journal of Neurology*, 26(11), pp. 1355–1361. doi: 10.1111/ene.13986.

Sun, M.-F. *et al.* (2018) 'Neuroprotective effects of fecal microbiota transplantation on MPTP-induced Parkinson's disease mice: Gut microbiota, glial reaction and TLR4/TNF-α signaling pathway', *Brain, Behavior, and Immunity*, 70, pp. 48–60. doi: 10.1016/j.bbi.2018.02.005.

Sweeney, M. (1998) 'Mycotoxin production by Aspergillus, Fusarium and Penicillium species', *International Journal of Food Microbiology*, 43(3), pp. 141–158. doi: 10.1016/S0168-1605(98)00112-3.

Synofzik, M. *et al.* (2010) 'The human G93A SOD1 phenotype closely resembles sporadic amyotrophic lateral sclerosis', *Journal of Neurology, Neurosurgery & Psychiatry*, 81(7), pp. 764–767. doi: 10.1136/jnnp.2009.181719.

Szewczyk, B. (2013) 'Zinc homeostasis and neurodegenerative disorders', *Frontiers in Aging Neuroscience*, 5. doi: 10.3389/fnagi.2013.00033.

Tahara, Y. *et al.* (2018) 'Gut Microbiota-Derived Short Chain Fatty Acids Induce Circadian Clock Entrainment in Mouse Peripheral Tissue', *Scientific Reports*, 8(1), p. 1395. doi: 10.1038/s41598-018-19836-7.

Takeshige, K. *et al.* (1992) 'Autophagy in yeast demonstrated with proteinase-deficient

mutants and conditions for its induction.', *The Journal of cell biology*, 119(2), pp. 301–311. doi: 10.1083/jcb.119.2.301.

Talpaert, M. J. *et al.* (2015) 'Candida biofilm formation on voice prostheses', *Journal of Medical Microbiology*, 64(3), pp. 199–208. doi: 10.1099/jmm.0.078717-0.

Tam, O. H. *et al.* (2019) 'Postmortem Cortex Samples Identify Distinct Molecular Subtypes of ALS: Retrotransposon Activation, Oxidative Stress, and Activated Glia', *Cell Reports*, 29(5), pp. 1164-1177.e5. doi: 10.1016/j.celrep.2019.09.066.

Tamanoi, F. (2011) 'Ras Signaling in Yeast', *Genes & Cancer*, 2(3), pp. 210–215. doi: 10.1177/1947601911407322.

Tanaka, M. and Nakayama, J. (2017) 'Development of the gut microbiota in infancy and its impact on health in later life', *Allergology International*, 66(4), pp. 515–522. doi: 10.1016/j.alit.2017.07.010.

Tashiro, Y. *et al.* (2012a) 'Motor neuron-specific disruption of proteasomes, but not autophagy, replicates amyotrophic lateral sclerosis.', *The Journal of biological chemistry*, 287(51), pp. 42984–94. doi: 10.1074/jbc.M112.417600.

Tashiro, Y. *et al.* (2012b) 'Motor Neuron-specific Disruption of Proteasomes, but Not Autophagy, Replicates Amyotrophic Lateral Sclerosis', *Journal of Biological Chemistry*, 287(51), pp. 42984–42994. doi: 10.1074/jbc.M112.417600.

Tateno, M. *et al.* (2004) 'Calcium-permeable AMPA receptors promote misfolding of mutant SOD1 protein and development of amyotrophic lateral sclerosis in a transgenic mouse model', *Human Molecular Genetics*, 13(19), pp. 2183–2196. doi: 10.1093/hmg/ddh246.

Tenreiro, S. *et al.* (2013) 'Harnessing the power of yeast to unravel the molecular basis of neurodegeneration', *Journal of Neurochemistry*, 127(4), pp. 438–452. doi: 10.1111/jnc.12271.

Territo, P. R. *et al.* (2000) 'Ca 2+ activation of heart mitochondrial oxidative phosphorylation: role of the F 0 /F 1 -ATPase', *American Journal of Physiology-Cell Physiology*, 278(2), pp. C423–C435. doi: 10.1152/ajpcell.2000.278.2.C423.

Therrien, M. and Parker, J. A. (2014) 'Worming forward: amyotrophic lateral sclerosis

toxicity mechanisms and genetic interactions in Caenorhabditis elegans', *Frontiers in Genetics*, 5. doi: 10.3389/fgene.2014.00085.

Thewes, S. (2014) 'Calcineurin-Crz1 Signaling in Lower Eukaryotes', *Eukaryotic Cell*, 13(6), pp. 694–705. doi: 10.1128/EC.00038-14.

Thibault, R. *et al.* (2010) 'Butyrate utilization by the colonic mucosa in inflammatory bowel diseases', *Inflammatory Bowel Diseases*, 16(4), pp. 684–695. doi: 10.1002/ibd.21108.

Thonhoff, J. R. *et al.* (2024) 'A phase 1 proof-of-concept study evaluating safety, tolerability, and biological marker responses with combination therapy of CTLA4-Ig and interleukin-2 in amyotrophic lateral sclerosis', *Frontiers in Neurology*, 15. doi: 10.3389/fneur.2024.1415106.

Thursby, E. and Juge, N. (2017) 'Introduction to the human gut microbiota', *Biochemical Journal*, 474(11), pp. 1823–1836. doi: 10.1042/BCJ20160510.

Tiwari, A. and Hayward, L. J. (2005) 'Mutant SOD1 Instability: Implications for Toxicity in Amyotrophic Lateral Sclerosis', *Neurodegenerative Diseases*, 2(3–4), pp. 115–127. doi: 10.1159/000089616.

Tiwari, A., Xu, Z. and Hayward, L. J. (2005) 'Aberrantly Increased Hydrophobicity Shared by Mutants of Cu,Zn-Superoxide Dismutase in Familial Amyotrophic Lateral Sclerosis', *Journal of Biological Chemistry*, 280(33), pp. 29771–29779. doi: 10.1074/jbc.M504039200.

Toepfer, C Folwaczny, A Klauser, RL, M. (2000) 'Gastrointestinal dysfunction in amyotrophic lateral sclerosis', *Amyotrophic Lateral Sclerosis and Other Motor Neuron Disorders*, 1(1), pp. 15–19. doi: 10.1080/146608299300079484.

Tokuda, E. *et al.* (2016) 'Low autophagy capacity implicated in motor system vulnerability to mutant superoxide dismutase', *Acta Neuropathologica Communications*, 4(1), p. 6. doi: 10.1186/s40478-016-0274-y.

Tollervey, J. R. *et al.* (2011) 'Characterizing the RNA targets and position-dependent splicing regulation by TDP-43', *Nature Neuroscience*, 14(4), pp. 452–458. doi: 10.1038/nn.2778.

Tong, Y. and Song, F. (2015) 'Intracellular calcium signaling regulates autophagy via calcineurin-mediated TFEB dephosphorylation', *Autophagy*, 11(7), pp. 1192–1195. doi: 10.1080/15548627.2015.1054594.

Tortarolo, M. *et al.* (2006) 'Glutamate AMPA receptors change in motor neurons of SOD1G93A transgenic mice and their inhibition by a noncompetitive antagonist ameliorates the progression of amytrophic lateral sclerosis-like disease', *Journal of Neuroscience Research*, 83(1), pp. 134–146. doi: 10.1002/jnr.20715.

Trachsel, J. *et al.* (2016) 'Function and Phylogeny of Bacterial Butyryl Coenzyme A:Acetate Transferases and Their Diversity in the Proximal Colon of Swine', *Applied and Environmental Microbiology*. Edited by H. L. Drake, 82(22), pp. 6788–6798. doi: 10.1128/AEM.02307-16.

Tsang, C. K. *et al.* (2018) 'SOD1 Phosphorylation by mTORC1 Couples Nutrient Sensing and Redox Regulation', *Molecular Cell*, 70(3), pp. 502-515.e8. doi: 10.1016/j.molcel.2018.03.029.

Tsekrekou, M. *et al.* (2024) 'Protein aggregation and therapeutic strategies in SOD1- and TDP-43- linked ALS', *Frontiers in Molecular Biosciences*, 11. doi: 10.3389/fmolb.2024.1383453.

Tsigos, C. and Chrousos, G. P. (2002) 'Hypothalamic–pituitary–adrenal axis, neuroendocrine factors and stress', *Journal of Psychosomatic Research*, 53(4), pp. 865–871. doi: 10.1016/S0022-3999(02)00429-4.

Tsujimoto, Y. and Shimizu, S. (2000) 'Bcl-2 family: Life-or-death switch', *FEBS Letters*, 466(1), pp. 6–10. doi: 10.1016/S0014-5793(99)01761-5.

Turner, M. R. *et al.* (2017) 'Genetic screening in sporadic ALS and FTD', *Journal of Neurology, Neurosurgery & Psychiatry*, 88(12), pp. 1042–1044. doi: 10.1136/jnnp-2017-315995.

Ueda, S. *et al.* (2002) 'Redox Control of Cell Death', *Antioxidants & Redox Signaling*, 4(3), pp. 405–414. doi: 10.1089/15230860260196209.

Uppuluri, P. *et al.* (2008) 'Synergistic Effect of Calcineurin Inhibitors and Fluconazole against Candida albicans Biofilms', *Antimicrobial Agents and Chemotherapy*, 52(3), pp. 1127–1132. doi: 10.1128/AAC.01397-07.

Uppuluri, P., Chaturvedi, A. K., *et al.* (2010) 'Dispersion as an Important Step in the Candida albicans Biofilm Developmental Cycle', *PLoS Pathogens*. Edited by T. L. Doering, 6(3), p. e1000828. doi: 10.1371/journal.ppat.1000828.

Uppuluri, P., Pierce, C. G., *et al.* (2010) 'The Transcriptional Regulator Nrg1p Controls

Candida albicans Biofilm Formation and Dispersion', *Eukaryotic Cell*, 9(10), pp. 1531–1537. doi: 10.1128/EC.00111-10.

Uppuluri, P. *et al.* (2018) 'Candida albicans Dispersed Cells Are Developmentally Distinct from Biofilm and Planktonic Cells.', *mBio*, 9(4). doi: 10.1128/mBio.01338-18.

Urushitani, M. *et al.* (2008) 'The endoplasmic reticulum-Golgi pathway is a target for translocation and aggregation of mutant superoxide dismutase linked to ALS', *The FASEB Journal*, 22(7), pp. 2476–2487. doi: 10.1096/fj.07-092783.

Vaisman, N. *et al.* (2009) 'Do patients with amyotrophic lateral sclerosis (ALS) have increased energy needs?', *Journal of the Neurological Sciences*, 279(1–2), pp. 26–29. doi: 10.1016/j.jns.2008.12.027.

Valero, T. (2014) 'Editorial (Thematic Issue: Mitochondrial Biogenesis: Pharmacological Approaches)', *Current Pharmaceutical Design*, 20(35), pp. 5507–5509. doi: 10.2174/1381612820351409111421l8.

Vallès, Y. *et al.* (2014) 'Microbial Succession in the Gut: Directional Trends of Taxonomic and Functional Change in a Birth Cohort of Spanish Infants', *PLoS Genetics*. Edited by D. S. Guttman, 10(6), p. e1004406. doi: 10.1371/journal.pgen.1004406.

Vance, C. *et al.* (2006) 'Familial amyotrophic lateral sclerosis with frontotemporal dementia is linked to a locus on chromosome 9p13.2–21.3', *Brain*, 129(4), pp. 868–876. doi: 10.1093/brain/awl030.

Vanhaecke, T. *et al.* (2004) 'Trichostatin A - like Hydroxamate Histone Deacetylase Inhibitors as Therapeutic Agents: Toxicological Point of View', *Current Medicinal Chemistry*, 11(12), pp. 1629–1643. doi: 10.2174/0929867043365099.

Vanhoutvin, S. A. L. W. *et al.* (2009) 'The effects of butyrate enemas on visceral perception in healthy volunteers', *Neurogastroenterology & Motility*, 21(9), p. 952. doi: 10.1111/j.1365-2982.2009.01324.x.

Vande Velde, C. *et al.* (2008) 'Selective association of misfolded ALS-linked mutant SOD1 with the cytoplasmic face of mitochondria', *Proceedings of the National Academy of Sciences*, 105(10), pp. 4022–4027. doi: 10.1073/pnas.0712209105.

Vercesi, A. E. *et al.* (1997) 'The Role of Reactive Oxygen Species in Mitochondrial Permeability Transition', *Bioscience Reports*, 17(1), pp. 43–52. doi: 10.1023/A:1027335217774.

Vernia, P. *et al.* (2003) 'Topical butyrate improves efficacy of 5-ASA in refractory distal ulcerative colitis: results of a multicentre trial', *European Journal of Clinical Investigation*, 33(3), pp. 244–248. doi: 10.1046/j.1365-2362.2003.01130.x.

Vidali, G. *et al.* (1978) 'Butyrate suppression of histone deacetylation leads to accumulation of multiacetylated forms of histones H3 and H4 and increased DNase I sensitivity of the associated DNA sequences.', *Proceedings of the National Academy of Sciences*, 75(5), pp. 2239–2243. doi: 10.1073/pnas.75.5.2239.

Vielhaber, S. (2000) 'Mitochondrial DNA abnormalities in skeletal muscle of patients with sporadic amyotrophic lateral sclerosis', *Brain*, 123(7), pp. 1339–1348. doi: 10.1093/brain/123.7.1339.

Villa, S. *et al.* (2020) 'Transcriptional control of hyphal morphogenesis in Candida albicans', *FEMS Yeast Research*, 20(1). doi: 10.1093/femsyr/foaa005.

Vital, M., Howe, A. C. and Tiedje, J. M. (2014) 'Revealing the Bacterial Butyrate Synthesis Pathways by Analyzing (Meta)genomic Data', *mBio*. Edited by M. A. Moran, 5(2). doi: 10.1128/mBio.00889-14.

Vlahakis, A. *et al.* (2014) 'TOR complex 2-Ypk1 signaling is an essential positive regulator of the general amino acid control response and autophagy', *Proceedings of the National Academy of Sciences*, 111(29), pp. 10586–10591. doi: 10.1073/pnas.1406305111.

de Vos, W. M. *et al.* (2022) 'Gut microbiome and health: mechanistic insights', *Gut*, 71(5), pp. 1020–1032. doi: 10.1136/gutjnl-2021-326789.

Wächtershäuser, A. *et al.* (2000) 'Expression of 5-Lipoxygenase by Human Colorectal Carcinoma Caco-2 Cells during Butyrate-Induced Cell Differentiation', *Biochemical and Biophysical Research Communications*, 268(3), pp. 778–783. doi: 10.1006/bbrc.2000.2213.

Wächtershäuser, A., Loitsch, S. M. and Stein, J. (2000) 'PPAR-γ Is Selectively Upregulated in Caco-2 Cells by Butyrate', *Biochemical and Biophysical Research Communications*, 272(2),

pp. 380–385. doi: 10.1006/bbrc.2000.2793.

Wächtershäuser, A. and Stein, J. (2000) 'Rationale for the luminal provision of butyrate in intestinal diseases', *European Journal of Nutrition*, 39(4), pp. 164–171. doi: 10.1007/s003940070020.

Walker, A. C. *et al.* (2021) 'Colonization of the Caenorhabditis elegans gut with human enteric bacterial pathogens leads to proteostasis disruption that is rescued by butyrate', *PLOS Pathogens*. Edited by A. J. Baumler, 17(5), p. e1009510. doi: 10.1371/journal.ppat.1009510.

Wang, A. *et al.* (2012) 'Butyrate Activates the cAMP-Protein Kinase A-cAMP Response Element-Binding Protein Signaling Pathway in Caco-2 Cells ', *The Journal of Nutrition*, 142(1), pp. 1–6. doi: 10.3945/jn.111.148155.

Wang, H.-G. *et al.* (1999) 'Ca 2+ -Induced Apoptosis Through Calcineurin Dephosphorylation of BAD', *Science*, 284(5412), pp. 339–343. doi: 10.1126/science.284.5412.339.

Wang, J. *et al.* (2003) 'Copper-binding-site-null SOD1 causes ALS in transgenic mice: aggregates of non-native SOD1 delineate a common feature', *Human Molecular Genetics*, 12(21), pp. 2753–2764. doi: 10.1093/hmg/ddg312.

Wang, Jiou *et al.* (2009) 'An ALS-linked mutant SOD1 produces a locomotor defect associated with aggregation and synaptic dysfunction when expressed in neurons of Caenorhabditis elegans', *PLoS Genetics*, 5(1). doi: 10.1371/journal.pgen.1000350.

Wang, J. *et al.* (2009) 'Progressive aggregation despite chaperone associations of a mutant SOD1-YFP in transgenic mice that develop ALS', *Proceedings of the National Academy of Sciences*, 106(5), pp. 1392–1397. doi: 10.1073/pnas.0813045106.

Wang, M.-D. *et al.* (2017) 'Identification of risk factors associated with onset and progression of amyotrophic lateral sclerosis using systematic review and meta-analysis', *NeuroToxicology*, 61, pp. 101–130. doi: 10.1016/j.neuro.2016.06.015.

Wang, P. *et al.* (2018) 'Sodium butyrate triggers a functional elongation of microglial process via Akt-small RhoGTPase activation and HDACs inhibition', *Neurobiology of Disease*, 111, pp. 12–25. doi: 10.1016/j.nbd.2017.12.006.

Wang, Q. and Ren, J. (2016) 'mTOR-Independent autophagy inducer trehalose rescues against insulin resistance-induced myocardial contractile anomalies: Role of p38 MAPK and Foxo1', *Pharmacological Research*, 111, pp. 357–373. doi: 10.1016/j.phrs.2016.06.024.

Wang, W.-Y. *et al.* (2013) 'Interaction of FUS and HDAC1 regulates DNA damage response and repair in neurons.', *Nature neuroscience*, 16(10), pp. 1383–91. doi: 10.1038/nn.3514.

Wang, W. *et al.* (2013) 'The ALS disease-associated mutant TDP-43 impairs mitochondrial dynamics and function in motor neurons', *Human Molecular Genetics*, 22(23), pp. 4706–4719. doi: 10.1093/hmg/ddt319.

Wang, X., Culotta, V. C. and Klee, C. B. (1996) 'Superoxide dismutase protects calcineurin from inactivation', *Nature*, 383(6599), pp. 434–437. doi: 10.1038/383434a0.

Wang, Y. *et al.* (2018) 'Superoxide dismutases: Dual roles in controlling ROS damage and regulating ROS signaling', *Journal of Cell Biology*, 217(6), pp. 1915–1928. doi: 10.1083/jcb.201708007.

Watanabe, M. *et al.* (2001) 'Histological Evidence of Protein Aggregation in Mutant SOD1 Transgenic Mice and in Amyotrophic Lateral Sclerosis Neural Tissues', *Neurobiology of Disease*, 8(6), pp. 933–941. doi: 10.1006/nbdi.2001.0443.

Weber, M. *et al.* (2021) 'Actin Cytoskeleton Regulation by the Yeast NADPH Oxidase Yno1p Impacts Processes Controlled by MAPK Pathways', *Antioxidants*, 10(2), p. 322. doi: 10.3390/antiox10020322.

Wedenoja, S., Holmberg, C. and Höglund, P. (2008) 'Oral Butyrate in Treatment of Congenital Chloride Diarrhea', *The American Journal of Gastroenterology*, 103(1), pp. 252–254. doi: 10.1111/j.1572-0241.2007.01562_14.x.

Weidberg, H., Shvets, E. and Elazar, Z. (2011) 'Biogenesis and Cargo Selectivity of Autophagosomes', *Annual Review of Biochemistry*, 80(1), pp. 125–156. doi: 10.1146/annurev-biochem-052709-094552.

Weiss, J. H., Sensi, S. L. and Koh, J. Y. (2000) 'Zn2+: a novel ionic mediator of neural injury in brain disease', *Trends in Pharmacological Sciences*, 21(10), pp. 395–401. doi: 10.1016/S0165-6147(00)01541-8.

Wiech, N. *et al.* (2009) 'Inhibition of Histone Deacetylases: A Pharmacological Approach to the Treatment of Non-Cancer Disorders', *Current Topics in Medicinal Chemistry*, 9(3), pp. 257–271. doi: 10.2174/156802609788085241.

Wiedemann, F. R. *et al.* (1998) 'Impairment of mitochondrial function in skeletal muscle of patients with amyotrophic lateral sclerosis', *Journal of the Neurological Sciences*, 156(1), pp. 65–72. doi: 10.1016/S0022-510X(98)00008-2.

Willemsen, L. E. M. (2003) 'Short chain fatty acids stimulate epithelial mucin 2 expression through differential effects on prostaglandin E1 and E2 production by intestinal myofibroblasts', *Gut*, 52(10), pp. 1442–1447. doi: 10.1136/gut.52.10.1442.

Williams, T. L. *et al.* (1997) 'Calcium-permeable ?-amino-3-hydroxy-5-methyl-4-isoxazole propionic acid receptors: A molecular determinant of selective vulnerability in amyotrophic lateral sclerosis', *Annals of Neurology*, 42(2), pp. 200–207. doi: 10.1002/ana.410420211.

Winterbourn, C. C. and Metodiewa, D. (1999) 'Reactivity of biologically important thiol compounds with superoxide and hydrogen peroxide', *Free Radical Biology and Medicine*, 27(3–4), pp. 322–328. doi: 10.1016/S0891-5849(99)00051-9.

Winzeler, E. A. *et al.* (1999) 'Functional Characterization of the S. cerevisiae Genome by Gene Deletion and Parallel Analysis', *Science*, 285(5429), pp. 901–906. doi: 10.1126/science.285.5429.901.

Withee, J. L. *et al.* (1997) 'An essential role of the yeast pheromone-induced Ca2+ signal is to activate calcineurin.', *Molecular Biology of the Cell*, 8(2), pp. 263–277. doi: 10.1091/mbc.8.2.263.

Withee, J. L., Sen, R. and Cyert, M. S. (1998) 'Ion Tolerance of Saccharomyces cerevisiae Lacking the Ca2+/CaM-Dependent Phosphatase (Calcineurin) Is Improved by Mutations in URE2 or PMA1', *Genetics*, 149(2), pp. 865–878. doi: 10.1093/genetics/149.2.865.

Wong, A. H.-H., Yan, C. and Shi, Y. (2012) 'Crystal Structure of the Yeast Metacaspase Yca1', *Journal of Biological Chemistry*, 287(35), pp. 29251–29259. doi: 10.1074/jbc.M112.381806.

Wong, J. M. W. *et al.* (2006) 'Colonic Health: Fermentation and Short Chain Fatty Acids', *Journal of Clinical Gastroenterology*, 40(3), pp. 235–243. doi: 10.1097/00004836-

200603000-00015.

Wurtele, H. *et al.* (2010) 'Modulation of histone H3 lysine 56 acetylation as an antifungal therapeutic strategy', *Nature Medicine*, 16(7), pp. 774–780. doi: 10.1038/nm.2175.

Wysong, D. R. *et al.* (1998) 'Cloning and sequencing of a Candida albicans catalase gene and effects of disruption of this gene.', *Infection and immunity*, 66(5), pp. 1953–61. doi: 10.1128/IAI.66.5.1953-1961.1998.

Xia, Q. *et al.* (2016) '<scp>TDP</scp> -43 loss of function increases <scp>TFEB</scp> activity and blocks autophagosome–lysosome fusion', *The EMBO Journal*, 35(2), pp. 121–142. doi: 10.15252/embj.201591998.

Xicoy, H., Wieringa, B. and Martens, G. J. M. (2017) 'The SH-SY5Y cell line in Parkinson's disease research: a systematic review', *Molecular Neurodegeneration*, 12(1), p. 10. doi: 10.1186/s13024-017-0149-0.

Xie, J. *et al.* (2016) 'The Paralogous Histone Deacetylases Rpd3 and Rpd31 Play Opposing Roles in Regulating the White-Opaque Switch in the Fungal Pathogen Candida albicans', *mBio*. Edited by J. Berman, 7(6). doi: 10.1128/mBio.01807-16.

Xu, Y.-F. *et al.* (2010) 'Wild-Type Human TDP-43 Expression Causes TDP-43 Phosphorylation, Mitochondrial Aggregation, Motor Deficits, and Early Mortality in Transgenic Mice', *The Journal of Neuroscience*, 30(32), pp. 10851–10859. doi: 10.1523/JNEUROSCI.1630-10.2010.

Xue, W., Zhang, J. and Li, Y. (2023) 'Enhancement of lysosome biogenesis as a potential therapeutic approach for neurodegenerative diseases', *Neural Regeneration Research*, 18(11), pp. 2370–2376. doi: 10.4103/1673-5374.371346.

Yamagata, M., Obara, K. and Kihara, A. (2013) 'Unperverted synthesis of complex sphingolipids is essential for cell survival under nitrogen starvation', *Genes to Cells*, 18(8), pp. 650–659. doi: 10.1111/gtc.12062.

Yamamura, R. *et al.* (2023) 'Intestinal and fecal pH in human health', *Frontiers in Microbiomes*, 2. doi: 10.3389/frmbi.2023.1192316.

Yamawaki, Y. *et al.* (2018) 'Sodium butyrate abolishes lipopolysaccharide-induced depression-like behaviors and hippocampal microglial activation in mice', *Brain Research*,

1680, pp. 13–38. doi: 10.1016/j.brainres.2017.12.004.

Yáñez, M. *et al.* (2011) 'CSF from amyotrophic lateral sclerosis patients produces glutamate independent death of rat motor brain cortical neurons: Protection by resveratrol but not riluzole', *Brain Research*, 1423, pp. 77–86. doi: 10.1016/j.brainres.2011.09.025.

Yang, L. *et al.* (2004) 'Calcineurin-mediated BAD Ser155 dephosphorylation in ammonia-induced apoptosis of cultured rat hippocampal neurons', *Neuroscience Letters*, 357(1), pp. 73–75. doi: 10.1016/j.neulet.2003.12.032.

Yang, W. *et al.* (2014) 'Fungal invasion of epithelial cells', *Microbiological Research*, 169(11), pp. 803–810. doi: 10.1016/j.micres.2014.02.013.

Yang, W. *et al.* (2020) 'Intestinal microbiota-derived short-chain fatty acids regulation of immune cell IL-22 production and gut immunity', *Nature Communications*, 11(1), p. 4457. doi: 10.1038/s41467-020-18262-6.

Yang, Z. and Klionsky, D. J. (2009) 'An Overview of the Molecular Mechanism of Autophagy', in, pp. 1–32. doi: 10.1007/978-3-642-00302-8_1.

Yin, H. Z., Tang, D. T. and Weiss, J. H. (2007) 'Intrathecal infusion of a Ca2+-permeable AMPA channel blocker slows loss of both motor neurons and of the astrocyte glutamate transporter, GLT-1 in a mutant SOD1 rat model of ALS', *Experimental Neurology*, 207(2), pp. 177–185. doi: 10.1016/j.expneurol.2007.07.011.

Yonezawa, T., Kobayashi, Y. and Obara, Y. (2007) 'Short-chain fatty acids induce acute phosphorylation of the p38 mitogen-activated protein kinase/heat shock protein 27 pathway via GPR43 in the MCF-7 human breast cancer cell line', *Cellular Signalling*, 19(1), pp. 185–193. doi: 10.1016/j.cellsig.2006.06.004.

Yoo, Y.-E. and Ko, C.-P. (2011) 'Treatment with trichostatin A initiated after disease onset delays disease progression and increases survival in a mouse model of amyotrophic lateral sclerosis', *Experimental Neurology*, 231(1), pp. 147–159. doi: 10.1016/j.expneurol.2011.06.003.

Yorimitsu, T. and Klionsky, D. J. (2005) 'Autophagy: molecular machinery for self-eating', *Cell Death & Differentiation*, 12(S2), pp. 1542–1552. doi: 10.1038/sj.cdd.4401765.

Yoshimoto, H. *et al.* (2002) 'Genome-wide Analysis of Gene Expression Regulated by the Calcineurin/Crz1p Signaling Pathway in Saccharomyces cerevisiae', *Journal of Biological Chemistry*, 277(34), pp. 31079–31088. doi: 10.1074/jbc.M202718200.

Yun, J. and Lee, D. G. (2016) 'Cecropin A-induced apoptosis is regulated by ion balance and glutathione antioxidant system in Candida albicans', *IUBMB Life*, 68(8), pp. 652–662. doi: 10.1002/iub.1527.

Zacchi, L. F., Schulz, W. L. and Davis, D. A. (2010) 'HOS2 and HDA1 Encode Histone Deacetylases with Opposing Roles in Candida albicans Morphogenesis', *PLoS ONE*. Edited by A. Alspaugh, 5(8), p. e12171. doi: 10.1371/journal.pone.0012171.

Zhai, C.-D. *et al.* (2019) 'Intestinal microbiota composition in patients with amyotrophic lateral sclerosis', *Chinese Medical Journal*, 132(15), pp. 1815–1822. doi: 10.1097/CM9.0000000000000351.

Zhang, L. *et al.* (2012) 'Inhibition of Histone Deacetylase-induced Myocardial Repair Is Mediated by c-kit in Infarcted Hearts', *Journal of Biological Chemistry*, 287(47), pp. 39338–39348. doi: 10.1074/jbc.M112.379115.

Zhang, M.-D. *et al.* (2014) 'Neuronal calcium-binding proteins 1/2 localize to dorsal root ganglia and excitatory spinal neurons and are regulated by nerve injury', *Proceedings of the National Academy of Sciences*, 111(12), pp. E1149–E1158. doi: 10.1073/pnas.1402318111.

Zhang, T. *et al.* (2025) 'Decoding the role of gut mycobiota in immune regulation and disease', *Virulence*, 16(1). doi: 10.1080/21505594.2025.2541704.

ZHANG, W. and LIU, H. T. (2002) 'MAPK signal pathways in the regulation of cell proliferation in mammalian cells', *Cell Research*, 12(1), pp. 9–18. doi: 10.1038/sj.cr.7290105.

Zhang, X. *et al.* (2014) 'MTOR-independent, autophagic enhancer trehalose prolongs motor neuron survival and ameliorates the autophagic flux defect in a mouse model of amyotrophic lateral sclerosis', *Autophagy*, 10(4), pp. 588–602. doi: 10.4161/auto.27710.

Zhang, Xiaojie *et al.* (2011) 'Rapamycin treatment augments motor neuron degeneration in SOD1 G93A mouse model of amyotrophic lateral sclerosis', *Autophagy*, 7(4), pp. 412–425. doi: 10.4161/auto.7.4.14541.

Zhang, Y. *et al.* (2017) 'Target Intestinal Microbiota to Alleviate Disease Progression in Amyotrophic Lateral Sclerosis', *Clinical Therapeutics*, 39(2), pp. 322–336. doi: 10.1016/j.clinthera.2016.12.014.

Zhang, Y. *et al.* (2021) 'Aberrant enteric neuromuscular system and dysbiosis in amyotrophic lateral sclerosis', *Gut Microbes*, 13(1). doi: 10.1080/19490976.2021.1996848.

Zhang, Y. *et al.* (2025) 'Synergistic Effects of Riluzole and Sodium Butyrate on Barrier Function and Disease Progression of Amyotrophic Lateral Sclerosis Through the Gut-Neuron Axis', *Comprehensive Physiology*, 15(2). doi: 10.1002/cph4.70009.

Zhao, G. and Rusche, L. N. (2021) 'Genetic Analysis of Sirtuin Deacetylases in Hyphal Growth of Candida albicans', *mSphere*. Edited by A. P. Mitchell, 6(3). doi: 10.1128/mSphere.00053-21.

Zhao, J. *et al.* (2022) 'The Impact of Mitochondrial Dysfunction in Amyotrophic Lateral Sclerosis', *Cells*, 11(13), p. 2049. doi: 10.3390/cells11132049.

Zhao, R. *et al.* (2019) 'Mitochondrial electron transport chain, ROS generation and uncoupling (Review)', *International Journal of Molecular Medicine*. doi: 10.3892/ijmm.2019.4188.

Zhen, M. and Samuel, A. D. (2015) 'C. elegans locomotion: small circuits, complex functions', *Current Opinion in Neurobiology*, 33, pp. 117–126. doi: 10.1016/j.conb.2015.03.009.

Zhou, Q. *et al.* (2017) 'n -butylidenephthalide treatment prolongs life span and attenuates motor neuron loss in SOD 1 G93A mouse model of amyotrophic lateral sclerosis', *CNS Neuroscience & Therapeutics*, 23(5), pp. 375–385. doi: 10.1111/cns.12681.

Zhu, W. *et al.* (2012) 'EGFR and HER2 receptor kinase signaling mediate epithelial cell invasion by Candida albicans during oropharyngeal infection', *Proceedings of the National Academy of Sciences*, 109(35), pp. 14194–14199. doi: 10.1073/pnas.1117676109.

Zhu, Y. and Yakel, J. L. (1997) 'Calcineurin Modulates G Protein-Mediated Inhibition of N-Type Calcium Channels in Rat Sympathetic Neurons', *Journal of Neurophysiology*, 78(2), pp. 1161–1169. doi: 10.1152/jn.1997.78.2.1161.

Zubenko, G. S., Park, F. J. and Jones, E. W. (1983) 'Mutations in PEP4 locus of Saccharomyces

cerevisiae block final step in maturation of two vacuolar hydrolases.', *Proceedings of the National Academy of Sciences*, 80(2), pp. 510–514. doi: 10.1073/pnas.80.2.510.

Zutz, C. *et al.* (2013) 'Small Chemical Chromatin Effectors Alter Secondary Metabolite Production in Aspergillus clavatus', *Toxins*, 5(10), pp. 1723–1741. doi: 10.3390/toxins5101723.

Zutz, C. *et al.* (2014) 'Fungi Treated with Small Chemicals Exhibit Increased Antimicrobial Activity against Facultative Bacterial and Yeast Pathogens', *BioMed Research International*, 2014, pp. 1–13. doi: 10.1155/2014/540292.

Zutz, C. *et al.* (2017) 'Butyrate influences intracellular levels of adenine and adenine derivatives in the fungus Penicillium restrictum', *Microbiological Research*, 197, pp. 1–8. doi: 10.1016/j.micres.2016.12.013.